pennsylvania
DEPARTMENT OF TRANSPORTATION

Evaluating Performance of Limestone Prone to Polishing

FINAL REPORT

December 31, 2009

By Zoltan Rado

The Thomas D. Larson
Pennsylvania Transportation Institute

PENNSTATE
1 8 5 5

COMMONWEALTH OF PENNSYLVANIA
DEPARTMENT OF TRANSPORTATION

DEPARTMENT OF TRANSPORTATION UNITED STATES OF AMERICA

Contract No. 510401
Work Order No. 015

Technical Report Documentation Page

1. Report No. FHWA-PA-2009-022-510401-015	**2. Government Accession No.**	**3. Recipient's Catalog No.**
4. Title and Subtitle Evaluating Performance of Limestone Prone to Polishing		**5. Report Date** December 31, 2009 **6. Performing Organization Code**
7. Author(s) Dr. Zoltan Rado, Ph.D.		**8. Performing Organization Report No.** LTI 2010-07 / MAUTC PSU-2007-02
9. Performing Organization Name and Address The Thomas D. Larson Pennsylvania Transportation Institute The Pennsylvania State University 201 Transportation Research Building University Park, PA 16802-4710		**10. Work Unit No. (TRAIS)** **11. Contract or Grant No.** 510401, Work Order 15
12. Sponsoring Agency Name and Address The Pennsylvania Department of Transportation Bureau of Planning and Research Commonwealth Keystone Building 400 North Street, 6th Floor Harrisburg, PA 17120-0064 The Mid-Atlantic Universities Transportation Center 201 Transportation Research Building University Park, PA 16802-4710		**13. Type of Report and Period Covered** Final Report 2/22/2008 – 12/31/2009 **14. Sponsoring Agency Code**
15. Supplementary Notes COTR: Patricia Miller, 717-787-2489		

16. Abstract

This research project evaluated the effect of blending Vanport limestone and other aggregates on the frictional surface characteristic properties of constructed trial road surfaces. The study undertook the evaluation of the performance of different mortar fractions and aggregate concentrations to determine the effect of coarse aggregate usage in the top mortar layer on pavement friction performance, as well as the effect of the substitution of different aggregates in place of Vanport limestone. The project developed a test matrix to evaluate the effect of the changes in these factors on portland cement concrete using state-of-the-art laboratory test equipment for assessing surface characteristics and using accelerated wearing for the evaluation of long-term pavement surface performance.

17. Key Words Limestone, aggregate friction, skid resistance, texture, polishing, mix design, PCC, pavement characteristics, safety	**18. Distribution Statement** No restrictions. This document is available from the National Technical Information Service, Springfield, VA 22161

19. Security Classif. (of this report)	**20. Security Classif. (of this page)**	**21. No. of Pages**	**22. Price**
Unclassified	Unclassified	196	

Form DOT F 1700.7 **(8-72)** **Reproduction of completed page authorized**

ACKNOWLEDGEMENTS

The author would like to acknowledge the Pennsylvania Department of Transportation for sponsoring this research. In particular, the author thanks Ms. Patricia Miller from the Bureau of Construction and Materials and Mr. Neal Fannin from the Engineering District 2-0, for their support, guidance, and many technical insights offered over the course of the study. Ms. Lisa Karavage from the Division of Bureau of Planning and Research is acknowledged for her support and management of the project. Finally, the author would like to acknowledge Ms. Robin Tallon and Mr. Dan Fura from the Larson Institute at Penn State for assisting in acquiring much of the laboratory data used in the study. Mr. Choongwoo Cho from the Larson Institute at Penn State is acknowledged for his contribution running the MMLS III accelerated wear cycle machine and using the various friction and texture measurement equipment for the data collection of the research project.

This work was sponsored by the Pennsylvania Department of Transportation and the U.S. Department of Transportation, Federal Highway Administration. The contents of this report reflect the views of the author, who is responsible for the facts and the accuracy of the data presented herein. The contents do not necessarily reflect the official views or policies of either the Federal Highway Administration, U.S. Department of Transportation, or the Commonwealth of Pennsylvania at the time of publication. This report does not constitute a standard, specification, or regulation.

TABLE OF CONTENTS

LIST OF FIGURES

LIST OF TABLES

CHAPTER 1 **INTRODUCTION**

1.1 Research Objectives and Scope

Road surfaces develop gradually deteriorating surface characteristics such as macro- and micro-texture, friction or skid resistance, among many others. The speed and form of the deterioration is a function of many parameters, including the road design, construction techniques, mix and aggregate types used, age, traffic magnitude and composition, weather, and many others. On road geometries and areas where vehicle maneuvers require the utilization of friction, traffic safety is strongly dependent on available surface friction. It was discovered that in Pennsylvania several roads manufactured according to standard design and construction techniques and paved with portland cement concrete have shown unwarranted rapid friction (skid resistance) deterioration well before the expected time limits and reached dangerously low levels of frictional characteristics. Based on preliminary studies it was assumed that these surfaces were constructed using Vanport limestone coarse aggregates. A task force committee was formed to investigate the surface performance degradation and to recommend possible solutions for research. Based on the committee's investigation and recommendation, the following research objectives were developed.

The objectives of this project were to:

- Using the outcome of the "Vanport Limestone Committee" (VLC), develop a research methodology to investigate the three priority recommendations of the VLC report for the solution of the problem:
- Evaluation of the effect of blending Vanport limestone with different other aggregates.
- Evaluation of the performance of different mortar fraction and aggregate concentrations.
- Determination of the effect of coarse aggregate usage in top mortar layer on pavement friction performance.
- Develop a test matrix to evaluate the effect of blending different aggregate materials in portland cement concrete using state-of-the-art laboratory test equipment for assessing surface characteristics and using accelerated wear testing for the evaluation of long-term pavement surface performance.
- Develop a test matrix to evaluate the effects of different mortar fraction and aggregate concentrations in Portland cement concrete using state-of-the-art laboratory test equipment for assessing surface characteristics and using accelerated wear testing for the evaluation of long-term pavement surface performance.

- Develop a test matrix to evaluate the effect of aggregate size in portland cement concrete using state-of-the-art laboratory test equipment for assessing surface characteristics and using accelerated wear testing for the evaluation of long-term pavement surface performance.

CHAPTER 2 **BACKGROUND AND LITERATURE REVIEW**

In this chapter the essential and relevant information from the research project Phase I results are presented. Phase I of the project conducted a thorough literature review with particular interest in the accelerated wearing, measurement and analysis techniques for evaluating the performance of pavement surfaces in relation to polishing and skid resistance characteristics. The work produced a comprehensive report on relevant literature in these areas.

In the following sections only the relevant and essential information from this report is presented to support the design and development of the methodology and testing of the experiment. For more information and for the full report please refer to APPENDIX C.

2.1 Background

The nature and severity of skidding accidents on wet pavements has been linked directly to the properties and chemical composition of aggregates and cement mortar layers in portland cement concrete (PCC) pavements. The characteristics of the selected materials, the type, size, and mixture of aggregates and the volumetric mixture and layering of larger aggregate and fine aggregate with high mortar content represents a critical safety issue for highway agencies. The characteristics of aggregates, depending on pavement construction technology, account for a substantial portion of essential friction and texture of PCC pavements and consequently play a major role in determining pavement safety related to skidding accidents. The frictional characteristics of wet and otherwise contaminated PCC surfaces depend to a very large extent on the micro-textural parameters and the polishing hardness of the used aggregates that are exposed on the pavement surface to the elements and to traffic. As vehicle speeds increase, the relative importance of the surface macro-texture of the pavement plays an ever-increasing role, not only to prevent hydroplaning, but also providing a means for precipitation contaminants like water or slush or wet snow to clear from the protruding aggregate tips into the macro-textural valleys thereby providing adequate tire-surface interaction interface for better friction. The two surface characteristic properties, the micro- and macro-textural features of the aggregates used in the PCC pavements, together provide the foundation of the frictional process to provide adequate friction over a wide speed range and in wet and contaminated surface conditions.

For PCC pavements the construction technology employed, specifically the finishing and texturing equipment utilized, provides the relatively short-lived initial texture features of the newly constructed pavement. Depending on traffic and climatic conditions the top layer mortar and cement paste micro- and macro-textural features wear and in a relatively short period of time the associated low- and high-speed frictional characteristics of the pavements deteriorate. In the specific case when the top mortar layer is constructed for the cover of coarse aggregates depending on traffic and climatic conditions, the wear course can deteriorate rapidly compared to the expected lifetime of the pavement and expose aggregates on the top of the surface. The fine aggregate exposed controls micro-texture frictional characteristics while the larger protruding aggregates will provide the macro-textural features that control high-speed and deep-precipitation frictional characteristics. While it is expected and indeed a correct assumption that the micro-textural features of the coarse aggregates will provide low-speed friction initially, depending on the aggregate properties, climate, and traffic conditions these micro-textural features can be polished in a relatively short amount of time, quite rapidly reducing the contribution of the coarse aggregates to the surface characteristics. In cold climates where studded tires, chains, and abrasives are common, the process of top layer surface wear is accelerated with additional effects on both micro- and macro-textural polishing.

A number of state agencies regulate the use of softer, usually manufactured fine aggregates from more polishing limestones in PCC surface layers. Some states and agencies allow the use of these aggregates but they require a blend with harder silica minerals. Most of the state agencies require the use of the ASTM D 3042 (ASTM, 2003) acid test to ensure that surface aggregates are not essentially all carbonate minerals like the limestone or dolomite that dissolve quickly in acidic environments. The exposed aggregates from these minerals wear and polish more rapidly under traffic especially in colder climates with heavier winter conditions. The rapid polishing of the pavement surface under traffic can be mitigated if the acid-insoluble residue represents a significant percentage of harder, plus No. 200 size, sandy mineral particles in the aggregate.

Proper selection of the aggregates and the construction technologies applied in the surface layers of PCC pavements can help provide adequate friction levels in wet and winter weathers for a prolonged period of time even under heavy traffic conditions. Hard minerals with Mohs hardness of 6 or greater withstand polishing for a longer period of time while maintaining better micro-textural features. Also, aggregates with good micro-texture, such as sandstone, or those having rough grains or a mix of minerals with different textures, will resist polishing and maintain good wet-weather frictional properties for a prolonged time. When easily polishing limestones or polished gravels are to be used in pavement surfaces, it is anticipated that frictional properties can be improved in the short and long term by blending in aggregates with hard minerals and desirable textures.

2.2 Pavement Surface Texture

2.2.1 Definition

Pavement surface texture is made up of the deviations of the pavement surface from a true planar surface. These deviations occur at three distinct levels of scale, each defined by the wavelength (λ) and peak-to-peak amplitude (A) of its components. Although there is a wide range of pavement surface texture ranging from micro-texture to unevenness, the range that influences pavement surface friction encompasses micro-texture and macro-texture.

Micro-texture and macro-texture were defined in 1987 by the Permanent International Association of Road Congresses (PIARC), as follows: (PIARC, 1987)

- Micro-texture (λ < 0.02 in [0.5 mm], A = 0.04 to 20 mils [1 to 500 μm])—Surface roughness quality at the sub-visible or microscopic level. It is a function of the surface properties of the aggregate particles contained in the asphalt or concrete paving material.
- Macro-texture (λ = 0.02 to 2 in [0.5 to 50 mm], A = 0.005 to 0.8 in [0.1 to 20 mm])—Surface roughness quality defined by the mixture properties (shape, size, and gradation of aggregate) of an asphalt paving material and the method of finishing/texturing (dragging, tining, grooving; depth, width, spacing and orientation of channels/grooves) used on a concrete paving material.

PIARC also defined mega-texture and unevenness as:

- Mega-texture (λ = 2 to 20 in [50 to 500 mm], A = 0.005 to 2 in [0.1 to 50 mm])—This type of texture is the texture which has wavelengths in the same order of size as the pavement–tire interface. It is largely defined by the distress, defects, or "waviness" on the pavement surface.
- Wavelengths longer than the upper limit (20 in [500 mm]) of mega-texture are defined as roughness or unevenness (Henry, 2000).

Figure 1 graphically illustrates the four texture ranges.

It is widely recognized that pavement surface texture influences many different pavement–tire interactions. Figure 2 shows the ranges of texture wavelengths affecting various vehicle–road interactions, including wet-weather friction, interior and exterior noise, splash and spray, rolling resistance, and tire wear. As can be seen, wet-weather friction is primarily affected by micro-texture and macro-texture, which correspond to the adhesion and hysteresis friction components, respectively.

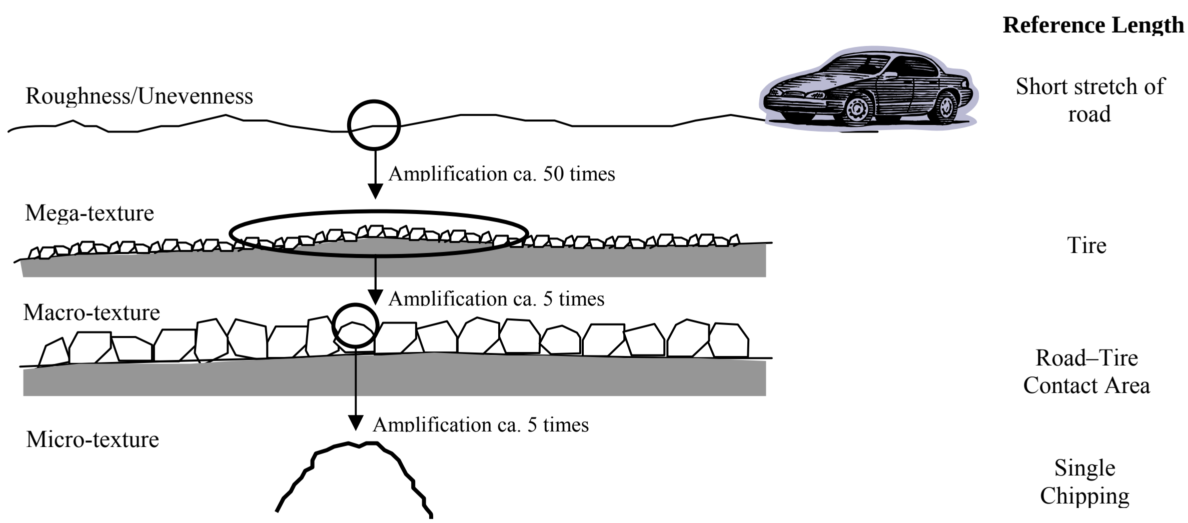

Figure 1. Simplified illustration of the various texture ranges that exist for a given pavement surface (Sandburg, 1998).

2.2.2 Factors Affecting Texture

There are many factors that affect pavement surface texture. These factors relate to the aggregate, binder, and mix properties of the pavement surface material and any intentional texturing done to the material after placement. A summary of the factors that influence pavement surface texture obtained from published literature is shown in Table 1. These factors can be optimized to obtain pavement surface characteristics required for a given design situation.

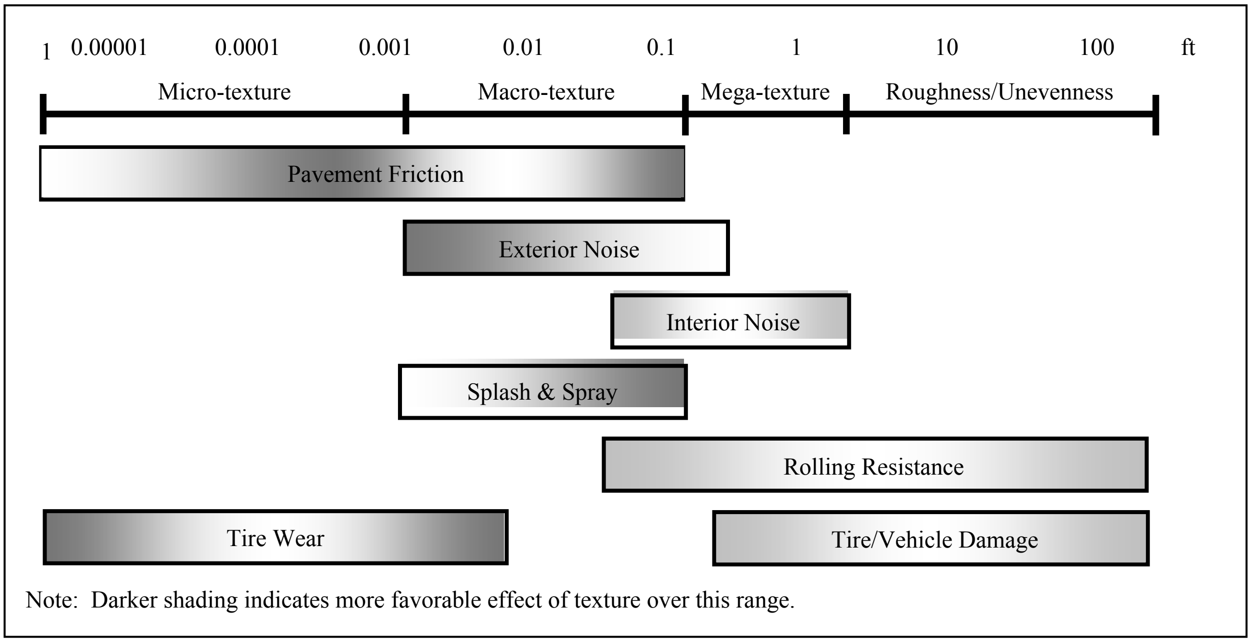

Figure 2. Texture wavelength influence on pavement–tire interactions (Henry, 2000; Sandburg and Ejsmont, 2002).

Table 1. Suggestions for optimizing pavement texture for friction and noise (Sandberg and Ejsmont, 2002; Henry, 2000; Rado 1994; Wambold et al., 1995; AASHTO, 1976).

Surface Type	Factor	Micro-Texture	Macro-Texture
Asphalt (includes chip seal)	Max. aggregate dimensions		X
	Coarse aggregate types	X (surface roughness)	X
	Fine aggregate types		X
	Mix gradation		X
	Mix air content		X
	Mix binder		X
Concrete	Coarse aggregate type	X (for exposed aggregate PCC)	X (for exposed aggregate PCC)
	Fine aggregate type	X	
	Mix gradation		X (for exposed

			aggregate PCC)
	Texture dimensions and spacing		X
	Texturing orientation		X
	Texture skew		X

2.3 Pavement Friction

2.3.1 Definition

Pavement friction has been described as the force that resists the relative motion between a vehicle tire and a pavement surface. This resistive force (illustrated in Figure 3) is generated as the tire rolls or slides over the pavement surface.

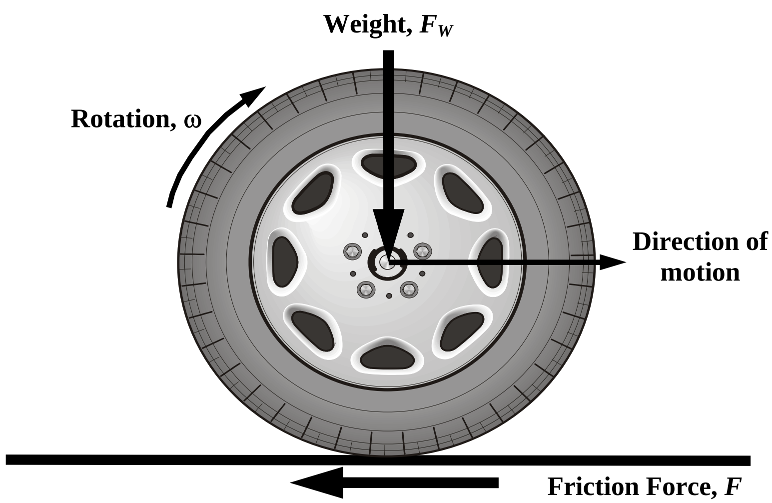

Figure 3. Simplified diagram of forces acting on a rotating wheel.

The resistive force (characterized using the non-dimensional friction coefficient, μ) is the ratio of the tangential friction force (F) between the tire tread rubber and the horizontal traveled surface to the perpendicular force or vertical load (F_W) and is computed using equation 1.

$$\mu = \frac{F}{Fw} \tag{1}$$

Pavement friction plays a vital role in keeping vehicles on the road, as it gives drivers the ability to control/maneuver their vehicles in a safe manner in both the longitudinal and lateral directions. It is a key input to highway geometric design, as it is used in determining if the minimum stopping sight distance, minimum horizontal radius, minimum radius of crest vertical curves, and maximum superelevation in horizontal curves provided in a given highway design are adequate. Generally speaking, the higher the friction available at the pavement-tire interface, the more control the driver has over the vehicle, whereas the lower the friction, the less control.

2.3.2 Friction Mechanisms

Pavement friction is the result of a complex interplay between two principal frictional force components—adhesion and hysteresis (see Figure 4). Adhesion is the friction that results from the small-scale bonding/interlocking of the vehicle tire rubber and the pavement surface as they come into contact with each other. It is a function of the interface shear strength and contact area. The hysteresis component of frictional forces results from the energy loss due to bulk deformation of the vehicle tire. When a tire compresses against the pavement surface, deformation energy is stored within the rubber. As the tire relaxes, part of the stored energy is recovered, while the other part is lost in the form of heat (hysteresis), which is irreversible.

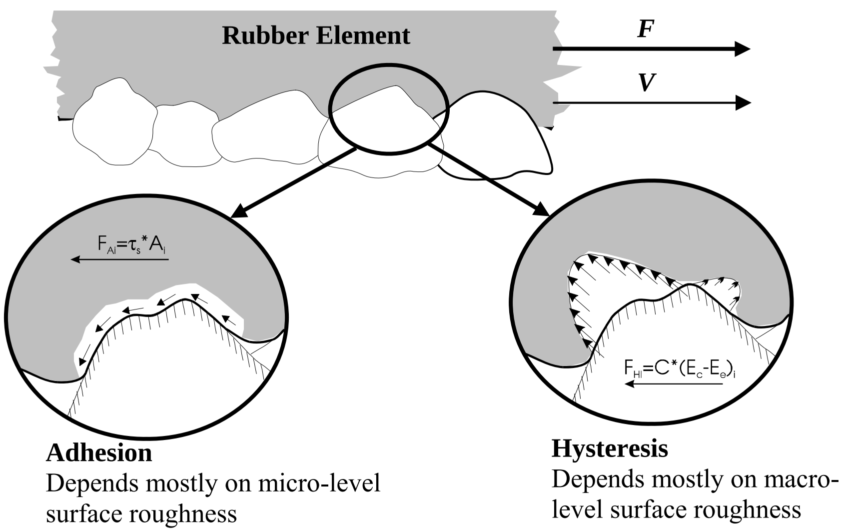

Figure 4. Mechanisms of pavement–tire friction.

Although there are other components of pavement friction (e.g., tire rubber shear), they are insignificant when compared to the adhesion and hysteresis force components. Thus, friction can be viewed as the sum of the adhesion and hysteresis frictional forces.

$$F = F_A + F_H \tag{2}$$

Both components depend to a large extent on pavement surface characteristics, the contact between tire and pavement, and the properties of the tire. Also, because tire rubber is a visco-elastic material, each component is affected by temperature and sliding speed.

Because adhesion force is developed at the pavement–tire interface, it is most responsive to the micro-level asperities (micro-texture) of the aggregate particles contained in the pavement surface. In contrast, the hysteresis force developed within the tire is most responsive to the macro-level asperities (macro-texture) formed in the surface via mix design and/or construction techniques. As a result of this phenomenon, adhesion governs the overall friction on smooth-textured and dry pavements, while hysteresis is the dominant component on wet and rough-textured pavements.

2.3.3 Braking Friction of Vehicles on Paved Surfaces

Vehicle braking frictional forces are the forces that occur between a rolling pneumatic tire (in the longitudinal direction) and the road surface when operating in the free rolling or constant-braked mode. In the free-rolling mode (no braking), the relative speed between the tire circumference and the pavement—referred to as the slip speed—is zero. In the constant-braked mode, the slip speed increases from zero to a potential maximum of the speed of the vehicle. The following mathematical relationship explains slip speed:

$$S = V - V_P = V - (0.68 \cdot \omega \cdot r) \tag{3}$$

where: S = Slip speed, mi/hr

V = Vehicle speed, mi/hr

V_P = Average peripheral speed of the tire, mi/hr

ω = Angular velocity of the tire, radians/sec

r = Average radius of the tire, ft

Again, during the free-rolling state of the tire, V_P is equal to the vehicle speed and thus S is zero. For a locked or fully-braked wheel, V_P is zero, so the sliding speed or slip speed is equal to the vehicle speed (V). A locked-wheel state is often referred to as a 100 percent slip ratio and the free-rolling state is a zero percent slip ratio. The following mathematical relationships give the calculation formula for slip ratio:

$$SR = \frac{V - V_P}{V} \cdot 100 = \frac{S}{V} \cdot 100 \tag{4}$$

where: SR = Slip ratio, percent

V = Vehicle speed, mi/hr

V_P = Average peripheral speed of the tire, mi/hr

S = Slip speed, mi/hr

Similarly to the previous explanation, during the free-rolling state of the tire, V_P is equal to the vehicle speed and S is zero, thus the slip ratio (SR) is zero percent. For a locked wheel, V_P is zero, S equals the vehicle speed (V), and so the slip ratio (SR) is 100 percent.

Figure 5 shows the ground forces acting on a tire under the free-rolling operation mode. In this mode, the ground force is at the center of pressure of the tire contact area and is off center by the amount a. This offset causes a moment that must be overcome to rotate the tire. The force required to counter this moment is called the rolling resistance force (F_R). The value a is a function of speed and increases with speed. Thus, F_R increases with speed.

In the constant-braked mode (Figure 6), an additional force called the braking slip force (F_B) is required to counter the added moment (M_B) created by braking. The force is proportional to the level of braking and the resulting slip ratio. The total frictional force is the sum of the free-rolling resistance force (F_R) and the braking slip force (F_B).

The coefficient of friction between a tire and the pavement changes with varying slip, as shown in figure 6 (Kulakowski et al., 1990). The coefficient of friction increases rapidly with increasing slip to a peak value that usually occurs between 10 and 20 percent slip (critical slip) (see Figure 7). The friction then decreases to a value known as the coefficient of sliding friction, which occurs at 100 percent slip. The difference between the peak and sliding coefficients of friction may equal up to 50 percent of the sliding value, and is much greater on wet pavements than on dry pavements. The relationship shown in figure 6 is the basis for anti-locking brake systems (ABS), the concept being to take advantage of the front side of peak friction and minimize the loss of side/steering friction due to sliding action.

Free Body diagram, steady state

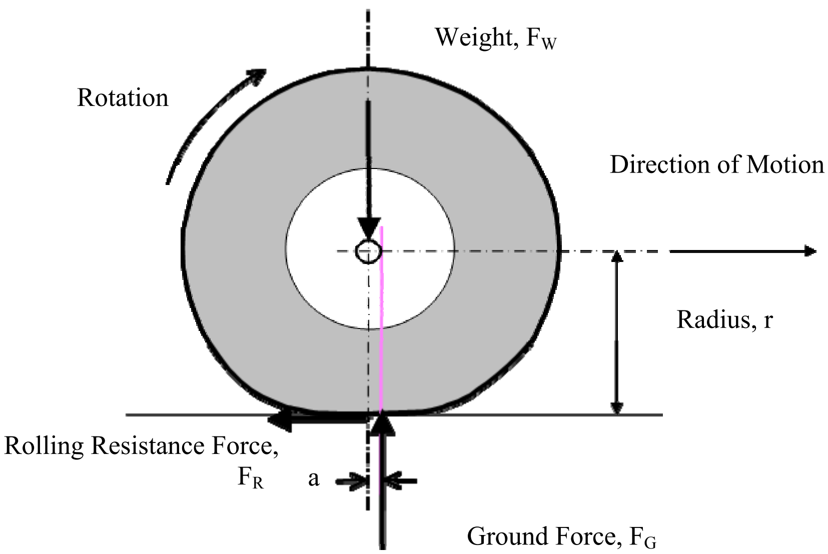

Figure 5. Rolling resistance force with a free-rolling tire at a constant speed on a bare, dry paved surface (Andresen and Wambold, 1999).

Free body diagram, steady state

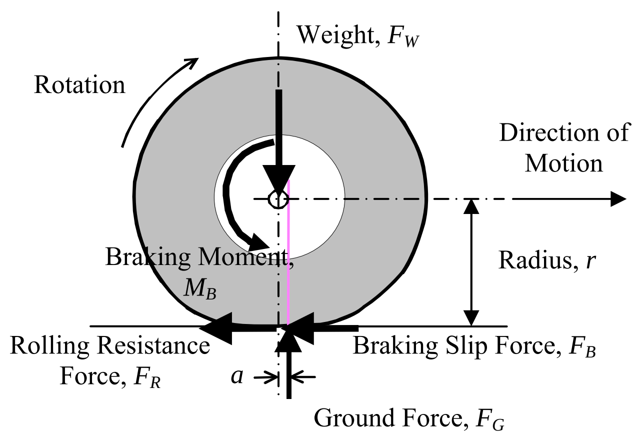

Figure 6. Forces and moments of a constant-braked wheel on a bare, dry paved surface (Andresen and Wambold, 1999).

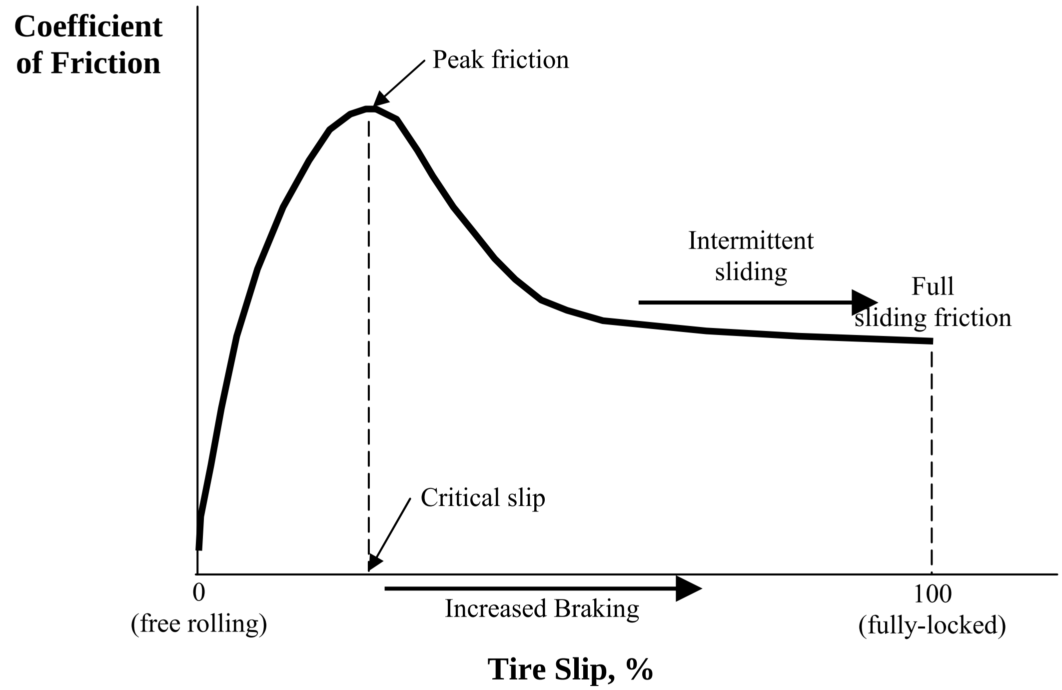

Figure 7. Pavement friction versus tire slip.

2.3.4 Relevant Factors Affecting Pavement Friction

The factors that influence pavement friction forces can be grouped into four categories—pavement surface characteristics, vehicle operational parameters, tire properties, and environmental factors. Table 2 lists the various factors comprising each category. Because each factor in this table plays a role in defining pavement friction, friction must be viewed as a process instead of an inherent property of the pavement alone. It is only when all these factors are fully specified that friction takes on a definite value. The more critical factors are highlighted in Table 2 (shown in bold) and discussed below.

Table 2. Factors affecting available pavement friction (modified from Wallman and Astrom, 2001).

Pavement Surface Characteristics	Vehicle Operating Parameters	Tire Properties	Environment
• **Micro-texture** • **Macro-texture** • Mega-texture/	• **Slip speed** ➢ vehicle speed ➢ braking action	• Width • **Tread design and condition**	• Climate ➢ Wind ➢ **Temperature**

unevenness • **Material properties** • Temperature	• Driving maneuver ➢ turning ➢ overtaking	• Rubber composition and hardness • **Inflation pressure** • Load • Temperature	➢ **Water** ▪ rainfall ▪ condensation ➢ **Snow and Ice** • **Contaminants** ➢ Anti-skid material (salt, sand) ➢ Dirt, mud, debris

Micro-texture and macro-texture are the two levels of pavement texture that affect pavement-tire friction (Henry, 2000). Micro-texture is mostly responsible for pavement friction at low speeds where there is sufficient contact between the tire and pavement surface to ensure that all friction available at the pavement tire interface is utilized. At higher speeds, however, available friction may be diminished or lost because of a reduction of the tire-pavement contact area due to phenomena such as hydroplaning. Pavement macro-texture is predominantly responsible for reducing potential separation of the tire and pavement surface due to hydroplaning and to induced friction caused by hysteresis for vehicles traveling at high speeds. Thus, micro-texture is the single most important factor at both low and high speeds in providing adequate friction at the tire-pavement interface (Papagouli and Kokkalis, 1998). Thus, micro-texture is the single most important factor at low speeds, providing a strong adhesional friction component, while at high speeds it can play a vital role provided adequate macro-texture presents sufficient contact area (Papagouli and Kokkalis, 1998). The influence of macro-texture in providing friction increases with speed, first at moderate speeds by supplying contact area for adhesion friction to develop, and for increasing speeds by providing hysteresis that becomes dominant at high speed. The difference between micro-texture and macro-texture is presented in Figure 8.

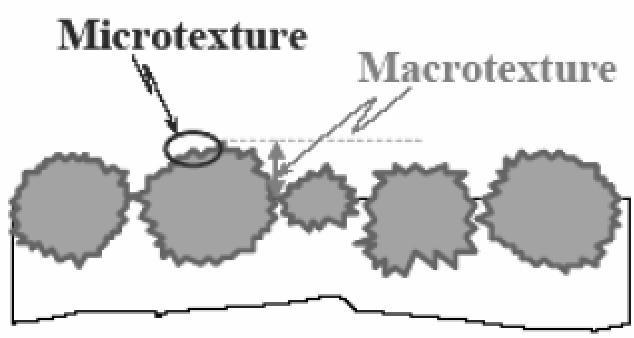

Figure 8. Micro-texture versus macro-texture (Flintsch et al., 2003).

Figure 9 shows the relative influences of micro-texture, macro-texture, and speed on wet pavement friction. As can be seen, micro-texture influences the magnitude of tire friction, while macro-texture impacts the friction–speed gradient. At low speeds, micro-texture dominates the wet friction level. At higher speeds, the presence of high macro-texture facilitates the drainage of water so that the adhesive component of friction afforded by micro-texture is re-established.

Hysteresis increases with speed exponentially, and at speeds above 65 mi/hr (105 km/hr) could account for over 95 percent of the friction.

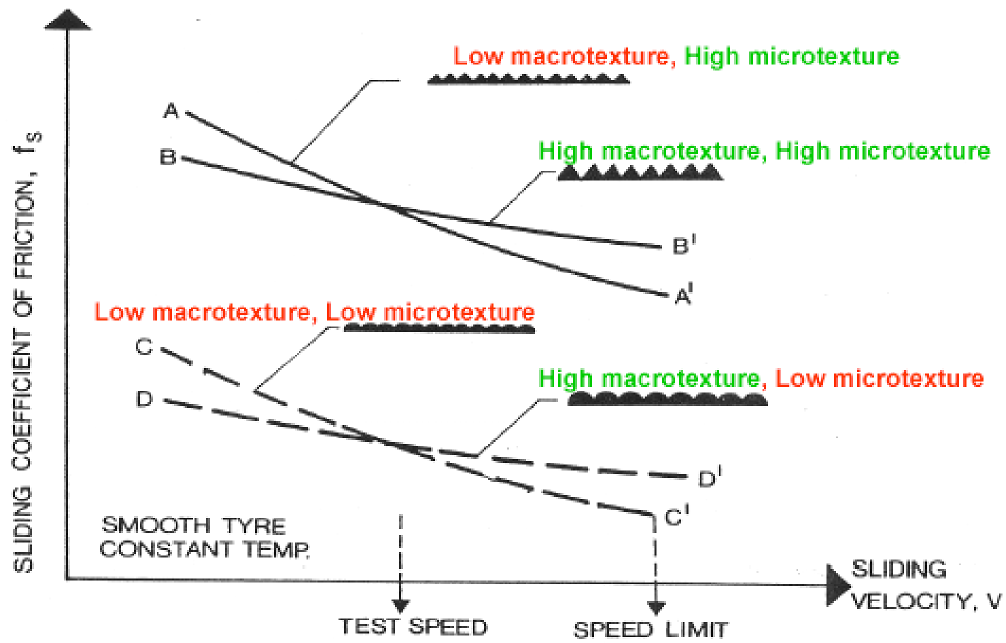

Figure 9. Effect of micro-texture and macro-texture on pavement–tire wet friction at different sliding speeds (Flintsch et al., 2002).

2.4 Recommended Measurements Methods and Indices

The two common devices used for the measurement of pavement friction characteristics in the laboratory or at low speeds in the field are the British Pendulum Tester (BPT) and the Dynamic Friction Tester (DFT). Both of these devices measure frictional properties by determining the loss in kinetic energy of a sliding pendulum or rotating disc when in contact with the pavement surface. The loss of kinetic energy is converted to a frictional force and thus pavement friction. The DFT has the added advantage of being able to measure the speed dependency of the pavement friction by measuring friction at various speeds (Saito et al., 1996). These two methods offer the advantage of being highly portable and easy to handle.

The DFT device is rapidly becoming the equipment of choice in research and harmonization projects to establish the basic frictional characteristics numbers of measured surfaces according to a number of established international standards.

For surfaces with low (minimal) macro-textural features, the measurements from the British Pendulum device are generally regarded as values representing the micro-textural features of the pavement. At the same time the variable speed data from the Dynamic Friction Tester used in the establishment of the International Friction Index incorporates both the measurement of macro- and micro-texture in the form of the calculated Mean Profile Depth and the low speed friction number. The use of the two devices enables the measurement and analysis of the frictional properties of pavement surfaces, taking both the micro- and macro-textural features of the pavement into account.

2.4.1 The British Pendulum Tester

The British Pendulum Test produces sliding contact between a rubber slider mounted on the swing arm of a pendulum tester and the test surface. It is a low-speed test in which the frictional resistance of the test material to the sliding of a standard rubber slider is measured. The rubber slider, while pressed against the surface by a spring during a swing produces frictional forces that slow down the swing of the arm, thus causing the upswing of the pendulum to be shortened due to the friction produced.

The apparatus (see Figure 10) consists of a tripod base where the swing arm of the pendulum is attached with bearings to the top section. The system is equipped with a quick-release mechanism and a fixed scale. The moving pendulum arm pushes in front of it a needle indicating the reached maximum upswing of the arm on the fixed scale.

Measurement procedure

The British Pendulum Tester is a hand-operated device where the data are also recorded by hand. The procedure begins with the leveling of the equipment above the test specimen, or the test surface is placed horizontally at the base of the tester, and the pivot point of the pendulum is adjusted so that the sliding distance of the rubber slider on the test surface will cover a pre-selected length. Sufficient water is applied at the tested portion of the surface. The test begins with the pendulum arm being held horizontally before it is allowed to freefall under its own weight by the quick-release mechanism. After the sliding contact, the pendulum arm will continue to swing until its velocity reaches zero. The needle indicates the maximum elevation of the upswing. The reading is recorded by hand. Usually five readings are averaged to calculate one measurement of the BP Tester.

Figure 10. British Pendulum Tester

Measurement Indices

The elevation at which the pendulum comes to a complete stop is calibrated to give a reading in BPN. BPN is a measure of the interface friction between the slider rubber and the test surface, and has been used as an indicator of the level of friction provided by the test material.

Advantages and disadvantages

The British Pendulum Test, as described in ASTM E 303, is probably the most widely used method in use today for laboratory and on-site spot measurements of pavement surface friction. The test result, reported as the British Pendulum Number (BPN), is often taken as a useful indirect measure of the micro-texture of the test material. Another important application of the British Pendulum Test is to measure the change in BPN of a paving material after it is subjected to wheel polishing treatment, as described in ASTM D 3319 and ASTM 2001a. One documented disadvantage of this testing method is that one must be careful when using this device as they are not generally reproducible and are subjected to operator and wind errors. It is a spot measurement technique applicable for laboratory and onsite research measurements.

With the exception of the British Pendulum Tester (which is an indicator of pavement micro-texture), the commonly applied texture measurement methods provide pavement surface macro-texture information. Modern methods used to characterize pavement surface texture are typically based on non-contact surface profiling techniques. An example of a non-contact profiler developed using both laboratory and a field study for characterizing pavement surface texture is the Circular Track Texture Meter (CTM). The CTM is a complementary device to the DFT, allowing the direct measurement of macro-texture profile and thus the calculation of all texture measures (such as the MPD or MTD) on the same physical surface as the DFT measurement took place.

2.4.2 Dynamic Friction Tester

The Dynamic Friction Tester uses the principle of measuring the necessary torque to turn three small rubber pads in a circular path on the measured surface at different speeds. The DFT consists of a horizontal spinning disk fitted with three spring-loaded rubber sliders that contact the paved surface as the disk rotational speed decreases due to the friction generated between the sliders and the paved surface. A water supply unit delivers water to the paved surface being tested. The torque generated by the slider forces measured during the spin down is then used to calculate the friction as a function of speed. The speed range is generally from 55 mi/hr (90 km/hr) down to 3 mi/hr (5 km/hr). The device uses an electric motor to spin the measuring disc to the desired speed and an electromagnetic device to lower the spinning disk to the ground at the highest revolutionary speed. The device is equipped with a rotational speed measurement device together with a rotational torque and a downward load measurement sensor. The DFT device is illustrated in Figure 11.

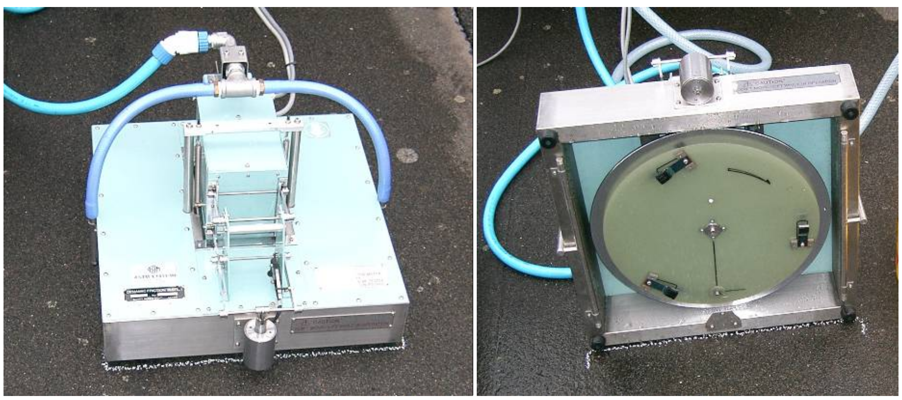

Figure 11. The Dynamic Friction Tester

Measurement Procedure

The device is usually carried in the trunk or back seat of a car together with the water tanks and a laptop computer. The device is manually placed on the pavement surface where the test is to take place. A laptop computer is used to control the test and record the data. Once the test initiated first the electronic motor accelerates the disk to the standard spinning speed where the equivalent tangential speed of the rubber pads is 55 mi/hr (90 km/hr). The electromagnetic release mechanism then drops the spinning disk to the ground and automatic data acquisition begins. The system finishes the data collection when the disk comes to a complete stop. The raw data are then filtered and the coefficient of friction is calculated from the measured and filtered torque and loading forces.

Measurement Indices

The DFT friction data are presented as a graph, plot of friction coefficient as a function of slip speed. The device also reports the peak friction and the slip speed at which the peak friction occurs. The device is calibrated and reports the International Friction Index (IFI) that consists of the friction number measured at 45 mph (72 km/h) designated by *FN60* and the *Sp* number that is the indication of the loss friction when speed increases.

Advantages and disadvantages

The DFT device produces measurements that are very repeatable and its results are reproducible. It is used as the standard device to calibrate friction devices to IFI. The DFT is relatively small and easy to transport. Disadvantages of the device are that it cannot be used for network-level monitoring or project measurements. It is a very promising device for laboratory and research use as well as for calibration purposes.

2.4.3 Circular Texture Meter

The Circular Texture Meter is designed to measure surface texture on the same circumference as the Dynamic Friction Tester. The charge-coupled device (CCD) laser displacement sensor used by this equipment is mounted on an arm that rotates at approximately 3 in (76 mm) above the road surface. The arm that holds the measurement sensor is rotated by an electric motor at a constant speed of 20 ft/min (6 m/min). The 5.625-in (142-mm) measurement radius yields a measurement length of 35.125 in (892 mm), which is sampled by the data acquisition system to collect 1,024 points in one rotation. The measurement results are recorded into a computer memory through an A/D converter. The stored data are then used by a computer program to report different surface texture indexes. The Circular Texture Meter is illustrated in Figure 12.

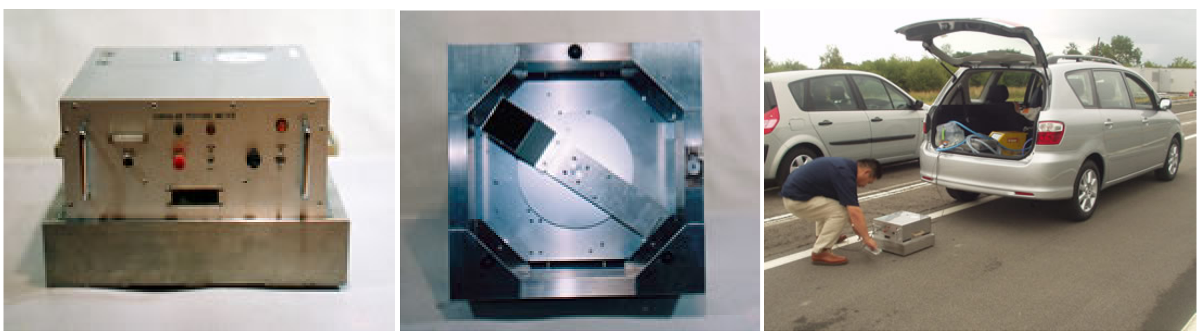

Figure 12. The circular texture Meter

Measurement Procedure

The measurement unit is hooked up to the 12V battery system of the vehicle in advance, before the measurement takes place. The power connection does not disturb the normal operation of the vehicle. The unit is placed on the ground above the desired test location. A laptop computer is used to check the calibration and control the test. After the initial information setup the operator triggers the data acquisition. The unit performs the test and the measured macro-texture profile is collected. After the test is done the profile is presented in graphical format and the calculated indices are displayed. The measurement can be repeated about 30 seconds after the previous was completed. The unit can be placed in the trunk of the car and driven to a new location.

Measurement Indices

The device reports the measured texture profile in graphical format. It also calculates the mean profile depth, the MPD index, and the root mean square of height, called the RMS index.

Advantages and disadvantages

Advantages of the unit include its small size (approx. 13 kg) and portability. It requires a relatively short time for setup (less than 1 min) and for measurement (approx. 45 seconds). The measurements are repeatable and reproducible, thus independent of operators. The unit can be operated using a standard automobile battery (12V DC, 24W).

2.4.4 The International Friction Index

The International Friction Index was proposed based on the PIARC International harmonization study conducted in 1992 by representatives from 16 countries covering each continent (PIARC, 1995). The experiment was conducted at 54 sites across the U.S. and Europe and included 51 different measurement systems. Various types of friction testing equipment were evaluated, including locked wheel, fixed slip, ABS, variable slip, side force, pendulum, and some new prototype devices. Surface texture was measured by means of the sand patch, laser profilometers (using the triangulation method), an optical system (using the light sectioning method), and outflow meters.

One of the main results of the PIARC experiment was the development of the IFI. The IFI standardized the practice of how the dependency of friction on the tire sliding speed is reported. As a measure of how strongly friction depends on the relative sliding speed of an automotive tire, the gradient of the friction values measured below and above 37 mi/hr (60 km/hr) is reported as the value of an exponential model for the IFI index. This gradient is named the Speed Number (S_P) and is reported in the range 0.6 to 310 mi/hr (1 to 500 km/hr).

The PIARC experiment strongly confirmed other research indicating that S_P is a measure of the macro-texture influence of the surfaces on friction. Macro-texture is in focus as a major contributor to friction safety characteristics for several reasons. The most well-known reason is the hydraulic drainage capability that macro-texture has for wet pavements during or immediately after a rainfall. This capability will also minimize the risk for hydroplaning. Another reason is that the wear or polishing of macro-texture can be interpreted from S_P as it changes value over time for a section of road.

A pronounced peak shape or a steep negative slope of the friction–slip speed curve is considered dangerous. The normal driver will experience an unexpected loss in braking power when the brake pedal is pushed to its maximum and the braking power is not at its maximum. A smallest possible negative slope or even a flat shape of the friction–slip speed curve is therefore desired and obtained with proper macro-texture.

The IFI is composed of two numbers—FN60 and S_P—and the designation and reporting of this index is IFI(FN60,S_p). The IFI is based on a mathematical model of the friction process called the PIARC Friction Model. It models the friction coefficient as a function of slip speed and macro-texture as follows:

$$S_P = a + bTX \tag{5}$$

where:

S_P = speed number

a, b = coefficients dependent on the device used for measuring macrotexture

TX = macro-texture measurement

$$FR60 = FRSe^{\frac{S-60}{S_P}} \tag{6}$$

where:

FR60 = adjusted value of friction for a slip speed of 60 km/h

FRS = measured friction value at speed S

S = slip speed (km/h)

$$F60 = A + B \text{ x } FR60 + C \text{ x } TX \tag{7}$$

where:

A, B = coefficients dependent on friction measuring device

C = regression constant required for measurements using ribbed tire

TX = macro-texture measurement required for ribbed tire readings

It should be noted that equation 11 can be used to adjust measurements made at speeds other than the standard 40 mi/hr (65 km/hr) with an ASTM E274 trailer to calculate FN40 (see equation 13).

$$FN(s) = FN_V \cdot e^{-\frac{s-V}{S_p}} \tag{8}$$

For example, a measurement made at low speed, say 20 mi/hr (32 km/hr), or one made at a high speed of 60 mi/hr (96 km/hr), can be adjusted to *FN40* by setting *S* to 40 and *V* to the measuring speed (20 or 60 mi/hr [32 or 96 km/hr]). Note that if the unit mi/hr is used, then *Sp* must also be in mi/hr.

The use of IFI to estimate friction values at any speed is illustrated in Figure 13. As shown, IFI utilizes the two indices contained in the IFI model (*FN60* and S_P). Having measured S_P and the friction value *FN60* at 60 km/hr, the friction value at any other slip speed can be estimated by choosing a value for S. The friction curve is plotted according to equation 13 and the *FN60* and S_p number are indicated on the graph.

The S_P for the pavement surface may be measured by a device that measures macro-texture. S_P can also be obtained by running a minimum of two measurement runs of the surface with each run at a different slip speed at the same vehicle speed. Some friction measuring devices measure both friction force and macro-texture in the same measurement. IFI or the PIARC model describes friction experienced by a driver in emergency braking using non-ABS brakes and deals with the friction from wheel lockup to stop.

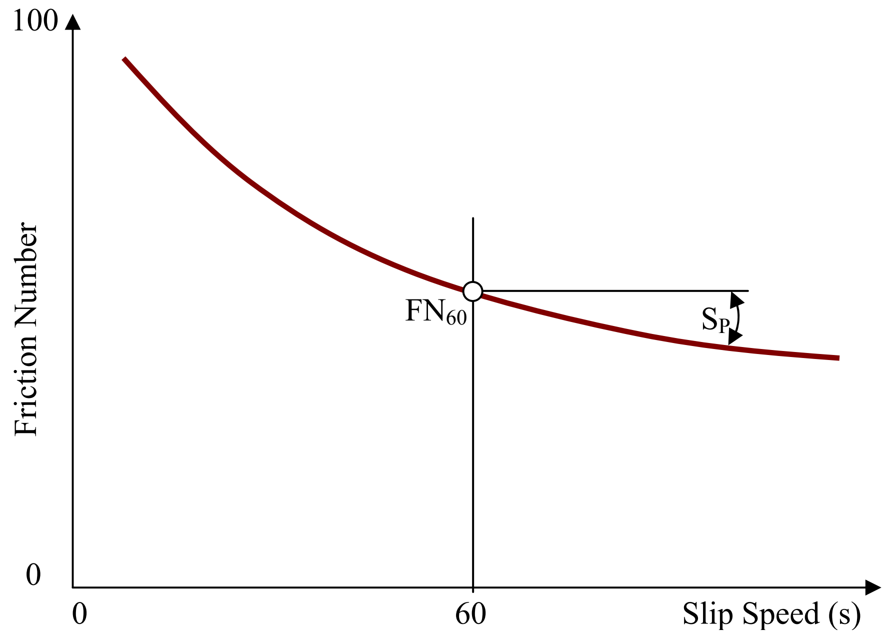

Figure 13. IFI and the PIARC Friction Model.

2.5 Accelerated Wear Testing

A review of the existing laboratory-scale accelerated polishing devices reveals that they can be categorized into three groups: one is capable of polishing the aggregate samples, a second is capable of polishing different sized manufactured PCC and asphalt surface samples, and the third is capable of polishing both (aggregate and pavement surface specimens). A brief review of the existing devices in each category follows.

Polishing Devices for Aggregates:

Within this category, there are three existing devices: British Polishing Wheel, Michigan Indoor Wear Track, and Micro-Deval device.

British Polishing Wheel

Most polishing machines used on aggregate specimens work on the principle of reducing the micro-texture of the aggregate. For example, the ASTM D3319 (ASTM, 1999) British Polishing Wheel method allows the curved specimens (aggregate coupons) clamped around the periphery of the wheel assembly to form a continuous strip of aggregate particles. The wheel is then rotated against a rubber-tire wheel that provides the polishing action. Silicon carbide grit No. 150, with a feeding rate of 6±2 g/min along with distilled water at a rate of 50-75 ml/min, is used to help accelerate the polishing. The aggregate specimens are formed by mounting uniformly sized coarse aggregate particles by hand in a curved mold and holding them in place with a bonding agent (polyester or epoxy resin). A catalyst could be used for faster curing of the resin. The companion British Pendulum Tester (BPT) specified in ASTM E303-93 (ASTM, 2005) is used to measure specimen friction values. The British polishing wheel is used for polishing microtexture of aggregate coupons only; however, it does not have the ability to alter macrotexture of aggregates or to test HMA specimens. In addition and as described above, the procedure used to prepare the aggregate coupons for the polishing test is tedious and time consuming.

Michigan Indoor Wear Track

Michigan Department of Transportation (MDOT) Indoor Wear Track device uses full-scale smooth tires to polish coarse aggregate specimens. After polishing, the specimens are subsequently tested by a laboratory version of the ASTM towed friction tester. According to Dewey et al. (2001), the circular wear track is very large, with a diameter of 7 ft. It accommodates 16 trapezoidal specimens. The individual specimens have parallel sides of 15.5 and 19.5 inches and non-parallel sides of 11 inches. Two wheels, with normal forces of 800 lb, pivot around the center. This device is used for polishing coarse aggregates only. It is by far the largest polishing device currently in use. As can be imagined, the sample preparation procedure is not only cumbersome but also time-consuming.

Micro-Deval Device

The Texas Transportation Institute (Luce et al., 2007) uses the Micro-Deval device as the mechanism to polish aggregates. Results have shown that the Micro-Deval test is an effective method for polishing aggregates within a short time (180 minutes). The Micro-Deval device can only polish aggregates and not HMA specimens.

Polishing Devices for HMA

Within this category there is currently one device that is the National Center for Asphalt Technology.

NCAT Polishing Machine

The National Center for Asphalt Technology (NCAT) laboratory-scale accelerated polishing device was designed to polish HMA surfaces. The NCAT (Voller and Hanson, 2006) device follows the same polishing principle as a Circular Track Polishing Machine. The NCAT machine can polish an area sufficiently large to accommodate the required measurements with the Dynamic Friction Tester and Circular Texture Meter to measure friction and texture, respectively. The NCAT polishing equipment uses three pneumatic tires made of resin or hard rubber, 8 inches in diameter, to polish an annulus that occupies a nominal 24-inch square slab. With rubber tires, water is used to wash the abraded rubber particles off the specimen surface during polishing. Dead weights are used to produce a total vertical force of 150 lb through the three wheels. Up to 100,000 revolutions at 40 rpm have been successfully applied to reach the terminal friction values of the HMA surface. NCAT uses a modified linear compactor to produce the slabs (24 inch square area) for polishing test. A somewhat prolonged test time, up to 41.7 hours, has been recorded by NCAT in order to reach the terminal friction values.

Polishing Devices for Aggregates and HMA:

Three devices exist within this category: NCSU Wear and Polishing Machine, Wehner/Schulze Polishing Machine, and Penn State Reciprocating Polishing Machine.

North Carolina State University Wear and Polishing Machine

Circular Track Polishing Machines represent yet another type of polishing concept. Some of these polishing machines can be used for polishing either aggregate specimens or HMA specimens. The North Carolina State University (NCSU) Wear and Polishing Machine, as specified in ASTM E660, utilizes four individually mounted, free-rolling wheel assemblies that pivot about a central shaft. The four wheels are loaded to 72 lb in vertical force. The tires are 11 inches in diameter and made of smooth nylon. Twelve specimens (aggregate or HMA mixes) are arranged around the perimeter of the track for polishing. The overall diameter of the track, to the center of the polishing wheels, is 36 inches. After 8 hours of polishing action, the surface friction of each specimen is measured using either the British Pendulum Tester (BPT) or the Variable Speed Friction Tester (VST). The test does not use slurry or water. Although the device is fairly large, it nevertheless polishes only a relatively small area of the specimen surface.

Wehner/Schulze Polishing Machine

The Wehner/Schulze polishing machine was developed in Germany 30 years ago (Do et al., 2007). It is comprised of two heads to facilitate polishing and friction measurement, respectively. Specimens are cores with a diameter of 8.9 inches. They can be taken from asphalt pavement or laboratory-prepared slabs (aggregate or asphalt specimens). The polishing action is achieved by means of three rubber cones mounted on a rotary disc, which rolls on the specimen surface. The rotation frequency is 500 rpm, giving a linear speed of 10.6 mph (17 km/h). The contact pressure between the cones and the specimen surface is 58.0 psi. The slip between the cone and the specimen surface is between 0.5% and 1%, which is roughly the slip between rolling tires and roads. A mix of water with quartz powder is sprayed on the specimen surface during the polishing action. The surface is polished on a ring that is roughly 6.3 inches in diameter and 2.4 inches in width. At each stop, water is sprayed on the specimen surface and 500 rotations are performed using the cones to wash all debris. This machine is not designed to handle typical specimen size compacted from the gyratory compactor.

Penn State Reciprocating Polishing Machine

The Penn State Reciprocating Polishing Machine (Nitta et al., 1990), ASTM E1393, represents a different style of polishing concept. It can be used in a laboratory or in the field to polish aggregates or HMA. In essence, a 3.5-by-3.5 inch rubber pad is oscillated back and forth on the specimen surface on which abrasive slurry is sprayed as well. Some of the critiques about this device include the relatively small polishing area (4.5 inch by 6.5 inch), the fact that the polishing action can only affect the aggregate macro-texture, and reciprocal movement.

2.6 Aggregates, Mix Design and Friction

Consideration of Aggregates

As pointed out in the previous section, texture plays a key role in the development of pavement–tire frictional forces and is primarily governed by the properties of the aggregate used in the pavement surface. While asphalt binder and cement paste can affect micro-texture—particularly just after a surface mix is placed—it is aggregate that makes up the bulk of asphalt and concrete mixtures, and thus serves as the primary contact medium with the vehicle tires.

Aggregate generally is viewed as two distinct fractions—coarse aggregate and fine aggregate. Coarse aggregate pieces are greater than the No. 4 sieve (0.19 in [4.75 mm]), with most pieces between 0.375 and 1.5 in (9.5 and 38 mm). Fine aggregate, on the other hand, is the collection of natural or crushed/manufactured particles less than 0.19 in (4.75 mm), but greater than the No. 200 sieve (0.003 in [75 µm]).

Aggregate testing and characterization must be targeted to the fraction(s) of aggregate in a mix that will control the frictional performance. In general, for asphalt mixtures, it is the coarse aggregate that controls, whereas for concrete mixes, it is the fine aggregate. Exceptions include fine-graded asphalt mixes, where fine aggregates are in greater abundance, and concrete mixes in which coarse aggregates are either intentionally exposed at the time of construction (exposed aggregate concrete) or will become exposed in the future (e.g., diamond grinding/grooving, surface abrading, porous concrete).

Research by Dahir and Henry (1978), Kandhal and Parker (1998), and Folliard and Smith (2003), among others, indicates that the following aggregate properties have a significant influence on pavement friction performance:

- Hardness
- Mineralogy (i.e., mineral composition and structure)
- Shape
- Texture
- Angularity
- Abrasion Resistance
- Polish Resistance
- Soundness

Aggregate hardness and mineralogy largely dictate the wear characteristics (i.e., durability, polish) of the aggregate. Aggregates that exhibit the highest levels of long-term friction are typically composed of hard, strongly bonded, interlocking mineral crystals (coarse grains) embedded in a matrix of softer minerals (Kulakowski, 1990). The differences in grain size and hardness provide a constantly renewed abrasive surface because of differential wear rates and the breaking off of the harder grains from the matrix of softer minerals.

Aggregates made up of hard minerals alone typically resist wear and other forms of degradation, yet may polish easily when subjected to traffic. Aggregates made up of moderately soft minerals alone resist polishing, but wear at very fast rates when subjected to traffic. Thus, while a wear-resistant aggregate is desired in the mixture, some wearing of the pavement surface must occur in order to ensure good levels of skid resistance (Davis, 2001).

As summarized in Table 3, aggregate angularity, shape, and texture are important parameters for defining both micro-texture and macro-texture. Fine aggregates that exhibit angular edges and cubical or irregular shapes generally provide higher levels of micro-texture, whereas those with rounded edges or elongated shapes generally produce lower micro-texture. For coarse aggregates, sharp and angular particles interlock and produce a deep macro-texture as compared to more rounded, smooth particles. Moreover, in asphalt mixes, platy (i.e., flat and elongated) aggregate particles tend to orient themselves horizontally, resulting in lower macro-texture depth.

Table 3. Effect of aggregate angularity, shape, and texture properties on pavement friction.

Aggregate Fraction	Aggregate Property	Effect of Aggregate Property on Pavement Friction	
		Asphalt Surface	Concrete Surface
Fine	Angularity and shape	No effect.	Defines pavement micro-texture, which highly impacts friction.
	Texture	No effect.	Little to no effect.
Coarse	Angularity and shape	Defines pavement macro-texture, which significantly impacts friction via hydroplaning potential.	If exposed, helps define pavement macro-texture, which impacts friction via hydroplaning potential.
	Texture	Defines pavement micro-texture, which highly impacts friction.	If exposed, helps define pavement micro-texture, which impacts friction.

The abrasion resistance of aggregates is an indicator of the aggregate resistance to mechanical degradation. The use of abrasion-resistant aggregates is important to avoid the breakdown of fine and/or coarse aggregates. During handling, stockpiling, mixing, and construction, the breakdown of fine and/or coarse aggregates can significantly alter the mix gradation, thereby affecting the porosity of open-graded friction course (OGFC) asphalt mixes and porous concrete mixes. For concrete mixes, it can result in the loss of strength due to the production of excess fines in the concrete mix. In asphalt mixes, the increase in fines can alter the volumetric properties and result in insufficient binder or may contribute to rutting and shoving. After construction, the breakdown of fine and/or coarse aggregates due to traffic shear forces can result in a loss of macro-texture.

Polish-resistant aggregates are those that are able to largely retain their harsh micro-texture under the grinding and shearing effects of repeated traffic loadings. For asphalt surface mixes, it is the hardness and mineralogy of the coarse aggregate particles that largely determine the degree of polishing that takes place. For concrete mixes, because the surface is composed primarily of mortar and is initially devoid of coarse aggregates, the polishing resistance of fine aggregates is the most critical parameter (Folliard and Smith, 2003). The coarse aggregate becomes an influencing factor only if it is made or becomes exposed.

Soundness refers to an aggregate's ability to resist degradation caused by climatic/ environmental effects (i.e., wetting and drying, freezing and thawing). Similar to abrasion resistance, sound and durable aggregate properties are important from the standpoint of avoiding the breakdown of fine and/or coarse aggregates, particularly when used in harsh climates.

Aggregate Types and Characteristics

Aggregates can be either natural or synthetic in nature. The most commonly used natural aggregates are those obtained by quarrying and crushing rocks, such as limestone, sandstone, and granite. Natural aggregates may also consist of stream and bank gravels that are obtained from dredging, washing, and screening, and are usually crushed to improve their angularity (Kulakowski et al., 1990).

Table 4. Natural aggregates used for different mix designs in the United States (Gransberg and James, 2005).

TYPE	PERCENTAGE USE IN UNITED STATES
Limestone	37
Quartzite	13
Granite	35
Trap Rock	13
Sandstone	10
Natural Gravels	58
Greywacke, Basalt	4

Synthetic aggregates are obtained by processing a wide variety of raw materials (natural or artificial). Sources of synthetic aggregates include such materials as blast-furnace slag, fly ash, and waste products from the glass, brick, tile, and other industries. The physical characteristics of different synthetic aggregates vary considerably depending on the source material and the manufacturing process. Because of these differences, the performance of these aggregates when used in pavement surfaces can vary widely (Kulakowski et al., 1990).

In general, synthetic aggregates are less susceptible to polishing than natural aggregates, but they tend to abrade more rapidly (Kulakowski et al., 1990).

Most limestones are very susceptible to polish. Aggregates derived from serpetinite, soapstone, siltstone, shale, and schists may also polish very rapidly (Kulakowski et al., 1990).

2.7 Conclusions

A number of major and very important conclusions can be drawn from the literature review that is pertinent to the design and execution of the present research project. These conclusions are centered on the subjects of:

(a) Surface characteristics for road safety and their measurements,

(b) The relationship of these characteristic measurements in a laboratory environment to the actual surface characteristics on roads,
(c) The issue of relevant accelerated wearing machine resembling traffic,
(d) Selection of aggregate types for the construction of the test samples and
(e) The construction of the test samples.

In the following paragraphs each of these major points will be separately discussed and the conclusions drawn and used in the research project summarized.

2.7.1 Surface Characteristics for Road Safety and their Measurements

The literature review has yielded the necessary insight of the best approach to assess the relevant surface characteristics parameters for the study directly related to the safety of travelled pavements. The characterization of these parameters requires the measurement of the following surface characteristics:

- Friction
- Macro-texture
- Micro-texture

It also can be concluded that these three surface characteristics parameters are interrelated and need to be assessed in a practical manner to serve two purposes at the same time. These two purposes are the following:

1) Measure the parameters using measuring techniques that enable the calculation of all relevant safety related parameters; and
2) Use parameters and measuring techniques that enable the transformation of the laboratory test results into quantities measured and directly relevant to actual road surface measurements and safety.

To achieve all of the above-stated purposes it was decided that three measurement devices would be employed in the study: (1) British Pendulum Tester, (2) Dynamic Friction Tester and (3) Circular Track Texture Meter. The selection of these devices ensure that all of the necessary parameters are measured and measured in a way that is relevant to vehicle friction and can be used to compute relevant international standards for road safety.

- The DFT device (ASTM, 2009) was used to measure the frictional properties of the sample surfaces. The device measures and delivers the coefficient of friction of the measured surface at all speeds between 0 and 80 km/h, thus allowing direct computation of the F60 parameter of the International Friction Index. The F60 parameter is a measure used around the world to assess frictional characteristics of road surfaces.
- The CTM device (ASTM, 2005) was used to measure the macro-texture of the test surfaces. The device measures the texture profile of the surface using a laser

in exactly the same track as the friction is measured by the DFT device. The measured texture profile is then used to calculate the international standard Mean Profile Depth parameter, which is a direct macro-texture parameter used around the world to assess texture characteristics of road surfaces. The MPD value then can be used to calculated the Sp parameter of the International Friction Index, which is a measure of the sensitivity of vehicle friction to vehicle speed and is used around the world to assess frictional characteristics of road surfaces.

- The BPT device (ASTM, 2003) will be used to assess the micro-texture of the test surfaces. The micro-texture is a relevant frictional determinant of pavement surfaces that directly effects absolute friction levels. The use of micro-texture and the IFI numbers together gives a complete picture of frictional characteristics of travelled surfaces.

Conclusion#1: The Dynamic Friction Tester, Circular Track Texture Meter and British Pendulum Tester were used to measure frictional parameters of the test surfaces.

2.7.2 The Relationship of Characteristic Measurements in a Laboratory Environment to the Actual Surface Characteristics on Roads.

The measured parameters from the three devices determined earlier will deliver substantial and relevant information on the frictional characteristics of the test surfaces under laboratory conditions. Although these are repeatable measurements in field studies and they are used in many states and countries, the measured values can be directly translated into measurements comparable to the ASTM E274 measuring trailer data used by PennDOT.

The employment of the International Friction Index was decided to achieve the purpose of translating the laboratory measurements obtained from the devices into relevant numbers corresponding to E274 measurements.

The measured values of the DFT and CTM devices were used to calculate the IFI numbers for each test surface according to the ASTM E1960 standard (ASTM, 2007). The IFI numbers then were utilized to determine the equivalent projected SN40S measurements of an E274 measurement device.

Conclusion#2: The International Friction Index was calculated from the measured DFT and CTM parameters. The IFI was used to calculate the relevant E274 friction tester parameter SN40S. The SN40S together with the obtained MPD and BPN numbers were presented for compatibility to PennDOT practice and evaluation in relation to real-world measurements.

2.7.3 The Issue of Relevant Accelerated Wearing Machine Resembling Traffic.

From the review of the relevant literature and the array of presently available machines and technologies for measuring accelerated wearing of pavement surfaces for the purpose of evaluating frictional surface performance, it could be concluded that no easily obtainable and practical technique exists today. The relevant parameters set as requirements were:

- Simulation of traffic with pneumatic rolling wheels,
- The achievement of at least 10 times accelerated polishing wear, and
- The capability of wearing surface samples large enough to be used for measurements by the DFT and CTM machines.

The conclusion was to suitably modify the presently available MMLS-3 machine at Penn State to achieve these results. The machine uses four pneumatic rubber tires for load testing of pavement surfaces at lengths of up to 6 ft. The machine also can simulate random traffic patterns with its random lateral movement of its loading wheels. The MMLS machine uses four wheels for load wear testing. For the present study to achieve the necessary polishing and wearing effects relevant to micro-texture, macro-texture, and friction, two of the machine wheels were suitably modified. The MMLS machine wears the surface by rolling the tires into the surface in a linear motion. The tires are moved in an oval shaped vertical rail system.

To achieve a truly accelerated frictional wear pattern two tires of the machine (every other tire) were coated with a high-resilience, high-impact epoxy material into which super-high-hardness silica carbide particles were embedded. The surface of the tires in this way was developed to be a sandpaper-like abrasive surface that can withstand the extreme use of many passes over the hard concrete surfaces. A detailed description of the tires and the wearing machine is given in CHAPTER 3 (section 3.7, Accelerated Wear Testing Setup on page 46).

Conclusion#3: The MMLS-3 machine was employed to perform an accelerated polishing and wear on the produced test surfaces. The machine was modified to include two out of the four tires altered with high-strength and high-hardness silica carbide material to ensure rapid and relevant wear of relevant surface characteristics.

2.7.4 Selection of Aggregate Types for the Construction of the Test Samples.

Comparing the available aggregate types in the Commonwealth of Pennsylvania that are practical and can be expected to be used in construction, it was decided that not all of the aggregate types suggested by the literature were examined in the study due to practical and availability limitations. Only the aggregate types presently available in quarries in acceptable proximity to Pennsylvania will be considered. After review of availability and practicality of the use of different aggregates three different types were selected in addition to the researched limestone: (a) gravel, (b) sandstone and (c) slag.

Conclusion#4: The study had examined three different aggregates in combination with the tested limestone: (a) gravel, (b) sandstone and (c) slag.

2.7.5 Construction of the Test Samples.

The literature review revealed that the texturing techniques of concrete surfaces are of paramount importance in the frictional behavior of the pavement surface. Because present study was evaluating the effect of different aggregates on the frictional performance of concrete pavements, it was necessary to devise a plan that would effectively take texturing out of the variables but at the same time deliver a surface that is prone to polishing and will deliver comparable results.

It was decided that the test samples would be manufactured without any texturing technique and the fabricated sample surfaces be cured for 28 days after construction. The samples after the curing period were subjected to sand blasting on their surface subjected to the wear testing plus 2 inches on either side of the wheel path.

This technique was used to ensure that there would be no macro-textural differences between the surfaces and the test samples would have minimum allowable macro-textural features that could effect the wearing process and deform the result regarding the polishing performance of the tested materials. At the same time, the use of sand blasting would preserve the micro-textural features of the surface and introduce a uniform and isometric sub-macro-texture that would allow the surfaces to be compared.

Conclusion#5: The test samples were constructed with no major macro-texture introduced through any texturing technique. Using sand blasting after curing, a comparative sub-macro texture was introduced to the surface that would not affect micro-texture but would allow the surfaces to be compared in regard to their polishing performance.

CHAPTER 3 **EXPERIMENTAL TEST PLAN**

3.1 Aggregate Selection

For the selection of the different available aggregate types, the committee report of the "Vanport Limestone Skid Resistance Analysis" study was used to gather frictional information(PennDOT internal publication). The study incorporated frictional measurements from six different aggregate types used in 378 different surfaces. The friction readings were collected in 19 counties and on pavements with different ages and widely differing ADT values. A summary of the data is given in Table 5.

Table 5. Average friction of PCC pavements with different aggregates

	Average Friction					
	E	L	G	H	M	Unknown
Gravel	39					
SLAG	24					
Limestone		32				
Dolomite			25	34	20	
Sandstone	53					
Dolomite, Limestone		31	29			
Vanport Limestone						27

As can be observed from the table, the friction values of the different aggregates for all pavement age levels vary between 20 and 53, showing a large spread. A better approach is to consider the performance of these pavements in the different age groups in average terms and also to take into account the spread of values around the means to see how volatile the frictional performance is. These statistics can be observed in Table 6.

Table 6. Average friction and standard deviation table [SN / STD]

	Combined Average and STD						
	0-5	5-10	10-15	15-20	20-25	25-30	30+
Gravel	52 / 4	47 / 2	36 / -	31 / 4			24 / 3
Sandstone	54 / 3			42 / -			
Limestone	40 / 6	25 / 6	36 / 8	28 / 5			34 / 12
Vanport Limestone		38 / 7					26 / 3
Dolomite, Limestone	40 / 7	31 / 6	33 / 6	29 / 8	12 / 2		26 / 3
Dolomite		26 / 9		20 / 3			

The numbers in Table 6 show the average friction numbers of each aggregate type in each age category for the tested PCC pavements. The second number shows the standard deviation, or the magnitude of spread in the data for each average friction number. A graphical interpretation of the numbers is shown in Figure 14.

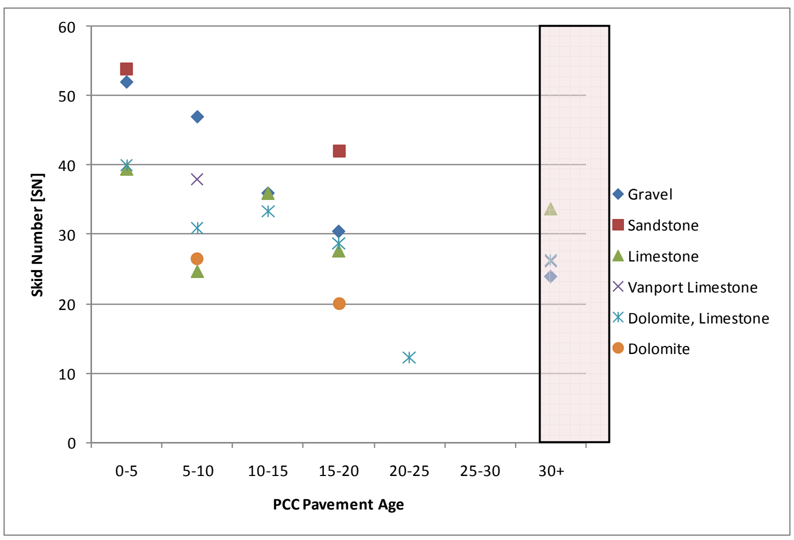

Figure 14. Friction levels vs. age of different aggregate PCC pavements

The figure shows both the absolute values and the time performance of the different surface materials. As can be observed, the sandstone and gravel are separated by a relatively large margin from the other aggregate materials at the beginning of the lifecycle between 0 and 5 years of age. The difference is more than 30% between these two aggregates and the rest of the analyzed materials. The time performance of the aggregate materials can also be observed from the chart. Although, data are missing from some of the age categories and from some of the aggregate types, general tendencies can be deduced. It can be observed that while the original performance of the gravel is equal to that of the sandstone, the frictional properties of the surfaces built from this aggregate deteriorate very rapidly and reach the level of limestone and dolomite, limestone within 15 years. The data available from the 30+ year performance of the surfaces is most an likely outlier; due to maintenance or other rehabilitation of the surfaces the data are measured on, and therefore these data were left out of the analysis. It was also a shortcoming of the available data that no more slag aggregate surface was included. The polishing values of the different aggregates in this project have been tested in many studies and a generally accepted range of the common values have been established (see Table 7).

Table 7. Polish values of aggregates of anterest

Aggregate Sources	Polish Values
Expanded Clay (Lightweight)	**~45**
Blast Furnace Slag	**~35**
Limestone (Sandy)	**~31**
Granites	**29~27**
Gravels	**27~25**
Limestones	**23~19**

3.1.1 Results from On-Site Testing of Surfaces of Interest

Preliminary measurements were taken on one of the sites available with the original surface of interest for which this investigation attempted to uncover the results of low friction. The site was located on I-79 northbound at station marker 1754. The site was transverse grooved portland cement concrete. The site and the measurement equipment are depicted in Figure 15.

Figure 15. Onsite measurements and core drilling

A number of core samples were also taken at the site to make it possible to analyze the construction of the original surfaces, since no design or construction data were available. The core samples were also utilized to estimate the used aggregate size and percentage of the original concrete mix used in the construction.

Table 8 contains the data measured on site with the same equipment as used in the laboratory experiment. The table contains measurements made in the right wheel path, the center of the lane, the left wheel path, and on the shoulder of the lane. Measurements were taken by both the DFT and CTM devices in exactly the same locations.

As can be observed from the measurement values of friction, the right and left wheel path friction values are significantly lower than the values of the center of the lane measurements. At the same time the measurements that were made on the shoulder with minimal or no traffic show an even larger increase in friction, practically doubling that of the friction in the wheel paths.

Table 8. Preliminary measurement results

		RWP	Center	LWP	Shoulder
1	Friction	0.35	0.60	0.37	0.73
2		0.40	0.63	0.39	0.91
3		0.44	0.64	0.43	0.93
4		0.39	0.68	0.37	-
5		0.39	0.64	0.40	-
Average		0.39	0.64	0.39	0.86
1	Texture	0.34	0.46	0.34	1.12
2		0.42	0.51	0.43	1.24
3		0.31	0.50	0.33	1.22
4		0.33	0.38	0.35	-
5		0.42	0.46	0.36	-
Average		0.36	0.46	0.36	1.19

The measurement of texture shows a very similar pattern with lower texture values in the wheel paths and a large increase in texture on the untraveled shoulder.

The preliminary measurements indicate very strong polishing and lack of macro-texture which points in the direction of lacking frictional characteristics due to deficient micro- and macro-texture of the surface.

3.2 Mix Selection for Aggregate Substitution Study

Based on the analysis, the preliminary measurements and analysis of the core samples and the conclusions of the literature review (see section 2.7 Conclusions, on page 26), the originally developed and submitted test matrix suggested for the analysis of the different aggregate mixtures was determined in cooperation with the PennDOT technical project managers and is given in Table 9.

Table 9. Original blending matrix

	Percentage Aggregate			
Sandstone	30% / 3 samples	40% / 3 samples*	50% / 3 samples	70% / 3 samples
Gravel	30% / 3 samples	40% / 3 samples*	50% / 3 samples	70% / 3 samples
SLAG	30% / 3 samples	40% / 3 samples*	50% / 3 samples	70% / 3 samples

* possible mixtures for elimination from test matrix.

The matrix includes three aggregates and four different aggregate/limestone blend percentages. The testing combinations were prepared such that a total of 48 test plates were required in 12 different blend mixture combinations. The statistical analysis of the obtained surface characteristic values required that multiple sample surfaces be tested from the same blend mixture types. It was suggested that three samples of each blend mixtures be prepared for the outer extreme aggregate combination percentages and three samples for the 40% and 50% combinations. Furthermore, in order to reduce the number of wear cycles and testing requirements it was determined that first only the 50% percentage blend mixture would be tested, and if the measurement results did not warrant the 40% blend mixture, testing would be eliminated (designated by the * symbol and light red background in the table). If the measurements of the first three blend combinations warranted, the testing on the 40% blend mixture was also performed. This measure effectively reduced the number of samples to be tested by 12 and thus sped the research project significantly.

3.2.1 Final Test Matrix for Aggregate Substitution Testing

Due to the fact that there were no previously available comparable accelerated polishing and surface characteristics wear tests or reports that would facilitate the estimation of the true time necessary for a complete wear cycle a pre-test evaluation was necessary. It was decided that a pre-test surface of comparable aggregate and mortar composition to the control surface be produced, and the MMLS wearing machine used to measure the performance of the modified machine and determine the cycle number intervals at which surface characteristics measurements would be performed. From the trial wearing tests, the following conclusions were drawn:

1. The MMLS machine is capable of producing highly accelerated wear and polishing on the test specimens.
2. For each test sample it was necessary to perform a minimum of 360,000 wearing cycles.
3. A complete 360,000 wearing cycle with the necessary intervals to measure surface properties during the wearing process takes 2 to 2.5 weeks in time.

Due to the time requirements of the wearing process, it became necessary to further reduce the total number of samples in the test matrix in order to be able to complete the testing within the allotted project execution time. In consultation with the project technical committee it was decided to modify the test matrix for the aggregate substitution, the test matrix for the mortar characteristics and the test matrix for the maximum aggregate size studies. The modified test matrix enabled a more rapid project execution while retaining the possibility to follow trends and observe performance differences. The final approved test matrix is given in Table 10.

Aggregate Substitution Test (AST)

Table 10. Final aggregate substitution test matrix

Aggregate	Substitution Percentage	Surface Code	# of samples
Gravel:	30% Gravel / 70% Vanport	AST-G-30-1	1 Slab
		AST-G-30-2	1 Slab
	50% Gravel / 50% Vanport*	AST-G-50-1*	1 Slab
		AST-G-50-2*	1 Slab
	70% Gravel / 30% Vanport	AST-G-70-1	1 Slab
		AST-G-70-2	1 Slab
Sandstone:	30% Sandstone / 70% Vanport	AST-S-30-1	1 Slab
		AST-S-30-2	1 Slab
	50% Sandstone / 50% Vanport*	AST-S-50-1*	1 Slab
		AST-S-50-2*	1 Slab
	70% Sandstone / 30% Vanport	AST-S-70-1	1 Slab
		AST-S-70-2	1 Slab

AASHTO #57 Coarse Aggregate Gradation
37% Fine Aggregate Fraction

For mix designs indicated with the red background, the "*" sign designates the designs that are optional designs. These mixes were intended to be tested only in the case where the testing of the two boundary mix designs would not yield conclusive results.

3.3 Mix Selection for Mortar Fraction Study

The significance of aggregate proportions and properties for PCC pavements lies in the assembly of aggregates bonded together with cement paste where the voids are completely filled with paste. Thus, the amount of paste depends on the amount of void space that must be filled and the total surface area of the aggregate that must be coated. The volume of voids between aggregate particles is greatest when the particles are of uniform size. When a wider range of sizes is used, the smaller particles pack between the larger ones, decreasing void space and lowering paste requirements. Using larger maximum aggregate sizes can also reduce void space even though the median void size is actually larger. At the same time for concrete pavements where the frictional, macro-, and micro-textural characteristics of the pavement surface are intended to be determined by the properties of the mortar layer the used fine aggregate (sand) and cement paste will have an overbearing influence.

The following test matrix has been designed to test the effects of different aggregate mixtures to the extremes in their composition with regard to fine and coarse aggregate content. The mixtures are intended to deliver a statistically significant number of samples with a distribution of aggregate sizes and mix combinations to the extremes, that will provide data that can be analyzed to assess the effect of increased fine aggregate (sand) components and the effects of decreasing course aggregate size on the frictional properties of the surfaces. The original proposed test matrix is given in Table 11.

Table 11. Original fine and coarse aggregate test matrix

		Coarse Aggregate Limestone			
		70% / 2”	50% / 2”	50% / 1”	30% 1”
Fine Aggregate	30%	Mix#1: 3 Samples			
	50%		Mix#2: 3 Samples		
	50%			Mix#3: 3 Samples	
	70%				Mix#4: 3 Samples

The original detailed mix designs from the preliminary planning stage of the project with the exact water/cement ratio, water content and determined weight ratios are given in Table 12.

Table 12. Original detailed mix designs for mortar fraction tests

	W/C	Water [Kg/m^3 (lb/ft^3)]	Cement [Kg/m^3 (lb/ft^3)]	Sand/Agg (%)	Course aggregate [Kg/m^3 (lb/ft^3)]	Sand [Kg/m^3 (lb/ft^3)]
Mix#1	0.47	150.00 (9.38)	319.15 (19.95)	30	1351.60 (84.47)	579.26 (36.20)
Mix#2	0.47	150.00 (9.38)	319.15 (19.95)	50	965.43 (60.34)	965.43 (60.34)
Mix#3	0.47	150.00 (9.38)	319.15 (19.95)	50	965.43 (60.34)	965.43 (60.34)
Mix#4	0.47	150.00 (9.38)	319.15 (19.95)	70	579.26 (36.20)	1351.60 (84.47)

3.3.1 Final Test Matrix for Mortar Fraction Testing

Due to the time limitations of the wearing test described earlier in this section, the fine aggregate content test matrix was also modified. The modifications also reflected a suggestion from the PennDOT technical committee to use material combinations and gradation that are practical and more relevant to the present construction practice. The use of artificial mixes in the test matrix was abandoned and a more practical approach taken in the design. It was decided that in this study the normally used AASHTO #57 coarse aggregate gradation would be employed using the tested Vanport Limestone aggregate. The variation of the fine-to-coarse aggregate ratio was also decided after the preliminary study in agreement with the technical committee to be limited to two mix designs; a preparation of a third middle mix ratio would be added to the testing only if measurement results are lacking clear trends. The final approved test matrix is given in Table 13.

Mortar Fraction Test

Table 13. Final Mortar fraction test matrix

Aggregate	Substitution Percentage	Surface Code	# of samples
Vanport Limestone	70% Coarse / 30% Fine	MFT-70/30-1	1 Slab
		MFT-70/30-2	1 Slab
	50% Coarse / 50% Fine *	MFT-50/50-1*	1 Slab
		MFT-50/50-2*	1 Slab
	30% Coarse / 70% Fine	MFT-30/70-1	1 Slab
		MFT-30/70-2	1 Slab

AASHTO #57 Vanport Limestone Coarse Aggregate Gradation

3.4 Mix Selection for Maximum Aggregate Size Study

During the preparation of the test matrix a number of mix combinations were eliminated from both the aggregate substitution study and the mortar fraction study to achieve economy and practical execution time for the project. At the same time a new test was added to the test matrix with a number of combinations of different gradations to test the effect of aggregate size of Vanport Limestone in PCC surfaces with regard to frictional characteristics and polishing performance.

A long and detailed discussion and planning process yielded the agreed-upon mix designs and the sizes of coarse aggregates to be used in the study of maximum aggregate size. The use of a blend of AASHTO #57 and #8 aggregate gradation was decided with the addition of gradation Class 1 fine aggregates. The AAHSTO Class 1 grading was added to make the mix based on a request from the PennDOT technical project managers. It was decided that the mix designs for the fine/coarse mixture study be updated with the #57 and #8 aggregates and included with the report, but the work on refining these with regard to practicality, workability and other issues will worked out throughout the study and therefore the finally tested mix designs might be different from the suggested preliminary designs in the interim report.

The final test matrix for the maximum aggregate size study is given in Table 14.

Table 14. Final maximum aggregate size test matrix

Aggregate	Aggregate Gradation	Surface Code	# of samples

Vanport Limestone	AASHTO #1 / #57	MAS-1/57-1*	1 Slab
		MAS-1/57-2*	1 Slab
	AASHTO #8 / #57	MAS-8/57-1	1 Slab
		MAS-8/57-2	1 Slab
	AASHTO #1	MAS-8-1	1 Slab
		MAS-8-2	1 Slab

*screened to max nominal size ≤ 2”

The selected different AASHTO gradations are given in Table 15.

Table 15. Selected AASHTO gradations table

Sieve Size		Percent Passing		
		AASHTO No. 57	AASHTO No. 8	AASHTO No. 1
100 mm	4 in	-	-	100 min
90 mm	2.5 in	-	-	90- 100
75 mm	3 in	-	-	-
63 mm	2.5 in	-	-	25 - 60
50 mm	2-inch	-	-	-
37.5 mm	1.5-inch	100 min	-	0 - 15
25 mm	1-inch	95 - 100	-	-
19.0 mm	0.75-inch	-	-	0 - 5
12.5 mm	0.5-inch	25 - 60	100 min	
9.5 mm	0.375-inch	-	85 - 100	
4.75 mm	No. 4	10 max	10 - 30	
2.36 mm	No. 8	5 max	10 max	
1.18 mm	No. 16	-	5 max	

Based on the planning process and the request from the PennDOT technical project managers, the AASHTO #1 graded aggregates were screened to maximum nominal size of not more than 2 inches of aggregate size. This has changed the original AASHTO gradation. The depiction of the gradation of the used aggregate sizes in the maximum aggregate size study can be found in Figure 16 through Figure 21Figure 18.

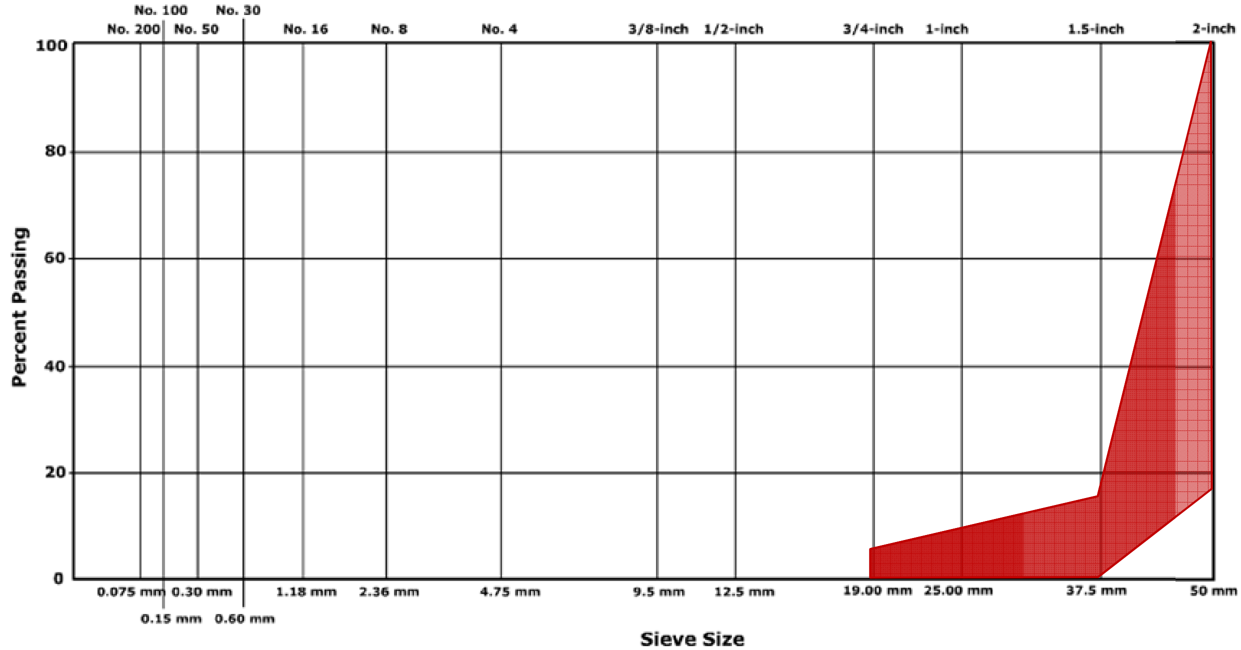

Figure 16. Coarse gradation AASHTO #1 (screened to max nominal size ≤ 2")

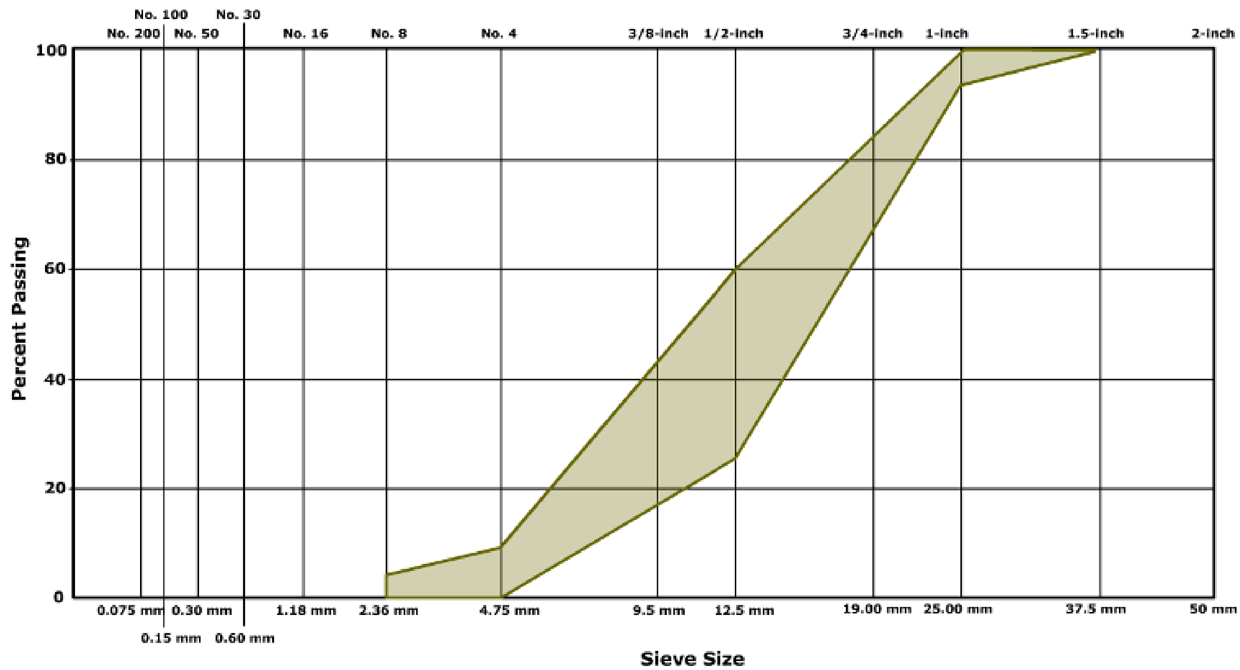

Figure 17. Coarse gradation AASHTO #57

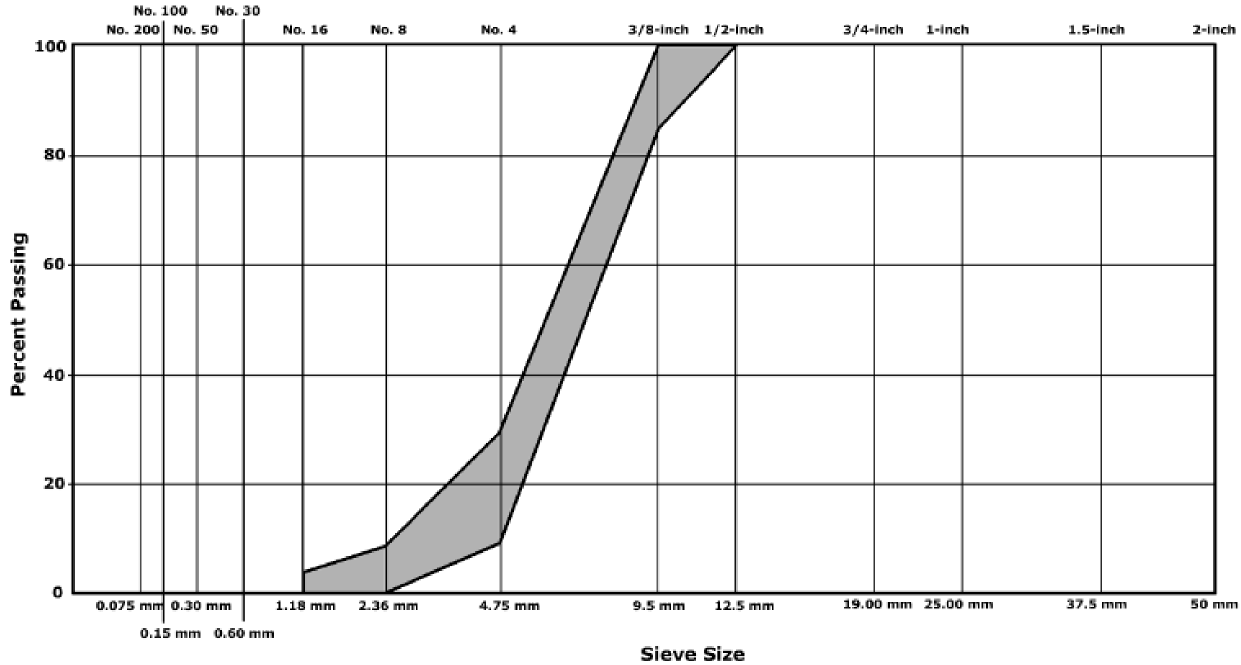

Figure 18. Coarse gradation AASHTO #8

The final three mixtures selected for the study, as described in Table 14, give a combination of modified AASHTO gradations, yielding the three surfaces for the maximum aggregate size study. The three mixtures, with their respective coarse aggregate gradations are given in Figure 19 through Figure 21

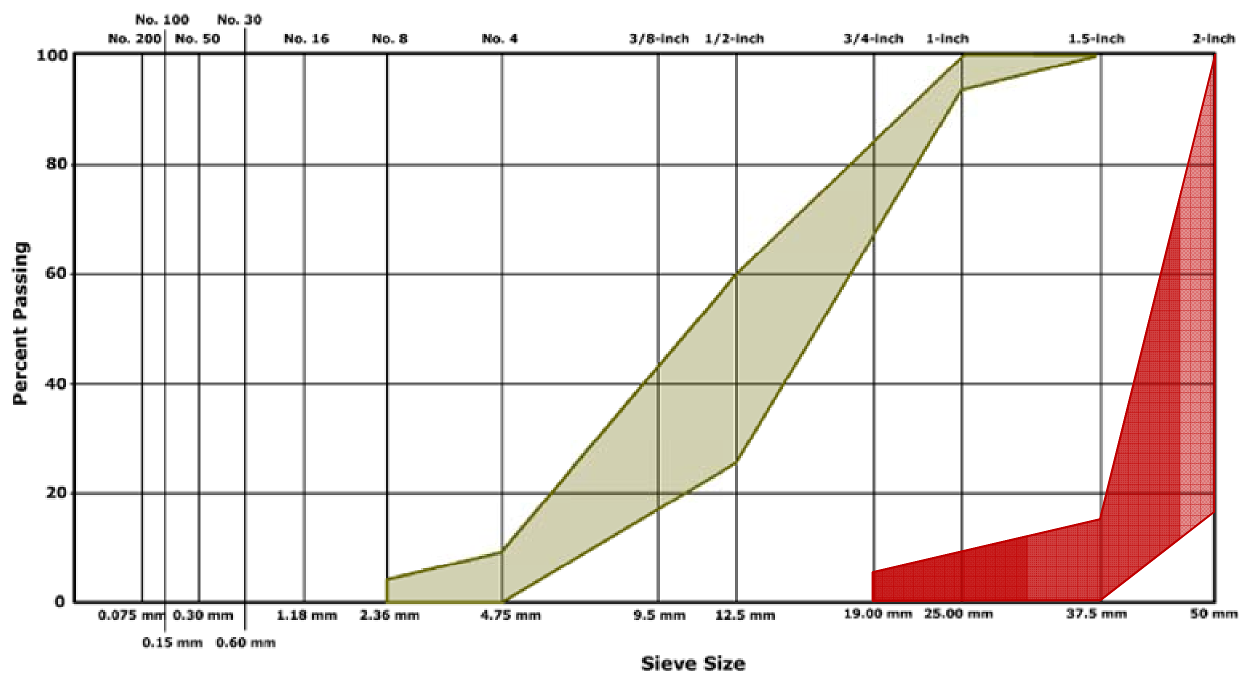

Figure 19. Coarse aggregate gradation for test surface MAS-1-57 **(AASHTO #1/AASHTO #57)**

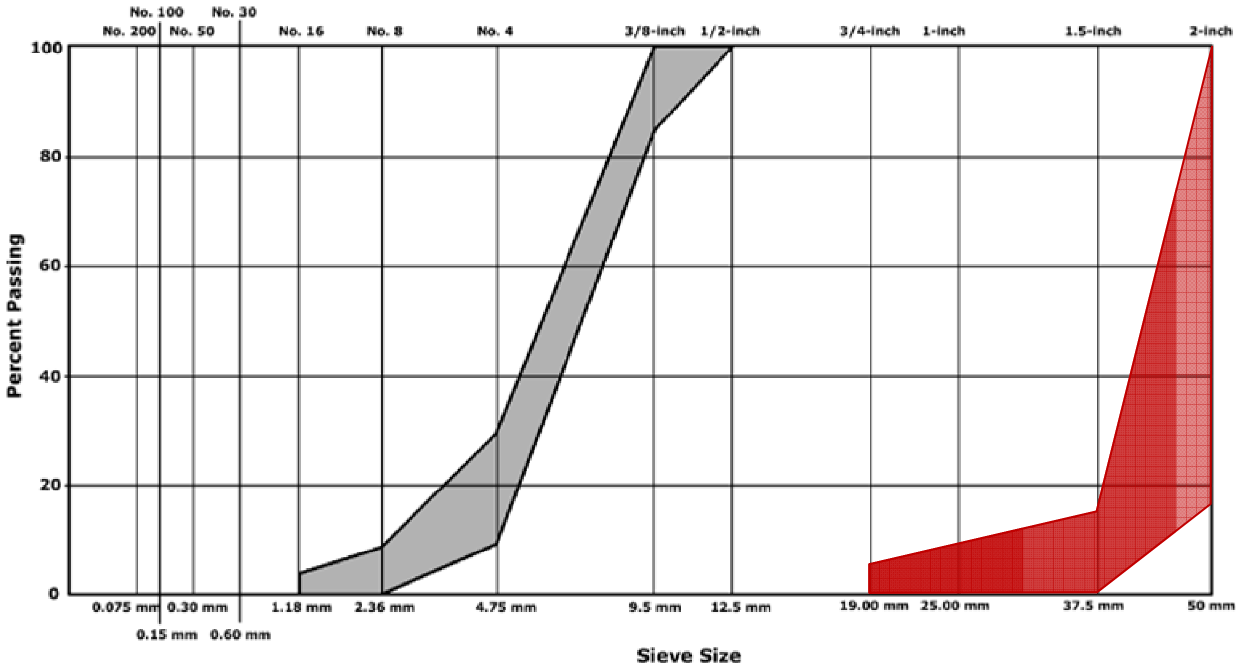

Figure 20. Coarse aggregate gradation for test surface MAS-8-57 (AASHTO #8/AASHTO #57)

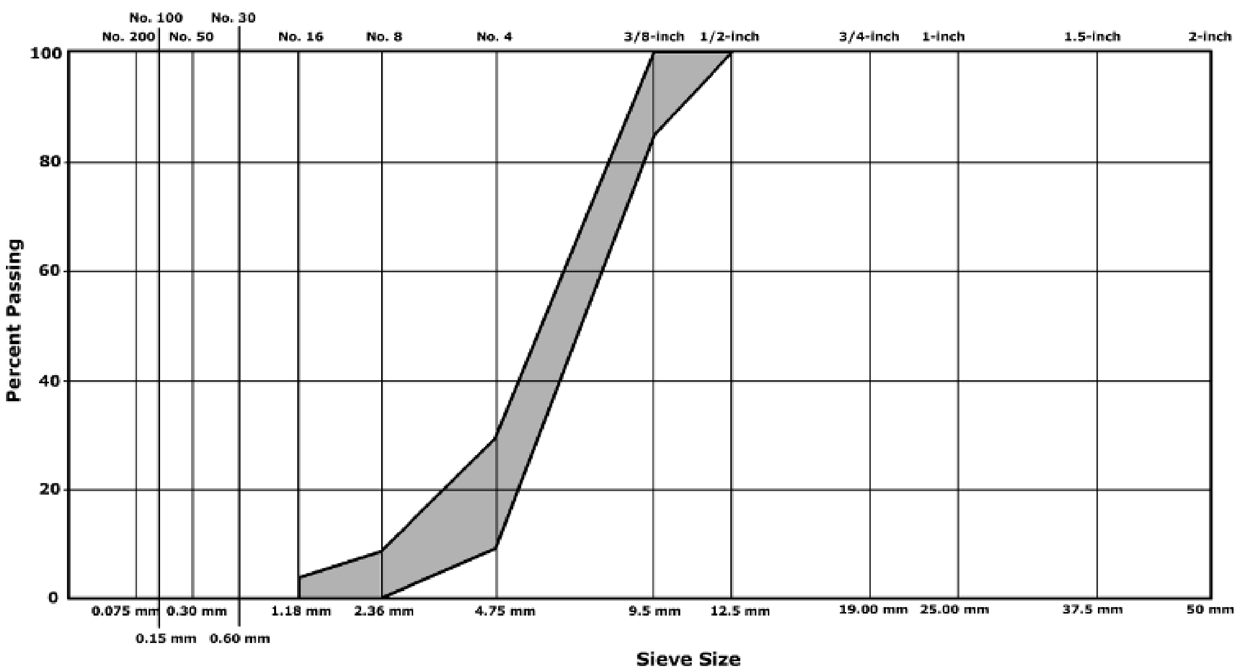

Figure 21. Coarse aggregate gradation for test surface MAS-8 (AASHTO #8)

3.5 Sample Construction

The final aggregate and mixture designs were agreed to be worked into a set of sample surfaces. Each sample had contained two independently cast and separated square samples of the same material. The sample materials were arranged such that the two separate squares were combined into a rectangular-shaped specimen, allowing the surfaces to be worn by the MMLS machine simultaneously, thus introducing exactly the same wearing load on both surfaces.

The concrete specimens were both cast and tested in the same forms. The forms consisted of a 74”X30”X0.25” steel base with bolts welded to the surface to mount wooden sides. The sides measured 48.5”X26”X5” with a 0.5” spacer inserted at the midpoint of the mold to create two 24”x26”x5” samples per mold.

One mix design was used for each pair of samples. The concrete was batched and mixed in the lab, placed into the form cavity and vibrated using a pencil vibrator. Percent air was determined with each mix design and 4”x8” compressive strength samples were cast for each mix.

Following placement, the concrete surface was finished by hand trowel and moist burlap was applied as well as a cover of plastic sheeting to maintain a moist cure. After 2 days of moist cure each sample was sandblasted in the area of the anticipated MMLS3 wheel path to expose the aggregate near the surface.

Samples were then aged for a minimum of 28 days and compressive strength determined. Following acceptable compressive strength the samples were subjected to trafficking using the MMLS3 apparatus.

Table 16. As-constructed mix parameters

	Water (lb)	Cement (lb)	Fly Ash (lb)	CA(lb)		FA (lb)	ABS(CA) Vanport (%)	ABS(CA) Gravel (%)	ABS(FA) (%)	Adjusted CA (lb)		Adjusted FA (lb)	Adjusted Water (lb)	AE (ml)	WR(ml)
				VP#57	Gr#57					VP#57	Gr#57				
Control	36.93	78.50	13.82	301.75		177.25	0.42	1.35	1.24	302.34	0.00	184.15	29.44	60.00	80.00
AST-G-30	36.93	78.50	13.82	211.23	90.52	177.25	0.42	1.35	1.24	211.50	93.69	189.25	21.49	60.00	80.00
AST-G-70	36.93	78.50	13.82	90.53	211.22	177.25	0.42	1.35	1.24	90.65	212.26	185.76	27.26	60.00	80.00
AST-G-50	36.93	78.50	13.82	150.88	150.87	177.25	0.42	1.35	1.24	151.04	149.87	184.01	31.00	40.00	50.00
	Water (lb)	**Cement (lb)**	**Fly Ash (lb)**	**CA(lb)**		**FA (lb)**	**ABS(CA) Vanport (%)**	**ABS(CA) Sandstone (%)**	**ABS(FA) (%)**	**Adjusted CA (lb)**		**Adjusted FA (lb)**	**Adjusted Water (lb)**		
				VP#57	**SS#57**					**VP#57**	**SS#57**				
AST-S-30	36.93	78.50	13.82	211.23	90.52	177.25	0.42	0.75	1.24	211.78	90.56	183.64	29.95	60.00	100.00
AST-S-70	36.93	78.50	13.82	90.53	211.22	177.25	0.42	0.75	1.24	90.78	212.81	183.68	28.65	60.00	100.00
	Water (lb)	**Cement (lb)**	**Fly Ash (lb)**	**CA(lb)**		**FA (lb)**	**ABS(CA) Vanport (%)**		**ABS(FA) (%)**	**Adjusted CA (lb)**		**Adjusted FA (lb)**	**Adjusted Water (lb)**		
				VP#57						**VP#57**					
MFT-70-30	36.93	78.50	13.82	335.30		143.70	0.42		1.24	335.54		148.31	32.08	80.00	80.00
MFT-30-70	36.93	78.50	13.82	143.70		335.30	0.42		1.24	143.81		342.68	29.44	80.00	100.00
	Water (lb)	**Cement (lb)**	**Fly Ash (lb)**	**CA(lb)**		**FA (lb)**	**ABS(CA) VP#57 (%)**	**ABS(CA) VP#1 / #8 (%)**	**ABS(FA) (%)**	**Adjusted CA (lb)**		**Adjusted FA (lb)**	**Adjusted Water (lb)**		
				VP#57	**VP#1 / #8**					**VP#57**	**VP#1 / #8**				
MAS-1-57	36.93	78.50	13.82	120.70	181.05	177.25	0.42	0.42	1.24	121.03	181.42	184.99	28.49	80.00	80.00
MAS-8-57	36.93	78.50	13.82	120.70	181.05	177.25	0.42	0.65	1.24	120.90	181.21	183.42	30.40	60.00	80.00
MAS-8	36.93	78.50	13.82	301.75		177.25	0.65		1.24	302.40		184.65	28.88	80.00	92.00

Mix Design (0.157 CU YD Batch Size) W/C=0.4

The concrete mix abbreviations used in Table 16 constitute the following naming conventions and indicators:

Experiment: <u>Control</u> Test **<u>CONTROL</u>**

100% Vanport Limestone Coarse Aggregate AST-V-1, AST-V-2

AASHTO #57 Coarse Aggregate Gradation

37% Fine Aggregate Fraction

Experiment: <u>A</u>ggregate <u>S</u>ubstitution <u>T</u>est **<u>AST</u>**

Gravel:	30% Gravel / 70% Vanport	**AST-G-30-1, AST-G-30-2**
	70% Gravel / 30% Vanport	**AST-G-70-1, AST-G-70-2**
Sandstone:	30% Sandstone / 70% Vanport	**AST-S-30-1, AST-S-30-2**
	70% Sandstone / 30% Vanport	**AST-S-70-1, AST-S-70-2**

AASHTO #57 Coarse Aggregate Gradation
37% Fine Aggregate Fraction

Experiment: <u>M</u>ortar <u>F</u>raction <u>T</u>est **<u>MFT</u>**

70% Coarse / 30% Fine	**MFT-70/30-1, MFT-70/30-2**
30% Coarse / 70% Fine	**MFT-30/70-1, MFT-30/70-2**

AASHTO #57 Vanport Limestone Coarse Aggregate Gradation

Experiment: <u>M</u>aximum <u>A</u>ggregate <u>S</u>ize **<u>MAS</u>**

AASHTO #1 / #57	**MAS-1/57-1*, MAS-1/57-2***
AASHTO #8 / #57	**MAS-8/57-1, MAS-8/57-2**
AASHTO #8	**MAS-8-1, MAS-8-2**

*screened to max nominal size ≤ 2”

The actual mixed concrete parameters were measured and recorded during the casting process and the data are given in Table 16.

During the casting of each test slab, three (3) 4”x8” compressive strength samples were cast. The compressive strength test samples were each used to determine, after the 28 day curing period, the concrete strength and tested against the required 3,750 psi strength. The criteria for each sample surface to be used in the study were established including that the compressive strength of the material had to exceed the threshold of 3,750 psi strength. The dates of the casting of each test specimen together with the dates for the testing of the compressive strength test samples were recorded. The data are given in Table 17. As can be observed, the resulting compressive strength of the materials used in this experiment for each individual test sample as well as the average sample strength passed the set criteria.

Table 17. As-built test sample compressive strength (sample: 4”x8”)

	Date Cast	Test Date	Sample #1	Sample #2	Sample #3	AVG
Control	4/21/2009	5/14/2009	5,565 Psi	5,560 Psi	5,405 Psi	5,510 Psi
AST-G-30	4/28/2009	5/14/2009	5,062 Psi	4,740 Psi	4,704 Psi	4,835 Psi
AST-G-70	4/21/2009	5/14/2009	4,425 Psi	4,951 Psi	4,204 Psi	4,527 Psi
AST-S-70	6/16/2009	7/13/2009	6,271 Psi	6,120 Psi	5,629 Psi	6,007 Psi
AST-S-30	7/15/2009	8/12/2009	4,991 Psi	4,897 Psi	4,832 Psi	4,907 Psi
MFT70-30	8/17/2009	9/14/2009	4,880 Psi	4,512 Psi	5,015 Psi	4,802 Psi
MFT30-70	7/27/2009	8/24/2009	4,366 Psi	4,116 Psi	-	4,241 Psi
MAS-1-57	8/18/2009	9/15/2009	5,116 Psi	4,713 Psi	3,711 Psi	4,915 Psi
MAS-8-57	9/4/2009	10/5/2009	5,685 Psi	5,584 Psi	5,878 Psi	5,635 Psi
MAS-8	9/15/2009	10/12/2009	4,955 Psi	4,624 Psi	4,703 Psi	4,790 Psi

3.6 Experimental Test Plan

Preliminary wear cycle tests were performed using a separate surface constructed according to the control surface specifications. The test surface was constructed before the testing of any of the designed test slabs took place, and the purpose of the manufacturing and testing of the pre-study surface was twofold:

1. Determine the optimal wearing cycle number necessary to be performed on a typical surface to achieve polishing and wearing that will predictably diminish the frictional, macro-and micro-textural surface properties to a point of unacceptable level; and
2. Determine the best combination intervals (number of wearing cycles) between measurements to follow the polishing and surface wear effects as a function of wearing cycles.

The preliminary study had yielded insights as to the overall number of wearing cycles and data for the determination of the best theoretical division of the wearing test to make periodic surface characteristics measurements.

The results of the pre-study testing yielded the following information for use in the polishing study:

1. The total combined number of wearing cycles: **360,000**
2. Optimal wearing cycle intervals to establish polishing and surface characteristics deterioration history and trend: **15,000; 30,000; 60,000; 120,000; 240,000**

In addition to the measurements to be made after the number of wearing cycles indicated in the previous list an original initial reading for all measurement characteristics parameter had to be made before the start of the wearing traffic on the test surface to establish initial conditions. Similarly, after the total 360,000 cycles of wearing traffic had been finished, the final surface characteristic measurements were performed to establish the final characteristics of the test surface at the end of the wearing.

3.6.1 Collected Test Parameters

As it was established during the background investigation and described in section 2.7, the Dynamic Friction Tester , Circular Track Texture Meter and the British Pendulum Tester were used to measure frictional parameters and other surface characteristic descriptors of the test surfaces during the study. The data from the measurements were be collected into a comprehensive database and used in the analysis of the experimental results to calculate the relevant in-laboratory and projected full-scale road testing relevant measurements and surface descriptor parameters.

In accordance with the discussion in chapter 2, the International Friction Index was calculated from the measured DFT and CTM parameters and the established IFI indices were be utilized for comparative study as well as the means to project actual, real-world, road-relevant, high-speed friction measurements. The IFI was used to calculate the relevant E274 friction tester friction number. The ASTM-suggested 40 mph friction index was estimated as it was measured using the ASTM 501 blank friction measurement tire. The designation of the blank tire friction measurement performed according to the ASTM E274 test at 40 mph speed was **FN40S**. In practice the E274 friction measurements sometimes are represented as whole numbers calculated from the measured coefficient of friction, multiplying it by 100 (e.g., a number corresponding to the coefficient of friction 1.0 is represented by an integer number 100); the designation of this number is usually referred to as SN40S. In this study, the coefficient of friction (FN40S) designation was followed. The FN40S, together with the obtained macro-texture descriptors of the mean texture depth and the PIARC speed number SP (part of the IFI index) and the British Pendulum Tester measurement numbers are presented and analyzed in the report. The IFI presentation provides a comprehensive analysis of the performance of each test surface comparatively evaluated against the other tested surfaces as well as the performance of the surface in terms of resistance of polishing on its own merit following the degradation of the measured parameters throughout the wearing process. The calculated FN40S numbers together with the measured MPD parameters will provide a strong foundation for compatibility evaluations to PennDOT practice and evaluation in relation to real-world measurements.

In addition, a complete set of photographs were prepared for the database. The photographs depict the surface's initial conditions, the progress of polishing and wearing with a picture taken at each interval of the wearing test, and a final set of pictures taken at the very end of the testing of each slab.

For the brevity of the report and to be able to limit the size and number of pages, photographs of the test surfaces are included in appendix A for each test surface at the initial, middle and end stages of the testing.

3.7 Accelerated Wear Testing Setup

The sample concrete slabs were exposed to traffic wearing and accelerated polishing using a one third scale accelerated wear testing device the Model Mobile Load Simulator (MMLS-3). It is commonly used to apply cycles to pavement markings, asphalt cement concrete pavements, and other highway materials to determine degradation phenomena. The MMLS-3 can apply up to 7,200 cycles per hour over an approximate 4 ft (1.26 m) distance, as shown in the longitudinal section of Figure 22. As it was anticipated that at least 500,000 cycles will have to be applied to begin observing significant skid resistance reduction the device was modified to conform to the commonly used practices described in chapter 2 for accelerated polishing and wear as well as to reduce the number of cycles necessary for the full testing of the surfaces.

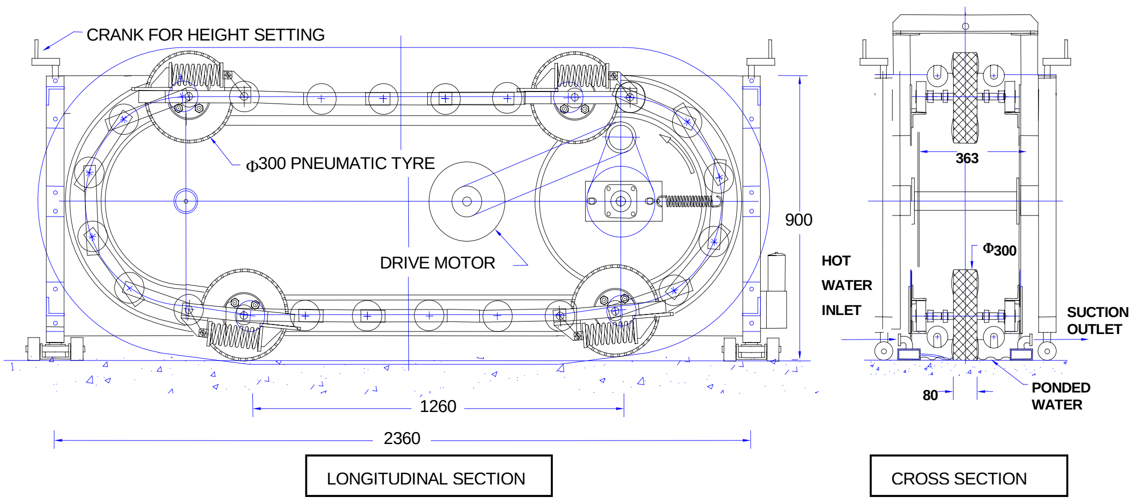

Figure 22. Model Mobile Load Simulator.

Based on the previously described preliminary experimental testing using the MMLS3, the research team determined that the first 6 inches (15 cm) of the MMLS3 contact area did not receive the same loading force (due to wheel bounce); therefore, only the middle 18”x18” (0.46x0.46 m) were used for the measurements and evaluation. A typical setup for the MMLS machine with a test surface is depicted in Figure 23.

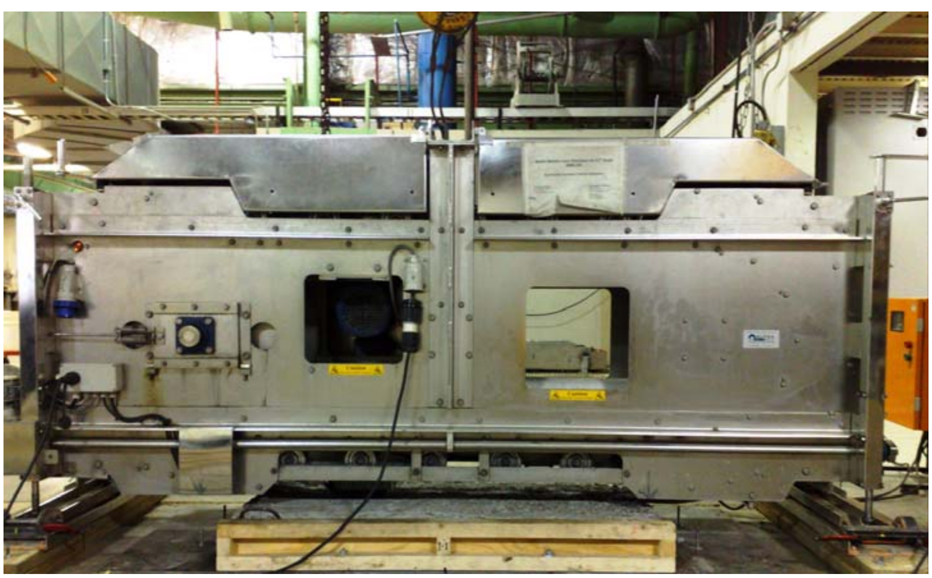

Figure 23. MMLS-3 machine setup with test surface

The modification to the machine was initiated to introduce significant polishing power to the wearing cycles in a similar manner as the polishing machines described in Chapter 2, but with the significant difference of closely simulating actual traffic conditions. The traffic conditions were simulated through the machine's capability to deliver straight longitudinal roll cycles of a pneumatic tire under load while at the same time move sideways, successfully introducing distributed traffic loads. The machine has four wheels that roll over the surface, thus one cycle contains four wheels passing over the tested surface area. Two of the pneumatic tires were modified in order to introduce significant polish and wear to the surface. The tires were coated using a high-strength and flexible polyurethane bonding agents into which ultra-high hardness silica carbide particles were embedded. The resultant tire surface gave a pneumatic wheel with high abrasive capability on a very fine scale. This combined with the unmodified two pneumatic wheels gave a capacity to the MMLS-3 machine to rapidly introduce heavy polishing and surface wear that is relevant to the surface characteristics of PCC pavements determining frictional performance.

CHAPTER 4 **EXPERIMENT RESULTS AND ANALYSIS**

Based on the test matrices, methods, wearing procedures, measurement intervals and measurement techniques described in CHAPTER 3, the complete testing and measurement program was executed and the measurement data collected. The measured and collected data in tabulated format are given in Appendix B.

4.1 Analysis of DFT Data

For the analysis, the measured DFT data had to be filtered and reduced into a manageable amount of data. As it has been discussed in the previous sections, the DFT device measures the coefficient of friction as a function of travel speed over the surface. Thus the measurement data from the device contain 1,000 pairs of data points of friction and rubber slider speed. A typical friction curve measured during the experiment can be observed in Figure 24.

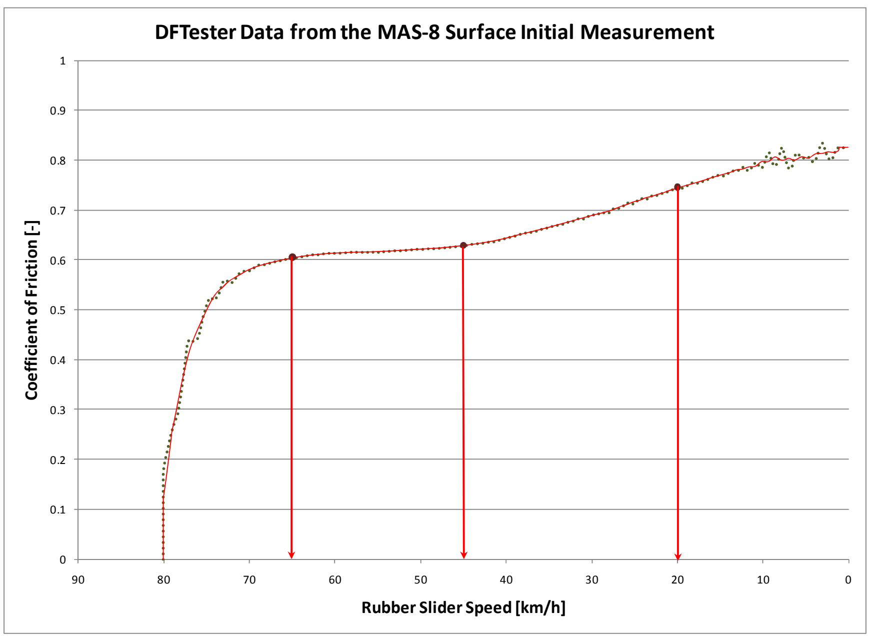

Figure 24. Interpretation of DFTester Measurement

The raw measured data are indicated by the dotted line in the figure, while the filtered and re-sampled measurement data are depicted by the red continuous line. For the analysis of the frictional characteristics of the pavements the filtered DFT data were further reduced to three single friction numbers characterizing the pavement surface. The frictional data at 65km/h, 45km/h, and 20km/h speeds were collected and separately assembled in a test data matrix for each of the tested surfaces at each of the wear intervals determined in the test matrix. These three numbers were collected for all repeated measurements and averaged to form the final measurement for the particular surface.

The averaged friction values for the three selected speeds were used in the analysis of surface performance and the calculation of surface characteristics parameters such as the IFI. The recorded DFT data for all of the studied surfaces have followed a similar general tendency in deterioration. The surfaces have shown an initial rapid drop in friction at all speed levels, which later leveled out to a less significant decline rate. A typical surface change with regard to wearing cycles is shown in Figure 25, where the lower graph shows wearing cycles in logarithmic scale.

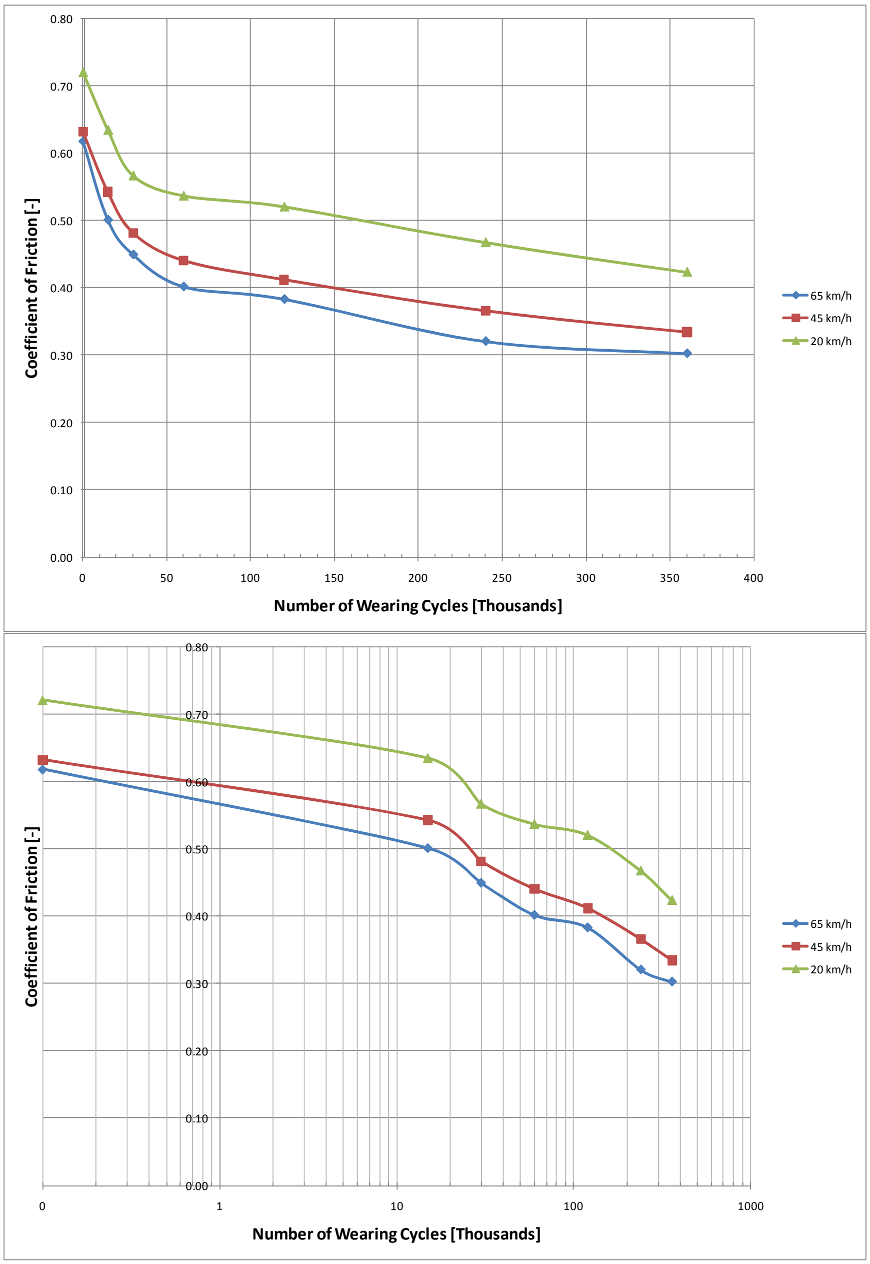

Figure 25. Deterioration of DFT friction levels with wearing

As can be observed from the figure, the deterioration of high-speed friction after the initial drop is close to linear in a logarithmic scale regarding the number of wearing cycles performed on the surface. This trend was observed in all of the tested materials without exception. A depiction of the decline of friction for all of the surfaces at 65km/h speed is presented in Figure 26.

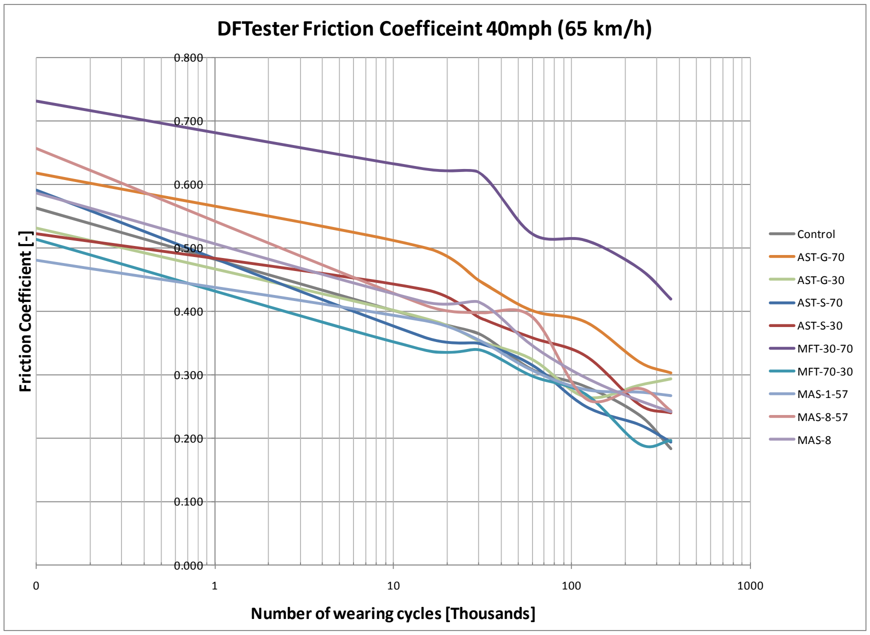

Figure 26. Friction Deterioration at 65km/h of all surfaces

Although a number of differences can already be observed from this figure, the performance differentiation of the surfaces is not yet clear and further processing of the data is clearly necessary. The measured texture and speed dependency changes captured by the calculation of the IFI and MPD indices will further refine the analysis.

It is worthwhile at this point in the analysis to observe the performance of the two highest friction surfaces in Figure 26. The three best frictional performances are clearly delivered by three surfaces: **MFT-30-70, MAS-1-57,** and the **AST-G-70,** if the absolute magnitude of the delivered friction values at 65 km/h speed is considered along the entire wearing curve. The surface performance can also be depicted considering the percent deterioration in measured coefficient of friction using the DFT results considering the initial and final measurements. The data organized to show these statistics are given in Table 18. As can be observed from the table, the very same two surfaces that delivered the best absolute performance considering only the DFT results also supplied the best performance regarding declining friction values along the wearing and polishing curve. The two surfaces are indicated in the table by red cell backgrounds containing the percentage decline in measured DFT coefficient of friction at the three pre-selected speeds.

Table 18. Percentage DFT friction deterioration of surfaces

	Initial			Finish			Percentage Decline		
	65 km/h	45 km/h	20 km/h	65 km/h	45 km/h	20 km/h	65 km/h	45 km/h	20 km/h
CONTROL	0.57	0.55	0.63	0.20	0.24	0.34	65%	56%	46%
AST-G-70	0.62	0.63	0.72	0.30	0.33	0.42	51%	47%	41%
AST-G-30	0.53	0.56	0.64	0.29	0.33	0.39	45%	42%	39%
AST-S-70	0.59	0.59	0.61	0.19	0.24	0.38	68%	59%	37%
AST-S-30	0.53	0.58	0.69	0.24	0.29	0.40	55%	51%	42%
MFT-30-70	0.76	0.80	0.89	0.44	0.48	0.61	42%	41%	32%
MFT-70-30	0.53	0.56	0.68	0.21	0.25	0.32	61%	56%	53%
MAS-1-57	0.49	0.54	0.64	0.26	0.30	0.38	47%	45%	40%
MAS-8-57	0.69	0.73	0.84	0.25	0.29	0.41	64%	60%	51%
MAS-8	0.47	0.64	0.62	0.25	0.29	0.39	47%	55%	37%

The overall deterioration graphs for all speeds and surfaces are given in Figure 27.

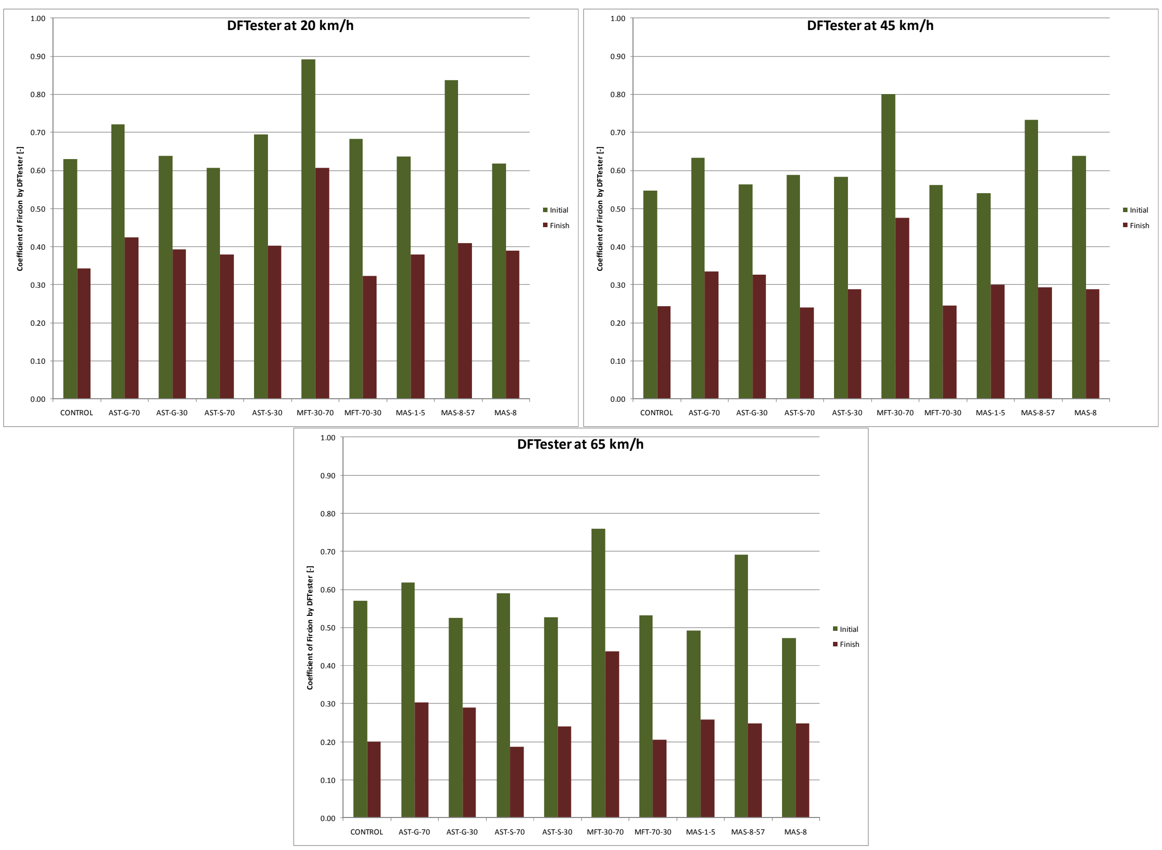

Figure 27. DFT friction decline for all surfaces

4.2 Analysis of the British Pendulum Tester Data

The British Pendulum Tester is generally regarded as a device that indicates surface micro-texture through its measurements. In this study all surfaces were prepared specifically to try to produce accurate macro- and micro-texture for the surfaces to ensure that the differences at the end of the wearing test reflect the true differences in the performance of the different surface mixtures. The test specimen fabrication discussed in section 2.7.5 was designed in regard to the surface finishing techniques to bring about these circumstances. The measured data from the BPT depicted in Figure 28.

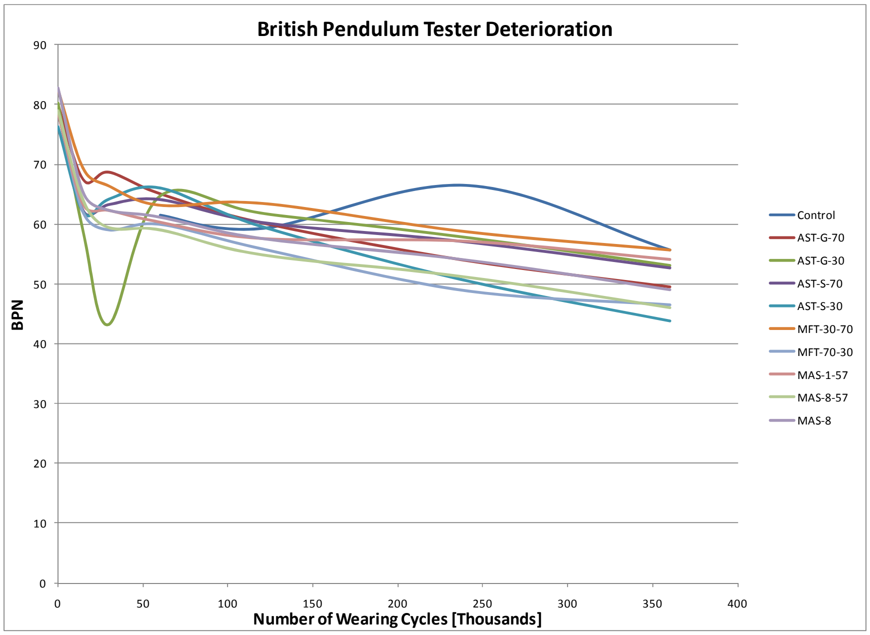

Figure 28. Progress of BPN data for all surfaces

It can clearly be observed from the figure that basically all surfaces had initially produced readings close to a nominal initial number. The initial BPN number averaged across the different surfaces was **78** with a standard deviation of **1.8**. This supports the efforts taken in the initial surface preparations to yield surfaces that deliver similar macro- and micro-textural features at the beginning of the study. A very similar pattern of BPN degradation to that of the degradation in DFT measurements over the entire course of surface wearing and polishing can be observed, as is illustrated in Figure 28, but the trends between the different surfaces are not clear. In fact, no clear trend can be observed, although a closer examination of the data shows that the same surfaces deliver marginally better results than other surfaces. The decline in the BPN measurements is better observed in Figure 29.

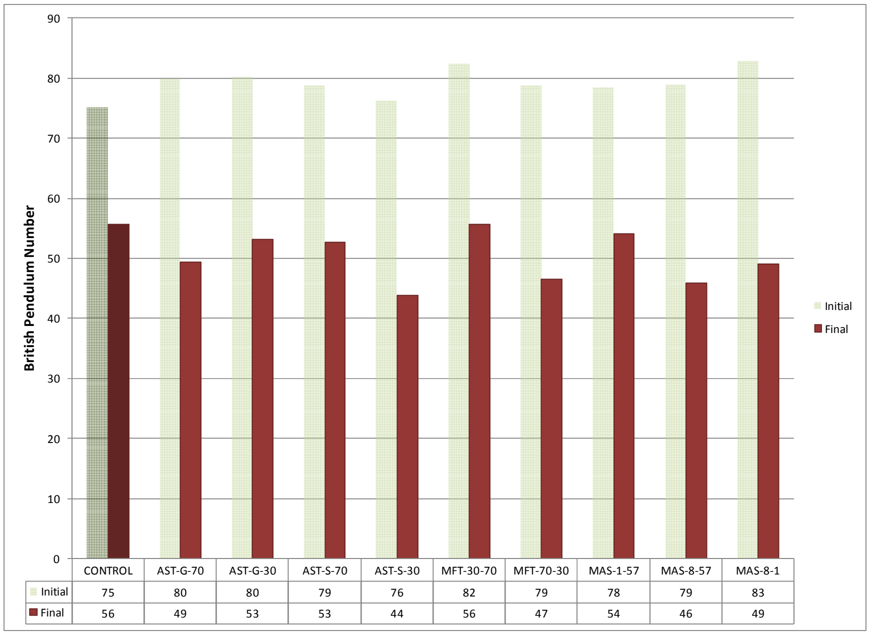

Figure 29. British Pendulum Tester measurement deterioration

4.3 Analysis of the CTM Data

The macro-texture of the surfaces was measured using a laser device that measures the pavement in the exact same physical area as is measured by the DFT device. The two devices therefore, form an ideal pair to produce the IFI friction index. The measurements of the macro-textural parameters of the surfaces are reported according to the mean profile depth measurement standards. The values measured by the CTM device generally follow the deterioration pattern of the BPN and DFT numbers. As has been indicated previously in the report, the importance of the MPD numbers is not only in the evaluation on their own merits but, more significantly, in their role in the international friction index and the PIARC friction model that allows the calculation of the E274 skid trailer measurements based on the IFI and the measured macro-texture numbers.

The macro-texture measurements and the deterioration in texture can be observed in Figure 30. The figure should be evaluated keeping in mind that all surfaces were prepared to produce minimal macro-textural features. Therefore it can be observed that all surfaces had calculated MPD values in the range of 0.3 to 0.5 mm (0.01 to 0.02 in). It also can be observed that these macro-texture readings were further reduced by only marginal numbers throughout the testing by the polishing machine. The ending measurement results show that the macro-texture of the surfaces after finishing the total number of 360,000 wearing cycles reduced MPD values to between almost the same limits. It also should be noted that that the largest drops in macro-texture measurements can be observed on those surfaces that had larger values to begin with, while the surfaces with smaller initial MPD features produced only marginal drops in macro-texture levels.

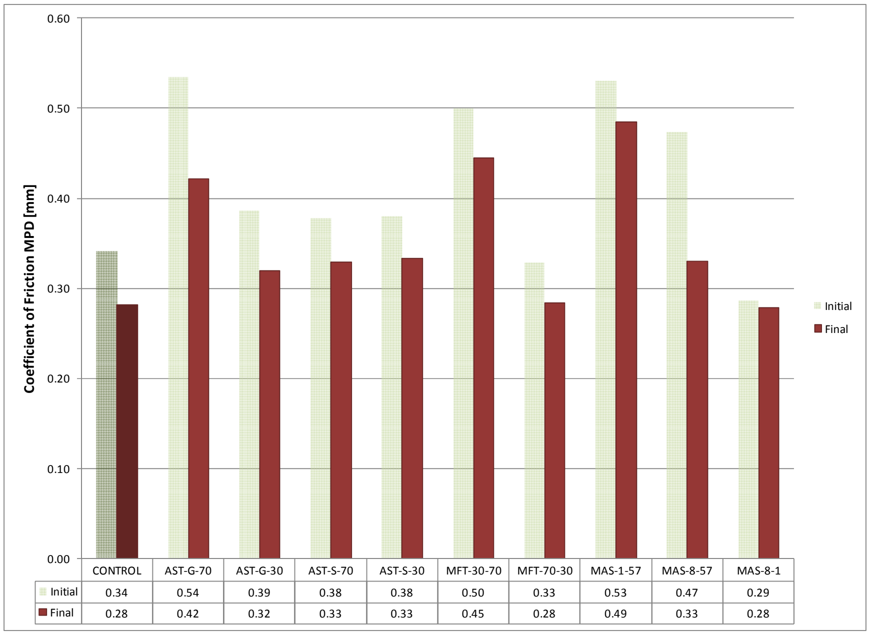

Figure 30. Deterioration of macro-texture of surfaces

One of the most important effects of the textural features of the tested surfaces is their effect on the frictional characteristics of the surface. The macro-texture of the surface together with micro-texture determines the surface's frictional performance in terms of travel speed of vehicles; the better the textural features the less the friction decline becomes at higher speeds. The dependency of friction on micro- and macro-texture plus vehicle speed (as explained in section 2.3) is illustrated in Figure 9. The speed dependency of friction can be very well described using equations 5 and 6. Using these equations one can depict the exact speed effects of the textural features of the surfaces using a single equation:

$$F(v) = F_{MeasurementSpeed} \cdot e^{\frac{MeasurementSpeed - v}{S_P}} \quad (9)$$

Equation 9 gives the relationship that can be used to evaluate the surface performance in terms of both texture and friction. Once a selected friction measurement together with the speed at which the friction is measured and the calculated speed parameter, *Sp*, from measured surface texture properties is inserted into equation 9, the surface friction can be calculated at any vehicle speed *v*.

Using the measures of the CTM device and the results of the PIARC experiment, we can calculate the *Sp* speed parameters for each of the studied surfaces. The speed numbers can be determined for each level of wear, thus allowing the analysis of the deterioration of the surface's friction-speed performance in terms of wear. The ASTM E1960 standard (ASTM, 2007) describes the equation to calculate the *Sp* speed number and gives the final equation to be used. The equation given in this ASTM standard is based on the PIARC friction model (PIARC, 1995) and is given in the following equation:

$$S_p = 14.2 + 89.7 \cdot MPD \qquad 10$$

Based on this equation the relevant *Sp* speed number, *Sp*, of the friction model can be calculated. The derived speed constants for all of the surfaces at each stage of the wearing cycle are given in Table 19.

Table 19. Complete table of PIARC speed constants

	CONT-ROL	AST-G-70	AST-G-30	AST-S-70	AST-S-30	MFT-30-70	MFT-70-30	MAS-1-57	MAS-8-57	MAS-8-1
Initial	44.77	62.19	48.88	48.13	48.28	59.05	43.65	61.74	56.65	39.91
15 Thousand Wearing Cycles	38.56	52.17	44.25	42.60	44.25	50.82	39.31	55.31	44.84	39.91
30 Thousand Wearing Cycles	41.70	50.37	43.35	41.11	46.49	51.27	38.86	56.06	45.14	37.97
60 Thousand Wearing Cycles	37.82	53.22	41.70	39.98	45.70	52.02	39.16	56.95	43.65	37.37
120 Thousand Wearing Cycles	39.87	52.62	43.95	38.56	43.05	51.27	40.81	58.00	45.59	38.41
240 Thousand Wearing Cycles	41.11	50.37	44.25	42.30	45.14	53.66	38.86	55.91	44.84	38.86
360 Thousand Wearing Cycles	39.46	52.02	42.90	43.72	44.10	54.11	39.61	57.70	43.80	39.16

A better visual representation of the data in Table 19 is a graph that gives an overview of the speed numbers as a function of wearing cycles. The graph is presented in Figure 31.

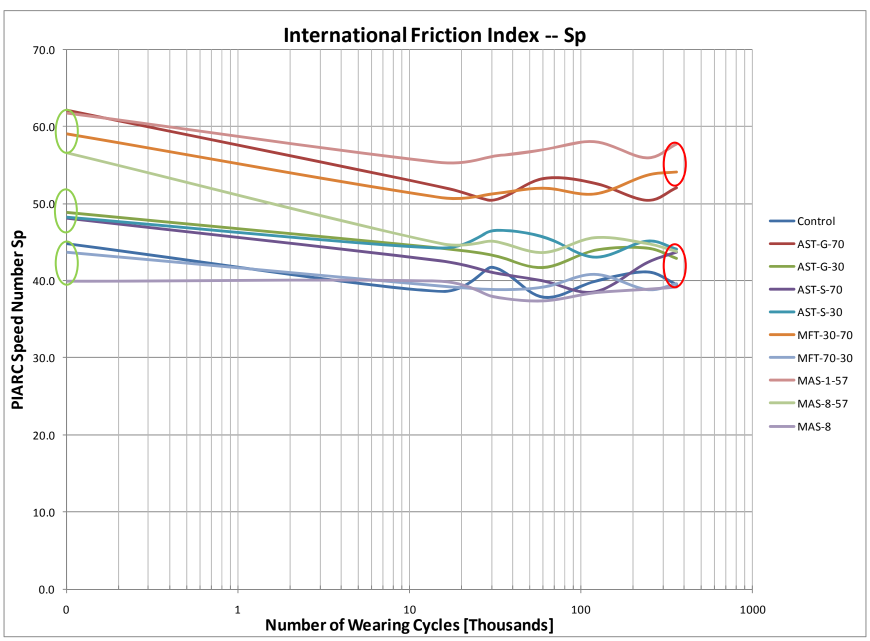

Figure 31. PIARC speed number of IFI for all surfaces

It can be clearly observed from Figure 31 that the tested surfaces form three distinct groups initially for which the measured speed numbers within each group are located very close, indicated by the green ovals in the figure. The three groups of surfaces at the initial conditions are in order of performance:

1. MAS-1-57, AST-G-70, MFT-30-70, MAS-8-57 — **Best** performers in terms of **Sp**.
2. AST-G-30, AST-S-30 and AST-S-70 — **Medium** performers in terms of **Sp**.
3. Control, MFT-70-30 and MAS-8 — **Low** performers in terms of **Sp**.

Throughout the wearing cycles these performances are altered by the polishing and wear effects and somewhat changed. At the end of the wearing process two distinctively different groups of the surfaces have emerged. The difference in their friction-speed relationship performance is relatively high, as indicated by the red ovals in Figure 31. The two groups of surfaces at the final conditions after the completed wearing cycles are in the order of their performance:

1. MAS-1-57, AST-G-70, and MFT-30-70 — **Best** performers in terms of **Sp**.
2. AST-G-30, AST-S-30 and AST-S-70, MAS-8-57, Control, MFT-70-30 and MAS-8 — **Low** performers in terms of **Sp**.

It can be observed from all the previous analysis, but particularly from the different speed measurements of the DFT and the surface performance — **both** in absolute terms and percentage friction deteriorations at the different speeds and the performance of the surfaces in regard to speed numbers (friction-speed relationships) — that a pattern is emerging. Three surfaces are outperforming the others by a relatively great margin. These three surfaces are:

MAS-1-57, AST-G-70, and MFT-30-70

4.4 Putting it All Together

In this section we are going to compile the results of all measurements and the analysis of the individual measuring processes to calculate and analyze the surfaces in regard to their performance in terms of the international friction index. The friction indexes then will be used in accordance with the ASTM standards and the PIARC friction harmonization procedure to calculate the friction values of the surfaces according to the ASTM E274 friction trailer reading (commonly known as K.J. Law Friction Tester). The calculated friction values will be presented in terms of the FN40S numbers corresponding to the friction measurements on real road surfaces by the K.J. Law tester using a 0.5 mm water depth and the ASTM E524 blank friction measurement tire.

4.4.1 Analysis of the IFI

Using the measurement of the DFT device and the results of the PIARC experiment together with the given standardized equations of the relevant ASTM standard E1960 (ASTM, 2007) we can calculate the **F60** friction index parameter of the international friction index for each of the studied surfaces. The F60 indices can be determined for each level of wear, thus allowing the analysis of the performance of the surface's high-level absolute friction performance in terms of wear. The ASTM E1960 standard (ASTM, 2007) describes the equation to calculate the **F60** friction index and gives the final equation to be used. The equation given in this ASTM standard is based on the PIARC friction model (PIARC, 1995) and is given in the following equation:

$$F60 = 0.081 + 0.732 \cdot e^{\frac{-40}{S_P}} \tag{11}$$

Based on this equation the relevant **F60** speed number of the IFI friction model can be calculated. The derived F60 indices for all the surfaces at each stage of the wearing cycle are given in Table 20.

Table 20. Complete table of PIARC F60 indices

	CONTROL	AST-G-70	AST-G-30	AST-S-70	AST-S-30	MFT-30-70	MFT-70-30	MAS-1-57	MAS-8-57	MAS-8-1
Initial	0.27	0.36	0.29	0.27	0.30	0.40	0.28	0.32	0.37	0.25
15 Thousand Wearing Cycles	0.23	0.30	0.24	0.24	0.26	0.34	0.23	0.28	0.28	0.25
30 Thousand Wearing Cycles	0.23	0.28	0.23	0.24	0.26	0.34	0.22	0.27	0.28	0.24
60 Thousand Wearing Cycles	0.21	0.29	0.22	0.23	0.25	0.34	0.22	0.26	0.27	0.23
120 Thousand Wearing Cycles	0.22	0.28	0.22	0.21	0.24	0.33	0.22	0.26	0.25	0.22
240 Thousand Wearing Cycles	0.21	0.26	0.23	0.22	0.23	0.33	0.20	0.25	0.26	0.22
360 Thousand Wearing Cycles	0.20	0.26	0.22	0.22	0.23	0.32	0.20	0.25	0.24	0.21

A better visual representation of the data in Table 20 is a graph that gives an overview of the derived friction indices of the international friction index numbers as a function of wearing cycles. The graph is presented in Figure 32.

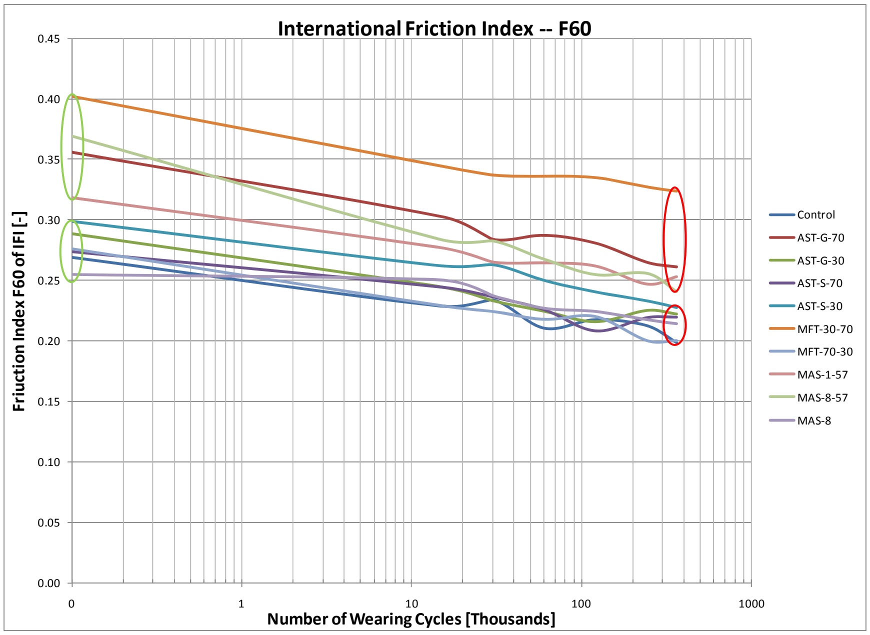

Figure 32. PIARC F60 index of IFI for all surfaces

It can be observed from the graph in Figure 32 that the tested surfaces, unlike in the case of the **Sp** speed numbers, do not form very clear groups but are more arranged along a range at the initial surface measurements. Nevertheless, there are four surfaces that deliver clearly superior performance compared to the other at the initial stage of the experiment, indicated by the green ovals in the figure. These surfaces are:

1. MFT-30-70, MAS-8-57, AST-G-70 and MAS-1-57 — **Best** performers in terms of **F60**.
2. AST-G-30, AST-S-30 and AST-S-70, Control, MFT-70-30 and MAS-8 — **Low** performers in terms of **F60**.

Throughout the wearing cycles these performances are altered by the polishing and wear effects by a considerable amount in absolute terms, but in terms of the relative performance of the surfaces the changes are very little and somewhat altered. At the end of the wearing process two distinctively different groups of the surfaces have emerged, similarly to that of the analysis of the speed numbers. The difference in their F60 friction index performance is relatively high, as indicated by the red ovals in Figure 32. The two groups of surfaces at the final conditions after the completed wearing cycles are, in the order of their performance:

1. MFT-30-70, AST-G-70, MAS-1-57, and MAS-8-57 — **Best** performers in terms of **F60**.
2. AST-G-30, AST-S-30 and AST-S-70, Control, MFT-70-30 and MAS-8 — **Low** performers in terms of **F60**.

It can be observed from all of the previous analysis, but particularly from the different speed measurements of the DFT and the surface performance —**both** in absolute terms and percentage friction deteriorations at the different speeds and the performance of the surfaces in regard to

IFI's friction index **F60,**— that the previously observed pattern is strengthened by the analysis of the F60 friction parameter. Three surfaces are outperforming the others by a relatively great margin. These three surfaces are:

MAS-1-57, AST-G-70, and MFT-30-70

Now that we have calculated and analyzed the two indices of the international friction index we can put it all together and paint a complete picture of the frictional performance of the surfaces in the study with regard to their performance against wearing and polishing effects using the model of the IFI. The model, discussed earlier, captures the surface performance in terms of both texture and friction and gives a complete picture of frictional surface characteristics as the friction-vehicle speed relationship.

4.4.2 Complete Surface Performance

Using the results of the previous analysis chapters and the calculated international friction index pairs (F60, Sp), we can now see a complete surface performance of each studied concrete mixture throughout the entire wearing study in a concise and comparative manner. We are going to use the graphs of the calculated friction curves using the IFI index numbers and plot the performance of each surface relative to the control surface's performance.

Figure 33 through Figure 36 give a complete picture of the surfaces' performance throughout the entire wearing cycle and depict the performance against the performance of the control surface. In each of the figures there are two shaded areas, (a) a green shaded area depicting the performance of the control surface, and (b) a red shaded area giving the performance of the corresponding individual surface in contrast to the control surface. The shaded areas for both the control surface and the paired studied surface give the range of surface friction performance throughout the wearing and polishing process. The top line in the shaded area represents the starting condition of the surfaces while the bottom boundary of the shaded area represents the final surface condition at the end of the wearing and polishing process. The relative positioning of the two shaded areas provide clear and easily observable comparative tool to contrast and match up the different concrete mixture performances against the control surface.

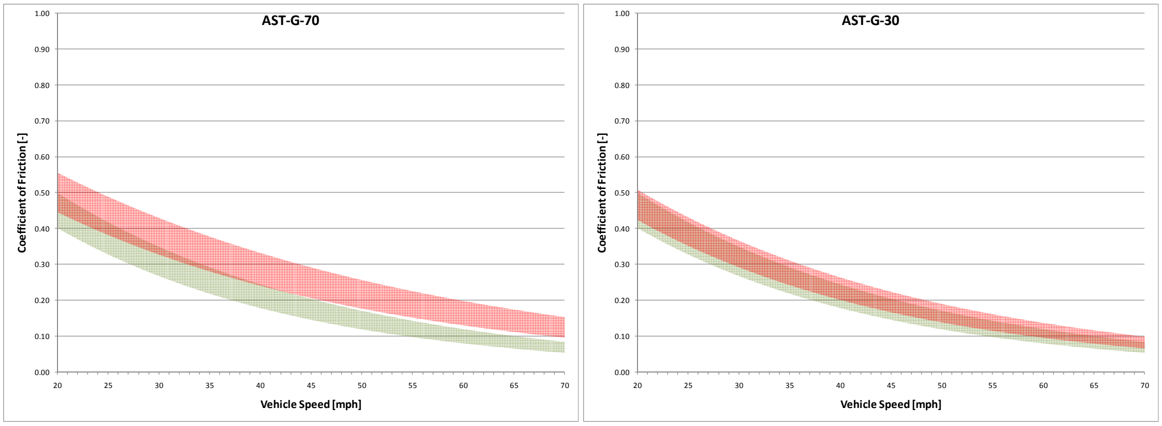

Figure 33. Complete surface performance of AST-G mixtures

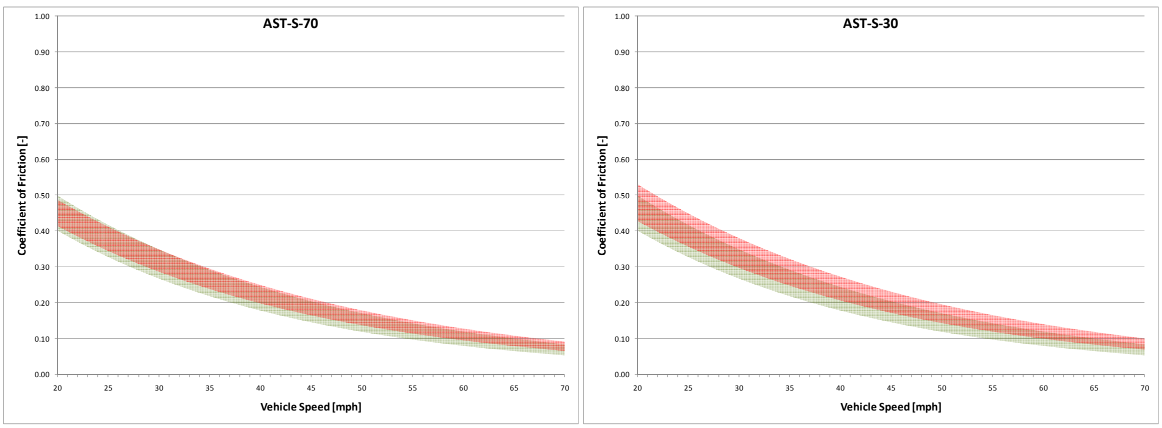

Figure 34. Complete surface performance of AST-S mixtures

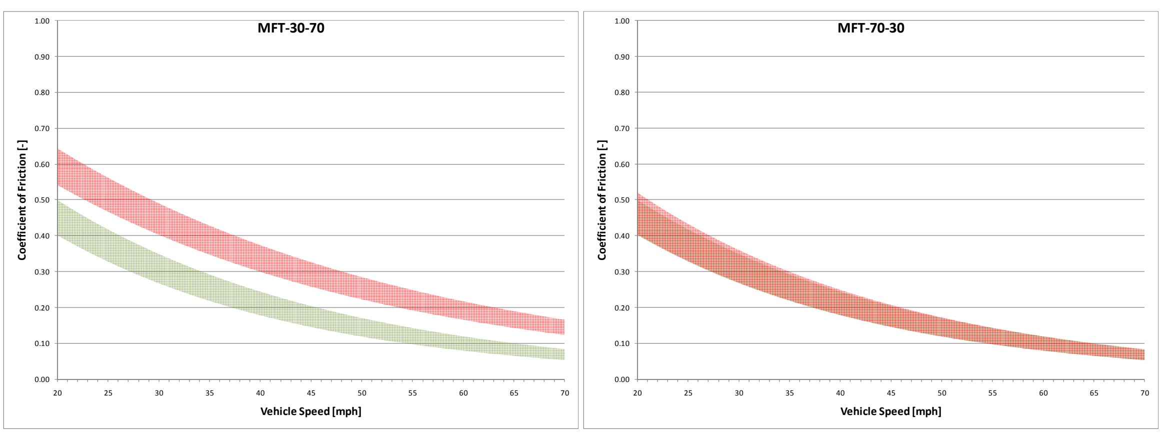

Figure 35. Complete surface performance of MFT mixtures

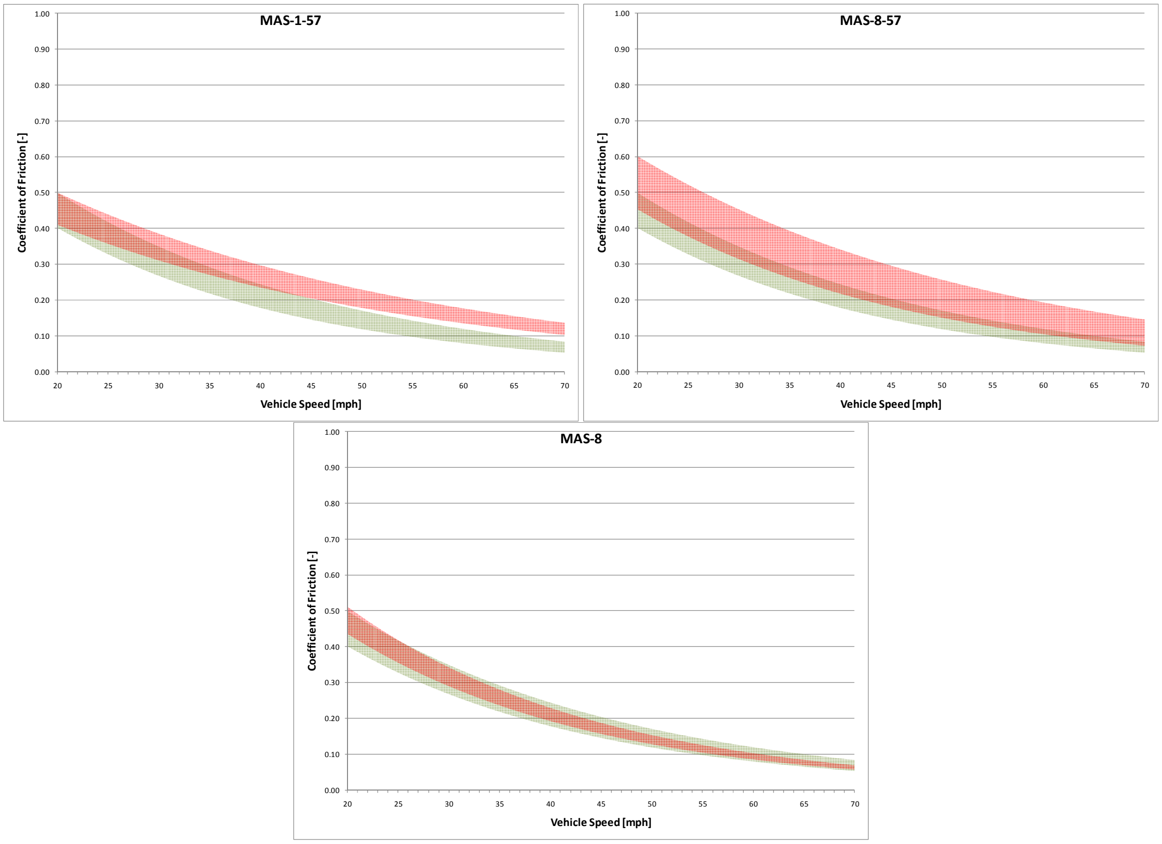

Figure 36. Complete surface performance of MAS mixtures

From the figures representing the complete frictional and textural performance of the different mixtures in the study, in both comparative numbers relative to the control surface and in absolute terms regarding differences amongst the mixtures, very much the same pattern of good surface performance emerged as observed in the previous analysis portions of the study. The four best performing surfaces, in **absolute, relative to control surface and resistance to wear and polishing** terms, are:

MAS-1-57, MAS-8-57, AST-G-70, and MFT-30-70

The superior performance of these surfaces can be observed in that the comparative friction performance of these mixtures consistently stays well above the control surface and over a large-range of vehicle speed ranges. The absolute initial frictional performance of these surfaces is higher than those of the others. At the same time, the frictional performance of these surfaces exceed the performance of the others in absolute terms at the end of the wearing and polishing process by a great margin.

Using the IFI indices the surface frictional properties also can be expressed in terms of projected E274 friction trailer reading at a 40 mph speed. This tool gives data that can easily be compared to the surface performance of real roads, as measured by an ASTM skid trailer. In the following section, the data and analysis of the projected data is presented.

4.4.3 Analysis of Projected E274 Skid Resistance Data FN40S

The IFI friction indices, together with the results of the PIARC (PIARC, 1995) friction harmonization experiment, provide a solid foundation to calculate and analyze projected ASTM skid trailer data. The PIARC experiment established a robust mathematical process and determined the necessary physical parameters that allow the use of the available IFI index pairs to calculate the projected ASTM skid trailer measurements with high confidence. The whole procedure and the background mathematical process are discussed in detail in section 2.4.4 and explained with mathematical background in the Interim Literature Review Report of this study (see Appendix C). The results of the mathematical processes to translate the obtained IFI friction values into a projected FN40S friction reading of the E274 skid trailer can be summarized in a single mathematical equation, given in equation X

$$FN40_{SmoothTire} = \frac{F60 - A_{IFI}}{B_{IFI}} \cdot \frac{1}{e^{-\frac{-4.36}{S_P}}} \qquad (12)$$

Where:

$FN40_{SmoothTire}$	= the projected ASTM Skid Trailer Measurement at 40mph with the smooth treaded ASTM E524 tire (SN40 divided by 100)
F60	= the friction index of IFI
S_P	= the speed number index of IFI
A_{IFI}; B_{IFI}	= parameters established by the PIARC International Experiment

The parameter values in equation 12 are the following (from PIARC, 1995):

$$A_{IFI} = 0.045; \; B_{IFI} = 0.925 \qquad (13)$$

Using equation 12 with the parameters from formula 13, together with the measurement results from the experiment yielding the IFI numbers at the end of the analysis for all surfaces at the different stages of the wearing cycle, we can calculate the projected measurement values of the ASTM skid trailer.

The determined skid trailer measurement projections for the final stage of the wearing and polishing process are presented in Table 21.

Table 21. Projected ASTM skid trailer measurements of all surfaces

	FN40S									
	CONTROL	AST-G-70	AST-G-30	AST-S-70	AST-S-30	MFT-30-70	MFT-70-30	MAS-1-57	MAS-8-57	MAS-8-1
Initial	0.22	0.31	0.24	0.23	0.25	0.36	0.23	0.28	0.32	0.20
15 Thousand Wearing Cycles	0.18	0.26	0.20	0.19	0.21	0.30	0.18	0.23	0.23	0.20

30 Thousand Wearing Cycles	0.18	0.24	0.18	0.19	0.21	0.29	0.17	0.22	0.23	0.19
60 Thousand Wearing Cycles	0.16	0.24	0.17	0.18	0.20	0.29	0.17	0.22	0.22	0.18
120 Thousand Wearing Cycles	0.17	0.23	0.17	0.16	0.19	0.29	0.17	0.22	0.21	0.17
240 Thousand Wearing Cycles	0.16	0.22	0.18	0.17	0.18	0.28	0.15	0.20	0.21	0.17
360 Thousand Wearing Cycles	0.15	0.21	0.17	0.17	0.18	0.28	0.15	0.21	0.19	0.16

A better visual representation of the data in Table 21 is a graph that gives an overview of the derived friction values of the ASTM skid trailer as a function of wearing cycles. The graph is presented in Figure 37. The data in the figure are presented for better compatibility as **SN40S,** which are basically 100 times the FN40S friction coefficients. The graph also only depicts the initial and the final results of the measured data. It gives a comprehensive picture of the surface performances in terms of the projected ASTM skid trailer measurements.

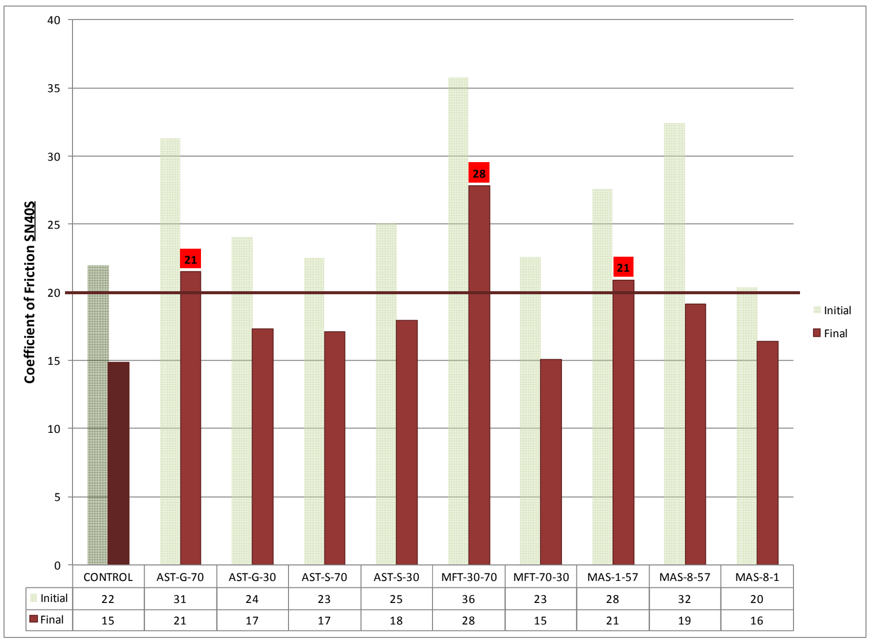

Figure 37. SN40S friction number of tested surfaces

In Figure 37 the acceptable SN40 friction level is indicated with a maroon colored line at the SN40=20 friction level.

Many state agencies use the friction numbers measured by the ASTM E274 friction trailer using the ribbed friction measurement tires for establishing minimum friction levels of roads due to historical reasons. The inability of the ribbed measurement tires (AST E501 tire) to measure and report frictional deterioration due to the lack of macro-texture has been discovered in 1992 and has been amply demonstrated in research projects. Although many state agencies are using and reporting friction levels using the ribbed tires more and more state departments and other highway organizations have started to use the smooth measurement tires (AST E524 tire) and establish minimum friction levels according to the PIARC and ASTM recommendations in the past years. The established friction levels using the smooth tires and somewhat variable but in all cases have been set close to the SN40S=20 level. In this study the SN40S=20 minimum friction level is used for threshold based on the ASTM recommendation (ASTM, 2005

"*Considerations in Developing a Network Pavement Inventory Friction Test Program for a State Highway Agency*"). The use of the smooth friction readings at 40mph speed allow the representation of frictional characteristics of the studied pavements taking both the micro- and macro-textural effect into account and thus truly reflecting the slippery when wet conditions on the surfaces.

It can be observed clearly that even though **all** surfaces exceeded the threshold friction level in the initial stage of the testing experiment, only **three (3)** surfaces retained enough frictional properties to stay above the threshold throughout the wearing and polishing process.

Again, a very similar pattern can be observed in the projected SN40S data, as in the previous analyses. The top performing surfaces are:

MFT-30-70, AST-G-70, and MAS-1-57

The best surface proved to be the MFT-30-70 mixture, which exceeded the required threshold level of SN40 by a relatively large margin at the end of the polishing cycles, while the control surface had diminished friction levels far below the threshold value.

The data also shows clear trends with regard to the variation of surface characteristics within each study groups. By comparing the final surface characteristics measurements of the different surfaces within each group unambiguous patterns can be observed. The maximum aggregate size surface group shows within itself a monotonic declining performance of the surfaces with decreasing aggregate size and gradation. The surface mix MAS-1-57 had performed better than MAS-8-57 which in turn performed better than MAS-8. The same performance pattern can observed within the aggregate substitution study. The surface of the mixture with higher gravel content performed significantly better than that with lower. The AST-G-70 mix had performed substantially better than the mix AST-G-30 the actual difference proved to be large enough to provide enough additional friction such that the AST-G-70 surface mix is one of the three mixtures exceeding the friction requirements. The mortar fraction study similarly produced a pattern where the higher the fine aggregate fraction is the higher the surface performance becomes. In this case the actual difference is very large. The MFT-30-70 mixture with 70% fine aggregate content far surpasses the MFT-70-30 surface with only 30% fine aggregate content and all other studied surfaces.

CHAPTER 5 **CONCLUSIONS**

Based on the results of the experiment and the outcome of data analysis the following conclusions can be drawn:

1. The determined surface mixtures, wearing and polishing process, and the fabrication of test surfaces, have delivered the expected results of:
    a. Comparable and deterministic testing;
    b. Relevant and significant polishing and wearing effects
    c. Tendencies according to expectations; and
    d. Results that are verifiable and follow common patterns with high confidence.
2. The selected measurement techniques and equipment, together with the chosen analysis methodology, have proven to:
    a. Be robust in processing and statistical terms;
    b. Deliver relevant and informative data;
    c. Be related to practice and theory; and
    d. Provide a solid and sound foundation for absolute and comparative study of the different surfaces and their frictional performance and resistance to wear and polishing.
3. The main results of the study show the following conclusions:

I. The examined surfaces had frictional properties above the required threshold levels despite the purposefully manufactured minimal macro-textural features.

II. All surfaces showed consistent and monotonic degradations in both texture and friction characteristics throughout the wearing and polishing process.

III. Only three surfaces showed significant resistance to polishing and consistently high performance in terms of frictional and texture characteristics.

IV. A clear and logical trend can be observed within each mixture design in regard to the variations in the mixture properties. These trends are clearly observable and can be used to approximate the performance of different mix designs.

V. The three clearly superior mix designs are the following:

1. MFT, where higher fine aggregate content delivers better performance

2. AST-G, where higher gravel aggregate content delivers better performance, and

3. MAS where higher maximum coarse aggregate size delivers better performance.

VI. The three superior mix designs show substantial benefits in comparison to the other tested and analyzed designs. The estimated wear acceleration factor of the MMLS III machine with the special polishing tires is 500 times. Thus, the research study is estimated to have simulated and average daily traffic of 16,500 for a span of 30 years. The mix design with high fine aggregate content delivered an estimated FN40S=28 at the end of the wearing and testing cycle while both the 70% gravel aggregate content and the maximum aggregate size of AASHTO gradation #1 surfaces yielded FN40S=21. Although these numbers exceed the minimum friction criteria the MFT surface has clearly delivered the best result by far surpassing the minimum set criteria.

REFERENCES AND BIBLIOGRAPHY

American Association of State Highway and Transportation Officials (AASHTO). 1976. Guidelines for Skid-Resistant Pavement Design, Task Force for Pavement Design.

American Society for Testing and Materials, 1999 "Accelerated Polishing of Aggregates Using the British Wheel," ASTM Standard Test Method D-3319, Book of ASTM Standards, Volume 04.03, Philadelphia, PA, 1999.

American Society for Testing and Materials, 2003 "Insoluble Residue in Carbonate Aggregates," ASTM Standard Test Method D-3042-03, Book of ASTM Standards, Volume 04.03, Philadelphia, PA, 2003

American Society for Testing and Materials 2003 "Measuring Surface Friction Properties Using the British Pendulum Tester" ASTM Standard Test Method E-303-93 (2003), Book of ASTM Standards, Volume 04.03, Philadelphia, PA, 2005.

American Society for Testing and Materials, 2005 "Standard Test Method for Measuring Pavement Macrotexture Properties Using the Circular Track Meter," ASTM Standard Test Method E-2157-01, Book of ASTM Standards, Volume 04.03, Philadelphia, PA

American Society for Testing and Materials, 2005 "Considerations in Developing a Network Pavement Inventory Friction Test Program for a State Highway Agency" ASTM International Journal of Testing and Evaluation, Volume 33, Issue 5 (September 2005)

American Society for Testing and Materials 2007 "Standard Practice for Calculating International Friction Index of a Pavement Surface" ASTM Standard Test Method E-1960-07, Book of ASTM Standards, Volume 04.03, Philadelphia, PA.

American Society for Testing and Materials, 2009 "Measuring Pavement Surface Frictional Properties Using the Dynamic Friction Tester", ASMT Standard Test Method E 1911-98 (2002), Book of ASTM Standards, Volume 04.03, Philadelphia, PA.

Andresen, A. and Wambold, J.C. 1999, "Friction Fundamentals, Concepts, and Methodology," Transportation Development Centre, Transport Canada, TP 13837E

Dahir, S.H. and J.J. Henry. 1978. Alternatives for the Optimization of Aggregate and Pavement Properties Related to Friction and Wear Resistance, Report No. FHWA-RD-78-209, Federal Highway Administration (FHWA), Washington, D.C.

Davis, R.M. 2001. Comparison of Surface Characteristics of Hot-Mix Asphalt Pavement Surfaces at the Virginia Smart Road, Thesis submitted to the faculty of Virginia Polytechnic Institute and State University, Blacksburg, Virginia.

Dewey, G. R., Robords, A. C., Armour, B. T., and Muethel, R. (2001) “Aggregate Wear and Pavement Friction” Transportation Research Board, Annual Meeting CD-ROM, 17p.

Do, M., Tang, Z., Kane, M., and Larrad, F. (2007) “Pavement Polishing-Development of a Dedicated Laboratory Test and its Correlation with Road Results” Wear 263, pp. 36-42.

Flintsch, G.W., I.L. Al-Qadi, C.A. Via Jr., R. Davis, and K.K. McGhee. 2002. “Effect of HMA Properties on Pavement Surface Characteristics,” Paper presented at *Pavement Evaluation 2002 Conference*, Roanoke, Virginia.

Flintsch G.W., E. De Leon, K.K. McGhee, and I.L. Al-Qadi. 2003. “Pavement Surface Macro-texture Measurement and Application,” Transportation Research Board (TRB), Washington, D.C.

Folliard, K.J. and K.D. Smith. 2003. “Aggregate Tests for Portland Cement Concrete Pavements: Review and Recommendations,” September edition (No. 281) of *NCHRP Research Results Digest*, National Cooperative Highway Research Program (NCHRP), Washington, D.C.

Gransberg, D. and D.M.B. James. 2005. “Chip Seal Best Practices,” *NCHRP Synthesis 342*, National Cooperative Highway Research Program (NCHRP), Washington, D.C.

Henry, J.J. 2000. “Evaluation of Pavement Friction Characteristics—A Synthesis of Highway Practice,” *NCHRP Synthesis 291*, Transportation Research Board, Washington, D.C.

Kandhal, P.S. and F. Parker Jr. 1998. 1997. *Aggregate Tests Related to Asphalt Concrete Performance in Pavements*, NCHRP Report 405, National Cooperative Highway Research Program (NCHRP), Washington, D.C.

Kulakowski, B.T., D.W. Harwood, D.R. Hiltunen, J.M. Mason, Jr., W.E. Meyer, S.L. Simoneau, and J.C. Wambold. 1990. “Skid Resistance Manual,” Report No. PTI 9016, Pennsylvania State University, University Park, Pennsylvania.

Nitta, N. Saito, K. and Isozaki, S. (1990) “Evaluating the Polishing Properties of Aggregates and Bituminous Pavement Surfaces by Means of the Penn State Reciprocating Polishing Machine” Surface Characteristics of Roadways, International Research and Technologies, ASTM SPT 1031, W. E. Meyer, and J. Reichert, Eds., American Society for Testing and Materials, Philadelphia, PA, pp. 113-126.

Panagouli, O.K., and Kokkalis, A.G. (1998). Skid Resistance and Fractal Structure of Pavement Surface. Chaos, Solutions & Fractals, 9(3), 493-505.

Permanent International Association of Road Congresses (PIARC). 1987. “Report of the Committee on Surface Characteristics,” *Proceedings of the 18th World Road Congress*, Brussels, Belgium.

Permanent International Association of Road Congresses (PIARC). 1995; Wambold, J.C., C.E. Antle, J.J. Henry, and Z. Rado. 1995. “International PIARC Experiment to Compare and Harmonize Texture and Skid Resistance Measurements,” AIPCR-01.04.T.

Rado, Z. 1994. “Analysis of Texture Models,” PTI Report No. 9510, PennsylvaniaTransportation Institute (PTI), Penn State University, State College, Pennsylvania.

Saito, K., T. Horiguchi, A. Kasahara, H. Abe, and J.J. Henry. 1996. “Development of Portable Tester for Measuring Skid Resistance and its Speed Dependency on Pavement Surfaces,” Transportation Research Record No. 1536, Transportation Research Board, Washington, D.C.

Sandberg, U. 1998. “Influence of Road Surface Texture on Traffic Characteristics Related to Environment, Economy, and Safety: A State-of-the-Art Study Regarding Measures and Measuring Methods,” VTI Report 53A-1997, Swedish National Road Administration, Borlange, Sweden.

Sandberg, U. and J.A. Ejsmont. 2002. *Tyre/Road Noise Reference Book*, ISBN 91-631-2610-9, Informex, Kisa, Sweden.

Voller, T. W., and Hanson, D. I. (2006) “Development of Laboratory Procedure for Measuring Friction of HMA Mixtures – Phase I,” Final Report of NCAT No. 06-06, National Center for Asphalt Technology.

Wallman, C.G. and H. Astrom. 2001. “Friction Measurement Methods and the Correlation Between Road Friction and Traffic Safety,” Swedish National Road and Transport Research Institute, VTI Meddelande 911A, Linkoping, Sweden.

Wambold, J.C., C.E. Antle, J.J. Henry, and Z. Rado. 1995. “International PIARC Experiment to Compare and Harmonize Texture and Skid Resistance Measurements,” AIPCR-01.04.T.

APPENDIX A: PHOTOGRAPHS OF TEST SURFACES

Initial Condition | After 120K Cycles | After 360K Cycles

MAS-1-57-1

Initial Condition | After 120K Cycles | After 360K Cycles

MAS-1-57-2

Initial Condition | After 120K Cycles | After 360K Cycles

MAS-8-1

Initial Condition After 120K Cycles After 360K Cycles

MAS-8-2

Initial Condition After 120K Cycles After 360K Cycles

MAS-8-57-1

Initial Condition After 120K Cycles After 360K Cycles

MAS-8-57-2

Initial Condition After 120K Cycles After 360K Cycles

AST-G-30-1

Initial Condition After 120K Cycles After 360K Cycles

AST-G-30-2

Initial Condition After 120K Cycles After 360K Cycles

AST-G-70-1

Initial Condition After 120K Cycles After 360K Cycles

AST-G-70-2

Initial Condition After 120K Cycles After 360K Cycles

AST-S-30-1

Initial Condition After 120K Cycles After 360K Cycles

AST-S-30-2

Initial Condition After 120K Cycles After 360K Cycles



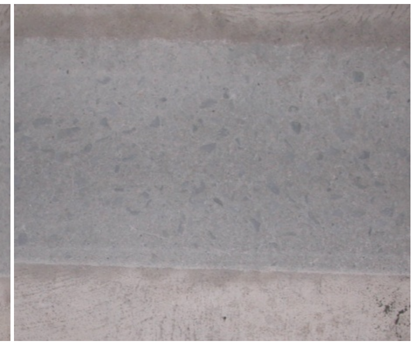

AST-S-70-1

Initial Condition After 120K Cycles After 360K Cycles



AST-S-70-2

Initial Condition After 120K Cycles After 360K Cycles

?


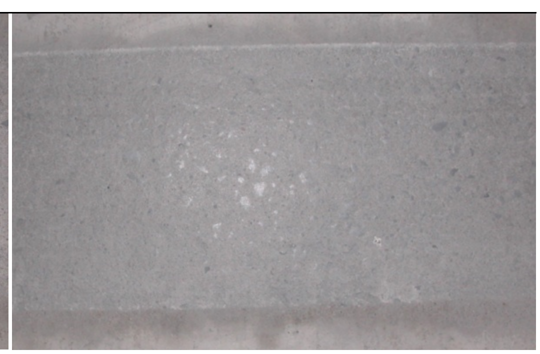

Control 57-1

Initial Condition After 120K Cycles After 360K Cycles

?

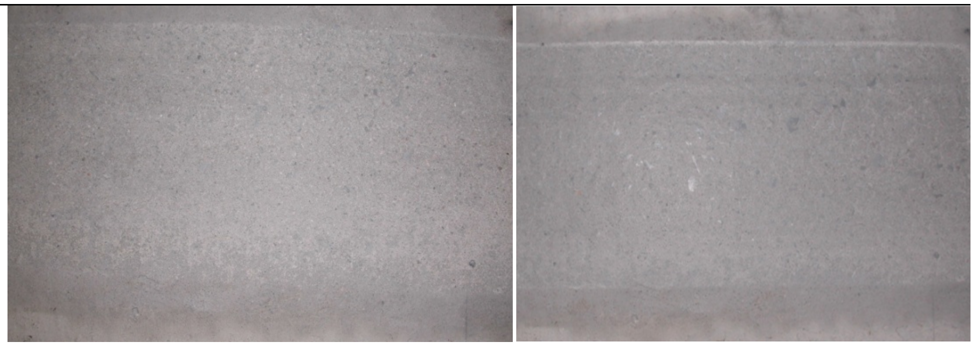

Control 57-2

Initial Condition After 120K Cycles After 360K Cycles

MFT-30-70-1

Initial Condition After 120K Cycles After 360K Cycles

MFT-30-70-2

Initial Condition After 120K Cycles After 360K Cycles

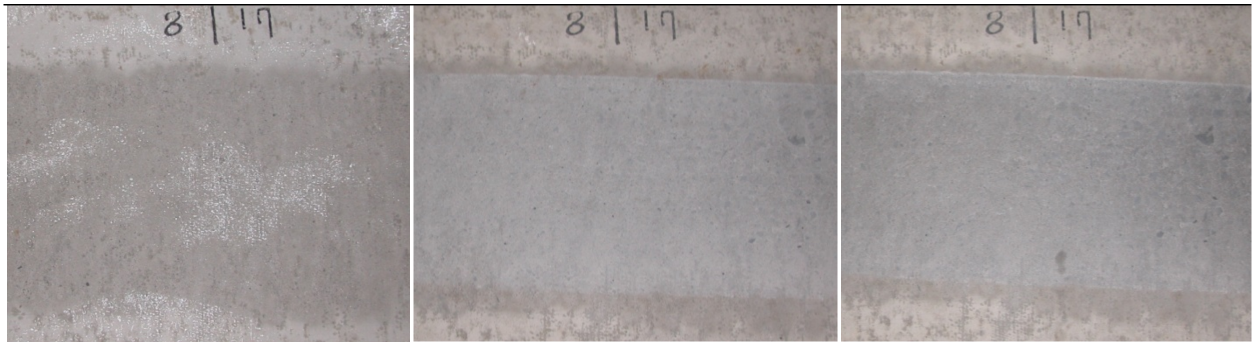

MFT-70-30-1

Initial Condition After 120K Cycles After 360K Cycles

MFT-70-30-2

APPENDIX B: TABULATED EXPERIMENT DATA

Friction Measurements with the DFTester Device

Surface	Speed of 65 km/h (40 mph)					Speed of 45 km/h (28 mph)					Speed of 20 km/h (12.5 mph)				
	1	2	3	Ave.	STD	1	2	3	Ave.	STD	1	2	3	Ave.	STD
CONTROL57-1-INI	0.56	0.53	0.51	0.54	0.025	0.58	0.55	0.53	0.55	0.025	0.67	0.63	0.61	0.64	0.029
CONTROL57-2-INI	0.60			0.60		0.54			0.54		0.62			0.62	
CONTROL57-1-15K	0.38	0.37	0.35	0.37	0.015	0.41	0.39	0.38	0.39	0.019	0.52	0.50	0.48	0.50	0.021
CONTROL57-2-15K	0.48	0.43	0.41	0.44	0.036	0.53	0.49	0.47	0.50	0.034	0.66	0.63	0.60	0.63	0.032
CONTROL57-1-30K	0.41	0.35	0.31	0.36	0.051	0.42	0.36	0.34	0.38	0.038	0.50	0.46	0.44	0.47	0.030
CONTROL57-2-3OK	0.45	0.40	0.37	0.40	0.037	0.48	0.45	0.42	0.45	0.026	0.62	0.58	0.56	0.59	0.032
CONTROL57-1-60K	0.32	0.28	0.27	0.29	0.027	0.34	0.31	0.29	0.31	0.025	0.45	0.42	0.39	0.42	0.029
CONTROL57-2-60K	0.39	0.35	0.34	0.36	0.027	0.42	0.39	0.37	0.39	0.022	0.56	0.54	0.51	0.53	0.026
CONTROL57-1-120K	0.29	0.26	0.25	0.26	0.020	0.31	0.29	0.27	0.29	0.018	0.41	0.40	0.38	0.40	0.014
CONTROL57-2-120K	0.33	0.33	0.33	0.33	0.004	0.38	0.38	0.36	0.37	0.008	0.52	0.52	0.51	0.52	0.009
CONTROL57-1-240K	0.23	0.23	0.24	0.23	0.004	0.25	0.25	0.26	0.25	0.006	0.32	0.32	0.34	0.33	0.010
CONTROL57-2-240K	0.29	0.26	0.26	0.27	0.017	0.33	0.31	0.31	0.32	0.011	0.47	0.46	0.45	0.46	0.011
CONTROL57-1-360K	0.19	0.19	0.20	0.19	0.004	0.21	0.22	0.21	0.22	0.001	0.29	0.30	0.30	0.30	0.005
CONTROL57-2-360K	0.20	0.21	0.21	0.21	0.006	0.27	0.28	0.27	0.27	0.006	0.39	0.39	0.38	0.39	0.006
AST-G-70-1-INI	0.63	0.62	0.60	0.62	0.013	0.66	0.64	0.63	0.64	0.011	0.75	0.74	0.73	0.74	0.012
AST-G-70-2-INI	0.64	0.62	0.60	0.62	0.018	0.64	0.62	0.61	0.62	0.016	0.73	0.70	0.69	0.71	0.018
AST-G-70-1-15K	0.52	0.50	0.49	0.50	0.019	0.59	0.55	0.53	0.56	0.031	0.68	0.65	0.63	0.65	0.025
AST-G-70-2-15K	0.54	0.49	0.47	0.50	0.033	0.57	0.52	0.49	0.53	0.042	0.66	0.61	0.59	0.62	0.038
AST-G-70-1-30K	0.46	0.45	0.45	0.45	0.008	0.51	0.49	0.48	0.49	0.016	0.60	0.58	0.56	0.58	0.016
AST-G-70-2-30K	0.47	0.44	0.43	0.44	0.020	0.50	0.47	0.45	0.47	0.025	0.58	0.55	0.53	0.55	0.028
AST-G-70-1-60K	0.43	0.42	0.41	0.42	0.008	0.47	0.46	0.44	0.46	0.016	0.57	0.55	0.54	0.55	0.014
AST-G-70-2-60K	0.40	0.38	0.37	0.38	0.018	0.45	0.43	0.40	0.43	0.022	0.54	0.53	0.50	0.52	0.017
AST-G-70-1-120K	0.41	0.38	0.38	0.39	0.018	0.45	0.42	0.41	0.43	0.024	0.58	0.55	0.52	0.55	0.028
AST-G-70-2-120K	0.39	0.37	0.36	0.37	0.014	0.41	0.39	0.38	0.40	0.016	0.52	0.48	0.48	0.49	0.021
AST-G-70-1-240K	0.35	0.34	0.33	0.34	0.010	0.38	0.38	0.36	0.37	0.010	0.51	0.49	0.48	0.49	0.019
AST-G-70-2-240K	0.32	0.30	0.30	0.31	0.011	0.36	0.36	0.35	0.36	0.008	0.46	0.44	0.43	0.44	0.011
AST-G-70-1-360K	0.33	0.31	0.31	0.32	0.012	0.36	0.35	0.34	0.35	0.009	0.46	0.44	0.43	0.45	0.012
AST-G-70-2-360K	0.29	0.29	0.29	0.29	0.001	0.32	0.32	0.32	0.32	0.005	0.41	0.40	0.40	0.40	0.007
AST-G-30-1-INI	0.55	0.54	0.53	0.54	0.010	0.58	0.58	0.56	0.57	0.012	0.68	0.66	0.60	0.65	0.041
AST-G-30-2-INI	0.54	0.51	0.49	0.51	0.025	0.58	0.55	0.54	0.56	0.023	0.67	0.64	0.59	0.63	0.042
AST-G-30-1-15K	0.44	0.39	0.36	0.40	0.037	0.46	0.42	0.40	0.42	0.033	0.59	0.55	0.46	0.53	0.066
AST-G-30-2-15K	0.40	0.37	0.35	0.37	0.022	0.44	0.40	0.39	0.41	0.027	0.53	0.49	0.43	0.49	0.050
AST-G-30-1-60K	0.41	0.36	0.33	0.37	0.036	0.42	0.39	0.38	0.39	0.021	0.51	0.49	0.42	0.47	0.047
AST-G-30-2-120K	0.36	0.33	0.31	0.33	0.024	0.38	0.35	0.34	0.36	0.022	0.47	0.44	0.39	0.43	0.041
AST-G-30-1-120K	0.33	0.31	0.30	0.31	0.018	0.37	0.37	0.34	0.36	0.019	0.47	0.44	0.38	0.43	0.047
AST-G-30-2-60K	0.35	0.32	0.31	0.33	0.020	0.39	0.36	0.34	0.36	0.026	0.48	0.45	0.39	0.44	0.046
AST-G-30-1-30K	0.28	0.28	0.27	0.28	0.008	0.33	0.30	0.29	0.31	0.018	0.41	0.40	0.34	0.38	0.040
AST-G-30-2-30K	0.28	0.24	0.22	0.25	0.034	0.30	0.25	0.24	0.26	0.030	0.37	0.33	0.26	0.32	0.054
AST-G-30-1-240K	0.32	0.31	0.30	0.31	0.013	0.36	0.34	0.33	0.34	0.016	0.45	0.43	0.37	0.42	0.045
AST-G-30-2-240K	0.25	0.26	0.24	0.25	0.009	0.30	0.30	0.29	0.30	0.009	0.39	0.38	0.32	0.36	0.038
AST-G-30-1-360K	0.33	0.32	0.28	0.31	0.026	0.38	0.35	0.33	0.35	0.027	0.44	0.43	0.37	0.41	0.036
AST-G-30-2-360K	0.28	0.27	0.25	0.27	0.012	0.32	0.30	0.29	0.30	0.017	0.40	0.39	0.33	0.37	0.039
AST-S-70-1-INI	0.66	0.62	0.60	0.63	0.030	0.66	0.63	0.61	0.64	0.026	0.68	0.65	0.63	0.66	0.024
AST-S-70-2-INI	0.58	0.55	0.53	0.55	0.021	0.56	0.54	0.52	0.54	0.018	0.58	0.56	0.54	0.56	0.018

Surface	Speed of 65 km/h (40 mph)					Speed of 45 km/h (28 mph)					Speed of 20 km/h (12.5 mph)				
AST-S-70-1-15K	0.33	0.36	0.36	0.35	0.018	0.44	0.44	0.43	0.43	0.003	0.59	0.59	0.59	0.59	0.004
AST-S-70-2-15K	0.36	0.31	0.30	0.32	0.030	0.42	0.37	0.36	0.38	0.032	0.55	0.50	0.48	0.51	0.039
AST-S-70-1-30K	0.44	0.36	0.37	0.39	0.039	0.50	0.42	0.41	0.44	0.048	0.67	0.59	0.57	0.61	0.054
AST-S-70-2-30K	0.31	0.30	0.29	0.30	0.008	0.35	0.34	0.33	0.34	0.009	0.49	0.48	0.46	0.48	0.016
AST-S-70-1-60K	0.33	0.33	0.33	0.33	0.002	0.39	0.38	0.38	0.38	0.004	0.55	0.53	0.53	0.54	0.008
AST-S-70-2-60K	0.25	0.26	0.26	0.26	0.008	0.29	0.29	0.29	0.29	0.002	0.44	0.43	0.43	0.43	0.010
AST-S-70-1-120K	0.24	0.25	0.25	0.25	0.004	0.29	0.30	0.30	0.29	0.003	0.43	0.44	0.43	0.43	0.003
AST-S-70-2-120K	0.21	0.21	0.21	0.21	0.001	0.26	0.25	0.24	0.25	0.007	0.39	0.38	0.38	0.38	0.009
AST-S-70-1-240K	0.24	0.24	0.24	0.24	0.002	0.28	0.28	0.29	0.29	0.002	0.44	0.43	0.42	0.43	0.006
AST-S-70-2-240K	0.19	0.19	0.19	0.19	0.002	0.24	0.24	0.23	0.23	0.003	0.38	0.37	0.37	0.37	0.005
AST-S-70-1-360K	0.23	0.22	0.22	0.22	0.004	0.28	0.28	0.27	0.27	0.004	0.43	0.42	0.41	0.42	0.010
AST-S-70-2-360K	0.15	0.14	0.15	0.15	0.005	0.20	0.20	0.21	0.20	0.004	0.35	0.34	0.34	0.34	0.005
AST-S-30-1-INI	0.57	0.55	0.54	0.55	0.015	0.60	0.60	0.58	0.59	0.012	0.73	0.71	0.69	0.71	0.019
AST-S-30-2-INI	0.52	0.50	0.49	0.50	0.015	0.59	0.57	0.56	0.57	0.018	0.70	0.68	0.66	0.68	0.023
AST-S-30-1-30K	0.49	0.47	0.45	0.47	0.021	0.53	0.50	0.49	0.51	0.021	0.66	0.63	0.61	0.63	0.029
AST-S-30-2-30K	0.42	0.40	0.40	0.40	0.011	0.46	0.44	0.44	0.45	0.014	0.57	0.55	0.54	0.55	0.017
AST-S30-1-15K	0.46	0.43	0.42	0.43	0.018	0.51	0.48	0.46	0.48	0.022	0.64	0.61	0.59	0.61	0.022
AST-S30-2-15K	0.39	0.35	0.34	0.36	0.027	0.45	0.39	0.38	0.41	0.034	0.56	0.49	0.48	0.51	0.042
AST-S-30-1-60K	0.40	0.39	0.40	0.40	0.005	0.47	0.45	0.46	0.46	0.010	0.58	0.56	0.56	0.57	0.011
AST-S-30-2-60K	0.32	0.31	0.30	0.31	0.009	0.37	0.35	0.35	0.36	0.013	0.46	0.45	0.43	0.45	0.011
AST-S-30-1-120K	0.35	0.35	0.35	0.35	0.002	0.42	0.40	0.40	0.41	0.007	0.53	0.53	0.52	0.52	0.005
AST-S-30-2-120K	0.32	0.30	0.29	0.30	0.013	0.36	0.34	0.34	0.35	0.013	0.46	0.45	0.44	0.45	0.014
AST-S-30-1-240K	0.29	0.27	0.26	0.28	0.012	0.35	0.33	0.32	0.33	0.014	0.48	0.46	0.45	0.47	0.016
AST-S-30-2-240K	0.25	0.23	0.22	0.23	0.014	0.29	0.27	0.26	0.27	0.018	0.39	0.37	0.36	0.37	0.015
AST-S-30-1-360K	0.29	0.27	0.26	0.27	0.011	0.35	0.33	0.32	0.33	0.012	0.48	0.46	0.45	0.46	0.012
AST-S-30-2-360K	0.21	0.20	0.20	0.20	0.009	0.26	0.24	0.24	0.25	0.009	0.35	0.34	0.34	0.34	0.008
MFT-30-70-1-INIT	0.76	0.73	0.71	0.73	0.023	0.80	0.77	0.75	0.78	0.025	0.91	0.87	0.85	0.88	0.026
MFT-30-70-2-INIT	0.80	0.79	0.77	0.79	0.012	0.86	0.82	0.80	0.83	0.029	0.93	0.91	0.88	0.90	0.023
MFT-30-70-1-15K	0.65	0.64	0.64	0.64	0.009	0.68	0.67	0.66	0.67	0.009	0.80	0.78	0.76	0.78	0.018
MFT-30-70-2-15K	0.64	0.63	0.63	0.63	0.009	0.67	0.65	0.66	0.66	0.010	0.77	0.76	0.74	0.76	0.015
MFT-30-70-1-30K	0.66	0.65	0.65	0.65	0.008	0.70	0.68	0.67	0.68	0.018	0.77	0.75	0.73	0.75	0.016
MFT-30-70-2-30K	0.64	0.63	0.62	0.63	0.012	0.68	0.65	0.64	0.66	0.020	0.72	0.70	0.68	0.70	0.017
MFT-30-70-1-60K	0.54	0.54	0.53	0.54	0.003	0.59	0.59	0.59	0.59	0.001	0.72	0.72	0.71	0.72	0.005
MFT-30-70-2-60K	0.51	0.50	0.49	0.50	0.010	0.56	0.54	0.53	0.55	0.013	0.70	0.68	0.67	0.68	0.013
MFT-30-70-1-120K	0.56	0.55	0.54	0.55	0.012	0.62	0.61	0.59	0.61	0.012	0.74	0.73	0.72	0.73	0.013
MFT-30-70-2-120K	0.53	0.53	0.51	0.52	0.013	0.58	0.57	0.56	0.57	0.011	0.71	0.69	0.68	0.69	0.014
MFT-30-70-1-240K	0.50	0.50	0.48	0.49	0.008	0.54	0.53	0.52	0.53	0.009	0.66	0.65	0.63	0.64	0.016
MFT-30-70-2-240K	0.47	0.47	0.47	0.47	0.002	0.51	0.50	0.50	0.50	0.005	0.63	0.62	0.62	0.62	0.005
MFT-30-70-1-360K	0.43	0.42	0.42	0.42	0.005	0.46	0.45	0.46	0.46	0.003	0.58	0.58	0.58	0.58	0.002
MFT-30-70-2-360K	0.46	0.46	0.44	0.45	0.014	0.50	0.50	0.48	0.49	0.010	0.65	0.64	0.62	0.63	0.014
MFT-70-30-1-INI	0.54	0.52	0.51	0.52	0.016	0.59	0.56	0.55	0.57	0.022	0.71	0.69	0.67	0.69	0.022
MFT-70-30-2-INI	0.56	0.54	0.52	0.54	0.020	0.58	0.56	0.54	0.56	0.020	0.70	0.67	0.65	0.67	0.025
MFT-70-30-1-15K	0.36	0.35	0.32	0.34	0.021	0.38	0.37	0.35	0.37	0.017	0.53	0.50	0.48	0.50	0.024
MFT-70-30-2-15K	0.40	0.37	0.36	0.38	0.018	0.42	0.40	0.38	0.40	0.018	0.55	0.53	0.51	0.53	0.020
MFT-70-30-1-30K	0.37	0.36	0.35	0.36	0.012	0.40	0.39	0.36	0.38	0.017	0.52	0.49	0.48	0.49	0.018
MFT-70-30-2-30K	0.35	0.34	0.33	0.34	0.010	0.37	0.36	0.35	0.36	0.009	0.50	0.48	0.47	0.48	0.016
MFT-70-30-1-60K	0.28	0.28	0.27	0.28	0.004	0.32	0.33	0.32	0.33	0.005	0.43	0.42	0.41	0.42	0.010
MFT-70-30-2-60K	0.35	0.35	0.33	0.34	0.011	0.39	0.39	0.37	0.38	0.011	0.47	0.47	0.45	0.47	0.011
MFT-70-30-1-120K	0.27	0.25	0.25	0.26	0.010	0.31	0.29	0.29	0.30	0.011	0.41	0.39	0.39	0.40	0.012
MFT-70-30-2-120K	0.31	0.29	0.29	0.30	0.011	0.35	0.34	0.34	0.34	0.008	0.45	0.44	0.43	0.44	0.012
MFT-70-30-1-240K	0.19	0.18	0.18	0.18	0.004	0.23	0.23	0.23	0.23	0.003	0.32	0.31	0.32	0.32	0.006
MFT-70-30-2-240K	0.23	0.21	0.21	0.22	0.012	0.26	0.25	0.25	0.25	0.002	0.36	0.35	0.34	0.35	0.007
MFT-70-30-1-360K	0.18	0.19	0.18	0.18	0.002	0.23	0.23	0.22	0.23	0.004	0.30	0.30	0.30	0.30	0.003

Surface	Speed of 65 km/h (40 mph)					Speed of 45 km/h (28 mph)					Speed of 20 km/h (12.5 mph)				
MFT-70-30-2-360K	0.24	0.23	0.22	0.23	0.012	0.27	0.27	0.26	0.26	0.005	0.36	0.35	0.34	0.35	0.009
MAS-1-57-1-INI	0.53	0.51	0.50	0.51	0.015	0.57	0.55	0.54	0.55	0.018	0.67	0.65	0.63	0.65	0.019
MAS-1-57-2-INI	0.50	0.46	0.45	0.47	0.030	0.56	0.53	0.50	0.53	0.028	0.65	0.62	0.60	0.62	0.027
MAS-1-57-1-15K	0.41	0.38	0.38	0.39	0.016	0.43	0.41	0.40	0.41	0.014	0.55	0.53	0.51	0.53	0.018
MAS-1-57-2-15K	0.39	0.37	0.37	0.38	0.010	0.42	0.41	0.40	0.41	0.009	0.52	0.50	0.49	0.50	0.011
MAS-1-57-1-30K	0.38	0.37	0.36	0.37	0.007	0.39	0.37	0.36	0.37	0.012	0.49	0.47	0.46	0.47	0.014
MAS-1-57-2-30K	0.35	0.33	0.33	0.34	0.009	0.40	0.38	0.37	0.38	0.014	0.45	0.43	0.42	0.43	0.012
MAS-1-57-1-60K	0.33	0.31	0.30	0.31	0.016	0.35	0.34	0.34	0.34	0.010	0.49	0.46	0.45	0.47	0.019
MAS-1-57-2-60K	0.32	0.31	0.30	0.31	0.014	0.36	0.34	0.34	0.35	0.010	0.44	0.42	0.41	0.43	0.015
MAS-1-57-1-120K	0.34	0.32	0.31	0.32	0.016	0.38	0.36	0.35	0.36	0.015	0.50	0.48	0.47	0.48	0.019
MAS-1-57-2-120K	0.24	0.23	0.22	0.23	0.007	0.27	0.26	0.26	0.26	0.004	0.37	0.35	0.35	0.36	0.009
MAS-1-57-1-240K	0.27	0.27	0.27	0.27	0.003	0.31	0.31	0.30	0.31	0.005	0.40	0.40	0.39	0.39	0.007
MAS-1-57-2-240K	0.26	0.26	0.26	0.26	0.003	0.30	0.29	0.29	0.29	0.008	0.35	0.35	0.34	0.35	0.005
MAS-1-57-1-360K	0.28	0.27	0.27	0.27	0.007	0.33	0.33	0.32	0.33	0.008	0.43	0.42	0.42	0.42	0.008
MAS-1-57-2-360K	0.24	0.24	0.25	0.24	0.003	0.27	0.27	0.28	0.27	0.005	0.33	0.34	0.33	0.33	0.005
MAS-8-57-1-INI	0.69	0.65	0.64	0.66	0.026	0.73	0.69	0.67	0.70	0.029	0.85	0.80	0.78	0.81	0.033
MAS-8-57-2-INI	0.75	0.73	0.70	0.72	0.025	0.79	0.77	0.74	0.77	0.025	0.90	0.86	0.83	0.86	0.032
MAS-8-57-1-15K	0.39	0.38	0.37	0.38	0.008	0.46	0.45	0.44	0.45	0.009	0.59	0.59	0.57	0.58	0.011
MAS-8-57-2-15K	0.48	0.48	0.47	0.48	0.005	0.55	0.53	0.53	0.54	0.014	0.67	0.66	0.65	0.66	0.010
MAS-8-57-1-30K	0.39	0.39	0.37	0.38	0.011	0.46	0.44	0.43	0.44	0.011	0.59	0.58	0.57	0.58	0.011
MAS-8-57-2-30K	0.47	0.45	0.45	0.46	0.009	0.52	0.51	0.51	0.51	0.008	0.65	0.64	0.63	0.64	0.012
MAS-8-57-1-60K	0.43	0.42	0.41	0.42	0.014	0.46	0.45	0.44	0.45	0.013	0.58	0.57	0.55	0.57	0.014
MAS-8-57-2-60K	0.42	0.40	0.40	0.41	0.011	0.45	0.44	0.43	0.44	0.008	0.57	0.56	0.55	0.56	0.014
MAS-8-57-1-120K	0.29	0.29	0.28	0.29	0.003	0.33	0.34	0.33	0.33	0.004	0.45	0.46	0.45	0.45	0.007
MAS-8-57-2-120K	0.26	0.26	0.26	0.26	0.004	0.31	0.31	0.31	0.31	0.003	0.44	0.45	0.44	0.44	0.002
MAS-8-57-1-240K	0.30	0.29	0.29	0.29	0.005	0.34	0.34	0.34	0.34	0.003	0.47	0.47	0.46	0.46	0.006
MAS-8-57-2-240K	0.28	0.28	0.29	0.28	0.003	0.35	0.34	0.34	0.34	0.005	0.49	0.48	0.47	0.48	0.008
MAS-8-57-1-360K	0.24	0.25	0.25	0.25	0.005	0.29	0.28	0.28	0.28	0.001	0.40	0.40	0.39	0.40	0.005
MAS-8-57-2-360K	0.24	0.25	0.26	0.25	0.007	0.30	0.30	0.30	0.30	0.002	0.42	0.42	0.41	0.42	0.003
MAS-8-1-INI	0.61	0.59	0.58	0.59	0.012	0.63	0.62	0.61	0.62	0.010	0.75	0.73	0.71	0.73	0.018
MAS-8-2-INI	0.36	0.35	0.35	0.35	0.003	0.69	0.65	0.63	0.66	0.026	0.52	0.51	0.50	0.51	0.010
MAS-8-1-15K	0.44	0.42	0.41	0.42	0.018	0.46	0.44	0.43	0.45	0.014	0.60	0.58	0.57	0.58	0.017
MAS-8-2-15K	0.47	0.45	0.43	0.45	0.017	0.50	0.47	0.46	0.48	0.024	0.63	0.60	0.59	0.61	0.022
MAS-8-1-30K	0.42	0.42	0.39	0.41	0.013	0.45	0.44	0.43	0.44	0.010	0.58	0.56	0.55	0.56	0.016
MAS-8-2-30K	0.47	0.45	0.44	0.46	0.015	0.51	0.48	0.47	0.49	0.022	0.61	0.58	0.56	0.58	0.026
MAS-8-1-60K	0.39	0.36	0.35	0.37	0.023	0.44	0.42	0.40	0.42	0.021	0.54	0.52	0.51	0.53	0.017
MAS-8-2-60K	0.36	0.35	0.35	0.35	0.003	0.41	0.39	0.39	0.40	0.009	0.52	0.51	0.50	0.51	0.010
MAS-8-1-120K	0.29	0.29	0.26	0.28	0.015	0.35	0.33	0.32	0.33	0.016	0.47	0.46	0.45	0.46	0.012
MAS-8-2-120K	0.35	0.33	0.33	0.34	0.010	0.39	0.36	0.36	0.37	0.016	0.49	0.47	0.47	0.48	0.012
MAS-8-1-240K	0.26	0.26	0.23	0.25	0.017	0.31	0.30	0.28	0.30	0.013	0.42	0.40	0.38	0.40	0.019
MAS-8-2-240K	0.30	0.30	0.29	0.30	0.006	0.36	0.34	0.33	0.34	0.012	0.46	0.44	0.43	0.45	0.013
MAS-8-1-360K	0.25	0.24	0.24	0.24	0.005	0.29	0.29	0.29	0.29	0.003	0.40	0.39	0.39	0.39	0.007
MAS-8-2-360K	0.26	0.25	0.25	0.25	0.006	0.30	0.29	0.28	0.29	0.007	0.40	0.39	0.38	0.39	0.008

Texture Measurements with the CTM Device

Surface	A	B	C	D	E	F	G	H	Average	STD
CONTROL57-1-INI	0.270	0.283	0.203	0.600	0.423	0.273	0.140	0.497	0.287	0.156
CONTROL57-2-INI	0.340	0.313	0.270	0.348	0.415	0.380	0.285	0.403	0.347	0.053
CONTROL57-1-15K	0.203	0.257	0.187	0.283	0.190	0.380	0.243	0.270	0.347	0.064
CONTROL57-2-15K	0.353	0.227	0.250	0.373	0.300	0.377	0.160	0.303	0.313	0.077
CONTROL57-1-30K	0.217	0.367	0.223	0.373	0.190	0.407	0.270	0.223	0.310	0.085
CONTROL57-2-3OK	0.275	0.300	0.258	0.460	0.433	0.325	0.238	0.355	0.310	0.081
CONTROL57-1-60K	0.243	0.417	0.233	0.293	0.200	0.457	0.230	0.210	0.363	0.098
CONTROL57-2-60K	0.270	0.197	0.163	0.240	0.237	0.370	0.157	0.283	0.340	0.070
CONTROL57-1-120K	0.257	0.253	0.237	0.410	0.217	0.487	0.197	0.263	0.323	0.102
CONTROL57-2-120K	0.363	0.230	0.198	0.338	0.268	0.355	0.205	0.308	0.323	0.067
CONTROL57-1-240K	0.213	0.350	0.227	0.447	0.217	0.553	0.207	0.253	0.350	0.130
CONTROL57-2-240K	0.310	0.260	0.257	0.357	0.247	0.417	0.220	0.250	0.330	0.067
CONTROL57-1-360K	0.213	0.237	0.240	0.280	0.263	0.303	0.240	0.347	0.327	0.043
CONTROL57-2-360K	0.333	0.247	0.200	0.333	0.320	0.330	0.237	0.353	0.410	0.057
AST-G-70-1-INI	0.590	0.457	0.400	0.607	0.520	0.627	0.597	0.680	0.417	0.093
AST-G-70-2-INI	0.493	0.593	0.390	0.467	0.483	0.620	0.613	0.457	0.430	0.084
AST-G-70-1-15K	0.597	0.363	0.267	0.457	0.460	0.447	0.297	0.567	0.407	0.118
AST-G-70-2-15K	0.553	0.323	0.280	0.563	0.550	0.460	0.277	0.327	0.423	0.128
AST-G-70-1-30K	0.537	0.397	0.270	0.513	0.453	0.380	0.327	0.503	0.417	0.095
AST-G-70-2-30K	0.597	0.340	0.293	0.410	0.457	0.487	0.200	0.277	0.423	0.129
AST-G-70-1-60K	0.677	0.323	0.180	0.430	0.410	0.487	0.367	0.523	0.557	0.147
AST-G-70-2-60K	0.580	0.390	0.327	0.483	0.640	0.393	0.257	0.497	0.440	0.128
AST-G-70-1-120K	0.573	0.397	0.303	0.383	0.457	0.447	0.283	0.510	0.417	0.098
AST-G-70-2-120K	0.493	0.457	0.400	0.377	0.647	0.387	0.267	0.493	0.400	0.112
AST-G-70-1-240K	0.517	0.287	0.207	0.480	0.453	0.527	0.360	0.440	0.383	0.114
AST-G-70-2-240K	0.570	0.333	0.377	0.510	0.503	0.347	0.290	0.277	0.427	0.111
AST-G-70-1-360K	0.587	0.307	0.197	0.443	0.410	0.533	0.437	0.420	0.447	0.122
AST-G-70-2-360K	0.523	0.393	0.343	0.457	0.700	0.380	0.300	0.327	0.513	0.132
AST-G-30-1-INI	0.283	0.327	0.437	0.347	0.390	0.397	0.360	0.370	0.270	0.047
AST-G-30-2-INI	0.290	0.383	0.527	0.417	0.310	0.467	0.370	0.510	0.303	0.087
AST-G-30-1-15K	0.237	0.363	0.370	0.383	0.357	0.357	0.327	0.350	0.287	0.046
AST-G-30-2-15K	0.287	0.273	0.240	0.380	0.287	0.437	0.227	0.453	0.280	0.088
AST-G-30-1-60K	0.220	0.323	0.287	0.373	0.377	0.307	0.293	0.293	0.267	0.050
AST-G-30-2-120K	0.237	0.323	0.267	0.373	0.327	0.437	0.277	0.467	0.260	0.082
AST-G-30-1-120K	0.220	0.327	0.283	0.290	0.300	0.253	0.307	0.307	0.363	0.034
AST-G-30-2-60K	0.247	0.293	0.307	0.350	0.380	0.407	0.217	0.417	0.373	0.074
AST-G-30-1-30K	0.237	0.353	0.257	0.340	0.347	0.320	0.340	0.307	0.417	0.044
AST-G-30-2-30K	0.387	0.380	0.317	0.423	0.297	0.413	0.187	0.393	0.403	0.079
AST-G-30-1-240K	0.250	0.373	0.313	0.417	0.370	0.300	0.330	0.400	0.390	0.056
AST-G-30-2-240K	0.240	0.293	0.283	0.370	0.383	0.360	0.267	0.393	0.400	0.059
AST-G-30-1-360K	0.253	0.353	0.290	0.320	0.373	0.303	0.263	0.317	0.443	0.041
AST-G-30-2-360K	0.250	0.283	0.337	0.303	0.387	0.370	0.300	0.400	0.397	0.053
AST-S-70-1-INI	0.308	0.428	0.450	0.560	0.545	0.343	0.393	0.343	0.310	0.094
AST-S-70-2-INI	0.237	0.353	0.363	0.363	0.417	0.330	0.323	0.297	0.363	0.053

Surface	A	B	C	D	E	F	G	H	Average	STD
AST-S-70-1-15K	0.357	0.360	0.253	0.513	0.473	0.290	0.367	0.310	0.343	0.089
AST-S-70-2-15K	0.233	0.243	0.167	0.357	0.357	0.240	0.233	0.347	0.330	0.072
AST-S-70-1-30K	0.370	0.383	0.220	0.420	0.450	0.253	0.307	0.237	0.350	0.088
AST-S-70-2-30K	0.320	0.207	0.193	0.330	0.360	0.267	0.217	0.280	0.305	0.062
AST-S-70-1-60K	0.307	0.317	0.245	0.395	0.363	0.273	0.283	0.265	0.420	0.051
AST-S-70-2-60K	0.250	0.283	0.257	0.263	0.337	0.263	0.237	0.237	0.233	0.032
AST-S-70-1-120K	0.340	0.413	0.263	0.353	0.333	0.233	0.237	0.293	0.270	0.063
AST-S-70-2-120K	0.220	0.173	0.197	0.350	0.277	0.220	0.163	0.267	0.283	0.062
AST-S-70-1-240K	0.350	0.387	0.330	0.413	0.393	0.293	0.243	0.327	0.270	0.056
AST-S-70-2-240K	0.350	0.280	0.320	0.253	0.277	0.217	0.227	0.323	0.308	0.048
AST-S-70-1-360K	0.333	0.423	0.310	0.387	0.307	0.357	0.297	0.377	0.270	0.045
AST-S-70-2-360K	0.297	0.382	0.297	0.302	0.290	0.312	0.260	0.325	0.337	0.035
AST-S-30-1-INI	0.280	0.303	0.350	0.487	0.320	0.483	0.360	0.313	0.290	0.080
AST-S-30-2-INI	0.293	0.270	0.393	0.397	0.430	0.433	0.663	0.297	0.250	0.126
AST-S-30-1-30K	0.200	0.273	0.233	0.243	0.333	0.357	0.327	0.267	0.310	0.055
AST-S-30-2-30K	0.307	0.267	0.423	0.360	0.350	0.483	0.613	0.300	0.283	0.115
AST-S30-1-15K	0.263	0.330	0.260	0.347	0.283	0.330	0.327	0.260	0.270	0.037
AST-S30-2-15K	0.310	0.313	0.373	0.430	0.387	0.493	0.710	0.310	0.287	0.135
AST-S-30-1-60K	0.205	0.220	0.285	0.285	0.200	0.270	0.330	0.295	0.337	0.047
AST-S-30-2-60K	0.258	0.295	0.383	0.393	0.535	0.488	0.840	0.355	0.283	0.185
AST-S-30-1-120K	0.213	0.273	0.273	0.320	0.297	0.230	0.287	0.253	0.293	0.035
AST-S-30-2-120K	0.267	0.377	0.380	0.373	0.343	0.483	0.507	0.287	0.290	0.084
AST-S-30-1-240K	0.240	0.277	0.320	0.333	0.290	0.240	0.313	0.257	0.293	0.036
AST-S-30-2-240K	0.263	0.313	0.503	0.373	0.327	0.457	0.677	0.300	0.330	0.138
AST-S-30-1-360K	0.263	0.247	0.237	0.253	0.260	0.343	0.320	0.200	0.240	0.046
AST-S-30-2-360K	0.277	0.353	0.453	0.400	0.340	0.430	0.637	0.313	0.345	0.112
MFT-30-70-1-INIT	0.387	0.637	0.387	0.427	0.370	0.520	0.610	0.540	0.477	0.106
MFT-30-70-2-INIT	0.437	0.530	0.573	0.530	0.477	0.517	0.517	0.493	0.473	0.041
MFT-30-70-1-15K	0.367	0.380	0.327	0.343	0.403	0.453	0.327	0.533	0.453	0.071
MFT-30-70-2-15K	0.550	0.413	0.350	0.437	0.430	0.507	0.283	0.443	0.463	0.083
MFT-30-70-1-30K	0.383	0.463	0.387	0.407	0.420	0.370	0.397	0.420	0.490	0.029
MFT-30-70-2-30K	0.433	0.523	0.380	0.437	0.413	0.410	0.343	0.430	0.477	0.052
MFT-30-70-1-60K	0.333	0.497	0.430	0.353	0.453	0.413	0.347	0.557	0.520	0.078
MFT-30-70-2-60K	0.447	0.480	0.357	0.413	0.490	0.397	0.287	0.513	0.500	0.076
MFT-30-70-1-120K	0.410	0.397	0.400	0.443	0.417	0.380	0.390	0.470	0.443	0.030
MFT-30-70-2-120K	0.420	0.580	0.330	0.397	0.463	0.337	0.380	0.413	0.477	0.080
MFT-30-70-1-240K	0.407	0.447	0.357	0.427	0.493	0.400	0.443	0.427	0.470	0.040
MFT-30-70-2-240K	0.460	0.627	0.410	0.533	0.407	0.323	0.397	0.493	0.480	0.094
MFT-30-70-1-360K	0.393	0.433	0.427	0.403	0.410	0.420	0.463	0.497	0.477	0.034
MFT-30-70-2-360K	0.430	0.690	0.400	0.417	0.487	0.383	0.310	0.503	0.540	0.113
MFT-70-30-1-INI	0.327	0.363	0.310	0.313	0.363	0.383	0.270	0.383	0.263	0.041
MFT-70-30-2-INI	0.373	0.310	0.330	0.310	0.283	0.313	0.280	0.313	0.270	0.029
MFT-70-30-1-15K	0.300	0.383	0.220	0.327	0.367	0.320	0.180	0.327	0.270	0.070
MFT-70-30-2-15K	0.357	0.257	0.173	0.280	0.233	0.293	0.143	0.290	0.267	0.069
MFT-70-30-1-30K	0.353	0.380	0.230	0.340	0.347	0.253	0.187	0.313	0.287	0.069
MFT-70-30-2-30K	0.320	0.240	0.210	0.283	0.217	0.273	0.183	0.277	0.253	0.046
MFT-70-30-1-60K	0.350	0.337	0.207	0.353	0.353	0.270	0.227	0.347	0.310	0.061

Surface	A	B	C	D	E	F	G	H	Average	STD
MFT-70-30-2-60K	0.317	0.220	0.203	0.250	0.220	0.267	0.183	0.313	0.277	0.049
MFT-70-30-1-120K	0.330	0.377	0.230	0.357	0.313	0.300	0.237	0.333	0.303	0.053
MFT-70-30-2-120K	0.493	0.200	0.303	0.273	0.217	0.233	0.220	0.280	0.280	0.094
MFT-70-30-1-240K	0.370	0.327	0.203	0.343	0.377	0.217	0.173	0.367	0.263	0.085
MFT-70-30-2-240K	0.340	0.257	0.210	0.303	0.233	0.263	0.160	0.240	0.270	0.055
MFT-70-30-1-360K	0.310	0.377	0.240	0.367	0.323	0.270	0.250	0.340	0.263	0.052
MFT-70-30-2-360K	0.327	0.267	0.200	0.297	0.260	0.220	0.153	0.293	0.363	0.057
MAS-1-57-1-INI	0.693	0.450	0.547	0.523	0.487	0.603	0.517	0.343	0.373	0.103
MAS-1-57-2-INI	0.703	0.600	0.380	0.703	0.500	0.680	0.423	0.333	0.337	0.151
MAS-1-57-1-15K	0.607	0.283	0.530	0.413	0.657	0.610	0.317	0.360	0.357	0.147
MAS-1-57-2-15K	0.497	0.493	0.267	0.683	0.367	0.730	0.170	0.323	0.363	0.197
MAS-1-57-1-30K	0.723	0.420	0.453	0.533	0.473	0.467	0.303	0.330	0.367	0.130
MAS-1-57-2-30K	0.620	0.620	0.253	0.667	0.453	0.540	0.247	0.347	0.350	0.169
MAS-1-57-1-60K	0.570	0.367	0.493	0.617	0.510	0.517	0.407	0.320	0.493	0.102
MAS-1-57-2-60K	0.643	0.607	0.287	0.650	0.390	0.513	0.317	0.397	0.327	0.147
MAS-1-57-1-120K	0.623	0.400	0.437	0.573	0.483	0.500	0.367	0.433	0.347	0.087
MAS-1-57-2-120K	0.697	0.550	0.313	0.647	0.630	0.473	0.377	0.330	0.327	0.151
MAS-1-57-1-240K	0.653	0.413	0.507	0.597	0.417	0.397	0.340	0.317	0.327	0.120
MAS-1-57-2-240K	0.647	0.633	0.300	0.620	0.453	0.550	0.247	0.373	0.293	0.158
MAS-1-57-1-360K	0.797	0.390	0.410	0.613	0.517	0.500	0.300	0.383	0.307	0.158
MAS-1-57-2-360K	0.613	0.627	0.240	0.663	0.443	0.490	0.333	0.427	0.453	0.149
MAS-8-57-1-INI	0.427	0.370	0.473	0.730	0.587	0.513	0.397	0.453	0.413	0.117
MAS-8-57-2-INI	0.580	0.443	0.390	0.363	0.513	0.450	0.407	0.477	0.390	0.070
MAS-8-57-1-15K	0.450	0.343	0.180	0.380	0.470	0.307	0.230	0.313	0.423	0.100
MAS-8-57-2-15K	0.510	0.367	0.150	0.367	0.467	0.300	0.313	0.297	0.407	0.111
MAS-8-57-1-30K	0.417	0.353	0.227	0.467	0.470	0.377	0.280	0.307	0.433	0.088
MAS-8-57-2-30K	0.483	0.307	0.163	0.333	0.427	0.303	0.293	0.297	0.420	0.096
MAS-8-57-1-60K	0.477	0.367	0.190	0.350	0.450	0.273	0.350	0.363	0.487	0.091
MAS-8-57-2-60K	0.423	0.347	0.203	0.290	0.417	0.263	0.223	0.273	0.413	0.083
MAS-8-57-1-120K	0.420	0.347	0.257	0.367	0.597	0.377	0.263	0.367	0.427	0.106
MAS-8-57-2-120K	0.470	0.300	0.163	0.287	0.413	0.283	0.317	0.387	0.457	0.095
MAS-8-57-1-240K	0.387	0.400	0.260	0.370	0.493	0.280	0.277	0.380	0.420	0.079
MAS-8-57-2-240K	0.420	0.330	0.210	0.310	0.397	0.257	0.250	0.450	0.457	0.087
MAS-8-57-1-360K	0.463	0.423	0.243	0.383	0.423	0.273	0.317	0.397	0.423	0.079
MAS-8-57-2-360K	0.463	0.270	0.153	0.270	0.367	0.263	0.250	0.307	0.513	0.091
MAS-8-1-INI	0.303	0.307	0.340	0.290	0.377	0.317	0.240	0.313	0.313	0.039
MAS-8-2-INI	0.283	0.287	0.243	0.287	0.320	0.273	0.170	0.260	0.303	0.045
MAS-8-1-15K	0.297	0.260	0.193	0.333	0.303	0.320	0.153	0.290	0.300	0.064
MAS-8-2-15K	0.447	0.267	0.243	0.350	0.357	0.323	0.180	0.260	0.300	0.083
MAS-8-1-30K	0.250	0.293	0.220	0.270	0.310	0.247	0.160	0.353	0.313	0.059
MAS-8-2-30K	0.347	0.237	0.210	0.303	0.320	0.250	0.147	0.283	0.307	0.065
MAS-8-1-60K	0.303	0.260	0.210	0.267	0.337	0.230	0.183	0.250	0.340	0.049
MAS-8-2-60K	0.283	0.287	0.243	0.287	0.320	0.273	0.170	0.260	0.280	0.045
MAS-8-1-120K	0.243	0.297	0.200	0.270	0.337	0.227	0.150	0.357	0.257	0.069
MAS-8-2-120K	0.273	0.347	0.210	0.280	0.350	0.290	0.160	0.287	0.250	0.064
MAS-8-1-240K	0.243	0.297	0.220	0.247	0.367	0.193	0.210	0.370	0.250	0.069
MAS-8-2-240K	0.333	0.310	0.237	0.253	0.300	0.313	0.203	0.303	0.253	0.045

Surface	A	B	C	D	E	F	G	H	Average	STD
MAS-8-1-360K	0.287	0.333	0.293	0.220	0.277	0.217	0.177	0.493	0.250	0.097
MAS-8-2-360K	0.270	0.330	0.237	0.257	0.307	0.240	0.167	0.340	0.317	0.057

British Pendulum Measurements with the BPT Device

Date	Operator	Sample Number	Sample Composition	Sample Condition	1	2	3	4	5	Average
5/14/2009	Robin Tallon	1	control57	initial	77	75	73	75	77	75.4
5/14/2009	Robin Tallon	1	control57	initial	77	77	75	75	75	75.8
5/14/2009	Robin Tallon	1	control57	initial	77	76	75	74	75	75.4
5/14/2009	Robin Tallon	2	control57	initial	75	74	75	70	70	72.8
5/14/2009	Robin Tallon	2	control57	initial	77	77	76	77	77	76.8
5/14/2009	Robin Tallon	2	control57	initial	75	75	75	74	75	74.8
6/2/2009	Robin Tallon	1	control57	60K	60	61	61	60	61	60.6
6/2/2009	Robin Tallon	1	control57	60K	62	63	63	64	62	62.8
6/2/2009	Robin Tallon	1	control57	60K	64	63	63	62	61	62.6
6/2/2009	Robin Tallon	2	control57	60K	60	62	63	62	61	61.6
6/2/2009	Robin Tallon	2	control57	60K	60	61	60	61	60	60.4
6/2/2009	Robin Tallon	2	control57	60K	60	62	62	60	61	61
6/3/2009	Zoltan Rado	1	control57	120K	59	60	60	60	60	59.8
6/3/2009	Zoltan Rado	1	control57	120K	62	61	61	61	61	61.2
6/3/2009	Zoltan Rado	1	control57	120K	62	61	61	60	61	61
6/3/2009	Zoltan Rado	2	control57	120K	60	60	60	60	60	60
6/3/2009	Zoltan Rado	2	control57	120K	58	57	57	57	57	57.2
6/3/2009	Zoltan Rado	2	control57	120K	56	57	57	57	56	56.6
6/12/2009	Robin Tallon	1	control57	240K	66	66	66	67	67	66.4
6/12/2009	Robin Tallon	1	control57	240K	67	67	69	68	68	67.8
6/12/2009	Robin Tallon	2	control57	240K	66	66	65	66	67	66
6/12/2009	Robin Tallon	2	control57	240K	64	65	66	67	66	65.6
6/15/2009	Robin Tallon	1	control57	360K	55	55	55	56	55	55.2
6/15/2009	Robin Tallon	1	control57	360K	54	55	55	55	55	54.8
6/15/2009	Robin Tallon	1	control57	360K	55	55	56	58	59	56.6
6/15/2009	Robin Tallon	2	control57	360K	54	55	56	57	57	55.8
6/15/2009	Robin Tallon	2	control57	360K	54	55	55	55	56	55
6/15/2009	Robin Tallon	2	control57	360K	55	57	57	58	58	57
8/14/2009	Robin Tallon	1	AST-S-30	initial	70	70	70	71	74	71
8/14/2009	Robin Tallon	1	AST-S-30	initial	83	80	76	80	78	79
8/14/2009	Robin Tallon	1	AST-S-30	initial	78	75	73	76	76	76
8/14/2009	Robin Tallon	2	AST-S-30	initial	80	79	79	78	76	78
8/14/2009	Robin Tallon	2	AST-S-30	initial	79	78	78	76	75	77
8/14/2009	Robin Tallon	2	AST-S-30	initial	78	76	75	75	75	76
8/18/2009	Choongwoo Cho	1	AST-S-30	15K	64	64	64	63	63	64
8/18/2009	Choongwoo Cho	1	AST-S-30	15K	66	66	66	65	65	66
8/18/2009	Choongwoo Cho	1	AST-S-30	15K	61	61	61	60	60	61
8/18/2009	Choongwoo Cho	2	AST-S-30	15K	60	60	60	60	60	60
8/18/2009	Choongwoo Cho	2	AST-S-30	15K	63	64	60	61	61	62
8/18/2009	Choongwoo Cho	2	AST-S-30	15K	60	60	60	60	61	60
8/19/2009	Choongwoo Cho	1	AST-S-30	30K	67	67	67	67	67	67
8/19/2009	Choongwoo Cho	1	AST-S-30	30K	65	65	65	64	64	65
8/19/2009	Choongwoo Cho	1	AST-S-30	30K	65	65	65	65	65	65

Date	Operator	Sample Number	Sample Composition	Sample Condition	1	2	3	4	5	Average
8/19/2009	Choongwoo Cho	2	AST-S-30	30K	60	60	60	60	60	60
8/19/2009	Choongwoo Cho	2	AST-S-30	30K	62	62	64	64	65	63
8/19/2009	Choongwoo Cho	2	AST-S-30	30K	65	65	65	65	65	65
8/20/2009	Robin Tallon	1	AST-S-30	60K	65	65	65	65	66	65
8/20/2009	Robin Tallon	1	AST-S-30	60K	68	69	68	68	68	68
8/20/2009	Robin Tallon	1	AST-S-30	60K	68	68	68	68	68	68
8/20/2009	Robin Tallon	2	AST-S-30	60K	63	63	62	63	63	63
8/20/2009	Robin Tallon	2	AST-S-30	60K	65	65	65	65	65	65
8/20/2009	Robin Tallon	2	AST-S-30	60K	66	66	67	68	68	67
8/31/2009	Robin Tallon	1	AST-S-30	120K	60	59	60	61	62	60
8/31/2009	Robin Tallon	1	AST-S-30	120K	60	60	62	64	64	62
8/31/2009	Robin Tallon	1	AST-S-30	120K	58	60	60	61	61	60
8/31/2009	Robin Tallon	2	AST-S-30	120K	56	58	58	58	58	58
8/31/2009	Robin Tallon	2	AST-S-30	120K	55	55	57	58	58	57
8/31/2009	Robin Tallon	2	AST-S-30	120K	59	60	62	62	62	61
9/1/2009	Choongwoo Cho	1	AST-S-30	240K	49	49	49	49	49	49
9/1/2009	Choongwoo Cho	1	AST-S-30	240K	51	51	53	55	55	53
9/1/2009	Choongwoo Cho	1	AST-S-30	240K	50	51	52	53	54	52
9/1/2009	Choongwoo Cho	2	AST-S-30	240K	46	47	48	49	49	48
9/1/2009	Choongwoo Cho	2	AST-S-30	240K	47	50	51	51	52	50
9/1/2009	Choongwoo Cho	2	AST-S-30	240K	50	51	51	53	53	52
9/2/2009	Zoltan Rado	1	AST-S-30	360K	46	47	47	46	48	47
9/2/2009	Zoltan Rado	1	AST-S-30	360K	45	45	45	45	46	45
9/2/2009	Zoltan Rado	1	AST-S-30	360K	47	49	50	50	49	49
9/2/2009	Zoltan Rado	2	AST-S-30	360K	40	41	41	42	41	41
9/2/2009	Zoltan Rado	2	AST-S-30	360K	39	40	40	40	40	40
9/2/2009	Zoltan Rado	2	AST-S-30	360K	40	40	42	42	43	41
8/3/2009	Robin Tallon	1	AST-S-70	initial	80	78	80	79	77	78.8
8/3/2009	Robin Tallon	1	AST-S-70	initial	80	80	80	79	79	80
8/3/2009	Robin Tallon	1	AST-S-70	initial	80	80	80	79	79	80
8/3/2009	Robin Tallon	2	AST-S-70	initial	77	79	80	79	79	79
8/3/2009	Robin Tallon	2	AST-S-70	initial	78	80	78	80	78	79
8/3/2009	Robin Tallon	2	AST-S-70	initial	76	80	76	77	76	77
8/4/2009	Zoltan Rado	1	AST-S-70	15K	60	60	60	60	60	60
8/4/2009	Zoltan Rado	1	AST-S-70	15K	61	60	61	60	60	60
8/4/2009	Zoltan Rado	1	AST-S-70	15K	63	62	65	65	65	64
8/4/2009	Zoltan Rado	2	AST-S-70	15K	62	62	63	62	63	62
8/4/2009	Zoltan Rado	2	AST-S-70	15K	63	63	64	63	64	63
8/4/2009	Zoltan Rado	2	AST-S-70	15K	62	62	63	63	63	63
8/5/2009	Zoltan Rado	1	AST-S-70	30K	65	65	64	63	64	64
8/5/2009	Zoltan Rado	1	AST-S-70	30K	62	62	61	61	60	61
8/5/2009	Zoltan Rado	1	AST-S-70	30K	59	61	61	60	59	60
8/5/2009	Zoltan Rado	2	AST-S-70	30K	65	61	64	60	64	63
8/5/2009	Zoltan Rado	2	AST-S-70	30K	65	67	66	65	67	66
8/5/2009	Zoltan Rado	2	AST-S-70	30K	65	65	66	65	65	65
8/7/2009	Zoltan Rado	1	AST-S-70	60K	63	64	64	65	63	64

Date	Operator	Sample Number	Sample Composition	Sample Condition	1	2	3	4	5	Average
8/7/2009	Zoltan Rado	1	AST-S-70	60K	65	65	64	65	64	65
8/7/2009	Zoltan Rado	1	AST-S-70	60K	66	66	67	66	65	66
8/7/2009	Zoltan Rado	2	AST-S-70	60K	61	61	61	61	61	61
8/7/2009	Zoltan Rado	2	AST-S-70	60K	63	63	62	63	64	63
8/7/2009	Zoltan Rado	2	AST-S-70	60K	65	66	66	66	67	66
8/10/2009	Zoltan Rado	1	AST-S-70	120K	59	60	60	60	60	60
8/10/2009	Zoltan Rado	1	AST-S-70	120K	60	60	60	60	60	60
8/10/2009	Zoltan Rado	1	AST-S-70	120K	63	63	62	62	60	62
8/10/2009	Zoltan Rado	2	AST-S-70	120K	57	60	63	64	64	62
8/10/2009	Zoltan Rado	2	AST-S-70	120K	55	57	56	57	58	57
8/10/2009	Zoltan Rado	2	AST-S-70	120K	60	61	62	62	62	61
8/13/2009	Choongwoo Cho	1	AST-S-70	240K	53	55	55	55	55	55
8/13/2009	Choongwoo Cho	1	AST-S-70	240K	57	59	60	60	60	59
8/13/2009	Choongwoo Cho	1	AST-S-70	240K	57	58	59	60	60	59
8/13/2009	Choongwoo Cho	2	AST-S-70	240K	57	59	59	59	59	59
8/13/2009	Choongwoo Cho	2	AST-S-70	240K	55	55	56	56	56	56
8/13/2009	Choongwoo Cho	2	AST-S-70	240K	54	55	55	56	56	55
8/14/2009	Choongwoo Cho	1	AST-S-70	360K	48	50	50	51	51	50
8/14/2009	Choongwoo Cho	1	AST-S-70	360K	54	55	55	55	55	55
8/14/2009	Choongwoo Cho	1	AST-S-70	360K	52	53	54	54	54	53
8/14/2009	Choongwoo Cho	2	AST-S-70	360K	52	53	54	55	55	54
8/14/2009	Choongwoo Cho	2	AST-S-70	360K	52	53	54	55	54	54
8/14/2009	Choongwoo Cho	2	AST-S-70	360K	49	50	50	51	51	50
7/14/2009	Choongwoo Cho	1	AST-G-30	initial	80	78	77	77	77	77.8
7/14/2009	Choongwoo Cho	1	AST-G-30	initial	80	80	78	80	75	79
7/14/2009	Choongwoo Cho	1	AST-G-30	initial	85	88	86	88	87	87
7/14/2009	Choongwoo Cho	2	AST-G-30	initial	80	78	76	75	75	77
7/14/2009	Choongwoo Cho	2	AST-G-30	initial	81	82	81	81	81	81
7/14/2009	Choongwoo Cho	2	AST-G-30	initial	82	80	79	79	79	80
7/16/2009	Choongwoo Cho	1	AST-G-30	15K	56	57	58	60	61	58
7/16/2009	Choongwoo Cho	1	AST-G-30	15K	56	57	58	59	59	58
7/16/2009	Choongwoo Cho	1	AST-G-30	15K	60	61	62	64	64	62
7/16/2009	Choongwoo Cho	2	AST-G-30	15K	60	60	60	61	61	60
7/16/2009	Choongwoo Cho	2	AST-G-30	15K	55	56	58	59	58	57
7/16/2009	Choongwoo Cho	2	AST-G-30	15K	55	55	57	56	56	56
7/17/2009	Choongwoo Cho	1	AST-G-30	30K	45	45	46	46	47	46
7/17/2009	Choongwoo Cho	1	AST-G-30	30K	45	44	44	44	43	44
7/17/2009	Choongwoo Cho	1	AST-G-30	30K	50	50	51	51	51	51
7/17/2009	Choongwoo Cho	2	AST-G-30	30K	47	47	48	48	48	48
7/17/2009	Choongwoo Cho	2	AST-G-30	30K	36	35	35	35	36	35
7/17/2009	Choongwoo Cho	2	AST-G-30	30K	37	37	36	36	35	36
7/20/2009	Choongwoo Cho	1	AST-G-30	60K	64	65	66	66	66	65
7/20/2009	Choongwoo Cho	1	AST-G-30	60K	65	67	67	70	67	67
7/20/2009	Choongwoo Cho	1	AST-G-30	60K	68	70	70	70	70	70
7/20/2009	Choongwoo Cho	2	AST-G-30	60K	62	62	63	65	64	63
7/20/2009	Choongwoo Cho	2	AST-G-30	60K	59	60	60	60	60	60

Date	Operator	Sample Number	Sample Composition	Sample Condition	1	2	3	4	5	Average
7/20/2009	Choongwoo Cho	2	AST-G-30	60K	60	61	63	65	64	63
7/21/2009	Choongwoo Cho	1	AST-G-30	120K	57	60	61	62	62	60
7/21/2009	Choongwoo Cho	1	AST-G-30	120K	63	65	65	66	66	65
7/21/2009	Choongwoo Cho	1	AST-G-30	120K	63	65	65	66	66	65
7/21/2009	Choongwoo Cho	2	AST-G-30	120K	58	60	60	61	62	60
7/21/2009	Choongwoo Cho	2	AST-G-30	120K	57	58	59	60	60	59
7/21/2009	Choongwoo Cho	2	AST-G-30	120K	60	61	62	62	62	61
7/22/2009	Choongwoo Cho	1	AST-G-30	240K	55	55	57	58	58	57
7/22/2009	Choongwoo Cho	1	AST-G-30	240K	55	57	57	59	60	58
7/22/2009	Choongwoo Cho	1	AST-G-30	240K	65	68	70	70	69	68
7/22/2009	Choongwoo Cho	2	AST-G-30	240K	54	55	55	55	56	55
7/22/2009	Choongwoo Cho	2	AST-G-30	240K	48	50	50	51	55	51
7/22/2009	Choongwoo Cho	2	AST-G-30	240K	55	57	60	60	60	58
7/23/2009	Choongwoo Cho	1	AST-G-30	360K	53	55	56	56	56	55
7/23/2009	Choongwoo Cho	1	AST-G-30	360K	50	51	53	54	54	52
7/23/2009	Choongwoo Cho	1	AST-G-30	360K	55	57	58	58	58	57
7/23/2009	Choongwoo Cho	2	AST-G-30	360K	45	47	47	50	50	48
7/23/2009	Choongwoo Cho	2	AST-G-30	360K	51	52	53	54	55	53
7/23/2009	Choongwoo Cho	2	AST-G-30	360K	50	52	54	54	55	53
6/22/2009	Robin Tallon	1	AST-G-70	initial	80	79	80	78	78	79
6/22/2009	Robin Tallon	1	AST-G-70	initial	82	80	80	80	81	81
6/22/2009	Robin Tallon	1	AST-G-70	initial	82	80	80	80	80	80
6/22/2009	Robin Tallon	2	AST-G-70	initial	83	80	80	80	82	81
6/22/2009	Robin Tallon	2	AST-G-70	initial	81	80	78	79	78	79
6/22/2009	Robin Tallon	2	AST-G-70	initial	81	80	79	78	79	79
6/23/2009	Robin Tallon	1	AST-G-70	15K	67	69	68	69	69	68
6/23/2009	Robin Tallon	1	AST-G-70	15K	65	67	66	66	65	66
6/23/2009	Robin Tallon	1	AST-G-70	15K	69	69	69	69	69	69
6/23/2009	Robin Tallon	2	AST-G-70	15K	66	67	68	69	68	68
6/23/2009	Robin Tallon	2	AST-G-70	15K	66	67	68	67	68	67
6/23/2009	Robin Tallon	2	AST-G-70	15K	65	66	66	67	67	66
7/1/2009	Robin Tallon	1	AST-G-70	30K	70	70	70	70	70	70
7/1/2009	Robin Tallon	1	AST-G-70	30K	66	66	67	68	68	67
7/1/2009	Robin Tallon	1	AST-G-70	30K	70	70	70	70	70	70
7/1/2009	Robin Tallon	2	AST-G-70	30K	70	70	70	71	70	70
7/1/2009	Robin Tallon	2	AST-G-70	30K	66	66	67	68	69	67
7/1/2009	Robin Tallon	2	AST-G-70	30K	66	67	68	68	69	68
7/2/2009	Robin Tallon	1	AST-G-70	60K	64	65	65	66	66	65
7/2/2009	Robin Tallon	1	AST-G-70	60K	64	65	65	65	65	65
7/2/2009	Robin Tallon	1	AST-G-70	60K	65	65	66	66	65	65
7/2/2009	Robin Tallon	2	AST-G-70	60K	65	66	68	68	68	67
7/2/2009	Robin Tallon	2	AST-G-70	60K	65	65	65	65	65	65
7/2/2009	Robin Tallon	2	AST-G-70	60K	62	63	65	63	62	63
7/6/2009	Robin Tallon	1	AST-G-70	120K	60	60	61	61	62	61
7/6/2009	Robin Tallon	1	AST-G-70	120K	60	61	61	62	62	61
7/6/2009	Robin Tallon	1	AST-G-70	120K	61	62	63	64	64	63

Date	Operator	Sample Number	Sample Composition	Sample Condition	1	2	3	4	5	Average
7/6/2009	Robin Tallon	2	AST-G-70	120K	59	60	60	60	60	60
7/6/2009	Robin Tallon	2	AST-G-70	120K	59	60	60	60	60	60
7/6/2009	Robin Tallon	2	AST-G-70	120K	56	56	57	57	57	57
7/7/2009	Robin Tallon	1	AST-G-70	240K	53	54	55	55	55	54
7/7/2009	Robin Tallon	1	AST-G-70	240K	53	54	55	55	55	54
7/7/2009	Robin Tallon	1	AST-G-70	240K	56	58	58	60	60	58
7/7/2009	Robin Tallon	2	AST-G-70	240K	53	54	55	55	55	54
7/7/2009	Robin Tallon	2	AST-G-70	240K	49	50	50	51	50	50
7/7/2009	Robin Tallon	2	AST-G-70	240K	50	51	52	52	53	52
7/10/2009	Choongwoo Cho	1	AST-G-70	360K	45	46	46	51	50	48
7/10/2009	Choongwoo Cho	1	AST-G-70	360K	51	52	54	55	56	54
7/10/2009	Choongwoo Cho	1	AST-G-70	360K	51	54	54	54	55	54
7/10/2009	Choongwoo Cho	2	AST-G-70	360K	49	50	51	51	51	50
7/10/2009	Choongwoo Cho	2	AST-G-70	360K	44	45	46	46	47	46
7/10/2009	Choongwoo Cho	2	AST-G-70	360K	45	45	46	46	47	46
9/3/2009	Zoltan Rado	1	MFT-30-70	initial	82	80	80	80	80	80.4
9/3/2009	Zoltan Rado	1	MFT-30-70	initial	78	78	78	78	78	78
9/3/2009	Zoltan Rado	1	MFT-30-70	initial	84	84	84	84	84	84
9/3/2009	Zoltan Rado	2	MFT-30-70	initial	80	81	82	80	80	81
9/3/2009	Zoltan Rado	2	MFT-30-70	initial	84	85	85	85	85	85
9/3/2009	Zoltan Rado	2	MFT-30-70	initial	87	86	87	87	86	87
9/4/2009	Choongwoo Cho	1	MFT-30-70	15K	69	71	70	70	71	70
9/4/2009	Choongwoo Cho	1	MFT-30-70	15K	66	67	68	68	69	68
9/4/2009	Choongwoo Cho	1	MFT-30-70	15K	72	74	75	75	74	74
9/4/2009	Choongwoo Cho	2	MFT-30-70	15K	65	66	65	65	65	65
9/4/2009	Choongwoo Cho	2	MFT-30-70	15K	67	68	69	69	69	68
9/4/2009	Choongwoo Cho	2	MFT-30-70	15K	70	70	70	70	70	70
9/9/2009	Choongwoo Cho	1	MFT-30-70	30K	65	65	65	65	65	65
9/9/2009	Choongwoo Cho	1	MFT-30-70	30K	66	67	67	67	68	67
9/9/2009	Choongwoo Cho	1	MFT-30-70	30K	67	67	68	68	68	68
9/9/2009	Choongwoo Cho	2	MFT-30-70	30K	66	69	69	69	69	68
9/9/2009	Choongwoo Cho	2	MFT-30-70	30K	64	63	63	64	64	64
9/9/2009	Choongwoo Cho	2	MFT-30-70	30K	65	67	67	67	67	67
9/10/2009	Choongwoo Cho	1	MFT-30-70	60K	62	62	63	64	65	63
9/10/2009	Choongwoo Cho	1	MFT-30-70	60K	61	62	64	65	65	63
9/10/2009	Choongwoo Cho	1	MFT-30-70	60K	64	65	65	65	65	65
9/10/2009	Choongwoo Cho	2	MFT-30-70	60K	61	63	63	63	64	63
9/10/2009	Choongwoo Cho	2	MFT-30-70	60K	60	61	61	61	60	61
9/10/2009	Choongwoo Cho	2	MFT-30-70	60K	63	64	63	65	65	64
9/10/2009	Choongwoo Cho	1	MFT-30-70	120K	60	61	62	63	60	61
9/10/2009	Choongwoo Cho	1	MFT-30-70	120K	62	63	63	64	63	63
9/10/2009	Choongwoo Cho	1	MFT-30-70	120K	63	63	63	64	64	63
9/10/2009	Choongwoo Cho	2	MFT-30-70	120K	60	62	62	62	62	62
9/10/2009	Choongwoo Cho	2	MFT-30-70	120K	65	65	66	65	66	65
9/10/2009	Choongwoo Cho	2	MFT-30-70	120K	66	66	66	66	67	66
9/11/2009	Choongwoo Cho	1	MFT-30-70	240K	57	58	59	59	59	58

Date	Operator	Sample Number	Sample Composition	Sample Condition	1	2	3	4	5	Average
9/11/2009	Choongwoo Cho	1	MFT-30-70	240K	61	61	61	59	61	61
9/11/2009	Choongwoo Cho	1	MFT-30-70	240K	59	60	60	60	60	60
9/11/2009	Choongwoo Cho	2	MFT-30-70	240K	58	60	60	62	62	60
9/11/2009	Choongwoo Cho	2	MFT-30-70	240K	57	57	59	60	60	59
9/11/2009	Choongwoo Cho	2	MFT-30-70	240K	57	57	53	53	53	55
9/12/2009	Choongwoo Cho	1	MFT-30-70	360K	53	55	55	56	56	55
9/12/2009	Choongwoo Cho	1	MFT-30-70	360K	56	57	57	57	57	57
9/12/2009	Choongwoo Cho	1	MFT-30-70	360K	57	57	57	57	57	57
9/12/2009	Choongwoo Cho	2	MFT-30-70	360K	55	55	56	56	55	55
9/12/2009	Choongwoo Cho	2	MFT-30-70	360K	53	55	55	56	56	55
9/12/2009	Choongwoo Cho	2	MFT-30-70	360K	53	55	55	56	56	55
9/16/2009	Choongwoo Cho	1	MFT-70-30	initial	80	80	81	78	78	79
9/16/2009	Choongwoo Cho	1	MFT-70-30	initial	79	79	79	80	80	79
9/16/2009	Choongwoo Cho	1	MFT-70-30	initial	81	80	80	80	80	80
9/16/2009	Choongwoo Cho	2	MFT-70-30	initial	78	79	79	79	80	79
9/16/2009	Choongwoo Cho	2	MFT-70-30	initial	78	78	76	76	77	77
9/16/2009	Choongwoo Cho	2	MFT-70-30	initial	80	79	79	76	76	78
9/16/2009	Choongwoo Cho	1	MFT-70-30	15K	65	65	65	65	65	65
9/16/2009	Choongwoo Cho	1	MFT-70-30	15K	60	62	62	64	62	62
9/16/2009	Choongwoo Cho	1	MFT-70-30	15K	64	64	64	65	64	64
9/16/2009	Choongwoo Cho	2	MFT-70-30	15K	60	60	60	61	60	60
9/16/2009	Choongwoo Cho	2	MFT-70-30	15K	60	60	60	60	60	60
9/16/2009	Choongwoo Cho	2	MFT-70-30	15K	60	60	60	60	61	60
9/17/2009	Choongwoo Cho	1	MFT-70-30	30K	56	56	56	56	56	56
9/17/2009	Choongwoo Cho	1	MFT-70-30	30K	59	60	59	60	59	59
9/17/2009	Choongwoo Cho	1	MFT-70-30	30K	60	60	60	60	60	60
9/17/2009	Choongwoo Cho	2	MFT-70-30	30K	61	60	61	60	60	60
9/17/2009	Choongwoo Cho	2	MFT-70-30	30K	56	59	58	59	59	58
9/17/2009	Choongwoo Cho	2	MFT-70-30	30K	60	61	60	60	61	60
9/17/2009	Choongwoo Cho	1	MFT-70-30	60K	63	63	63	63	63	63
9/17/2009	Choongwoo Cho	1	MFT-70-30	60K	60	60	61	62	62	61
9/17/2009	Choongwoo Cho	1	MFT-70-30	60K	60	60	60	60	60	60
9/17/2009	Choongwoo Cho	2	MFT-70-30	60K	59	59	59	59	59	59
9/17/2009	Choongwoo Cho	2	MFT-70-30	60K	57	59	59	57	59	58
9/17/2009	Choongwoo Cho	2	MFT-70-30	60K	56	59	60	60	59	59
9/18/2009	Choongwoo Cho	1	MFT-70-30	120K	55	55	57	58	59	57
9/18/2009	Choongwoo Cho	1	MFT-70-30	120K	55	57	59	57	57	57
9/18/2009	Choongwoo Cho	1	MFT-70-30	120K	56	57	57	59	57	57
9/18/2009	Choongwoo Cho	2	MFT-70-30	120K	55	55	55	55	55	55
9/18/2009	Choongwoo Cho	2	MFT-70-30	120K	52	54	54	55	55	54
9/18/2009	Choongwoo Cho	2	MFT-70-30	120K	55	55	55	56	56	55
9/20/2009	Choongwoo Cho	1	MFT-70-30	240K	48	50	50	50	50	50
9/20/2009	Choongwoo Cho	1	MFT-70-30	240K	50	52	53	53	53	52
9/20/2009	Choongwoo Cho	1	MFT-70-30	240K	54	54	54	54	53	54
9/20/2009	Choongwoo Cho	2	MFT-70-30	240K	46	47	47	47	47	47
9/20/2009	Choongwoo Cho	2	MFT-70-30	240K	44	45	46	46	46	45

Date	Operator	Sample Number	Sample Composition	Sample Condition	1	2	3	4	5	Average
9/20/2009	Choongwoo Cho	2	MFT-70-30	240K	45	45	46	46	46	46
9/21/2009	Choongwoo Cho	1	MFT-70-30	360K	46	49	49	49	50	49
9/21/2009	Choongwoo Cho	1	MFT-70-30	360K	46	46	49	50	50	48
9/21/2009	Choongwoo Cho	1	MFT-70-30	360K	50	50	50	51	52	51
9/21/2009	Choongwoo Cho	2	MFT-70-30	360K	42	42	42	42	42	42
9/21/2009	Choongwoo Cho	2	MFT-70-30	360K	42	44	45	45	45	44
9/21/2009	Choongwoo Cho	2	MFT-70-30	360K	45	45	46	46	46	46
9/30/2009	Choongwoo Cho	1	MAS-1-57	initial	74	71	71	70	70	71
9/30/2009	Choongwoo Cho	1	MAS-1-57	initial	83	80	80	80	77	80
9/30/2009	Choongwoo Cho	1	MAS-1-57	initial	85	86	85	85	85	85
9/30/2009	Choongwoo Cho	2	MAS-1-57	initial	75	76	76	76	78	76
9/30/2009	Choongwoo Cho	2	MAS-1-57	initial	80	78	76	77	78	78
9/30/2009	Choongwoo Cho	2	MAS-1-57	initial	80	81	80	80	80	80
10/1/2009	Choongwoo Cho	1	MAS-1-57	15K	60	60	56	56	58	58
10/1/2009	Choongwoo Cho	1	MAS-1-57	15K	63	65	65	65	65	65
10/1/2009	Choongwoo Cho	1	MAS-1-57	15K	60	60	60	61	60	60
10/1/2009	Choongwoo Cho	2	MAS-1-57	15K	60	60	60	60	60	60
10/1/2009	Choongwoo Cho	2	MAS-1-57	15K	65	67	70	70	70	68
10/1/2009	Choongwoo Cho	2	MAS-1-57	15K	67	68	68	68	68	68
10/1/2009	Choongwoo Cho	1	MAS-1-57	30K	60	60	62	63	60	61
10/1/2009	Choongwoo Cho	1	MAS-1-57	30K	59	60	60	60	61	60
10/1/2009	Choongwoo Cho	1	MAS-1-57	30K	59	60	60	61	61	60
10/1/2009	Choongwoo Cho	2	MAS-1-57	30K	60	61	63	64	65	63
10/1/2009	Choongwoo Cho	2	MAS-1-57	30K	61	64	64	64	65	64
10/1/2009	Choongwoo Cho	2	MAS-1-57	30K	65	66	66	67	67	66
10/2/2009	Choongwoo Cho	1	MAS-1-57	60K	57	60	60	60	60	59
10/2/2009	Choongwoo Cho	1	MAS-1-57	60K	59	60	60	61	61	60
10/2/2009	Choongwoo Cho	1	MAS-1-57	60K	60	60	62	62	62	61
10/2/2009	Choongwoo Cho	2	MAS-1-57	60K	55	58	58	58	58	57
10/2/2009	Choongwoo Cho	2	MAS-1-57	60K	61	62	63	65	65	63
10/2/2009	Choongwoo Cho	2	MAS-1-57	60K	60	62	64	64	64	63
10/3/2009	Choongwoo Cho	1	MAS-1-57	120K	51	54	54	54	55	54
10/3/2009	Choongwoo Cho	1	MAS-1-57	120K	55	57	57	57	59	57
10/3/2009	Choongwoo Cho	1	MAS-1-57	120K	56	57	58	58	58	57
10/3/2009	Choongwoo Cho	2	MAS-1-57	120K	52	55	55	55	55	54
10/3/2009	Choongwoo Cho	2	MAS-1-57	120K	59	59	59	60	60	59
10/3/2009	Choongwoo Cho	2	MAS-1-57	120K	56	57	59	60	60	58
10/4/2009	Choongwoo Cho	1	MAS-1-57	240K	54	55	57	57	58	56
10/4/2009	Choongwoo Cho	1	MAS-1-57	240K	55	57	57	57	57	57
10/4/2009	Choongwoo Cho	1	MAS-1-57	240K	60	60	61	61	60	60
10/4/2009	Choongwoo Cho	2	MAS-1-57	240K	51	54	54	55	55	54
10/4/2009	Choongwoo Cho	2	MAS-1-57	240K	54	55	56	57	58	56
10/4/2009	Choongwoo Cho	2	MAS-1-57	240K	58	60	60	60	60	60
10/5/2009	Choongwoo Cho	1	MAS-1-57	360K	52	54	55	55	55	54
10/5/2009	Choongwoo Cho	1	MAS-1-57	360K	52	52	52	52	52	52
10/5/2009	Choongwoo Cho	1	MAS-1-57	360K	56	57	57	58	58	57

Date	Operator	Sample Number	Sample Composition	Sample Condition	1	2	3	4	5	Average
10/5/2009	Choongwoo Cho	2	MAS-1-57	360K	51	51	51	51	51	51
10/5/2009	Choongwoo Cho	2	MAS-1-57	360K	54	55	56	57	57	56
10/5/2009	Choongwoo Cho	2	MAS-1-57	360K	51	55	55	55	55	54
10/6/2009	Choongwoo Cho	1	MAS-8-57	15K	67	67	67	67	67	67
10/6/2009	Choongwoo Cho	1	MAS-8-57	15K	63	65	65	63	63	64
10/6/2009	Choongwoo Cho	1	MAS-8-57	15K	63	64	64	63	63	63
10/6/2009	Choongwoo Cho	2	MAS-8-57	15K	60	61	61	61	60	61
10/6/2009	Choongwoo Cho	2	MAS-8-57	15K	62	64	64	65	65	64
10/6/2009	Choongwoo Cho	2	MAS-8-57	15K	63	64	65	65	65	64
10/7/2009	Choongwoo Cho	1	MAS-8-57	30K	57	59	60	60	60	59
10/7/2009	Choongwoo Cho	1	MAS-8-57	30K	59	60	60	60	60	60
10/7/2009	Choongwoo Cho	1	MAS-8-57	30K	60	60	60	60	60	60
10/7/2009	Choongwoo Cho	2	MAS-8-57	30K	55	57	59	59	60	58
10/7/2009	Choongwoo Cho	2	MAS-8-57	30K	57	59	60	60	62	60
10/7/2009	Choongwoo Cho	2	MAS-8-57	30K	59	60	60	60	60	60
10/7/2009	Choongwoo Cho	1	MAS-8-57	60K	60	61	61	61	61	61
10/7/2009	Choongwoo Cho	1	MAS-8-57	60K	59	60	60	60	61	60
10/7/2009	Choongwoo Cho	1	MAS-8-57	60K	58	58	58	58	60	58
10/7/2009	Choongwoo Cho	2	MAS-8-57	60K	58	58	58	58	58	58
10/7/2009	Choongwoo Cho	2	MAS-8-57	60K	58	59	60	61	61	60
10/7/2009	Choongwoo Cho	2	MAS-8-57	60K	56	56	57	59	58	57
10/8/2009	Choongwoo Cho	1	MAS-8-57	120K	56	58	59	59	59	58
10/8/2009	Choongwoo Cho	1	MAS-8-57	120K	57	57	57	57	57	57
10/8/2009	Choongwoo Cho	1	MAS-8-57	120K	55	56	56	56	56	56
10/8/2009	Choongwoo Cho	2	MAS-8-57	120K	50	51	53	53	53	52
10/8/2009	Choongwoo Cho	2	MAS-8-57	120K	53	55	55	55	55	55
10/8/2009	Choongwoo Cho	2	MAS-8-57	120K	50	51	52	52	52	51
10/10/2009	Choongwoo Cho	1	MAS-8-57	240K	53	55	55	55	56	55
10/10/2009	Choongwoo Cho	1	MAS-8-57	240K	51	52	52	52	54	52
10/10/2009	Choongwoo Cho	1	MAS-8-57	240K	55	54	54	54	54	54
10/10/2009	Choongwoo Cho	2	MAS-8-57	240K	46	46	46	46	46	46
10/10/2009	Choongwoo Cho	2	MAS-8-57	240K	48	50	50	50	50	50
10/10/2009	Choongwoo Cho	2	MAS-8-57	240K	50	50	50	50	50	50
10/11/2009	Choongwoo Cho	1	MAS-8-57	360K	49	50	50	50	50	50
10/11/2009	Choongwoo Cho	1	MAS-8-57	360K	45	45	46	46	46	46
10/11/2009	Choongwoo Cho	1	MAS-8-57	360K	47	48	48	48	49	48
10/11/2009	Choongwoo Cho	2	MAS-8-57	360K	43	44	44	44	44	44
10/11/2009	Choongwoo Cho	2	MAS-8-57	360K	44	45	45	45	45	45
10/11/2009	Choongwoo Cho	2	MAS-8-57	360K	43	44	44	44	44	44
10/12/2009	Choongwoo Cho	1	MAS-8-1	initial	86	85	85	84	84	85
10/12/2009	Choongwoo Cho	1	MAS-8-1	initial	84	85	83	83	82	83
10/12/2009	Choongwoo Cho	1	MAS-8-1	initial	83	82	81	81	81	82
10/12/2009	Choongwoo Cho	2	MAS-8-1	initial	86	85	85	83	83	84
10/12/2009	Choongwoo Cho	2	MAS-8-1	initial	83	82	82	81	80	82
10/12/2009	Choongwoo Cho	2	MAS-8-1	initial	82	82	81	80	80	81
10/12/2009	Choongwoo Cho	1	MAS-8-1	15K	65	66	66	66	65	66

Date	Operator	Sample Number	Sample Composition	Sample Condition	1	2	3	4	5	Average
10/12/2009	Choongwoo Cho	1	MAS-8-1	15K	65	66	66	66	66	66
10/12/2009	Choongwoo Cho	1	MAS-8-1	15K	66	65	65	65	65	65
10/12/2009	Choongwoo Cho	2	MAS-8-1	15K	60	61	61	60	60	60
10/12/2009	Choongwoo Cho	2	MAS-8-1	15K	66	68	70	70	70	69
10/12/2009	Choongwoo Cho	2	MAS-8-1	15K	65	66	66	65	66	66
10/13/2009	Choongwoo Cho	1	MAS-8-1	30K	63	64	64	64	64	64
10/13/2009	Choongwoo Cho	1	MAS-8-1	30K	60	60	63	61	60	61
10/13/2009	Choongwoo Cho	1	MAS-8-1	30K	65	65	65	65	65	65
10/13/2009	Choongwoo Cho	2	MAS-8-1	30K	61	61	61	61	61	61
10/13/2009	Choongwoo Cho	2	MAS-8-1	30K	62	63	62	62	62	62
10/13/2009	Choongwoo Cho	2	MAS-8-1	30K	61	61	61	61	62	61
10/14/2009	Choongwoo Cho	1	MAS-8-1	60K	60	60	60	60	60	60
10/14/2009	Choongwoo Cho	1	MAS-8-1	60K	60	62	62	62	62	62
10/14/2009	Choongwoo Cho	1	MAS-8-1	60K	59	60	60	60	60	60
10/14/2009	Choongwoo Cho	2	MAS-8-1	60K	60	60	60	60	60	60
10/14/2009	Choongwoo Cho	2	MAS-8-1	60K	59	60	61	62	62	61
10/14/2009	Choongwoo Cho	2	MAS-8-1	60K	63	65	65	66	66	65
10/15/2009	Choongwoo Cho	1	MAS-8-1	120K	55	56	56	58	57	56
10/15/2009	Choongwoo Cho	1	MAS-8-1	120K	55	57	57	57	57	57
10/15/2009	Choongwoo Cho	1	MAS-8-1	120K	57	57	59	59	59	58
10/15/2009	Choongwoo Cho	2	MAS-8-1	120K	53	55	55	55	55	55
10/15/2009	Choongwoo Cho	2	MAS-8-1	120K	57	60	60	60	60	59
10/15/2009	Choongwoo Cho	2	MAS-8-1	120K	60	60	60	61	61	60
10/16/2009	Choongwoo Cho	1	MAS-8-1	240K	52	53	54	54	54	53
10/16/2009	Choongwoo Cho	1	MAS-8-1	240K	56	56	57	57	57	57
10/16/2009	Choongwoo Cho	1	MAS-8-1	240K	55	55	55	55	55	55
10/16/2009	Choongwoo Cho	2	MAS-8-1	240K	53	53	54	54	54	54
10/16/2009	Choongwoo Cho	2	MAS-8-1	240K	50	51	51	50	51	51
10/16/2009	Choongwoo Cho	2	MAS-8-1	240K	55	55	55	55	55	55
10/17/2009	Choongwoo Cho	1	MAS-8-1	360K	50	50	50	50	50	50
10/17/2009	Choongwoo Cho	1	MAS-8-1	360K	49	50	50	50	50	50
10/17/2009	Choongwoo Cho	1	MAS-8-1	360K	52	52	52	52	52	52
10/17/2009	Choongwoo Cho	2	MAS-8-1	360K	45	45	45	45	45	45
10/17/2009	Choongwoo Cho	2	MAS-8-1	360K	46	46	47	47	47	47
10/17/2009	Choongwoo Cho	2	MAS-8-1	360K	50	51	51	51	51	51

APPENDIX C: INTERIM LITERATURE REVIEW REPORT

WO 15: Evaluating Performance of Limestone Prone to Polishing

Literature Review

Problem Statement

Pavements must provide appropriate surface friction, so that loss of vehicle control does not occur in normally expected situations when the pavement is wet. Surface friction is largely affected by the pavement surface texture which is a function of aggregate properties, size, and gradation in addition to other variables, such as durability of cement paste for rigid pavements, and asphalt binder for flexible pavements. It is thus vital that state highway agencies control aggregate properties and surface texture to minimize the accidents attributed to skidding on pavements exhibiting poor surface friction.

Pavement surface friction also referred to as skid resistance is the retarding force developed at the interface between the tire and the pavement when the vehicle tires are prevented from rotating slides along the pavement surface (HUANG, 2004).

Road surfaces develop gradually deteriorating surface characteristics such as macro and micro-texture, skid resistance amongst many others with time. It was discovered that in Pennsylvania, several roads built according to standard design and construction techniques and paved with Portland cement concrete have shown unwarranted rapid skid resistance deterioration well before the expected time limits (PennDOT, 2008). It was also found that a significant number of those PCC (Portland Cement Concrete) roadways were built using concrete mixtures with Vanport Limestone coarse aggregate.

The Vanport Limestone found in Pennsylvania has a low percentage of acid insoluble residue and polishes to a smooth surface when exposed to traffic loading rates greater than 1000 vehicles per day (PennDOT, 2008)

A report prepared by The Pennsylvania DoT compared several existing PCC pavements containing Vanport limestone aggregate, some which have been performing well for over 30 years and others characterized by unacceptable skid numbers after less than 12 years of normal use or in less than 3 years after surface grinding. The study has found that some portions of this aggregate have low acid insoluble residue which causes its premature polishing. The polishing occurs once the surface texture and mortar layer is worn off the pavement. In the pavements that the surface mortar layer and macro-texture remained intact, skid resistance levels remained acceptable (PennDOT, 2008).

The study also pointed out some problems caused by diamond grinding using conventional blade spacing and shot blasting. The surfaces where this king of intervention was used presented an abrupt reduction in its lifetime. However roads that were finished with a burlap drag, maintained an acceptable friction level for an average of 30 years regardless of coarse aggregate (Vanport, Dolomite, other limestone) in the mixture on several different roads.

Based on these findings, the committee recommended the following alternatives for further consideration:

1. Utilize the Minnesota texturing method using artificial turf carpeting drag.

2. Blend Vanport with better frictional aggregates.

3. Investigate the frictional properties affected by increasing the mortar fraction compared to the coarse aggregate concentration of mixes.

4. Design two layer composite pavements consisting of a concrete base and an asphalt wearing surface.

Aiming to collect research results and practice evaluation of similar studies, valuable information have been summarized and grouped according to the following major topics.

- Pavement surface texture

- Pavement friction

- Friction and texture measurement methods

- Indices for characterizing friction and surface texture

- Friction and design

Results from on site testing

Preliminary measurements were taken on one of the sites available with the original surface for which this investigation attempts to uncover the results of low friction. The site was located on I-79 Northbound at a station marker 1754. The site was transverse grooved Portland cement concrete. The site and the measurement equipment are depicted in the following pictures.



Several core samples were also taken from the locations close to that of the measurements for further analysis. The results of the measurements are given in the table below:

		RWP	Center	LWP	Shoulder
1	Friction	0.35	0.60	0.37	0.73
2	Friction	0.40	0.63	0.39	0.91
3	Friction	0.44	0.64	0.43	0.93
4	Friction	0.39	0.68	0.37	-
5	Friction	0.39	0.64	0.40	-
Average		0.39	0.64	0.39	0.86
1	Texture	0.34	0.46	0.34	1.12
2	Texture	0.42	0.51	0.43	1.24
3	Texture	0.31	0.50	0.33	1.22
4	Texture	0.33	0.38	0.35	-
5	Texture	0.42	0.46	0.36	-
Average		0.36	0.46	0.36	1.19

As it can be observed from the measurement values of friction the right and left wheel path friction values are significantly lower than the values of the center of the lane measurements. At the same time the measurements that were made on the shoulder with minimal or no traffic shows an even larger increase in friction, practically doubling that of the friction in the wheel paths.
The measurement of texture shows a very similar pattern with lower texture values in the wheel paths and a large increase in texture on the untraveled shoulder.

The preliminary measurements indicate very strong polishing and lack of macro-texture which points to the direction of lacking frictional characteristics due to deficient micro- and deficient macro texture of the surface.

In the following literature review we will give comprehensive overview of the measurement and relationship of friction and texture surface characteristic values and they connection to surface materials, construction techniques, weather and environmental conditions and traffic as well as the possible rehabilitation techniques and other relevant information.

PAVEMENT SURFACE TEXTURE

Definition

Pavement surface texture is made up of the deviations of the pavement surface from a true planar surface. These deviations occur at three distinct levels of scale, each defined by the wavelength (λ) and peak-to-peak amplitude (A) of its components. Although there is a wide range of pavement surface texture ranging from micro-texture to unevenness, the range that influences pavement surface friction are micro-texture and macro-texture.

Micro-texture and macro-texture were defined in 1987 by the Permanent International Association of Road Congresses (PIARC), are as follows: (PIARC 1987)

- Micro-texture (λ < 0.02 in [0.5 mm], A = 0.04 to 20 mils [1 to 500 μm])—Surface roughness quality at the sub-visible or microscopic level. It is a function of the surface properties of the aggregate particles contained in the asphalt or concrete paving material.
- Macro-texture (λ = 0.02 to 2 in [0.5 to 50 mm], A = 0.005 to 0.8 in [0.1 to 20 mm])—Surface roughness quality defined by the mixture properties (shape, size, and gradation of aggregate) of an asphalt paving material and the method of finishing/texturing (dragging, tining, grooving; depth, width, spacing and orientation of channels/grooves) used on a concrete paving material.

PIARC also defined mega-texture and unevenness as:

- Mega-texture (λ = 2 to 20 in [50 to 500 mm], A = 0.005 to 2 in [0.1 to 50 mm])—This type of texture is the texture which has wavelengths in the same order of size as the pavement–tire interface. It is largely defined by the distress, defects, or "waviness" on the pavement surface.
- Wavelengths longer than the upper limit (20 in [500 mm]) of mega-texture, are defined as roughness or unevenness (Henry, 2000).

Figure 1 graphically illustrates the four texture ranges.

It is widely recognized that pavement surface texture influences many different pavement–tire interactions. Figure 2 shows the ranges of texture wavelengths affecting various vehicle–road interactions, including wet-weather friction, interior and exterior noise, splash and spray, rolling resistance, and tire wear. As can be seen, wet-weather friction is primarily affected by micro-texture and macro-texture, which correspond to the adhesion and hysteresis friction components, respectively.

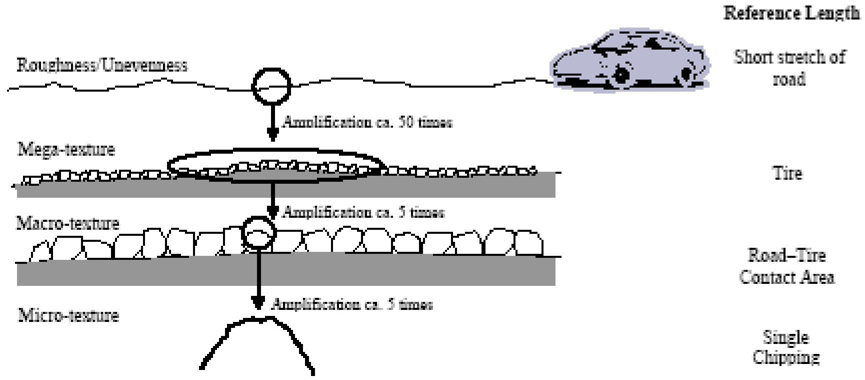

Figure 1. Simplified illustration of the various texture ranges that exist for a given pavement surface (Sandburg, 1998).

Factors Affecting Texture

There are many factors that affect pavement surface texture. These factors, relate to the aggregate, binder, and mix properties of the pavement surface material and any intentional texturing done to the material after placement. A summary of the factors that influence pavement surface texture obtained from published literature are shown in table 1. These factors can be optimized to obtain pavement surface characteristics required for a given design situation.

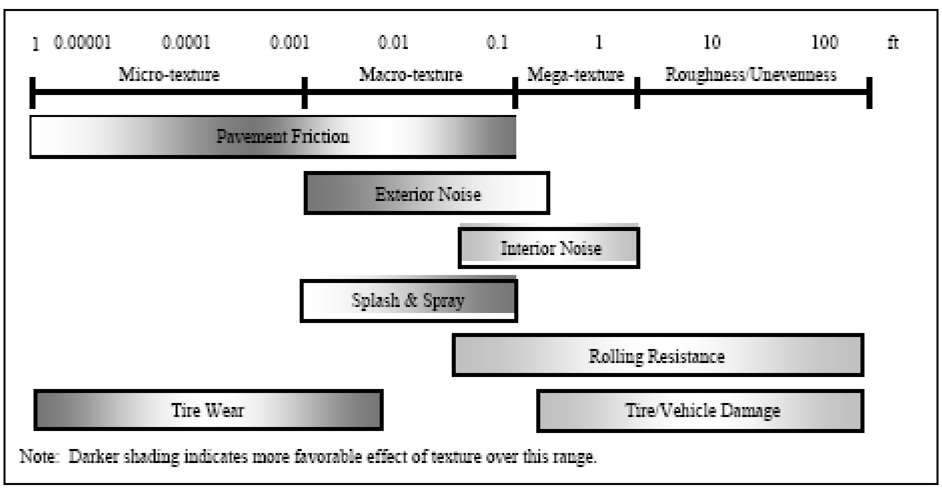

Figure 2. Texture wavelength influence on pavement–tire interactions (Henry, 2000; Sandburg and Ejsmont, 2002).

Table 1. Suggestions for optimizing pavement texture for friction and noise (Sandberg 2002; Henry 2000; Rado 1994; Wambold et al. 1995; AASHTO 1976).

Surface Type	Factor	Micro-Texture	Macro-Texture
Asphalt (includes chip seal)	Max. aggregate dimensions		X
	Coarse aggregate types	X (surface roughness)	X
	Fine aggregate types		X
	Mix gradation		X
	Mix air content		X
	Mix binder		X
Concrete	Coarse aggregate type	X (for exposed aggregate PCC)	X (for exposed aggregate PCC)
	Fine aggregate type	X	
	Mix gradation		X (for exposed aggregate PCC)
	Texture dimensions and spacing		X
	Texturing orientation		X
	Texture skew		X

PAVEMENT FRICTION

Definition

Pavement friction is described as the force that resists the relative motion between a vehicle tire and a pavement surface. This resistive force (illustrated in figure 3) is generated as the tire rolls or slides over the pavement surface.

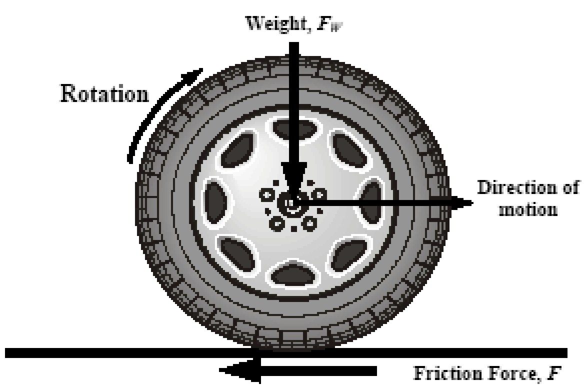

Figure 3. Simplified diagram of forces acting on a rotating wheel.

The resistive force (characterized using the non-dimensional friction coefficient, μ) is the ratio of the tangential friction force (F) between the tire tread rubber and the horizontal traveled surface to the perpendicular force or vertical load (F_W) and is computed using equation 1.

$$\mu = \frac{F}{Fw} \qquad 1$$

Pavement friction plays a vital role in keeping vehicles on the road, as it gives drivers the ability to control/maneuver their vehicles in a safe manner, both in the longitudinal and lateral directions. It is a key input to highway geometric design as it is used in determining if the minimum stopping sight distance, minimum horizontal radius, minimum radius of crest vertical curves, and maximum superelevation in horizontal curves provided in a given highway design are adequate. Generally speaking, the higher the friction available at the pavement-tire interface, the more control the driver has over the vehicle, whereas the lower the friction, the less control.

Longitudinal Frictional Forces

Longitudinal frictional forces are the forces that occur between a rolling pneumatic tire (in the longitudinal direction) and the road surface when operating in the free rolling or constant-braked mode. In the free-rolling mode (no braking), the relative speed between the tire circumference and the pavement—referred to as the slip speed—is zero. In the constant-braked mode, the slip speed increases from zero to a potential maximum of the speed of the vehicle. The following mathematical relationship explains slip speed:

$$S = V - V_p = V - (0.68 \cdot \omega \cdot r) \qquad 2$$

where: S = Slip speed, mi/hr.
V = Vehicle speed, mi/hr.
V_P = Average peripheral speed of the tire, mi/hr.
ω = Angular velocity of the tire, radians/sec.
r = Average radius of the tire, ft.

Again, during the free-rolling state of the tire, V_P is equal to the vehicle speed and thus S is zero. For a locked or fully-braked wheel, V_P is zero, so the sliding speed or slip speed is equal to the vehicle speed (V). A locked-wheel state is often referred to as a 100 percent slip ratio and the free-rolling state is a zero percent slip ratio. The following mathematical relationships give the calculation formula for slip ratio:

$$SR = \frac{V - V_P}{V} \cdot 100 = \frac{S}{V} \cdot 100 \qquad 3$$

where: SR = Slip ratio, percent.
V = Vehicle speed, mi/hr.
V_P = Average peripheral speed of the tire, mi/hr.
S = Slip speed, mi/hr.

Similarly to the previous explanation, during the free-rolling state of the tire, V_P is equal to the vehicle speed and S is zero, thus the slip ratio (SR) is zero percent. For a locked wheel, V_P is zero, S equals the vehicle speed (V), and so the slip ratio (SR) is 100 percent.

Figure 4 shows the ground forces acting on a tire under the free-rolling operation mode. In this mode, the ground force is at the center of pressure of the tire contact area and is off center by the amount a. This offset causes a moment that must be overcome to rotate the tire. The force required to counter this moment is called the rolling resistance force (F_R). The value a is a function of speed and increases with speed. Thus, F_R increases with speed.

In the constant-braked mode (figure 5), an additional force called the braking slip force (F_B) is required to counter the added moment (M_B) created by braking. The force is proportional to the level of braking and the resulting slip ratio. The total frictional force is the sum of the free-rolling resistance force (F_R) and the braking slip force (F_B).

The coefficient of friction between a tire and the pavement changes with varying slip, as shown in figure 6 (Kulakowski et al., 1990). The coefficient of friction increases rapidly with increasing slip to a peak value that usually occurs between 10 and 20 percent slip (critical slip). The friction then decreases to a value known as the coefficient of sliding friction, which occurs at 100 percent slip. The difference between the peak and sliding coefficients of friction may equal up to 50 percent of the sliding value, and is much greater on wet pavements than on dry pavements. The relationship shown in figure 6 is the basis for anti-locking brake systems (ABS); the concept being to take advantage of the front side of peak friction and minimize the loss of side/steering friction due to sliding action.

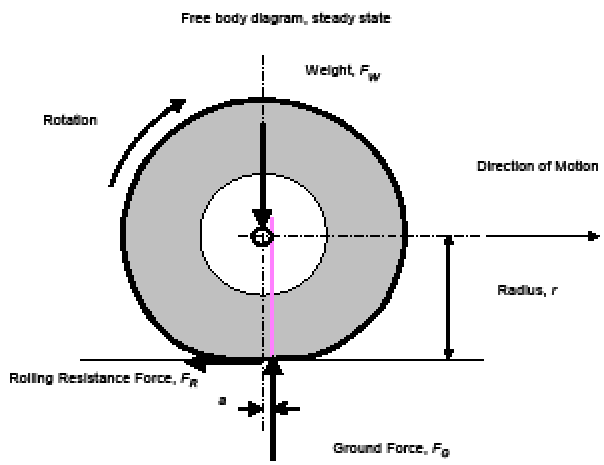

Figure 4. Rolling resistance force with a free-rolling tire at a constant speed on a bare, dry paved surface (Andresen and Wambold, 1999).

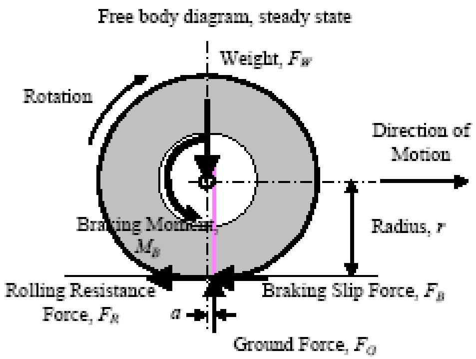

Figure 5. Forces and moments of a constant-braked wheel on a bare, dry paved surface (Andresen and Wambold, 1999).

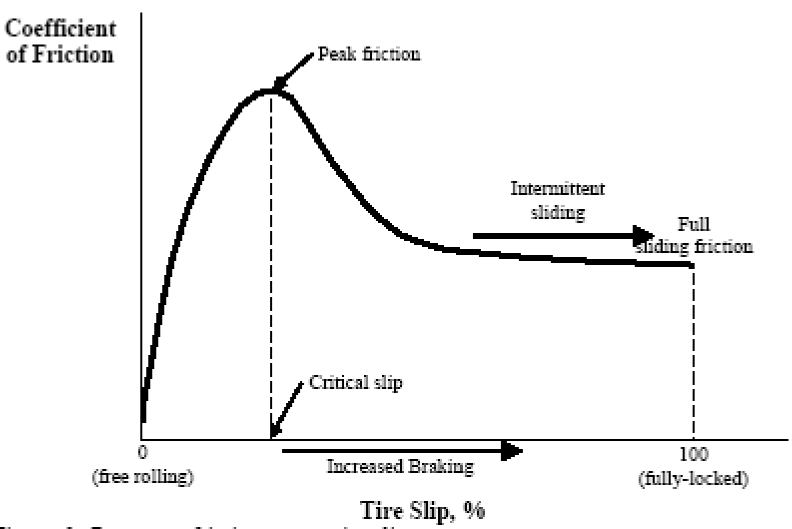

Figure 6. Pavement friction versus tire slip.

Lateral Frictional Forces

The preceding discussion has pertained to the longitudinal frictional forces associated with traversing and braking along a tangent (i.e., straight segment) of highway. Another important aspect of friction relates to the lateral or side force friction that occurs as a vehicle changes direction or compensates for pavement cross-slope and/or cross wind effects. The basic relationship between the forces acting on the vehicle tire and the pavement surface as the vehicle steers around a curve, changes lanes, or compensates for lateral forces is as follows:

$$F_S = \frac{V^2}{15\,R} - e \qquad 4$$

where: F_S = Side friction.
V = Vehicle speed, mi/hr.
R = Radius of the path of the vehicle's center of gravity (also, the radius of curvature in a curve), ft.
e = Pavement super-elevation

Equation 4 is based on the pavement–tire steering/cornering force diagram in figure 7. It shows how the side force friction factor acts as a counter balance to the centripetal force developed as a vehicle performs a lateral movement.

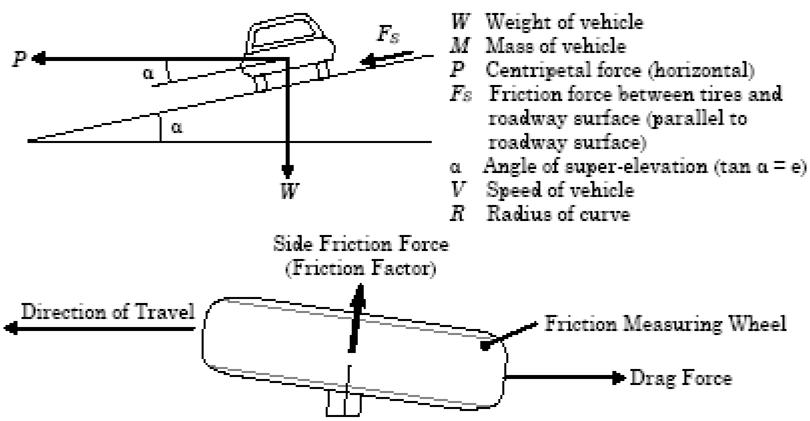

Figure 7. Dynamics of a vehicle traveling around a constant radius curve at a constant speed, and the forces acting on the rotating wheel.

Friction Mechanisms

Pavement friction is the result of a complex interplay between two principal frictional force components—adhesion and hysteresis (figure 8). Adhesion is the friction that results from the small-scale bonding/interlocking of the vehicle tire rubber and the pavement surface as they come into contact with each other. It is a function of the

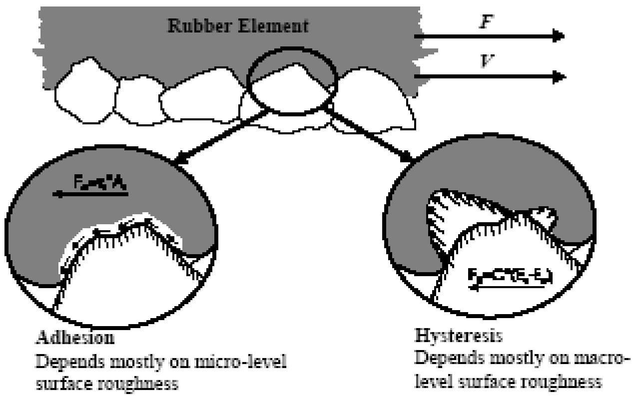

Figure 8. Key mechanisms of pavement–tire friction.

interface shear strength and contact area. The hysteresis component of frictional forces results from the energy loss due to bulk deformation of the vehicle tire. When a tire compresses against the pavement surface, deformation energy is stored within the rubber. As the tire relaxes, part of the stored energy is recovered, while the other part is lost in the form of heat (hysteresis), which is irreversible.

Although there are other components of pavement friction (e.g., tire rubber shear), they are insignificant when compared to the adhesion and hysteresis force components. Thus, friction can be viewed as the sum of the adhesion and hysteresis frictional forces.

$$F = F_A + F_H \qquad 5$$

Both components depend to a large extent on pavement surface characteristics, the contact between tire and pavement, and the properties of the tire. Also, because tire rubber is a visco-elastic material, each component is affected by temperature and sliding speed.

Because adhesion force is developed at the pavement–tire interface, it is most responsive to the micro-level asperities (micro-texture) of the aggregate particles contained in the pavement surface. In contrast, the hysteresis force developed within the tire is most responsive to the macro-level asperities (macro-texture) formed in the surface via mix design and/or construction techniques. As a result of this phenomenon, adhesion governs the overall friction on smooth-textured and dry pavements, while hysteresis is the dominant component on wet and rough-textured pavements.

Factors Affecting Available Pavement Friction

The factors that influence pavement friction forces can be grouped into four categories—pavement surface characteristics, vehicle operational parameters, tire properties, and environmental factors. Table 2 lists the various factors comprising each category. Because each factor in this table plays a role in defining pavement friction, friction must be viewed as a process instead of an inherent property of the pavement alone. It is only when all these factors are fully specified that friction takes on a definite value. The more critical factors are highlighted in table 2 (shown in bold) and discussed below.

Table 2. Factors affecting available pavement friction
(modified from Wallman and Astrom, 2001).

Pavement Surface Characteristics	Vehicle Operating Parameters	Tire Properties	Environment
• **Micro-texture** • **Macro-texture** • Mega-texture/ unevenness • **Material properties** • Temperature	• **Slip speed** ➢ vehicle speed ➢ braking action • Driving maneuver ➢ turning ➢ overtaking	• Width • **Tread design and condition** • Rubber composition and hardness • **Inflation pressure** • Load • Temperature	• Climate ➢ Wind ➢ **Temperature** ➢ **Water** ▪ rainfall ▪ condensation ➢ **Snow and Ice** • **Contaminants** ➢ Anti-skid material (salt, sand) ➢ Dirt, mud, debris

Pavement Surface Characteristics

Texture

Micro-texture and macro-texture are the two levels of pavement texture which affect the pavement-tire friction (Henry 2000). Micro-texture is mostly responsible for pavement friction at low speeds where there is sufficient contact between the tire and pavement surface to ensure that all friction available at the pavement tire interface is utilized. At higher speeds, however, available friction may be diminished or lost because of a reduction of the tire and pavement contact area due phenomenon's such as hydroplaning. Pavement macro-texture is predominantly responsible for reducing potential separation of the tire and pavement surface due to hydroplaning and to induce friction caused by hysteresis for vehicles traveling at high speeds. Thus, micro-texture is the single most important factor at both low and high speeds in providing adequate friction at the tire pavement interface (Papagouli and Kokkalis 1998). Thus, micro-texture is the single most important factor at low speeds providing strong adhesional friction component while at high speeds can play vital role provided adequate macro-texture presents sufficient contact area (Papagouli and Kokkalis 1998). The influence of macro-texture in providing friction increases with speed, first at moderate speeds with supplying contact area through for adhesion friction to develop and for increasing speeds with providing hysteresis that becomes dominant at high speed. The difference between micro-texture and macro-texture is presented in Figure 9.

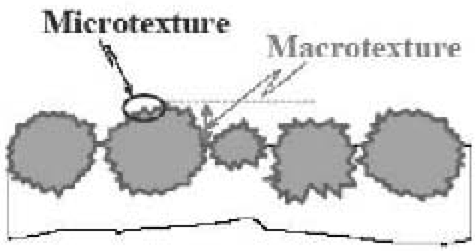

Figure 9. Micro-texture versus macro-texture. (Flintsch et al. 2003)

Figure 10 shows the relative influences of micro-texture, macro-texture, and speed on wet pavement friction. As can be seen, micro-texture influences the magnitude of tire friction, while macro-texture impacts the friction–speed gradient. At low speeds, micro-texture dominates the wet friction level. At higher speeds, the presence of high macro-texture facilitates the drainage of water so that the adhesive component of friction afforded by micro-texture is re-established. Hysteresis increases with speed exponentially, and at speeds above 65 mi/hr (105 km/hr) could account for over 95 percent of the friction.

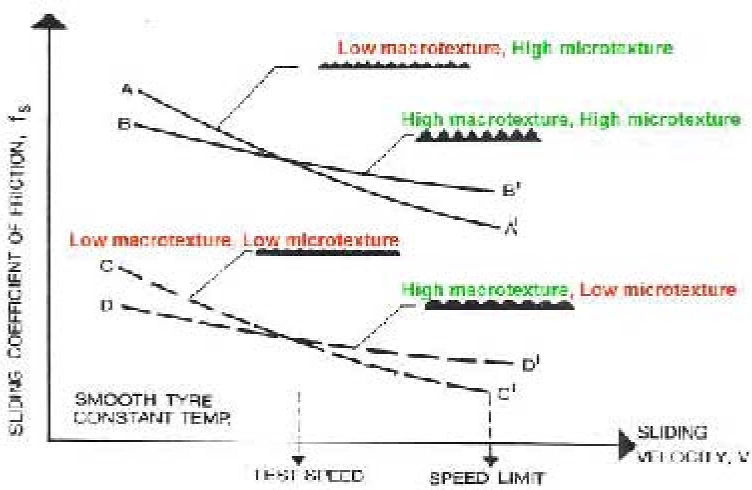

Figure 10. Effect of micro-texture and macro-texture on pavement–tire wet friction at different sliding speeds (Flintsch et al., 2002).

Pavement Surface Material Properties

As indicated previously, pavement material properties (i.e., aggregate and mix characteristics, surface texture patterns) influence both micro-texture and macro-texture. These properties also affect the long-term durability of texture through their capacities to resist aggregate polishing and abrasion/wear of both aggregate and mix under accumulated traffic and environmental loadings.

<u>Tire Properties</u>

Tire Tread Design and Condition

Tire tread design (i.e., type, pattern, and depth) and condition have a significant influence on draining water that accumulates at the pavement surface. Water trapped between the pavement and the tire can be expelled through the channels provided by the pavement macro-texture and by the tire tread. The depth of tread is particularly important for vehicles driving over thick films of water at high speeds. Some studies have reported a decrease in wet friction of 45 to 70 percent for fully worn tires as compared to new ones.

Tire Inflation Pressure

Low inflation pressure, can significantly reduce friction at high speeds. This is because a significantly under-inflated tire allows the center of the tire tread to collapse and become very concave resulting in the constriction of drainage channels within the tire tread and a reduction of contact pressure. The effect is for the tire to trap water at the pavement surface rather than allow it to flow through the treads. As a consequence, hydroplaning speed is decreased.

High inflation pressure, on the other hand, causes only a small loss of pavement friction (Kulakowski et al., 1990). Increasing the tire pressure reduces the trapping effect and also yields higher pressure for forcing water from below the vehicle's tire. The increased tire pressure and thus smaller tire contact area, results in a higher hydroplaning speed.

Thermal Properties

Automotive tires are visco-elastic materials and thus their properties can be significantly affected by changes in temperature and other thermal properties, such as thermal conductivity and specific heat. Reviews of research reports indicate that in general pavement–tire friction decreases with increasing tire temperature though this is difficult to quantify.

Environment

Water

Water, in the form of rainfall or condensation, can act as a lubricant, significantly reducing the friction between tire and pavement. The effect of water film thickness (*WFT*) on friction is minimal at low speeds (<20 mi/hr [32 km/hr]) and quite pronounced at higher speeds (>40 mi/hr [64 km/hr]). As shown in figure 11, the coefficient of friction of a vehicle tire sliding over a wet pavement surface, decreases exponentially as *WFT* increases. The rate at which the coefficient of friction decreases generally becomes smaller as *WFT* increases. In addition, the effect of *WFT* is influenced by tire design and condition, with worn tires being most sensitive to *WFT*.

A very small amount of water can significantly reduce pavement friction. Test results from an FHWA-sponsored study (Harwood, 1987) indicate that as little as 0.002 in (0.05 mm) of water on the pavement surface can reduce the coefficient of friction by 20 to 30 percent of the dry coefficient of friction. In some cases, a 0.001-in (0.025-mm) water film can reduce friction significantly. Such a thin water film is likely to be formed during any hour in which at least 0.01 in (0.25 mm) of rain has fallen.

A particularly hazardous situation involving relatively thick water layers or films and vehicles traveling at higher speeds is hydroplaning. Hydroplaning occurs when a vehicle tire is separated from the pavement surface by the water pressure that builds up at the pavement–tire interface (Horne and Buhlmann, 1983), causing friction to drop to a near-zero level.

Hydroplaning is a complex phenomenon that is affected by several parameters, including water depth, vehicle speed, pavement macro-texture, tire tread depth, tire inflation pressure, and tire contact area.

Relatively thick water films form on a pavement surface when drainage is inadequate during heavy rainfalls or when pavement rutting or wearing creates puddles. Loss of direct pavement–tire contact via hydroplaning can occur at speeds as low as 40 to 45 mi/hr (64 to 72 km/hr) on puddles about 1 in (25 mm) deep and 30 ft (9 m) long (Hayes et al., 1983).

Pavement macro-texture and tire tread depth influence the onset of dynamic hydroplaning in two ways. First, they have a direct effect on the critical hydroplaning speed because they provide a pathway for water to escape from the pavement–tire interface. Secondly, they have an indirect effect on the critical hydroplaning speed since larger the macro-texture, the deeper the water must be to cause hydroplaning. Thus, increases in macro-texture depth and tire tread depth tend to increase the critical hydroplaning speed. However, the pavement surface must also have the proper micro-texture to develop adequate friction.

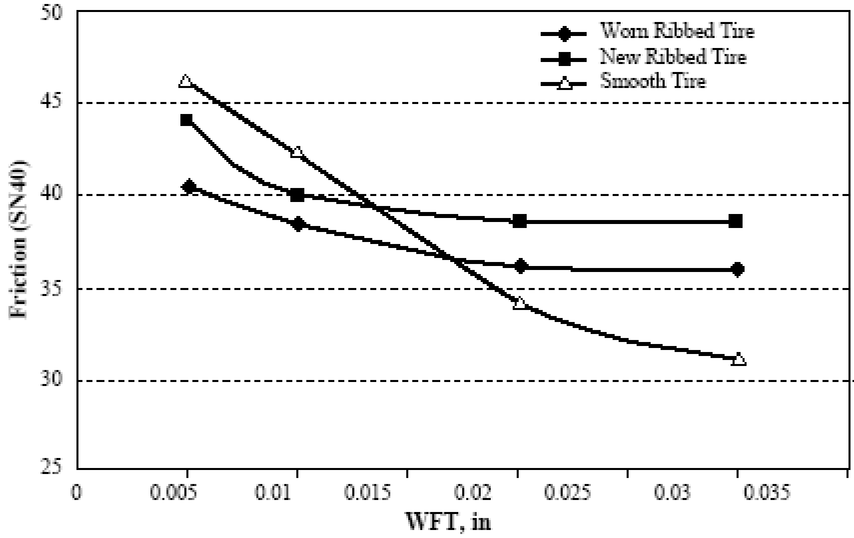

Figure 11. Effect of water film thickness on pavement friction (Henry, 2000).

Snow and Ice

Ice and snow covering the pavement surface present the most hazardous condition for vehicle braking or cornering. The level of friction between the tires and the snow- or ice-covered pavement is such that almost any abrupt braking or sudden change of direction results in locked-wheel sliding and loss of vehicle directional stability. As stated previously, this Guide does not address winter-related friction issues, such as the treatment of snow and ice. However, the NCHRP Project 6-14 final report (Al Qadi et al., 2002) covering winter-related friction measurement noted that vehicle friction performance can be drastically degraded if the tire contact area does not reach the pavement surface because of contaminate (ice and snow) amount.

<u>Contaminants</u>

Any kind of contamination at the pavement–tire interface will have an adverse effect on pavement–tire friction. This is because particles of foreign material act as the balls in a ball bearing or as lubricant between a piston and cylinder in an engine, which thus reduces friction between the two surfaces. The thicker or more viscous the contaminant, the greater the reduction in pavement–tire friction. Types of contaminants commonly found on highways include dirt, sand, oil, water, snow, and ice. The grinding effect of contaminants of considerable hardness, such as sand, helps accelerate the rate of wearing at the pavement surface.

The most common type of surface contamination is due to water. A wet pavement surface generally has a lower level of friction than a comparable dry surface. Water on a pavement surface can also accumulate as a film under the tire footprint causing the tire to lift from the road surface, losing traction at high speeds. This phenomenon is called hydroplaning. The degree of hydroplaning is also affected by vehicle speed, tire tread pattern, and the depth of water at the pavement surface. In general, deeper water, higher speeds, lighter vehicles, wider tires, lover tire pressure, less tread depth, and less efficient tread designs will cause tires to hydroplane at lower speeds. However, all tires will be forced to hydroplane at some speed. The occurrence of hydroplaning can be reduced considerably by increasing the rate at which water is drained from a pavements surface (i.e., increasing pavement macrotexture and cross slope).

FRICTION AND TEXTURE MEASUREMENT METHODS

Overview

The measurement of pavement friction and texture has been of primary importance for the last 50 years. Many different types of equipment have been developed and used to measure these properties, and their differences in terms of measurement principles and procedures and the way measurement data are processed and reported, can be significant.

For friction-testing alone, there are over a dozen, commercially produced devices that can operate at fixed or variable slip, at speeds up to 100 mi/hr (161 km/hr), and under variable test tire conditions, such as load, size, tread design, inflation pressure, and construction. Measurement of pavement surface texture, whether it be micro-, macro-, or mega-texture, can be measured using a variety of laser devices, volumetric techniques, water drainage rates (outflow meter), and sliding rubber pad apparatus (British portable pendulum tester).

This section provides an overview of the different friction and texture measurement methods and available representative equipment. ASTM and AASHTO have developed a set of surface characteristic standards and measurement practice standards to ensure comparable texture and friction data reporting. Since the standards ensure comparability of the measurements for practical purposes, the methods and devices are discussed in pairs and are grouped according to measurements performed at highway speeds and measurements requiring lane closure (i.e., low-speed/walking and stationary devices).

In general, the measurement devices requiring lane closure are simpler and relatively inexpensive, whereas the highway-speed devices are more complex, require more training to maintain and operate, and are more expensive. With the recent development of technology in data acquisition, sensor technology, and data processing power of computers, the once true superiority of data quality for the stationary and low-speed devices is diminishing. The resolution and accuracy of the acquired data for the measurement devices that are low-speed or stationary can be still superseding that of the high-speed devices, but with smaller and smaller margins.

Friction

The two common devices used for the measurement of pavement friction characteristics in the laboratory or at low speeds in the field are the British Pendulum Tester (BPT) and the Dynamic Friction Tester (DFT). Both these devices measure frictional properties by determining the loss in kinetic energy of a sliding pendulum or rotating disc when in contact with the pavement surface. The loss of kinetic energy is converted to a frictional force and thus pavement friction. The DFT has the added advantage of being able to measure the speed dependency of the pavement friction by measuring friction at various speeds. (Saito et al. 1996)These two methods offer the advantage of being highly portable and easy to handle.

Full scale friction measurements utilize one or two full-scale test tires to measure pavement friction properties in the following modes (1) locked wheel, (2) side-force, (3) fixed-slip, and (4) variable slip.

The most common method for measuring pavement friction in the United States is the locked-wheel method. (Henry 2000) The locked-wheel method is specified in ASTM E
274. This method is meant to test the frictional properties of the surface under emergency braking conditions for a vehicle without anti-lock brakes. As opposed to the side force and fixed slip methods, the locked-wheel approach tests at a slip speed equal to the vehicle speed, this means that the wheel is locked and unable to rotate. (Henry1986) The results of a locked-wheel test conducted under ASTM specifications are reported as a skid number (SN) or friction number (FN). Equation 6 is used for computing SN or FN.

$$SN\ (V, \%\ SLIP\ ) = \frac{F}{N} * 100 \qquad 6$$

Where:

F = friction force

N = vertical load on the test tire

Locked-wheel friction testers usually operate at speeds between 40 and 60 mph. Testing can be done using a smooth or ribbed tire. The ribbed tire is insensitive to the pavement surface water film thickness, thus it is insensitive to the pavement macro-texture. The smooth tire on the other hand is sensitive to macro-texture.

Locked wheel skid testers are used in some fashion in all 50 states for measuring pavement surface friction. (Wambold et al. 1995)

The side-force method is used to measure the ability of vehicles to maintain control in curves and involves maintaining a constant angle, the yaw angle, between the tire and the direction of motion. Equation 7 shows how the side-force coefficient (SFC) is calculated.

$$SFC\ (V, \alpha) = \frac{F_s}{N} * 100 \qquad 7$$

Where:

V = velocity of the test tire

α = yaw angle
N = normal force on the test tire
F_s = force perpendicular to plane of rotation

Since the yaw angle is typically small, between 7.5 and 20 degrees, the slip speed is also quite low; this means that side-force testers are particularly sensitive to the pavement micro-texture but are generally insensitive to changes in the pavement macro-texture. The two most common side-force measuring devices are the Mu-Meter and the Side-Force Coefficient Road Inventory Machine (SCRIM). The primary advantage offered by side-force measuring devices is the ability for continuous friction measurement throughout a test section (Henry 2000). This ensures that areas of low friction are not skipped due to a sampling procedure.

Fixed-slip devices measure the friction observed for vehicles with anti-lock brakes. Fixed-slip devices maintain a constant slip, typically between 10 and 20 percent, as a vertical load is applied to the test tire; the frictional force in the direction of motion between the tire and pavement is measured. (Henry 2000). Equation 8 is used
for calculating the percent slip:

$$Percent\ \ Slip = \frac{(V - r\omega)}{V} * 100 \tag{8}$$

Where:

Percent Slip	= the ratio of slip speed to test speed (in percent)
V	= test speed
r	= effective tire rolling radius
ω	= angular velocity of test tire

These devices are also more sensitive to micro-texture as the slip speed is low.

Variable slip devices measure the frictional force as the tire is taken through a predetermined set of slip ratios.

Texture

With the exception of the British Pendulum Tester (which is an indicator of pavement micro-texture), the commonly applied texture measurement methods provides pavement surface macro-texture information. Other means of measuring (estimating) micro-texture include low-speed testing with friction measurement devices, such as the Dynamic Friction Tester (DFT) and the locked-wheel skid trailer equipped with a smooth test tire (Flintsch et al., 2002).

Modern methods used to characterize pavement surface texture are typically based on non-contact surface profiling techniques. An example of a non-contact profiler developed by the FHWA for use in characterizing pavement surface texture is the Road Surface Analyzer ($ROSAN_V$). $ROSAN_V$ is a portable, vehicle-mounted, automated system for the measurement of pavement texture at highway speeds along a linear path. $ROSAN_V$ incorporates a laser sensor mounted on the vehicle's front bumper and the device can be operated at speeds of up to 70 mi/hr (113 km/hr). The system calculates both MPD and estimated texture depth (ETD), which is an estimate of MTD derived from MPD using a transformation equation.

An automated measurement system such as $ROSAN_V$ provides a large quantity of valuable and less expensive (when a large amount is needed) texture data while greatly reducing the safety and traffic control problems inherent to the manually performed Volumetric Patch Methods. Some of the applications of $ROSAN_V$ include the following (FHWA 2002):

- Texture measurements for pavement management systems.
- Site specific texture measurements for safety investigations.
- Quality control (QC) measurements for new pavement for certifying pavement meeting contract specifications for texture and aggregate segregation limits.
- Combining friction-testing equipment, such as a skid trailer, with $ROSAN_V$ for simultaneous surface friction and texture measurement.
- Texture and surface detail measurements (grooving, tining) in noise research studies.

Texture measurements from non-contact surface profiling techniques generally correlate well with the texture depths measured using the volumetric methods. Several procedures have been developed to improve such correlations and provide uniform worldwide compatibility of such measurements.

As a result of the international PIARC experiment to compare and harmonize texture and skid resistance measurements, there is a clear preference for both volumetric and profiler-derived texture depth measurements to be reported in terms of MPD. MPD has been standardized as reported in ISO 13473, "Characterization of Pavement Textures Using Pavement Profiles—Part 1: Determination of Mean Profile Depth" (ISO, 1997c). ASTM provides the following model for relating mean texture depth (measured from the volumetric testing procedure) and mean profile depth (measured using profilers) as follows: (ASTM 19??)

$$MTD = 0.79*MPD + 0.23 \qquad 9$$

Summary of Test Methods and Equipment

Friction measurement equipment capable of highway speeds (high-speed devices) are described and illustrated in tables 3 and 4, whereas friction measurement equipment requiring lane closure (stationary and walking/low-speed devices) are described and illustrated in tables 5 and 6. Tables 7 and 8 provide summary information for texture measurement equipment capable of highway speeds (high-speed devices), whereas descriptions and illustrations of texture measurement equipment requiring lane closure (stationary and walking/low-speed devices) are shown in tables 9 and 10.

INDICES FOR CHARACTERIZING FRICTION AND SURFACE TEXTURE

International Friction Index (PIARC Model)

The International Friction Index (IFI) was proposed based on the PIARC International harmonization study conducted in 1992 by representatives from 16 countries covering each continent. The experiment was conducted at 54 sites across the U.S. and Europe and included 51 different measurement systems. Various types of friction testing equipment were evaluated, including locked wheel, fixed slip, ABS, variable slip, side force, pendulum, and some new prototype devices. Surface texture was measured by means of the sand patch, laser profilometers (using the triangulation method), an optical system (using the light sectioning method), and outflow meters.

One of the main results of the PIARC experiment was the development of the IFI. The IFI standardized the practice of how the dependency of friction on the tire sliding speed is reported. As a measure of how strongly friction depends on the relative sliding speed of an automotive tire, the gradient of the friction values measured below and above 37 mi/hr (60 km/hr) is reported as value of an exponential model for the IFI index. This gradient is named the Speed Number (S_P), and is reported in the range 0.6 to 310 mi/hr (1 to 500 km/hr).

The PIARC experiment strongly confirmed other research that S_P is a measure of the macro-texture influence of the surfaces on friction. Macro-texture is in focus as a major contributor to friction safety characteristics for several reasons. The most well known reason is the hydraulic drainage capability that macro-texture has for wet pavements during or immediately after a rainfall. This capability will also minimize the risk for hydroplaning. Another reason is that the wear or polishing of macro-texture can be interpreted from S_P as it changes value over time for a section of road.

A pronounced peak shape or a steep negative slope of the friction–slip speed curve is considered dangerous. The normal driver will experience an unexpected loss in braking power when the brake pedal is pushed to its maximum, and the braking power is not at its maximum. A smallest possible negative slope or even a flat shape of the friction–slip speed curve is therefore desired and obtained with proper macro-texture.

Table 3. Overview of highway-speed pavement friction test methods.

TEST METHO D	ASSOCIATE D STANDAR D	DESCRIPTION	EQUIPMENT	
Locked-Wheel	ASTM E 274	This device is installed on a trailer which is towed behind the measuring vehicle at a typical speed of 40 mi/hr (64 km/hr). Water (0.02 in [0.5 mm] thick) is applied in front of the test tire, the test tire is lowered as necessary, and a braking system is forced to lock the tire. Then the resistive drag force is measured and averaged for 1 to 3 seconds after the test wheel is fully locked. Measurements can be repeated after the wheel reaches a free rolling state again.	Testing requires a tow vehicle and locked-wheel skid trailer, equipped with either a ribbed tire (ASTM E 501) or a smooth tire (ASTM E 524). The smooth tire is more sensitive to pavement macro-texture, and the ribbed tire is more sensitive to micro-texture changes in the pavement.	
Side-Force	ASTM E 670	Side-force friction measuring devices measure the pavement side friction or cornering force perpendicular to the direction of travel of one or two skewed tires. Water is placed on the pavement surface (4 gal/min [1.2 L/min]) and one or two skewed, free rotating wheels are pulled over the surface (typically at 40 mi/hr [64 km/hr]). Side force, tire load, distance, and vehicle speed are recorded. Data is typically collected every 1 to 5 in (25 to 125 mm) and averaged over 3-ft (1-m) intervals.	-The British Mu-Meter, shown at right, measures the side force developed by two yawed (7.5 degrees) wheels. Tires can be smooth or ribbed. -The British Sideway Force Coefficient Routine Investigation Machine (SCRIM), shown at right, has a wheel yaw angle of 20 degrees.	 
Fixed-Slip	ASTM E 274	Fixed-slip devices measure the rotational resistance of smooth tires slipping at a constant slip speed (12 to 20 percent). Water (0.02 in [0.5 mm] thick) is applied in front of a retracting tire mounted on a trailer or vehicle typically traveling 40 mi/hr [64 km/hr]. Test tire rotation is inhibited to a percentage of the vehicle speed by a chain or belt mechanism or a hydraulic braking system. Wheel loads and frictional forces are measured by force transducers or tension and torque measuring devices. Data are typically collected every 1 to 5 in (25 to 125 mm) and averaged over 3-ft (1-m) intervals.	-Roadway and runway friction testers (RFTs). -Airport Surface Friction Tester (ASFT), shown at right. -Saab Friction Tester (SFT), shown at right. -U.K. Griptester, shown at right. -Finland BV-11. -Road Analyzer and Recorder (ROAR). -ASTM E 1551 specifies the test tire suitable for use in fixed-slip devices.	 
Variable-Slip	ASTM E 1859	Variable-slip devices measure friction as a function of slip (0 to 100 percent) between the wheel and the highway surface. Water (0.02 in [0.5 mm] thick) is applied to the pavement surface and the wheel is allowed to rotate freely. Gradually the test wheel speed is reduced and the vehicle speed, travel distance, tire rotational speed, wheel load, and frictional force are collected at 0.1-in (2.5-mm) intervals or less. Raw data are recorded for later filtering.	-French IMAG. -Norwegian Norsemeter RUNAR, shown at right. -ROAR and SALTAR systems.	

		smoothing, and reporting.		

Table 4. Additional information on highway-speed pavement friction test methods.

TEST METHOD	MEASUREMENT INDEX	APPLICATIONS	ADVANTAGES	DISADVANTAGES
Locked-Wheel	The measured resistive drag force and the wheel load applied to the pavement are used to compute the coefficient of friction, μ. Friction is reported as friction number (FN) or skid number (SN).	Field testing (straight segments). Network-level friction monitoring.	Well developed and very widely used in the U.S. More than 40 states use locked-wheel devices. Systems are user friendly, relatively simple, and not time consuming.	Can only be used on straight segments (no curves, T-sections, or roundabouts). Can miss slippery spots because measurements are intermittent.
Side-Force	The side force perpendicular to the plane of rotation is measured and averaged to compute the Mu Number, *MuN*, or the sideways force coefficient, *SFC*.	Field testing straight sections, curves, steep grades. Data in different applications should be collected separately.	Relatively well controlled skid condition similar to fixed-slip device results. Measurements are continuous throughout a test pavement section. Method is commonly used in Europe.	Very sensitive to road irregularities (potholes, cracks, etc.) which can destroy tires quickly. Mu-Meter is primarily only used for airports in the U.S.
Fixed-Slip	The measured resistive drag force and the wheel load applied to the pavement are used to compute the coefficient of friction, μ. Friction is reported as FN.	Field testing (straight segments). Network-level friction monitoring. Project-level friction monitoring.	Continuous, high resolution friction data collected.	Fixed-slip devices take readings at a specified slip speed. Their slip speeds do not always coincide with the critical slip speed value, especially over ice- and snow-covered surfaces. Uses large amounts of water in continuous mode. Requires skillful data reduction.
Variable-Slip	When used for variable-slip measurements, the system provides a chart of the relationship between slip friction number and slip speed. The resulting indices are: • Longitudinal slip friction number • Peak slip friction number • Critical slip ratio • Slip ratio • Slip to skid friction number • Estimated friction number • Rado Shape factor When used for locked-wheel measurements, the system provides friction number (μ) values.	Field testing (straight or curved segments). Network-level friction monitoring. Project-level friction monitoring.	Can provide continuously any desired fixed or variable slip friction results. Can provide the Rado shape factor for detailed evaluation.	Large, complex equipment with high maintenance costs and complex data processing and analysis needs. Uses large amounts of water in continuous mode.

Table 5. Overview of pavement friction test methods requiring traffic control.

TEST METHOD	ASSOCIATED STANDARD	DESCRIPTION	EQUIPMENT	
Stopping Distance Measurement	ASTM E 445	The pavement surface is sprayed with water until saturated. A vehicle is driven at a constant speed (40 mi/hr [64 km/hr] specified) over the surface. The wheels are locked, and the distance the vehicle travels while reaching a full stop is measured. Alternatively, different speeds and a fully engaged antilock braking system (ABS) have been used.	A passenger car or light truck (at least 3,200 lb [preferable equipped with a heavy-duty suspension system]) is specified. The braking system should be capable of full and sustained lockup. Tires should be ASTM E 501 ribbed design.	
Deceleration Rate Measurement	ASTM E 2101	Testing is typically done in winter contaminated conditions. While traveling at standard speed (20 to 30 mi/hr [32 to 48 km/hr]), the brakes are applied to lock the wheels, until deceleration rates can be measured. The deceleration rate is recorded for friction computation.	Mechanical or electronic equipment, shown at right, is installed on any vehicle to measure and record deceleration rate during stopping.	
Portable Testers	ASTM E 303 ASTM E 1911	Portable testers can be used to measure the frictional properties of pavement surfaces. These testers use pendulum or slider theory to measure friction in a laboratory or in the field. The pendulum tester produces a low-speed sliding contact between a standard rubber slider and the pavement surface. The elevation to which the arm swings after contact provides an indicator of the frictional properties. Data from five readings are typically collected and recorded by hand. The Dynamic Friction Tester measures the torque necessary to rotate three small, spring-loaded, rubber pads in a circular path over the pavement surface at speeds from 3 to 55 mi/hr (5 to 89 km/hr). Water is applied at 0.95 gal/min (3.6 L/min) during testing. Rotational speed, rotational torque, and downward load are measured and recorded electronically.	-The British Pendulum Tester (BPT) is manually operated and documented, as shown at top right. -The Dynamic Friction Tester (DFT), shown at bottom right, is a modular system that is controlled electronically. Results are typically recorded at 12, 24, 36, and 48 mi/hr (20, 40, 60, and 80 km/hr), and the speed, friction relationship can be plotted. It fits in the trunk of a car and is accompanied by a water tank and portable computer.	 

Table 6. Additional information on pavement friction test methods requiring traffic control.

TEST METHOD	MEASUREMENT INDEX	APPLICATIONS	ADVANTAGES	DISADVANTAGES
Stopping Distance Measurement	Stopping distance number (*SDN*) or coefficient of friction (μ) is determined using the following equation: $$\mu = \frac{v^2}{2 * g * d}$$ where: μ = Coefficient of friction. v = Vehicle brake application speed, ft/sec (m/sec). g = Acceleration due to gravity, 32.2 ft/sec² (9.81 m/sec²). d = Stopping distance, ft (m).	Field testing (straight segments). Accident investigations.	Simplest method for determining pavement surface friction.	Test values obtained are not very repeatable. Traffic control is required.
Deceleration Rate Measurement	The measured deceleration force is used to calculate the pavement surface friction coefficient, μ, using the equation: $$\mu = \frac{\text{Measured Deceleration}}{g}$$ where: μ = Coefficient of friction. g = Acceleration due to gravity, 32.2 ft/sec² (9.81 m/sec²). The measured deceleration can be directly measured for the complete stopping operation or determined for a partial stop as the difference between the initial and final deceleration divided by the braking time.	Field testing (straight segments). Accident investigations.	System is easy to use, small, portable, lightweight, and easy to install and remove.	Requires a sudden braking maneuver to be made, and such maneuvers may not be operationally desirable (Al-Qadi et al., 2002). Cannot be used for network evaluation. Generally requires traffic lane closure.
Portable Testers	The British Pendulum Tester (BPT) provides a British Pendulum Number (BPN) based on the pendulum swing height of a calibrated BPT. The Dynamic Friction Tester (DFT) produces DFT numbers or friction coefficients and a graph of the friction coefficient for different rotational speeds. This device also reports the peak friction, associated peak slip speed, and the International Friction Index (IFI), designated by FN60 and S_p.	The BPT provides friction and micro-texture indicators for any pavement, whether in the field or from laboratory analysis of cored or prepared samples. It is also used to evaluate the effect of wear on friction and texture. The DFT can be used for field and laboratory testing for quality control, project, and investigatory friction data collection.	The BPT is used worldwide as a measure of friction and texture. It is suitable for both laboratory and field evaluation. The BPT can be used to measure both longitudinal and lateral pavement-tire friction. The DFT provides good repeatability and reproducibility and is unaffected by operators or wind. It also provides friction coefficients that are representative of high speed values. It can produce the IFI statistics, and it correlates well with BPN.	BPN variability is large and can be affected by operator procedures and wind effects. Traffic control is required for both portable testers. They do not always simulate pavement–tire characteristics. Both devices collect only spot measurement and cannot be used for network evaluation. To quantify a given section of pavement, several measurements must be made over the length of the section.

Table 7. Overview of highway-speed pavement surface texture test methods.

TEST METHOD/ EQUIPMENT	ASSOCIATED STANDARD	DESCRIPTION	EQUIPMENT
Electro-optic (laser) method (EOM)	ASTM E 1845 ISO 13473-1 ISO 13473-2 ISO 13473-3	Non-contact very high-speed lasers are used to collect pavement surface elevations at intervals of 0.01 in (0.25 mm) or less. This type of system, therefore, is capable of measuring pavement surface macro-texture (0.5 to 50 mm) profiles and indices. Global Positioning Systems (GPS) are often added to this system to assist in locating the test site. Data collecting and processing software filters and computes the texture profiles and other texture indices.	High-speed laser texture measuring equipment (such as the FHWA ROSAN system shown at right) uses a combination of a horizontal distance measuring device and a very high speed (64 kHz or higher) laser triangulation sensor. Vertical resolution is usually 0.002 in (0.5 mm) or better. The laser equipment is mounted on a high-speed vehicle, and data is collected and stored in a portable computer.  

Table 8. Additional information on highway-speed pavement surface texture test methods.

TEST METHOD/EQUIPMENT	MEASUREMENT INDEX	ADVANTAGES	DISADVANTAGES
Electro-optic (laser) method (EOM)	Using the measured texture profiles, the EOM system computes mean profile depth (*MPD*) as the difference between the peak and average elevations for consecutive 2-in (50-mm) segments, averaged in 4 in (100 mm) profile segments. Estimated texture depth (*ETD*), in units of millimeters, can then be estimated as: $ETD = 0.2 + 0.8\,MPD$ RMS macro-texture levels can also be computed. The power of texture wavelengths can also be determined using power spectral density computations.	• Collects continuous data at high speeds. • Correlates well with MTD. • Can be used to provide a speed constant to accompany friction data.	• Equipment is very expensive. • Skilled operators are required for collection and data processing.

Table 9. Overview of pavement surface texture test methods requiring traffic control.

TEST METHOD/ EQUIPMENT	ASSOCIATED STANDARD	DESCRIPTION	EQUIPMENT	
Sand Patch Method (SPM)	ASTM E 965, ISO 10844	This volumetric-based spot test method provides the mean depth of pavement surface macro-texture. The operator spreads a known volume of glass beads in a circle onto a cleaned surface and determines the diameter and subsequently mean texture depth (MTD).	Equipment includes: Wind screen, 1.5 in³ (25,000 mm³) container, scale, brush, and disk (2.5- to 3-in [60- to 65-mm] diameter). ASTM D 1155 glass beads.	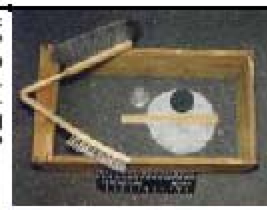
Outflow Meter (OFM)	ASTM WK 364	This volumetric test method measures the water drainage rate through surface texture and interior voids. It indicates the hydroplaning potential of a surface by relating to the escape time of water beneath a moving tire. Correlations with other texture methods have also been developed.	Equipment is a cylinder with a rubber ring on the bottom and an open top. Sensors measure the time required for a known volume of water to pass under the seal or into the pavement.	
Circular Texture Meter (CTM)	ASTM E 2157	This non-contact laser device measures the surface texture in an 11.25-in (286-mm) diameter circular profile of the pavement surface at intervals of 0.034 in (0.868 mm), matching the measurement path of the DFT. It rotates at 20 ft/min (6 m/min) and provides profile traces and mean profile depths for the pavement surface.	Equipment includes a water supply, portable computer, and the texture meter device.	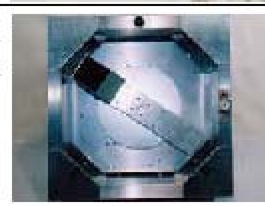 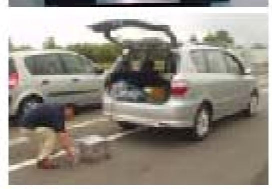
Texture Depth Gauge (TDG)	AASHTO T 261	This device provides an average depth of PCC grooves or tining. The gauge is inserted into 10 grooves to measure their depths.	A digital depth gauge, illustrated at right, can be used.	

Table 10. Additional information on pavement surface texture test methods requiring traffic control.

TEST METHOD/EQUIPMENT	MEASUREMENT INDEX	ADVANTAGES	DISADVANTAGES
Sand Patch Method (SPM)	Mean texture depth (MTD) of macro-texture is computed as: $MTD = \frac{4V}{\Pi D^2}$ where: *MTD* = Mean texture depth, in (mm) *V* = Sample volume, in³ (mm³) *D* = Average material diameter, in (mm)	• Simple and inexpensive methods and equipment. • When combined with other data, can provide friction information. • Widely used method.	• Method is slow and requires lane closure. • Only represents a small area. • Only macro-texture is evaluated. • Sensitive to operator variability. • Labor intensive activity.
Outflow Meter (OFM)	Output is the time in milliseconds for outflow of specified volume of water. Shorter outflow times indicate rougher surface texture.	• Simple methods and relatively inexpensive equipment. • Provides an indication of hydroplaning potential in wet weather.	• Method is slow and requires lane closure. • Only represents a small area of the pavement surface. • Output does not have a good correlation with MPD or MTD
Circular Texture Meter (CTM)	Indices provided by the CTM include the mean profile depth (*MPD*) and the root mean square (*RMS*) macro-texture. *MPD* has been correlated to *MTD* according to the following relationship (units of mm): $MTD = 0.947\, MPD + 0.069$	• Measures same diameter as DFT, allowing texture-friction comparisons. • Repeatable, reproducible, and independent of operators • Correlates well with *MTD*. • Measures positive and negative texture. • Is small (29 lb [13 kg]) and portable. • Setup time is short (less than 1 minute)	• Method is slow (about 45 seconds to complete) and requires lane closure. • Represents a small surface area.
Texture Depth Gauge (TDG)	TDG provides the average groove/tine depth with a reporting accuracy of 0.03 in (1 mm).	• Simple method and inexpensive equipment.	• Method is slow and requires lane closure. • Only represents a small area of the pavement. • Does not provide complete macro-texture information. • Labor intensive activity.

The IFI is composed of two numbers—FN60 and S_p—and the designation and reporting of this index is IFI(FN60,S_p). The IFI is based on a mathematical model of the friction process called the PIARC Friction Model. It models the friction coefficient as a function of slip speed and macro-texture as follow:

$$S_p = a + bTX \qquad 10$$

Where:

S_p = speed number
a, b = coefficients dependent on the device used for measuring macrotexture
TX = macro-texture measurement

$$FR60 = FRS e^{\frac{S-60}{S_p}} \tag{11}$$

Where:

FR60 = adjusted value of friction for a slip speed of 60 km/h
FRS = measured friction value at speed S
S = slip speed (km/h)

$$F60 = A + B \times FR60 + C \times TX \tag{12}$$

Where:

A, B = coefficients dependent on friction measuring device
C = regression constant required for measurements using ribbed tire
TX = macro-texture measurement required for ribbed tire readings

It should be noted that the equation 11 can be used to adjust measurements made at speeds other than the standard 40 mi/hr (65 km/hr) with an ASTM E 274 trailer to calculate FN40 (see equation 13).

$$FN(s) = FN_V \cdot e^{-\frac{s-V}{S_p}} \tag{13}$$

For example, a measurement made at low speed, say 20 mi/hr (32 km/hr), or one made at a high speed of 60 mi/hr (96 km/hr), can be adjusted to FN40 by setting *S* to 40 and *V* to the measuring speed (20 or 60 mi/hr [32 or 96 km/hr]). Note that if the unit mi/hr is used, then *Sp* must also be in mi/hr.

The use of IFI to estimate friction values at any speed is illustrated on figure 12. As shown, IFI utilizes the two indices contained in the IFI model (FN60 and S_p). Having measured S_p and the friction value FN60 at 60 km/hr, the friction value at any other slip speed can be estimated by choosing a value for *S*. The friction curve is plotted according to equation 13 and the FN_{60} and S_p number are indicated on the graph.

The S_p for the pavement surface may be measured by a device that measures macro-texture. S_p can also be obtained by running a minimum of two measurement runs of the surface with each run at a different slip speed at the same vehicle speed. Some friction measuring devices measure both friction force and macro-texture in the same measurement. IFI or the PIARC model describes friction experienced by a driver in emergency braking using non-ABS brakes and deals with the friction from wheel lock-up to stop, whereas the Rado model (discussed next) describes the same braking process using ABS brakes and deals with friction experienced in the initial braking mechanisms.

International Friction Index and the Rado Model

The PIARC friction model basically deals with the high slip speed and locked wheel phase of the friction range. It does not apply to the relatively low speed and low slip speed frictional segment where the friction number rises sharply to a maximum value.

With the advent of ABS brake functions, it is also of great interest to model the initial curve segment of the first phase of a braking scenario.

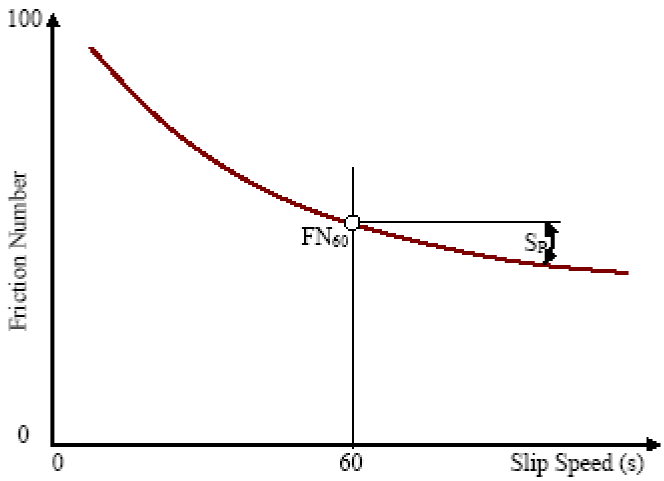

Figure 12. The PIARC Friction Model.

For estimating braking action with ABS brakes, the maximum friction value, when the wheel is still rolling with low slip ratios, is essential. Under such conditions the tire will work to give the vehicle directional control, as well as perform braking. In the locked wheel state, the tire is unable to contribute to directional control.

There is a need for a friction model which complements the PIARC friction model for the above reasons. A mathematical model for the behavior of the maximum friction value has been accomplished. It is in the following form:

$$FN(s) = \mu_{max} \cdot e^{-\left(\frac{\ln\left(\frac{s}{S_{max}}\right)}{\bar{C}}\right)^2} \qquad 14$$

In this relation, μ_{max} is the maximum friction value and S_{max} is the corresponding slip speed, also known as the critical slip speed. In other words, when the tire is slipping on the pavement with S_{max} slip speed while still rolling, it develops μ_{max} friction.

$\bar{C}$ is a shape factor which is closely related to the speed constant (S_P) in the PIARC model. The parameter $\bar{C}$ determines the skewed shape of the full friction curve (see figure 13). The Rado model also treats μ_{max} as a function of surface and tire properties, measuring speed and slip speed.

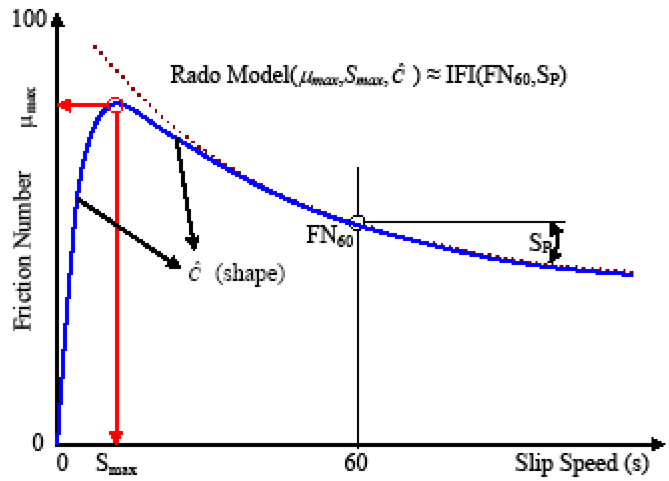

Figure 13. The PIARC and Rado friction models.

The Rado friction model lends itself to determining the actual friction curve for a braking process from free rolling to a locked wheel state. Variable slip measurement devices can utilize this model to characterize their measurement with three parameters that fully describe the whole friction process (μ_{max}, S_{max}, $\hat{c}$). Utilizing different mathematical procedures, the three parameters can be estimated from raw measured data. This reduces the thousands of measured data points making up the friction curve from a measurement to three numbers that together with the mathematical form can re-create the whole friction curve.

The technique is characterized by doing controlled wheel braking on the measuring tire while keeping a constant traveling speed. The measuring wheel is braked gradually from free rolling to locked state through the range of available slip speeds.

By sampling hundreds of friction values at known slip speeds, a friction number curve is fitted to the acquired data points. The equation for the friction number curve is determined. An equation for the maximum friction values is also derived.Having the equations, friction values can be estimated and presented for any slip- and sliding speeds, as well as different traveling speeds under the same environmental conditions.

The Rado friction model applied can directly report the IFI, FN_{60}, and S_P. In this model, S_P is the derivative of the curve at the FN_{60} point, when it is transformed to a logarithmic form. Figure 13 depicts both the Rado and PIARC friction models. Maximum friction values can be predicted for the measured surface stripe at all other traveling speeds for the same tire using this model. The RADO friction index is a three-number index—peak friction (μ_{peak}), critical slip speed (S_{max}), and the form factor ($\hat{c}$).

PAVEMENT FRICTION AND CONSTRUCTION DESIGN

The design and construction design of pavement with regard to friction is a relatively small component of the overall pavement design process yet it is a critical component because of the safety issue. Its importance and complexity have increased over the years due to increased demands for safer roads and the desire for greater highway user comfort, which sometimes contradicts friction. Friction design requires a thorough understanding of the factors that influence friction and knowledge of the materials and construction techniques (including equipment) that ultimately dictate initial and long-term friction. It also requires an understanding of the economic and engineering tradeoffs associated with different materials and techniques. Analyzing and indeed designing pavement surfaces for both new pavement structures and a rehabilitation activity so that they have adequate friction is a unique process that involves identifying materials and construction activities that produce an appropriate combination of micro-texture and macro-texture. Generally the micro-texture is a function of the type of aggregate used in the surface mix or if it is a sealed pavement the function of the properties and construction techniques used for the sealing, while the macro-texture is generally dictated by the gradation/size of the aggregate in the mix or the type of texturing applied to the surface of the in-place mix.

FRICTION AND DESIGN

Consideration of Aggregate in Friction Design

As pointed out in previous section, texture plays a key role in the development of pavement–tire frictional forces and is primarily governed by the properties of the aggregate used in the pavement surface. While asphalt binder and cement paste can affect micro-texture—particularly just after a surface mix is placed—it is aggregate that makes up the bulk of asphalt and concrete mixtures, and thus serves as the primary contact medium with the vehicle tires.

Aggregate generally is viewed as two distinct fractions—coarse aggregate and fine aggregate. Coarse aggregate pieces are greater than the No. 4 sieve (0.19 in [4.75 mm]), with most pieces between 0.375 and 1.5 in (9.5 and 38 mm). Fine aggregate, on the other hand, is the collection of natural or crushed/manufactured particles less than 0.19 in (4.75 mm), but greater than the No. 200 sieve (0.003 in [75 µm]).

Aggregate testing and characterization must be targeted to the fraction(s) of aggregate in a mix that will control the frictional performance. In general, for asphalt mixtures, it is the coarse aggregate that controls, whereas for concrete mixes, it is the fine aggregate. Exceptions include fine-graded asphalt mixes, where fine aggregates are in greater abundance, and concrete mixes in which coarse aggregates are either intentionally exposed at the time of construction (exposed aggregate concrete) or will become exposed in the future (e.g., diamond grinding/grooving, surface abrading, porous concrete).

Research by Dahir and Henry (1978), Kandhal and Parker (1998), and Folliard and Smith (2003), among others, indicates that the following aggregate properties have a significant influence on pavement friction performance:

- Hardness.
- Mineralogy (i.e., mineral composition and structure).
- Shape.
- Texture.
- Angularity.
- Abrasion Resistance.
- Polish Resistance.
- Soundness.

Aggregate hardness and mineralogy largely dictate the wear characteristics (i.e., durability, polish) of the aggregate. Aggregates that exhibit the highest levels of long-term friction are typically composed of hard, strongly bonded, interlocking mineral crystals (coarse grains) embedded in a matrix of softer minerals (Kulakowski, 1990). The differences in grain size and hardness provide a constantly renewed abrasive surface because of differential wear rates and the breaking off of the harder grains from the softer matrix of softer minerals.

Aggregates made up of hard minerals alone typically resist wear and other forms of degradation, yet may polish easily when subjected to traffic. Aggregates made up of moderately soft minerals alone resist polishing, but wear at very fast rates when subjected to traffic. Thus, while a wear-resistant aggregate is desired in the mixture, some wearing of the pavement surface must occur in order to ensure good levels of skid resistance (Davis, 2001).

As summarized in table 11, aggregate angularity, shape, and texture are important parameters for defining both micro-texture and macro-texture. Fine aggregates that exhibit angular edges and cubical or irregular shapes generally provide higher levels of micro-texture, whereas those with rounded edges or elongated shapes generally produce lower micro-texture. For coarse aggregates, sharp and angular particles interlock and produce a deep macro-texture as compared to more rounded, smooth particles. Moreover, in asphalt mixes, platy (i.e., flat and elongated) aggregate particles tend to orient themselves horizontally, resulting in lower macro-texture depth.

Table 11. Effect of aggregate angularity, shape, and texture properties on pavement friction.

Aggregate Fraction	Aggregate Property	Effect of Aggregate Property on Pavement Friction	
		Asphalt Surface	Concrete Surface
Fine	Angularity and shape	No effect.	Defines pavement micro-texture, which highly impacts friction.
	Texture	No effect.	Little to no effect.
Coarse	Angularity and shape	Defines pavement macro-texture, which significantly impacts friction via hydroplaning potential.	If exposed, helps define pavement macro-texture, which impacts friction via hydroplaning potential.
	Texture	Defines pavement micro-texture, which highly impacts friction.	If exposed, helps define pavement micro-texture, which impacts friction.

The abrasion resistance of aggregates is an indicator of the aggregate resistance to mechanical degradation. The use of abrasion-resistant aggregates is important to avoid the breakdown of fine and/or coarse aggregates. During handling, stockpiling, mixing, and construction, the breakdown of fine and/or coarse aggregates can significantly alter the mix gradation, thereby affecting the porosity of open-graded friction course (OGFC) asphalt mixes and porous concrete mixes. For concrete mixes, it can result in the loss of strength due to the production of excess fines in the concrete mix. In asphalt mixes, the increase in fines can alter the volumetric properties and result in insufficient binder or may contribute to rutting and shoving. After construction, the breakdown of fine and/or coarse aggregates due to traffic shear forces can result in a loss of macro-texture.

Polish-resistant aggregates are those that are able to largely retain their harsh micro-texture under the grinding and shearing effects of repeated traffic loadings. For asphalt surface mixes, it is the hardness and mineralogy of the coarse aggregate particles that largely determine the degree of polishing that takes place. For concrete mixes, because the surface is composed primarily of mortar and is initially devoid of coarse aggregates, the polishing resistance of fine aggregates is the most critical parameter (Folliard and Smith, 2003). The coarse aggregate becomes an influencing factor only if it is made or becomes exposed.

Soundness refers to an aggregate's ability to resist degradation caused by climatic/ environmental effects (i.e., wetting and drying, freezing and thawing). Similar to abrasion resistance, sound and durable aggregate properties are important from the standpoint of avoiding the breakdown of fine and/or coarse aggregates, particularly when used in harsh climates.

Aggregate Types and Characteristics

Table 12. Natural Aggregates used for chip seals (Gransberg and James, 2005).

TYPE	PERCENTAGE USE IN UNITED STATES
Limestone	37
Quartzite	13
Granite	35
Trap Rock	13
Sandstone	10
Natural Gravels	58
Greywacke, Basalt	4

Aggregates can be either natural or synthetic in nature. The most commonly used natural aggregates are those obtained by quarrying and crushing rocks, such as limestone, sandstone, and granite. Natural aggregates may also consist of stream and bank gravels that are obtained from dredging, washing, and screening, and are usually crushed to improve their angularity (Kulakowski et al., 1990).

Synthetic aggregates are obtained by processing a wide variety of raw materials (natural or artificial). Sources of synthetic aggregates include such materials as blast-furnace slag, fly ash, and waste products from the glass, brick, tile, and other industries. The physical characteristics of different synthetic aggregates vary considerably depending on the source material and the manufacturing process. Because of these differences, the performance of these aggregates when used in pavement surfaces can vary widely (Kulakowski et al., 1990).

In general, synthetic aggregates are less susceptible to polishing than natural aggregates, but they tend to abrade more rapidly (Kulakowski et al., 1990).

Most limestones are very susceptible to polish. Aggregates derived from serpetinite, soapstone, siltstone, shale, and schists may also polish very rapidly (Kulakowski et al., 1990).

Aggregate Tests

Many laboratory material tests were note d in the literature as being useful or pertinent in defining aggregate frictional properties. Many of these same tests were reported in the state friction survey (see listing in appendix C) as being used to ensure the use of aggregates with good frictional properties.

Several of the tests cited are often conducted for reasons other than friction performance. For example, for concrete pavements, mineralogical tests are very important in assessing the potential development of alkali-aggregate reactivity, D-cracking, and spalling. For asphalt pavements, coarse and fine aggregate particle shape and texture are good indicators of permanent deformation and fatigue cracking potential.

Based on recent comprehensive evaluations of aggregate tests related to performance (Kandhal and Parker, 1998; Folliard and Smith, 2003) and the proactive work of various states—Maryland, Michigan, Ohio, New York, and Texas, to name a few—the following tests are considered to be most relevant in characterizing frictional properties and potential performance.

- Scratch Hardness (Mohs).
- Petrographic Analysis (ASTM C 295).
- Uncompacted Voids (UV) for Fine Aggregate (AASHTO T 304 or ASTM C 1252).
- UV for Coarse Aggregate (AASHTO T 326).
- Fractured-Face Particles (ASTM D 5821).
- Micro-Deval for Fine Aggregates (Canadian Standards Association [CSA] A23.2-23A).
- Micro-Deval for Coarse Aggregates (AASHTO TP 58 or ASTM D 6928).
- LA Abrasion (AASHTO T 96 or ASTM C 131 for small-sized coarse aggregates; ASTM C 535 for large-sized coarse aggregates).
- Acid Insoluble Residue (AIR) (ASTM D 3042).
- Polished Stone Value (PSV) (AASHTO T 278 and T 279 or ASTM E 303 and D 3319).
- Magnesium Sulfate Soundness (AASHTO T 104 or ASTM C 88).

Table 12 provides a brief description of each test and shows their recommended applications. Further discussion about the selection of tests is provided below. It is important to note that each test in of itself cannot be fully relied upon to predict friction performance. The selection and use of multiple tests will add to the reliability, but, even then, there is no total guarantee of friction performance in the field. Thus, it is essential that testing be used in conjunction with field performance history to identify acceptable aggregate types.

Table 13. Test methods for characterizing aggregate frictional properties.

Aggregate Property	Aggregate Type	Test Name	Test Protocol	Test Description	Applications
Hardness	Fine	Scratch Hardness test	Mohs	Rough measure of the resistance of a mineral's surface to scratching. Expressed using a 1-to-10 scale (1 being very soft, 10 being very hard), Mohs hardness is determined by observing whether its surface is scratched by minerals of a known or defined hardness.	• New concrete surfacings.
	Coarse	Scratch Hardness test	Mohs	Same as above.	• New asphalt surfacings and asphalt mixes used for friction restoration. • New concrete surfacings (conventional and innovative).*
Mineralogy (i.e., Aggregate Composition & Structure)	Fine	Descriptive Nomenclature for Constituents of Concrete Aggregates	ASTM C 294	Provides brief descriptions of commonly occurring natural or artificial aggregates from which mineral aggregates are derived. The descriptions provide a basis for understanding the potential effects on pavement friction of using different aggregate materials.	• New concrete surfacings.
		Petrographic Analysis	ASTM C 295	Used to assess aggregate (1) constituent minerals and structure, (2) surface texture, and (3) mineralogy, and to develop a petrographic database for aggregate sources to serve as a basis for linking aggregate sources to pavement field performance (Folliard and Smith, 2003).	
	Coarse	Descriptive Nomenclature for Constituents of Concrete Aggregates	ASTM C 294	Same as above.	• New asphalt surfacings and asphalt mixes used for friction restoration. • New concrete surfacings (conventional and innovative).*
		Petrographic Analysis	ASTM C 295	Same as above	

* For conventional PCC surfaces, where coarse aggregates are expected to be exposed, and innovative surfaces, such as porous concrete and exposed aggregate concrete.

Table 13. Test methods for characterizing aggregate frictional properties (continued).

Aggregate Property	Aggregate Type	Test Name	Test Protocol	Test Description	Applications
Angularity, Shape, & Texture	Fine	Uncompacted Voids (UV) test for fine aggregates	AASHTO T 304 (or ASTM C 1252)	Fine aggregate of prescribed gradation is allowed to flow through orifice of a funnel and fill a 6.1-in^3 (100-cm^3) cylinder. Excess material is struck off and cylinder with aggregate is weighed. Uncompacted void content is computed using this weight and the bulk dry specific gravity of the aggregate (Kandhal et al., 1997). Higher uncompacted void contents are generally the result of more fractured faces and rougher textures, which are desirable for pavement friction.	• New concrete surfacings.
	Coarse	Uncompacted Voids (UV) test for coarse aggregates	AASHTO T 326[b]	Coarse aggregate angularity, shape, and texture can be determined using principles similar to those described above for fine aggregates. Again, higher uncompacted void contents are generally the result of more fractured faces and rougher textures, which are desirable for pavement friction.	• New asphalt surfacings and asphalt mixes used for friction restoration. • New concrete surfacings (conventional and innovative).[a]
		Fractured-Face Particles test	ASTM D 5821	Determines the amount (percent) of fractured-faced (an angular, rough, or broken surface of an aggregate particle) aggregate particles, by visual inspection. The fractured face of each aggregate particle must meet a minimum cross-sectional area.	• New asphalt surfacings and asphalt mixes used for friction restoration. • New concrete surfacings (conventional and innovative).[a]
Abrasion/Wear Resistance	Fine	Micro-Deval test for fine aggregates	Canadian Standards Association (CSA) A23.2-23A	A fine aggregate sample is subjected to wet attrition by placing it in a steel jar with 0.375-in (9.5-mm) diameter steel balls and water. The jar is rotated at 100 rpm for 15 minutes, after which aggregate damage is assessed by mass loss using a No. 200 (75 μm) sieve. Higher percentages of loss indicate greater potential for aggregate breakdown (Folliard and Smith, 2003).	• New concrete surfacings (conventional).
	Coarse	LA Abrasion test	AASHTO T 96 (or ASTM C 131 [for small-sized coarse aggregates] ASTM C 535 [for large-sized coarse aggregates])	A dry aggregate sample is placed in a steel drum with six to twelve 420-gram steel balls, and the drum is rotated for 500 to 1,000 revolutions. Degradation by impact of the aggregate sample is determined by the percentage passing the No. 12 (1.7-mm) sieve.	• New asphalt surfacings and asphalt mixes used for friction restoration. • New concrete surfacings (conventional and innovative)[a]
		Micro-Deval test for coarse aggregates	AASHTO TP 58 (or ASTM D 6928)	A coarse aggregate sample is subjected to wet attrition by placing it in a steel jar with 0.375-in (9.5-mm) diameter steel balls and water. The jar is rotated at 100 rpm for 2 hours, after which aggregate damage is assessed by mass loss using a No. 16 (1.18-mm) sieve.	• New asphalt surfacings and asphalt mixes used for friction restoration. • New concrete surfacings (conventional and innovative)[a]

[a] For conventional PCC surfaces, where coarse aggregates are expected to be exposed, and innovative surfaces, such as porous concrete and exposed aggregate concrete.
[b] Formerly AASHTO TP 56.

Table 13. Test methods for characterizing aggregate frictional properties (continued).

Aggregate Property	Aggregate Type	Test Name	Test Protocol	Test Description	Applications
Polish Resistance	Fine	Acid Insoluble Residue (AIR) test	ASTM D 3042	Estimates the percent by weight of insoluble, hard, non-carbonate residue in carbonate aggregates (e.g., limestone, dolomite), using hydrochloric acid solution to react the carbonates. Higher acid insoluble residue (AIR) values indicate larger percentages of siliceous minerals, which are considered more polish resistant than carbonate materials (Kandhal et al., 1997).	• New concrete surfacings.
	Coarse	Polished Stone Value (PSV) test	AASHTO T 278 & T 279 (or ASTM E 303 & D 3319)	Aggregate coupons (aggregates embedded in epoxy resin) are fabricated, subjected to accelerated polishing (using British polish wheel) for a specified time (usually 9 hrs), and then tested for frictional resistance (expressed as British Pendulum Number [BPN]) using the British Pendulum Tester. The BPN value associated with accelerated polishing is defined as the polished stone value (PSV), which is a quantitative representation of the aggregate's terminal frictional characteristics. Higher values of PSV indicate greater resistance to polish.	• New asphalt surfacings and asphalt mixes used for friction restoration. • New concrete surfacings (conventional and innovative)*
		Acid Insoluble Residue (AIR) test	ASTM D 3042	Same as above.	• New asphalt surfacings and asphalt mixes used for friction restoration. • New concrete surfacings (conventional and innovative)*
Soundness	Fine	Magnesium Sulfate Soundness test	AASHTO T 104 (or ASTM C 88)	An aggregate sample is immersed in a solution of magnesium sulfate for a period of 16 to 18 hours at a temperature of 70°F (21°C). The sample is then removed, drained for 15 minutes, and oven-dried to a constant weight (5 cycles of immersion and drying is typical). During the immersion process, the salt solution penetrates the permeable pore spaces of the aggregate. Oven drying dehydrates the sulfate salt precipitated in the pores. The internal expansive force of the re-hydration upon re-immersion simulates the expansion of water upon freezing. Upon completion of the final cycle, the sample is sieved over various sieves and the maximum weighted average loss is reported as the sulfate soundness loss. Higher percentages of loss indicate less sound or durable aggregate (Khandal et al., 1997).	• New concrete surfacings.
	Coarse				• New asphalt surfacings and asphalt mixes used for friction restoration. • New concrete surfacings (conventional and innovative)*

* For conventional PCC surfaces, where coarse aggregates are expected to be exposed, and innovative surfaces, such as porous concrete and exposed aggregate concrete.

Aggregate Composition/Structure and Mineral Hardness

While a visual inspection (using the descriptive nomenclature in ASTM C 294) of the subject aggregate can provide a basic understanding of mineral composition and structure, much more detailed information can be obtained through advanced testing using petrographic analysis (ASTM C 295). Among other things, petrographic analysis provides important information on the types and relative amounts of constituent minerals comprising an aggregate. Although Mohs hardness test can be performed on the individual mineral components, an experienced petrographer will know the approximate hardness values of each component. Thus, a range of hardness can be established, as well as the proportion of hard versus soft minerals.

Aggregate Angularity, Shape, and Texture

The uncompacted voids (UV) test (AASHTO T 304 [ASTM C 1252]) is the most commonly used test for assessing fine aggregate angularity, sphericity, and texture (Folliard and Smith, 2003). As indicated by Meininger (1998), this test does not require performing detailed petrographic evaluations of shape and texture.

Three feasible options for assessing coarse aggregates are the fractured-face particles test (ASTM D 5821), the UV test (AASHTO T 326 [formerly AASHTO TP 56]), and the flat/elongated particles test. Both the fractured-face and flat/elongated particles tests are used extensively by highway agencies, primarily for the control of rutting in asphalt mixes. Because of the concern for subjectivity with the former test, NCHRP Project 4-19 recommended the UV test as a replacement for it (Prowell et al., 2005). However, given that the UV test has yet to be adopted by any state, the option of either test is recommended. Furthermore, because it is believed that the fractured particles test conveys a better sense of the micro-texture characteristics of an aggregate as compared to the flat/elongated test, it is recommended over the flat/elongated test.

Abrasion/Wear Resistance

While the Micro-Deval test (AASHTO TP 58 [ASTM D 6928]) for coarse aggregates has been reported (Folliard and Smith, 2003; Kandhal and Parker, 1998) in recent years to be a better indicator of the potential for aggregate breakdown, the LA Abrasion test is commonly used with good success. Both tests are recommended.

Polish Resistance

There are no direct tests for assessing fine aggregate polish characteristics. The acid insoluble residue (AIR) test (ASTM D 3042), which indicates the amount of softer polishing carbonate material in an aggregate, is widely used and accepted, and has been reported to best relate to friction in concrete pavements. It is therefore recommended for fine aggregate.

For coarse aggregates, both the AIR test and the polished stone value (PSV) test (AASHTO T 278 & T 279 [ASTM E 303 & D 3319]) have been used with good success. Both tests are recommended.

It should be recognized that feasible alternatives to the PSV test exist in the form of Circular Track Polishing tests. Like the PSV test, these tests consist of polishing an aggregate sample using an accelerated polishing device and then evaluating the micro-texture of the aggregate using a friction testing device. Three particular tests examined in this study include the North Carolina State University (NCSU) wear and polishing test (represented by ASTM standard E 660, *Standard Practice for Accelerated Polishing of Aggregates or Pavement Surfaces Using a Small-Wheel, Circular Track Polishing Machine*), the Michigan aggregate wear test, and the NCAT polishing test.

The polishing devices used in these tests are bigger than the accelerated polishing machine (APM) used in the PSV test, with polishing tracks ranging from about 12 in (305 mm) (NCAT device) to 7 ft (2.1 m) (Michigan device) in diameter and test tires ranging from 8 in (203 mm) in diameter (NCAT device) to full-scale smooth friction test tires (Michigan device). Although the size, configuration, and operation of these devices appear to simulate real-world conditions better than the APM, the equipment and operational costs tend to be greater than the APM.

At issue also is the availability and usage of the various polishing-type tests. McDaniel and Coree (2003) reported that, although ASTM E 660 was re-approved in 2002, it is not being used by the university or the North Carolina DOT. Further, no states reported using this test in the NCHRP 1-43 friction survey. Though the Michigan DOT has reported good success with the Michigan aggregate wear test (which uses a laboratory version of the ASTM towed friction tester), it is the only agency that uses it.

The NCAT test is primarily designed for mixture samples instead of aggregate samples. Nominal 20-in (508 mm) square slabs are polished and tested with the Dynamic Friction Tester (DFT) and Circular Texture Meter (CTM), resulting in both micro-texture and macro-texture assessments of the prepared mix. This test is more appropriate for use as a mix design and/or QA/QC test.

Soundness

The test method considered to best characterize aggregate soundness is the sulfate soundness test (AASHTO T 104 [ASTM C 88]). This widely used test was developed to simulate, without the need for refrigeration equipment, the effects of freeze-thaw water action on aggregate particles (Khandal and Parker, 1998).

Two options for sulfate solution are given in this test—sodium sulfate and magnesium sulfate. The preferred option is the latter, as it has been reported to produce less variation in mass loss (Folliard and Smith, 2003) and provide a better indication of good versus poor aggregates (Kandhal and Parker, 1998).

<u>Aggregate Test Criteria</u>

Just as there is no single test that can be used to distinguish good friction performance from bad, there is no single test value that can be used as a standard for the same purpose. The factors that influence friction performance do so in an interactive manner and on a continuous scale, making it difficult to pinpoint specific discrimination values.

Nevertheless, past research and current practices does shed light on what can be considered as basic guidance in establishing friction performance-related test criteria. Table 13 provides guideline values in the form of acceptable ranges for the tests recommended in the previous section. It also presents and discusses the source information used to support the guideline criteria. The information presented pertains to typical virgin aggregates and may not apply to lightweight, heavyweight, or recycled aggregates.

Table 14. Typical range of test values for aggregate properties.

Aggregate Property	Aggregate Type	Test Type	Typical Property Range for Good Friction Performance*	Supporting Documentation
Hardness	Fine	Mohs Scratch Hardness	≥ 6	• Dahir and Henry (1978) provided Mohs hardness values for a variety of minerals, as follows: Diamond: 10 Feldspar: 6 - 6.5 Corundum: 9 Pyroxene Group: 5 - 7 Topaz: 8 Amphibole Group: 4 - 6.5 Sillimanite: 7.5 Apatite: 5 Cordierite: 7 - 7.5 Zeolites: 3.5 - 5.5 Quartz: 7 Flourite: 4 Garnet Group: 6.5 - 7.5 Dolomite: 3.5 - 4 Olivine Group: 6.5 - 7 Calcite: 3 Epidote Group: 6 - 7 Gypsum: 2 Chalcedony: 6 • As noted by Dahir and Henry (1978), arbitrarily, but rather widely, Mohs Hardness of 5 has been used as dividing number between minerals termed as soft and those termed as hard. • Dahir and Henry (1978) reported that aggregates made up of hard minerals (Mohs hardness ≥ 6) alone typically resist wear and other forms of degradation, yet may polish easily when subjected to traffic. Aggregates made up of moderately soft minerals (Mohs hardness of 3 to 6) alone resist polishing, but wear quickly when subjected to traffic. • The ideal coarse aggregate should consist of 50 to 70 percent coarse-grained and hard minerals embedded in a matrix of 30 to 50 percent softer minerals (Dahir and Henry, 1978). Coarse aggregates that contain larger and more angular mineral grains or crystals exhibit higher levels of micro-texture and have a higher frictional resistance.
	Coarse	Mohs Scratch Hardness	Hard minerals: ≥ 6 Soft minerals: 3 to 5 Differential hardness (hard minus soft): 2 to 3	
Aggregate Composition & Structure	Fine	Visual Examination (Constituents of Concrete Aggregates)	Hard siliceous mineral aggregate	
	Coarse	Visual Examination (Constituents of Concrete Aggregates) and Petrographic Analysis	<u>Percent of Hard Fraction</u> Natural Aggregate: 50 to 70 Artificial Aggregate: 20 to 40 <u>Hard Grain or Crystal Size</u> 150 to 300 μm, average 200 μm <u>Hard Grain or Crystal Shape</u> Angular Tips	

Table 14. Typical range of test values for aggregate properties (continued).

Aggregate Property	Aggregate Type	Test Type	Typical Property Range for Good Friction Performance*	Supporting Documentation
Angularity, Shape, & Texture	Fine	Uncompacted Voids content, %	≥45	• Guideline value of 45% minimum is based solely on addressing permanent deformation concerns (as noted by Prowell et al. [2005], several studies have supported the 45% minimum criteria). No research was available to indicate what minimum value should be used from a friction performance standpoint.
	Coarse	Uncompacted Voids content, %	≥45	
		Fractured-Face Particles	Agg. Particle Size: 0.12 to 0.5 in (3 to 13 mm) Agg. Particle Shape: Conical, Angular At least 90% by weight of the combined aggregates retained on No. 4 (4.75 mm) sieve should have two or more mechanically fractured faces.	• Guideline value of 90% minimum is based on addressing rutting potential (as suggested by Prowell et al. [2005], a reasonable minimum target for high traffic pavements is 95% with two or more crushed faces). No research was available to indicate what minimum criteria should be used from a friction performance standpoint.
Abrasion/Wear Resistance	Fine	Micro-Deval, % Loss	≤ 15 to 20	• Research performed under NCHRP Project 4-19 (Kandhal and Parker, 1998) resulted in a recommendation of 18% as the maximum allowable percentage loss. Ontario has longstanding requirement of 17% for aggregate used in surface courses (Kandhal and Parker, 1998).
	Coarse	Micro-Deval, % Loss	≤ 15 to 20	
		LA Abrasion, % Loss	≤ 35 to 45	• As reported by Prowell et al. (2005), the LA abrasion test is used extensively by state agencies, with specification values ranging from 30 to 55% maximum and the most frequently cited specification value being 40% maximum • Wu et al. (1998) reported that majority of states have a maximum allowable loss of 40 or 45%, and noted that criteria are more restrictive for surface courses than base courses. • FHWA (2005) recommended range of 35 to 45% as maximum loss using the LA Abrasion test.

Table 14. Typical range of test values for aggregate properties (continued).

Aggregate Property	Aggregate Type	Test Type	Typical Property Range for Good Friction Performance*	Supporting Documentation
Polish Resistance	Fine	Acid Insoluble Residue (AIR), %	≥ 40 to 60	• Dahir and Henry (1978) recommended 50 to 70 percent minimum for heavily traveled pavements. • According to Liang (2003), Kentucky DOT specifies 50% minimum for class A aggregate sources. • Liang and Chyi (2000) reported that New York DOT requires minimum of 15% for ADT greater than 3,000 veh/day.
	Coarse	AIR, %	≥ 50 to 70	
		Polished Stone Value (PSV)	≥ 30 to 35	• Texas DOT criteria for PSV for different traffic levels (Liang and Chyi, 2000): ➢ ADT < 750: No requirements ➢ ADT between 750 and 2,000: 28 min. ➢ ADT between 2,000 and 5,000: 30 min. ➢ ADT > 5,000: 32 min. • Louisiana DOT governs use of asphalt mixtures based on four levels of PSV (Liang, 2003): ➢ Friction Rating I: PSV > 37 ➢ Friction Rating II: PSV between 35 and 37 ➢ Friction Rating III: PSV between 24 and 30 ➢ Friction Rating IV: PSV between 20 and 29 • New Jersey DOT rated surface coarse aggregates with minimum PSV between 25 and 30 as marginal and with minimum PSV greater than 30 as good (Liang, 2003). To ensure year-round SN40S greater than 35, they recommended minimum PSV of 33 (Liang, 2003). • Tennessee DOT categorizes aggregates based on silica dioxide content, calcium carbonate content, AIR, and PSV. Minimum PSV values for each category are as follows (Liang, 2003): ➢ Type I: 33 ➢ Type II: 30 ➢ Type III: 25 • Utah DOT specifies minimum PSV of 38 for aggregates to be used in surface courses (Liang, 2003). • Senior and Rogers (1991) recommended minimum PSV of 50 for high-volume roadways in Ontario.
Soundness	Fine	Magnesium Sulfate Soundness (5 cycles), % Loss	≤ 10 to 20	• While Kandhal et al. (1997) reported a fairly wide range (10 to 30) in the maximum percentage loss specified by some states, subsequent research performed under NCHRP Project 4-19 (Kandhal and Parker, 1998) resulted in a recommendation of 18% as the maximum value. • FHWA (2005) recommended a range of 15 to 20% as the maximum loss using the magnesium sulfate test.
	Coarse	Magnesium Sulfate Soundness (5 cycles), % Loss	≤ 10 to 20	

Surface Mix Types and Texturing Techniques

Pavement surface drainage is in part a function of the surface macro-texture, and macro-texture is defined largely by the aggregate gradation characteristics and finish quality of the surface mix. Surfaces with greater amounts of macro-texture provide greater resistance to sliding via hysteresis, and they help facilitate drainage, thereby reducing the potential for vehicle hydroplaning.

Several different surface mix types and finishing/texturing techniques are available for use in constructing new pavements and overlays, or for restoring friction on existing pavements. Tables 14 and 15 describe the more commonly used mix types and texturing techniques, respectively, and they present the typical macro-texture levels achieved and how those levels influence hydroplaning potential, noise, and splash/spray. Considerations, such as constructability, cost, and structural performance, are not discussed here, but they must be an integral part of any policies developed for these mixes and texturing techniques.

Design Policy for Friction and Texture

The way aggregates and/or surface mixtures/textures are specified and selected for pavement projects varies widely throughout the U.S. While the NCHRP 1-43 state friction survey (appendix C) provides some indication of states' current practices, an earlier survey by Jayawickrama et al. (1996) provided an insightful characterization of friction design practices that most likely hasn't changed. The approaches are categorized as follows:

- Category I—No Specific Guidelines to Address Skid Resistance. Past experience indicates that no prior classification of aggregates is necessary and, as such, no special procedure is followed to ascertain that the frictional characteristics of the aggregate used are satisfactory. The primary reason cited for such a policy is the availability of good quality aggregates.
- Category II—Skid Resistance is Accounted for Through Mix Design. States in this category also do not use any procedure to evaluate the frictional properties of their aggregates. Instead, they base their friction policies on proper mix design. Again, the experience of these states has indicated that they have no major problems related to pavement friction.
- Category III—No Specific Guidelines to Address Skid Resistance. States in this category consider friction of surface courses in the design of new pavements. Sufficient friction is obtained by controlling the quality of aggregate used in the construction of the pavement surface courses. Quality of the aggregates is controlled through experience by specifying the type and allowable percentages of a particular type of aggregate.
- Category IV—Evaluate Aggregate Frictional Properties Using Laboratory Test Procedures. States in this category use laboratory tests, such as AIR, PSV, fractured particles, and soundness, to determine the acceptability of an aggregate or aggregate source for a particular job.
- Category V—Incorporates Field Performance in Aggregate Qualification—With shortcomings in the correlation between laboratory test results and actual field

performance, some states incorporate a two-pronged design approach consisting of laboratory testing and historical field performance.

Table 15. Asphalt pavement surface mix types and texturing techniques.

Application	Mix/ Texture Type	Description	Macro-texture Depth	General Remarks
New AC or AC Overlay	Dense Fine-Graded HMA	Dense-graded HMA is a dense, continuously graded mixture of coarse and fine aggregates, mineral filler, and asphalt cement (5 to 6 percent). It is produced in a hot-mix plant, delivered, spread, and compacted on site. Dense-graded HMA can be modified with polymers or crumb rubber[a], and may include recycled materials. Nominal maximum sizes for surfacing applications can range from 0.38 in (9.5 mm) to 0.75 in (19.0 mm). Fine HMA mixes contain gradations that pass above the MDL at the No. 8 sieve (WSDOT, 2005).	Typically ranges from 0.015 to 0.025 in (0.4 to 0.6 mm) (Meegoda et al., 2002).	• Increased hydroplaning potential corresponding to increased rutting over time. • Moderate to high splash/spray levels. • Low noise. Noise benefits decrease with surface wear (Wayson, 1998).
	Dense Coarse-Graded HMA	Coarse HMA mixes have gradations that pass below the maximum density line (MDL) at the No. 8 sieve (WSDOT, 2005).	Typically ranges from 0.025 to 0.05 in (0.6 to 1.2 mm) (Meegoda et al., 2002).	• Increased hydroplaning potential corresponding to increased rutting over time. • Moderate to high splash/spray levels. • Low noise.
	Gap-Graded HMA or Stone Matrix Asphalt (SMA)[b]	SMA is a gap-graded mixture of course aggregate (typically, 0.4 to 0.6 in [10 to 15 mm]), filler, fibers and polymer-modified asphalt (typically, between 6 and 9 percent) produced in a hot-mix plant. Its primary advantage is resistance to deformation, but its relatively coarse surface yields good frictional characteristics.	Typically exceeds 0.04 in (1.0 mm) (Hanson and Prowell, 2004; Richardson, 1999).	• Reduced hydroplaning potential. • Reduced splash/spray (Mergenmeier, 2004). • Reduced noise (Mergenmeier, 2004). • Excellent long-term rut resistance helps keep hydroplaning potential low. • Increased durability and abrasion resistance (Emery et al., 1993). • Reduced glare (Emery et al., 1993).
	Open-Graded HMA or Open-Graded Friction Course (OGFC)[b]	OGFC is an open-graded mixture of mostly coarse aggregate, mineral filler, and asphalt cement (3 to 6 percent). It is produced in a hot-mix plant, contains a high percentage of air voids (17-22 percent) in the mix, and is spread and compacted on site. Friction, texture, and drainage properties can be controlled by the aggregate gradation, size, angularity, and type. Open-graded HMA can be modified with polymers, fibers, and/or crumb rubber[a].	Typically ranges from 0.06 to 0.14 in (1.5 to 3.0 mm) (Meegoda et al., 2002; Hanson and Prowell, 2004).	• Reduced potential for hydroplaning (FHWA, 1990; NHI, 1998; Noyce et al., 2005). • Reduced splash/spray (FHWA, 1990; Noyce et al., 2005). • Reduced noise (FHWA, 1990; Noyce et al., 2005). • Long-term friction, noise, and splash/spray benefits diminish as voids fill with debris. • Reduced headlight glare (FHWA, 1996; Noyce et al., 2005).

[a] Crumb rubber asphalt is a blend of 5 to 10 percent asphalt cement, reclaimed tire rubber, and additives in which the rubber component is 15 to 20 percent by weight of the total blend. The rubber must react in the hot asphalt cement sufficiently to cause swelling of the rubber particles.
[b] Fine- and coarse-graded SMAs and OGFCs are being developed and increasingly used.

53

Table 15. Asphalt pavement surface mix types and texturing techniques (continued).

Application	Mix/ Texture Type	Description	Macro-texture Depth	General Remarks
Friction Restoration of Existing AC Pavement	Chip Seal	Thin surface treatment containing single-sized, high-quality, angular aggregates (0.38 to 0.63 in [9.5 to 15 mm]), spread over and rolled into a liquid asphalt or asphalt emulsion binder. Aggregates are sometimes pre-coated with asphalt emulsion prior to spreading. Completed surface is somewhat course, yielding good frictional characteristics.	Typically exceeds 0.04 in (1 mm) (Wade et al., 2001; Gransberg and James, 2005; Mockensturm et al, 2002).	• Reduced hydroplaning potential and splash/spray. • Low to moderate noise; higher noise if larger-sized aggregates used. • Limited use on high-volume roads due to loose chips (NHI, 1998).
	Slurry Seal	Slurry mixtures of fine aggregate, mineral filler, and asphalt emulsion. They are similar to micro-surfacing, without interlocking aggregates. Polymers are not always used in the emulsion. Their surface is typically gritty.	Typically range from 0.01 to 0.025 in (0.3 to 0.6 mm).	• Reduced hydroplaning potential (NHI, 1998). • Low to moderate noise
	Micro-Surfacing (polymer-modified slurry seal)	A slurry mixture containing high-quality crushed, dense-graded aggregate, mineral filler, and polymer-modified asphalt emulsion. It is placed over a tack coat and is capable of being spread in variable thickness layers for rut-filling, correction courses, and wearing course applications.	Typically range from 0.02 to 0.04 in (0.5 to 1 mm) (McNerney et al., 2000; Hanson and Waller, 2005).	• Reduced hydroplaning potential (NHI, 1998). • Low to moderate noise.
	HMA Overlay	See HMA surface mixes above.		
	Ultra-Thin Polymer-Modified Asphalt (e.g., NovaChip)	Thin gap-graded asphalt surfaces placed using specialized equipment immediately over a thick polymer-modified asphalt emulsion membrane. Following slight compaction the surface provides a semi-porous texture.	Typically exceeds 0.04 in (1 mm) (Hanson and Prowell, 2004; McNerney et al., 2000; Hanson and Waller, 2005).	• Reduced hydroplaning potential (Uhlmeyer et al., 2003). • Reduced splash/spray (Uhlmeyer et al., 2003). • Low noise (Henry, 2000).
	Epoxied Synthetic Treatment (e.g., Italgrip)	A very thin surface treatment consisting of a two-part polymer resin placed on an existing pavement and covered with a man-made aggregate of re-worked steel slag (0.12 to 0.16 in [3 to 4 mm]). The surface is designed to substantially improve the frictional characteristics of pavements.	Typically exceeds 0.06 in (1.5 mm) (HITEC, 2003).	• Reduced hydroplaning potential (HITEC, 2003). • Reduced splash/spray. • Reduced noise (Kuemmel et al., 2000 ; HITEC, 2003). • Reduced glare. • Best suited for heavily trafficked roads.
Retexturing of Existing AC Pavement	Micro-Milling	Milling equipment, consisting of a self-propelled machine with carbide teeth mounted on a rotating drum, typically removes 0.75 to 1.25 in (19 to 32 mm) from the asphalt surface. Spacing of cuts is approximately 0.2 in (5 mm) versus 0.62-in (6-mm) cut of conventional cold-milling machines. Resulting surface has a fine, smooth pattern that gives smoother ride.	Typically exceeds 0.04 in (1 mm) (Yaron and Nesichi, 2005)	• Reduced hydroplaning potential. • Reduced noise.

Table 16. Concrete pavement surface mix types and texturing techniques.

Application	Mix/ Texture Type	Description	Macro-texture Depth	General Remarks
New PCC or PCC Overlay	Broom Drag (longitudinal or transverse)	A long-bristled broom is mechanically or manually dragged over the concrete surface in either the longitudinal or transverse direction. Texture properties are controlled by adjusting the broom angle, bristle properties (length, strength, density), and delay behind the paver. Uniform striations approximately 0.06 to 0.12 in (1.5 to 3.0 mm) deep are produced by this method.	Typically ranges from 0.008 to 0.016 in (0.2 to 0.4 mm) (Hoerner et al., 2003).	• Increased hydroplaning potential (Henry, 2000). • Reduced noise (Hoerner and Smith, 2002).
	Artificial Turf Drag (longitudinal)	An inverted section of artificial turf is dragged longitudinally over a concrete surface following placement. Texture properties are controlled by raising/lowering the support boom, adding weight to the turf, and delaying application to allow surface hardening. This method produces uniform 0.06 to 0.12 in (1.5 to 3.0 mm) deep surface striations.	Typically ranges from 0.008 to 0.016 in (0.2 to 0.4 mm) (Hoerner et al., 2003; FHWA, 1996), but a deep texture (min depth of 0.04 in [1.0 mm]) has been specified[a].	• Increased hydroplaning potential, except for deep textures. • Reduced noise (Hoerner and Smith, 2002).
	Burlap Drag (longitudinal)	One or two layers of moistened coarse burlap sheeting are dragged over the concrete surface following placement. Texture properties are controlled by raising/lowering the support boom and adjusting the delay following concrete placement. This method produces uniform 0.06 to 0.12 in (1.5 to 3.0 mm) deep striations in the surface.	Typically ranges from 0.008 to 0.016 in (0.2 to 0.4 mm) (Hoerner et al., 2003; FHWA, 1996).	• Increased hydroplaning potential and splash/spray potential (Henry, 2000; Hoerner et al., 2003). • Reduced noise (Hoerner and Smith, 2002).
	Longitudinal Tine	A mechanical assembly drags a wire comb of tines ($\gtrsim$ 5 in [127 mm] long and 10 ft [3 m] wide) behind the paver (and usually following a burlap or turf drag). Texture properties are controlled by the tine angle, tine length, tine spacing, and delay for surface curing. Grooves from 0.12 to 0.25 in (3 to 6 mm) deep and 0.12 in (3 mm) wide are produced by this method, typically spaced at 0.75 in (19 mm).	Typically ranges from 0.015 to 0.04 in (0.4 to 1.0 mm) (Hoerner and Smith, 2002; FHWA, 1996).	• Compared to transverse tining, reduced friction and more rapid rate of friction deterioration over time (Wayson, 1998). • Improved resistance to lateral skidding. • Increased splash/spray. • Reduced interior and exterior noise.
	Transverse Tine	Accomplished using methods similar to longitudinal tining, however, the mechanical assembly drags the wire comb perpendicular to the paving direction. Variations include skewing the tines 9 to 14° from perpendicular and using random or uniform tine spacing from 0.5 to 1.5 in (12 to 38 mm).	Typically ranges from 0.015 to 0.04 in (0.4 to 1.0 mm) (Hoerner and Smith, 2002; FHWA, 1996).	• Reduced hydroplaning potential (transverse channels/grooves). • Reduced splash/spray. • Increased whine with uniform transverse tine. • Reduced noise with random skewed tine (Wayson, 1998).

[a] Minnesota Department of Transportation.

Table 16. Concrete pavement surface mix types and texturing techniques (continued).

Application	Mix/ Texture Type	Description	Macro-texture Depth	General Remarks
New PCC or PCC Overlay	Diamond Grinding (longitudinal)	A self-propelled grinding machine with a grinding head of gang-mounted diamond sawing blades removes 0.12 to 0.75 in (3 to 19 mm) of cured concrete surface, leaving a corduroy-type surface. Blades are typically 0.08 to 0.16 in (2 to 4 mm) wide and spaced 0.18 to 0.25 in (4.5 to 6 mm) apart, leaving 0.08 to 0.16 in (2 to 4 mm) high ridges. This method is most commonly used to restore surface characteristics of existing pavements, however, in recent years, it has been used to enhance the surface qualities of new PCC pavements or PCC overlays.	Typically ranges from 0.03 to 0.05 in (0.7 to 1.2 mm) (Rao et al. 1999).	• Reduced hydroplaning potential (Hoerner et al., 2003). • Reduced noise (Hoerner et al., 2003)
	Porous PCC	Gap-graded, small-diameter aggregate are combined with cement, polymers, and water to form a drainable surface layer (typically 8 in [200 mm] thick). That surface layer is bonded to the underlying wet or dry dense concrete layer. Texture properties are controlled by aggregate sizes and gradations. Air voids range from 15 to 25 percent.	Typically exceeds 0.04 in (1 mm) (FHWA, 1996).	• Similar characteristics as OGFC (i.e., reduced hydroplaning potential, reduced splash/spray, and reduced noise (Hoerner et al., 2003).
	Exposed Aggregate PCC	A set retarder is applied to the wet concrete surface and the surface is protected for curing. After 12 to 24 hours, the unset mortar is removed to a depth of 0.04 to 0.08 in (1 to 2 mm) using a power broom. The large diameter aggregate is exposed by this process leaving a uniform surface.	Typically exceeds 0.035 in (0.9 mm) (Hoerner et al., 2003; FHWA, 1996; FHWA, 2005).	• Reduced hydroplaning potential. • Low splash/spray (Hoerner et al., 2003) • Low noise (Hoerner et al., 2003).
Friction Restoration of Existing PCC Pavement*	HMA Overlay	See HMA surface mixes above.		
Retexturing of Existing PCC Pavement	Diamond Grinding (longitudinal)	See diamond grinding above.		
	Longitudinal Diamond Grooving	A self-propelled grooving machine saws longitudinal grooves in the road surface about 0.12 to 0.25 in (3 to 6 mm) deep and spaced 0.5 to 1.5 (13 to 38 mm) apart. This method adds macro-texture for drainage but relies on the original surface for micro-texture.	Typically ranges from 0.035 to 0.055 in (0.9 to 1.4 mm) (FHWA, 1996).	• Traditional means of improving friction in high-crash locations (Hoerner et al., 2003) • Increased drainage reduces hydroplaning potential and splash/spray. • Increased lateral control at transitions and super-elevated curves (Hoerner et al., 2003).
	Transverse Diamond Grooving	Completed in a manner similar to longitudinal diamond grooving, except the grooves are sawn transverse to the travel direction. This method also adds macro-texture and positive drainage for surface water. It relies on the original surface for micro-texture.	Typically ranges from 0.035 to 0.055 in (0.9 to 1.4 mm) (FHWA, 1996).	• Useful at intersections (Henry, 2000). • Increased noise associated with uniform transverse grooves (Henry, 2000). • Reduced noise associated with randomly spaced transverse grooves (Henry, 2000).
	Shot Abrading	An automated machine hurls recycled round steel abrasive material at the pavement surface, abrading the surface and/or removing the mortar and sand particles surrounding the coarse aggregate to a depth of up to 0.25 in (6 mm). Texture properties are controlled by adjusting the steel abrasive material velocity and approach angle and by modifying the forward equipment speed.	Typically ranges from 0.025 to 0.05 in (0.6 to 1.2 mm) (FHWA, 1996; HITEC, 2005).	• Reduced hydroplaning potential (Henry, 2000). • Reduced pavement–tire noise (Henry, 2000).

* Other treatments, such as micro-surfacing, ultra-thin polymer-modified asphalt, epoxy-bonded laminates, and thin-bonded PCC overlays, have been used but often have structural performance and/or cost issues.

Thus, while some states are fortunate to have good quality aggregates or are less in need of special mixes or textures for macro-texture, others are compelled, at some level, to more fully evaluate and specify their aggregates and mixes/textures.

Presented in the sections below are some of the friction design practices reported in the literature and through the surveys and interviews with selected state agencies. The practices described represent examples of how traffic and other site conditions can be utilized in specifying aggregates and mixes/textures.

Illinois DOT

The Illinois DOT selects and designs pavement surfaces in accordance with the following criteria (Rowden, 2004):

- PCC Pavements: Final finishing on highways with posted speed limits in excess of 40 mi/hr (65 km/hr) receives a Type A final finish (transverse tining with 0.75-in [19-mm] spacing, 0.1- to 0.125-in [2.5- to 3.1-mm] width, and 0.125- to 0.19-in [3.1- to 4.8-mm] depth. Final finishing on highways with posted speed limits not exceeding 40 mph (65 km/hr) receives a Type A or Type B (artificial turf drag) final finish.

- HMAC Pavements: New surface courses must have friction qualities equivalent to or greater than those provided by the following guidelines. Traffic levels from the expected year of construction are used to determine the mixture.
  - Mixture C is used as the Class I surface course on roads and streets having an ADT of 5,000 veh/day or less.
  - Mixture D is used as the Class I surface course on two-lane roads and streets having an ADT greater than 5,000 veh/day, on four-lane highways having an ADT between 5,001 and 25,000 veh/day, and on six-lane (or greater) highways having an ADT of 60,000 veh/day or less.
  - Mixture E is used as the Class I surface course on four-lane highways having an ADT between 25,001 and 100,000 veh/day or on six-lane (or greater) highways having an ADT between 60,001 and 100,000 veh/day.
  - Mixture F is used as the Class I surface course on any facility having an ADT greater than 100,000 veh/day.

The HMAC specification describes the allowable coarse aggregates and proportions for use in each mixture type. For instance, aggregates for mixture C may consist of one of the following: crushed gravel, crushed stone, crushed sandstone, crushed slag, crushed steel slag, and gravel (in certain instances). Aggregates for the highest mixture type (F), on the other hand, may only consist of either crushed sandstone or crushed gravel or crushed stone (except limestone), adequately blended crushed sandstone.

Although the Department employs some friction-related lab tests, such as sodium sulfate soundness and LA Abrasion, they place much greater emphasis on testing friction in the field and linking the results to the respective aggregates/aggregate sources.

Louisiana DOT

Although the Louisiana DOT does not utilize a friction demand identification process, the Department does classify aggregates for asphalt mixtures according to four different friction ratings, that are based on PSV test results (Rasoulian, 2004). These friction rating categories are distinguished by layer and application, as illustrated below.

- Friction Rating 1 (all mixtures): PSV > 37.
- Friction Rating 2 (all mixtures): PSV = 35 to 37.
- Friction Rating 3 (all mixtures, except wearing courses with ADT > 7,000 veh/day): PSV = 30 to 34.
- Friction Rating 4 (all mixtures except wearing courses): PSV = 20 to 29.

Maryland SHA

Maryland ensures HMAC friction by recommending minimum levels of coarse aggregate PSV in the HMAC mixture. The actual PSV required to ensure adequate levels of pavement surface friction is dependent on friction demanded by a specific site (i.e., site category) and expected traffic level, as depicted in table 17 (Flintsch et al., 2002). According to the Maryland procedure, the use of limestone, marble, or serpent aggregates in the surface mixture is avoided regardless of their PSV value.

Table 17. Recommended levels of aggregate PSV for various site and friction requirement categories (Flintsch et al., 2002).

Site/Demand Category	PSV of Coarse Aggregates						Design FN
	Traffic (Heavy Commercial Vehicles per Lane per Day)						
	250	1,000	1,750	2,500	3,250	4,000	
1—Approach railroad crossing, traffic lights, pedestrian crossing, roundabouts, stop and give way controlled intersections.	7	7	8	8	9	9	55
2—Curves with radius < 820 ft (250 m), downhill gradients > 10 percent, and 164-ft (50-m) long freeway/highway on/off ramp.	6	7	7	8	8	9	50
3—Approach to intersections, downhill gradients 5 to 10%.	6	6	7	7	8	8	45
4—Undivided highways without any other geometrical constraints which influences frictional demand.	5	6	6	7	7	8	40
5—Divided highways without any other geometrical constraints which influences frictional demand.	5	5	6	6	7	7	35

Michigan DOT

Michigan determines the polishing potential of HMAC coarse aggregates for design of high-friction pavements through laboratory testing (wear track testing or petrographic analysis) (Skerritt, 2004). The wear-track testing program consists of a large-scale indoor polishing track and a tire-mounted friction tester. Aggregate test specimens are subjected to 4 million wheel passes on the wear track, during which surface friction is measured. The normalized value of friction at the end of the test is used to calculate an Aggregate Wear Index (AWI), which is a measure of the polishing potential of the aggregate source tested. Aggregates are specified for use as follows, based on anticipated traffic (Liang, 2003):

- ADT < 100 veh/day/lane: no AWI requirement.
- ADT ≥ 100 and < 500 veh/day/lane: AWI ≥ 220.
- ADT ≥ 500 veh/day/lane: AWI ≥ 260.

Pennsylvania DOT

All coarse aggregate sources approved by the Pennsylvania DOT are assigned a Skid Resistance Level (SRL) rating that is used to decide (for asphalt wearing courses only) what aggregate sources may be used in which wearing courses. The five levels of SRL ratings are defined as low (L), medium (M), good (G), high (H), and excellent (E). Based on the SRL, aggregates are specified for pavements with different ADT values as follows (Liang, 2003):

- ADT > 20,000 veh/day: E
- 5,000 < ADT < 20,000 veh/day: E, H, E/M blend, or E/G blend.
- 3,000 < ADT < 5,000 veh/day: E, H, G, H/M blend, or E/L blend
- 1,000 < ADT < 3,000 veh/day: E, H, G, M, H/L blend, G/L blend, or E/L blend
- ADT < 1,000 veh/day: Any

After the results of the above tests are available, they are evaluated and the SRL rating is assigned to the new aggregate source, based on the petrography of the aggregate, and how closely it matches that of older, petrographically similar aggregate sources whose skid performance is known from previous skid studies.

Texas DOT

Designing for friction in Texas begins with the identification of friction demand. The Texas DOT uses various factors for assessing overall friction demand, including rainfall, traffic, speed, trucks, grade, curves, intersections, cross slope, surface design life, and the macro-texture of the proposed surface (Stampley, 2004)

For asphalt pavements, the Department has developed an aggregate rating system that classifies coarse aggregate source materials into four categories (A, B, C, and D) to match their demand classifications. These ratings are updated semi-annually based on aggregate properties from approved resources (Texas DOT, 2004). Source aggregates are rated according to PSV, LA

Abrasion, and magnesium sulfate soundness for HMAC and surface treatment applications. Suggestions for blending are also provided (Texas DOT, 2004).

Framework for Comprehensive Friction and Texture Policy

Highway agencies are encouraged to develop or update policies concerning the friction and texture design of new and restored pavements. Such policies should clearly define the aggregate friction testing protocol (test types and criteria) and surface mix/texturing techniques that are applicable for different roadway types requiring different levels of friction. In essence, friction design categories should be established that link (a) the recommended level and types of aggregate testing to be performed and (b) the recommended surfacing options, with roadways requiring different levels of micro-texture and macro-texture.

As a minimum, friction design categories should be established according to highway design speed and traffic (or design loadings in terms of equivalent single axle loads [ESALs]), since these factors largely determine micro-texture and macro-texture needs. Other factors that could be used in establishing categories include roadway facility type (i.e., functional or highway class, access type), facility setting (rural, urban), climate (e.g., wet, dry), number of lanes, and truck percentages.

Although several factors can be used in establishing friction design categories, the number of categories should be limited to between three and five. In addition, agencies should be mindful of any existing classification schemes set forth in their wet-weather accident reduction programs, materials and/or construction specifications, or other pavement-related policies and systems, as they may by and large reflect the desired friction priorities.

Table 18 provides an example illustration of friction design categories. Five categories are shown corresponding to a simple matrix comprised of five different facility types, two levels of traffic, two types of climate, and two levels of speed. In this example, design category I represents those scenarios where friction and texture requirements are lowest, whereas category V represents those scenarios with the greatest requirements.

Once the design categories have been set, aggregate test protocols and mix/texture type options can be developed for each category. The test protocol should list the specific tests to be performed and the criteria/parameters to be used. The criteria should be based on established links between historical friction performance and laboratory test data.

Table 19 provides a matrix that can be used to in establishing tests and criteria for each design category. Agencies likely already utilize some of the recommended tests as part of their standard mix design processes. Such tests and corresponding criteria, along with the basic criteria given in table 13, should serve as the basis for developing a more thorough testing protocol for friction design. Agencies are advised to consider the interaction between tests and the consequences of selecting specific criteria. As an example, some aggregates with high PSV values may not be very resistant to abrasion (Prowell et al., 2005).

Table 18. Example illustration of friction design categories used in developing friction design policy.

Facility Type	Traffic Volume	Friction Design Categories			
		Dry Climate (annual precipitation <32 in)[a]		Wet Climate (annual precipitation ≥32 in)[a]	
		Low Speed (<50 mi/hr)[a]	High Speed (≥50 mi/hr)[a]	Low Speed (<50 mi/hr)[a]	High Speed (≥50 mi/hr)[a]
Local & Frontage Roads	All	I		I	
2-lane highways	Low (ADT ≤ 5,000 veh/day)[a]	II	II	II	III
	High (ADT > 5,000 veh/day)[a]	II	III	III	IV
4-lane roads	Low (ADT ≤ 25,000 veh/day)[a]	II	II	II	III
	High (ADT > 25,000 veh/day)[a]	II	III	III	IV
6-lane roads	Low (ADT ≤ 50,000 veh/day)[a]	III	III	III	IV
	High (ADT > 50,000 veh/day)[a]	III	IV	III	V
Entrance & Exit Ramps	All	III	IV	IV	V

[a] Example break-out values. Agencies should define their own break-out values.
1 in = 25.4 mm 1 mi/hr = 1.61 km/hr

Table 19. Aggregate test requirements for friction design.

Design Category	Aggregate Fraction	Aggregate Test Protocol									
		Mineral Hardness		Structure/Composition		Angularity, Shape, & Texture					
		Mohs		ASTM C 294 & C 295		AASHTO T 304 (ASTM C 1252)		AASHTO T 326		ASTM D 5821	
		Required	Criteria	Required	Criteria	Required	Criteria	Required	Criteria	Required	Criteria
I	Fine										
	Coarse										
II	Fine										
	Coarse										
III	Fine										
	Coarse										
IV	Fine										
	Coarse										
V	Fine										
	Coarse										

Table 19. Aggregate test requirements for friction design (continued).

Design Category	Aggregate Fraction	Aggregate Test Protocol											
		Abrasion/Wear Resistance						Polish Resistance				Soundness	
		CSA A23.2-23A		AASHTO T 96 (ASTM C 131 & C 535)		AASHTO TP 58 (ASTM D 6928)		ASTM D 3042		AASHTO T 278 & T 279 (ASTM E 303 & D 3319)		AASHTO T 104 (ASTM C 88)	
		Required	Criteria	Required	Criteria	Required	Criteria	Required	Criteria	Required	Criteria	Required	Criteria
I	Fine												
	Coarse												
II	Fine												
	Coarse												
III	Fine												
	Coarse												
IV	Fine												
	Coarse												
V	Fine												
	Coarse												

Table 20 shows the types of asphalt mixes and concrete textures that would be most applicable for the five example friction design categories. Similarly, table 20 shows the types of restoration treatments most applicable for existing asphalt and concrete pavements for the five design categories. Micro-texture aspects aside, mixes/textures with greater texture depths are generally more appropriate for the higher friction demand situations.

Because state experiences with the various mixes, textures, and treatments will vary, and because other viable options may exist or are currently being developed, agencies should develop their own matrices for the design categories they create. Such matrices should also consider limitations of use with respect to noise, splash/spray, and other pavement–tire interaction issues.

Table 20. Recommended mix and textures types for different friction design categories.

Design Category	New AC or AC Overlay [a]	New PCC or PCC Overlay[b]
I	Dense fine-graded HMA	Broom Drag Burlap Drag Artificial Turf Drag
II	Dense fine-graded HMA Dense coarse-graded HMA	Broom Drag Burlap Drag Artificial Turf Drag
III	Dense fine-graded HMA Dense coarse-graded HMA SMA	Artificial Turf Drag[c] Transverse Tine[d] Longitudinal Tine[d] Diamond Grind Diamond Groove
IV	Dense fine-graded HMA Dense coarse-graded HMA SMA OFGC	Artificial Turf Drag[c] Transverse Tine[d] Longitudinal Tine[d] Diamond Grind Diamond Groove
V	Dense coarse-graded HMA SMA OGFC	Artificial Turf Drag[c] Transverse Tine[d] Longitudinal Tine[d] Diamond Grind Diamond Groove Porous PCC Exposed Aggregate PCC

[a] Based in part on FHWA, 2005.
[b] Based in part on ACPA, 2000; Hoerner et al., 2003; FHWA, 2005.
[c] Deep texture, as per Minnesota specification.
[d] Preceded by burlap or turf drag.

Table 21. Recommended restoration treatments for different friction design categories.

Design Category	Existing Asphalt Pavement [a]	Existing Concrete Pavement [b]
I	Chip Seal Slurry Seal Micro-surfacing HMA Overlay Ultra-thin Polymer Modified Asphalt	HMA Overlay Diamond Grinding
II	Chip Seal Slurry Seal Micro-surfacing HMA Overlay Ultra-thin Polymer Modified Asphalt	HMA Overlay Diamond Grinding
III	Micro-surfacing HMA Overlay	HMA Overlay Diamond Grinding Diamond Grooving
IV	Micro-surfacing[c] HMA Overlay	HMA Overlay Diamond Grinding Diamond Grooving
V	Micro-surfacing[c] HMA Overlay	HMA Overlay Diamond Grinding Diamond Grooving

[a] Based in part on ODOT, 2001; FHWA, 2005; Uhlmeyer et al., 2003.
[b] Based in part on FHWA, 2005.
[c] Double application for higher design categories to ensure durable wearing surface.

PROJECT-LEVEL FRICTION DESIGN

Project-level friction design entails selecting aggregates and mix types/texturing techniques that satisfy both initial and long-term friction requirements. Although safety over the established pavement design life is the paramount concern, the design process should strive for the ideal surface consisting of the following characteristics:

- Adequate levels of pavement friction (produced by a sharp, gritty micro-texture).
- Little or no decrease in pavement friction with increased speed (adequate levels of macro-texture for efficient displacement of water on the pavement surface).
- Little or no reduction in pavement friction with time and traffic applications (durable, polish and wear resistant surface.
- Low levels of splash/spray.
- Low noise generation.
- Low tire wear and rolling resistance.
- Low glare.

A five-step process for designing surfaces for new asphalt or concrete pavement, as well as restoration treatments of existing asphalt or concrete pavement, is as follows:

1. Determine design friction and texture levels.
2. Select aggregates and conduct mix design.
3. Identify concrete pavement texturing technique.
4. Develop construction specifications.
5. Formulate design strategies.

These design steps are described in detail in the sections below.

Step 1—Determining Design Friction and Texture Levels

Design pavement friction/texture levels must be selected to satisfy agency policy requirements. Ultimately, the design friction/texture levels must ensure that adequate levels of friction/texture are available throughout the design period.

Once an agency sets a goal for friction for a class of road in their design process, the texture levels can be established by using equation 1 and the relationship between macro-texture and the speed gradient given in ASTM E 1960, as outlined below.

Given the level of *FN* desired by the agency for the design, pairs of *BPN* (micro-texture) and *MTD* (macro-texture) can be determined as follows:

From ASTM E 1960:

$$FN(S) = FN(S_0) * e^{(S_0-S)/Sp} \qquad 15$$

where: $FN(S)$ = Friction number at some selected slip speed S.

S = Selected slip speed, mi/hr.
$FN(S_0)$ = Friction number at some desired slip speed S_0.
S_0 = Desired slip speed, mi/hr.
S_P = Speed number, mi/hr.

And, S_P (in mi/hr) is given in terms of *MTD* (in inches) by.

$$S_P = 1802*MTD - 7.25 \tag{16}$$

BPN speed is about 6.25 mi/hr (10 km/hr). Thus, $FN(S_0)$ can be set to *BPN* at S_0 equal to 6.25 mi/hr (10 km/hr). Furthermore, it is known that for a locked-wheel trailer, the vehicle velocity V is equal to slip speed S. Substituting S with V, *BPN* at S_0 = 6.25 mi/hr (10 km/hr), and S_P as per equation 16 into equation 15, one gets the following:

$$FN(V) = BPN * e^{(6.25-V)/(1802*MTD - 7.25)} \tag{17}$$

Solving for *BPN* gives the following relation of *BPN* as a function of *FN(V)* and *MTD*:

$$BPN = FN(V) * e^{(V-6.25)/(1802*MTD - 7.25)} \tag{18}$$

Consider an example where it is desired that a smooth tire give a friction number of 40 at a speed limit of 40 mi/hr (64 km/hr). Then, *FN40S* is *FN(V)* with V = 40 mi/hr (64 km/hr) and equation 18 becomes as follows:

$$BPN = FN40S * e^{(33.75)/(1802*MTD - 7.25)} \tag{19}$$

Figure 12 is a plot of equation 19. To achieve the design friction level of 40, the pairs of *BPN* and *MTD* given in table 20 are needed. The first set is not usable, as the scale for *BPN* only goes from 0 to 100. Therefore, one of the last four pairs would need to be selected to give the minimum *MTD* and *BPN* needed.

If the polishing characteristics have been measured or are already known, higher levels of micro-texture and/or macro-texture should be selected to meet the required levels at the end of the design life. For example, if the polished *BPN* (i.e., *PSV*) and the *MTD* are satisfactory, then the initial *BPN* from the test would need to be specified. If the polished *BPN* is too low and thus requires a *MTD* that is too high to meet, then a higher *BPN* or different aggregate is needed to get the required polished *BPN* at the end of the design life.

This method is then a guide to find what levels of micro-texture (*BPN*) and macro-texture (*MTD*) are required to meet a design for a desired *FN*. This can be used in choosing the aggregate that is known to meet these requirements or laboratory tests can be used to ensure the samples meet the required micro-texture and macro-texture.

A more robust method would be to use DF (20) of the DFT for BPN/100 and use S_0 = 12 mi/hr (20 km/hr) in the equations. The DF (20) has been shown to be much more repeatable (NASA Wallops runway friction workshops). However, very few state agencies presently have DFT, but that is changing. Smartly, the following method could use the DF (20).

An alternative method for determining friction and texture requirements for asphalt pavements was developed by Sullivan (2005). This method, illustrated in figure 14, uses *PSV* and *MPD* to compute *IFI* (as given in ASTM E 1960) and subsequently determine the design vehicle stopping distance. Figure 15 shows an example vehicle response chart for a selected speed of 50 mi/hr (80 km/hr).

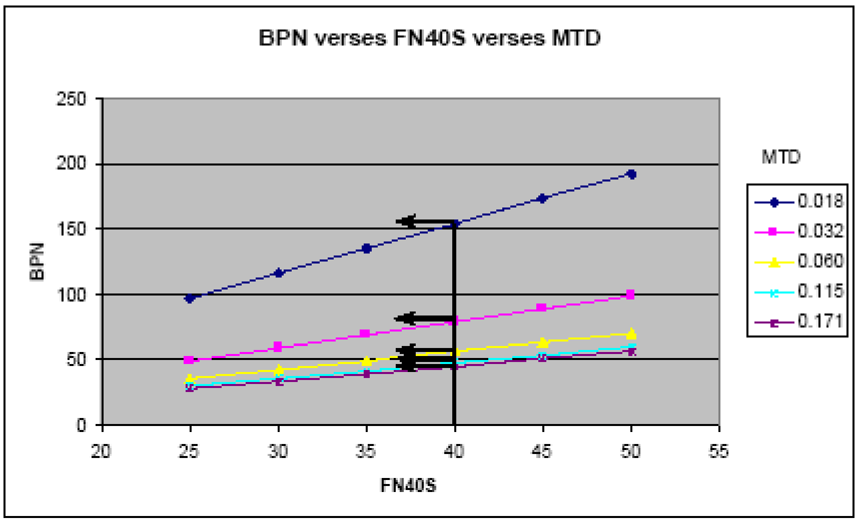

Figure 14. Example of determining *BPN* and *MTD* needed to achieve design friction level.

Table 22. Pairs of *MTD* and *BPN* needed to achieve *SN40S* equal to 40.

MTD, in	0.018	0.032	0.060	0.115	0.171
BPN	154.297	78.561	56.058	47.353	44.748

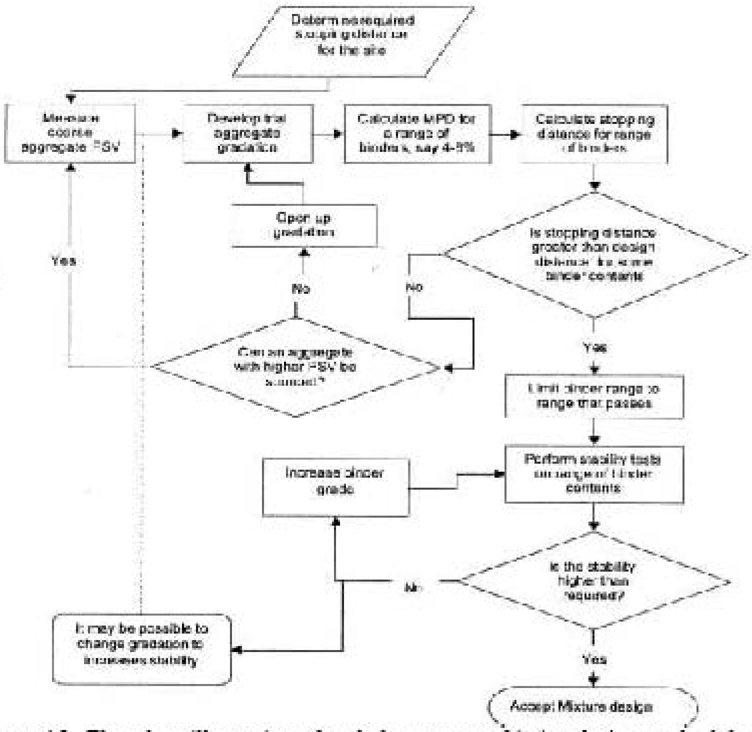

Figure 15. Flowchart illustration of asphalt pavement friction design methodology (Sullivan, 2005).

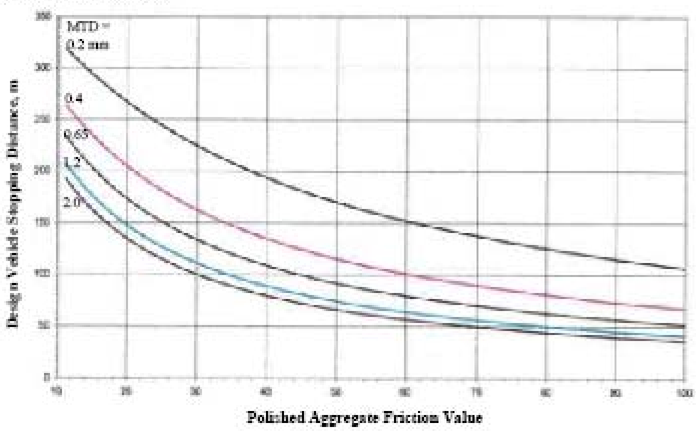

Figure 16. Illustration of vehicle response as function of *PSV* and *MTD* (Sullivan, 2005).

The method uses an equation for computing the *MPD* based on key asphalt mix characteristics (maximum aggregate size, gradation, binder content). While historical data on asphalt surface mix textures (or concrete pavement surface textures) can be used in this process, the *MPD* equation (derived using comprehensive mix design and surface texture data from the NCAT test track) gives the mix designer greater flexibility in establishing a mix design that will meet friction requirements.

Since most state agencies measure and use FN40, the first method relates to FN40. However, the second method might be more practical for agencies since stopping distance (SD) may be more meaningful to the personnel that a friction value. In reality, the two values are related to each other as SD is the double integral of FN (V) multiplied by gravity.

Step 2—Selection of Aggregates and Conduct of Mix Design

The most important factor in achieving long-lasting friction is aggregate selection. Pavement designers must select aggregates that have the right physical, chemical, and mechanical properties to satisfy both the initial and long-term friction requirements of a pavement project.

Aggregates must comply with the testing requirements established by the agency. Aggregate samples should be submitted early in a project so that tests can be conducted to determine their suitability and compliance with specifications. Generally, two or more aggregate sources must be combined in appropriate percentages to meet project gradation requirements. Aggregates not meeting the specified test parameters should be rejected (prior to any mix design effort) and either new materials should be submitted and tested or a suitable blend of good quality aggregates and the original aggregates should be identified.

Micro-Texture

As discussed earlier, micro-texture in asphalt surface mixes is provided by the coarse aggregate surface texture. Coarse aggregates that exhibit "rough sandpaper" surface textures provide higher levels of micro-texture than those with smooth "fine sandpaper" textures.

Micro-texture in concrete surfaces is generally provided by the fine aggregates in the cement mortar/paste (for concrete mixes with exposed aggregates, the surface properties of the coarse aggregate will dictate micro-texture). Fine aggregates that exhibit angular edges and cubical or irregular shapes generally provide higher levels of micro-texture, whereas those with rounded edges or elongated shapes generally produce lower micro-texture.

Aggregates comprised of a matrix of both hard and soft minerals offer a continuously renewable micro-texture that helps ensure friction durability. Ascertaining the long-term micro-texture of the selected aggregate is a crucial part of the design process. It generally entails either retrieving historical *PSV* test data (if available) for the aggregate or aggregate source in question or conducting formal *PSV* testing of the aggregate.

Macro-Texture

Macro-texture in asphalt surface mixes (and exposed concrete surfaces) is primarily governed by the size and gradation of the aggregate used. Generally speaking, the larger the aggregates in the mix, the greater the macro-texture produced. Also influencing macro-texture are mix volumetric properties, such as voids in the mineral aggregate (VMA), voids in the total mix (VTM), and the percentage of aggregate passing the 0.38-in (9.5-mm) through No. 10 (2.36-mm) sieve sizes.

Mix type selection and design are important from the standpoint of identifying a mix with sufficient macro-texture (*MTD*) that, when combined with the aggregate *PSV*, satisfies the friction design requirements (Step 1). Further discussion about asphalt mix design, and in particular aggregate size/gradation and volumetric properties, is provided in the sections below.

Aggregate Size

Aggregate size may be qualified in terms of either maximum size (*MS*) or nominal maximum size (*NMS*). The *MS* of an aggregate is defined as the smallest sieve that all of a particular aggregate must pass through. The *NMS* of an aggregate is defined as the smallest sieve size through which the major portion of the aggregate must pass. The *NMS* sieve may retain 5 to 15 percent of the aggregate depending on the size number. Superpave defines *NMS* as one sieve size larger than the first sieve to retain more than 10 percent of the material (ASTM, 2004; ACI, 2000; Roberts et al., 1996).

Aggregate Gradation

The gradations of commonly used asphalt surface mixes can be categorized and described as follows:

- Dense- or well-graded—Refers to a gradation that is near maximum density. The most common HMA mix designs tend to use either dense fine-graded or dense coarse-graded aggregate.
- Gap-graded—Refers to a gradation that contains only a small percentage of aggregate particles in the mid-size range. The curve is flat in the mid-size range. Gap-graded surface mixes include SMA and proprietary mixes such as NovaChip.
- Open-graded—Refers to a gradation that contains only a small percentage of aggregate particles in the small range. This results in more air voids because there are not enough small particles to fill in the voids between the larger particles. The curve is flat and near-zero in the small-size range. Open-graded surface mixes include OGFC.
- Uniformly graded—Refers to a gradation that contains most of the particles in a very narrow size range. In essence, all the particles are the same size. The curve

is steep and only occupies the narrow size range specified. Common uniformly graded surface mixes include most slurry seals, micro-surfacing, and chip seals.

Figure 17 illustrates the four gradations listed above. Note that dense fine-graded HMA mixes contain gradations that pass above the maximum density line (MDL) at the No. 8 (2.36-mm) sieve, whereas the gradations for dense coarse-graded HMA pass below the MDL at the No. 8 (2.36-mm) sieve.

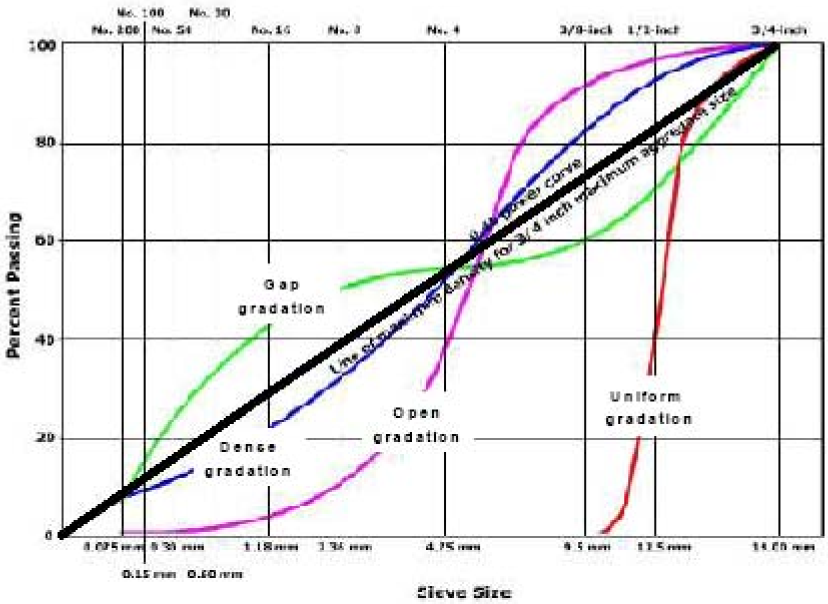

Figure 17. Typical asphalt mix aggregate gradations.

Percentage of Aggregate Material Passing the 0.38-in (9.5-mm) through No. 10 (2.36-mm) Sieve Sizes

The percentage of material passing the 0.375-in (9.5-mm) through No. 10 (2.36-mm) sieve sizes affects the asphalt mix macro-texture. Evidence suggests that increasing the amount of material passing these sieve sizes reduces the asphalt mix macro-texture. Generally, the amount of aggregate passing these sieve sizes depends on the asphalt mix type (i.e., dense graded, open graded, and so on). To increase asphalt mix macro-texture, the lower bound values of agency recommendations for percentage of aggregate material passing these sieve sizes should be used.

Voids in the Mineral Aggregate (VMA)

Increasing the VMA increases macro-texture and porosity. Excessively high VMA can, however, adversely affect asphalt mix durability. Hence, increasing this asphalt mix property must be done with caution. Where a high VMA is required to meet macro-texture requirements or to ensure that the asphalt mix is open or porous, additives (i.e., polymers) can be added to the mix to increase durability.

Typically, a minimum VMA value ranging from 13 to 15 percent is specified a dense aggregate mix. This value can be increased to enhance the asphalt mix macro-texture requirements by altering the packing characteristics of aggregate particles in the asphalt mix. In particular, lowering the minus No. 200 content in a mixture to the lower end of the specification or reducing the amount of aggregate particles between two successive sieves (i.e., gap grading) will increase VMA and thus macro-texture.

Estimating Texture Depth Using Mix Design Parameters

Several studies have been conducted attempting to model texture depth as a function of aggregate gradation/size characteristics and mix volumetric properties. Presented below are three particular models reported in the literature which could be considered for use in assessing macro-texture of laboratory-designed asphalt mixes.

- NCHRP Report 441 (Stroup-Gardiner and Brown, 2000)—The model below predicts estimated mean texture depth (*ETD*) based on aggregate size and gradation characteristics. As also shown, the sieve sizes associated with 10, 30, and 60 percent passing are used to compute the coefficients of uniformity and curvature (C_C and C_U, respectively).

$$ETD = 0.0198MS - 0.004984P200 + 0.1038C_C + 0.004861\underline{C_U} \qquad 20$$

where: *ETD* = Estimated texture depth (an estimate of MTD computed using ROSAN$_V$ laser texture measurement.

MS = Maximum size of the aggregate, mm.

P200 = Percentage passing No. 200 (4.75-mm) sieve.

$C_C = \dfrac{D_{30}^2}{D_{10} * D_{60}}$

$C_U = \dfrac{D_{60}}{D_{10}}$

D_{10} = Sieve size associated with 10 percent passing, mm.

D_{30} = Sieve size associated with 30 percent passing, mm.

D_{60} = Sieve size associated with 60 percent passing, mm.

- Virginia Smart Road (Davis, 2001)—Mean profile depth (*MPD*) at the Virginia Smart Road, as measured using a laser profiler, was analyzed according to mixture properties of the pavement to determine which properties had the largest effect on MPD. The equation resulting from the regression analysis is provided below. The regression coefficient for the equation was 0.9724, indicating an excellent fit.

$$MPD = -3.596 + 0.1796*NMS + 0.0913*P200 - 0.0294*VTM + 0.1503*VMA \quad 21$$

where:
- MPD = Mean profile depth.
- NMS = Nominal maximum size of the aggregate.
- $P200$ = Percentage passing No. 200 (4.75-mm) sieve.
- VTM = Total voids in the mixture.
- VMA = Voids in the mineral aggregate.

- NCAT-Derived Model (Sullivan, 2005)—The results of an evaluation of the effect of mix gradation and binder content on in-service surface texture measurements from 17 NCAT test mixes found that texture depth can be accurately estimated using binder content and the gradation's weighted mean distance from the MDL. The developed model is presented below. The correlation between predicted and measured texture depth (in the form of *MPD*) was excellent, with an R^2 of 0.96.

$$\Omega = \sum \left[\left\{ \left[(SivS/MaxAgg)^{0.45} \text{ x } 100 \right] - \%Pass \right\} \text{x } SivS \right] \quad 22$$

where:
- Ω = Weighted distance from maximum density line.
- $SivS$ = Sieve size.
- $MaxAgg$ = Maximum aggregate size in mix.
- $\%Pass$ = Percent of mix passing the sieve size.

$$MPD = 0.025\Omega^2 + 0.037\Omega - 0.0265P_b + 0.052 \quad 23$$

where: P_b = Percent binder by weight.

Macro-Texture Durability

For asphalt mix types, high permeability, high air voids, and thin asphalt coatings on aggregate particles are the primary causes of excessive aging of the asphalt binder. This aging contributes to lack of durability and hence, loss of long-term pavement friction. (Kandhal, Foo, and Mallick, 1998). Thus, mix proportioning that ensures long-term durability, and hence pavement friction, must optimize the asphalt mix properties.

In the special case of open-graded asphalt mixes, maintaining the long-term durability and pavement friction while ensuring a high porosity/permeability is required. Additives and polymers can be used to prevent moisture damage and excessive aging of the asphalt binder. Specific recommendations for ensuring durable asphalt mixes are presented below.

- Dense, Uniform, and Gap-Graded Mixes—As a consequence of their low void content and thick binder films, these mixes have generally proven to be durable and resistant to age hardening. Some pavement friction-related considerations are as follows:
  - Make a careful choice of aggregate size, shape, and grading to produce a dense asphalt surface that will meet micro-texture and macro-texture requirements.
  - Limit the voids in the asphalt mix to ensure adequate durability. However, if the void content is too low, deformation can occur resulting in a loss of macro-texture.
  - Ensure a thick film of asphalt binder around the coarse aggregate to prevent thin asphalt binder films and excessive aging. However, the binder content must not be excessive to cause bleeding.
  - SMA mixes may require a stiff asphalt binder to ensure durability. This can be achieved by using the harder asphalt binder grades or by adding polymers to the binder.

- Open-Graded Mixes—Maintaining high levels of permeability/porosity are important for maintaining the drainage characteristics of open-graded asphalt mixes. This is achieved by using open-graded aggregates held together by asphalt binder to form a matrix with interconnecting voids through which water can pass. Unfortunately the interconnected voids allow excellent access to air; so aging and embrittlement of the asphalt binder is potentially exacerbated. To ensure both permeability and durability in the long term, the following is recommended for design:
  - Enhance asphalt mix durability by using softer grade binders and as high a binder content as possible. The binder content must be optimized through testing to ensure adequate permeability.
  - Avoid lean asphalt mixes, as these types of mixes are mostly not durable.
  - Avoid rich asphalt mixes, as these types of mixes are likely to flush/bleed, resulting in patches of binder on the road surface causing low pavement friction and an impermeable surface (poor drainage).
  - The design binder content (optimized through testing) represents the maximum quantity of binder that can be safely incorporated into the porous asphalt mix without introducing excessive binder drainage causing segregation during mixing, transportation, and placement.
  - Excessive binder content and/or excessive mixing temperature causes binder drainage and mixture segregation during transportation from the mixing plant, leading to inconsistency of the finished surface, with areas either rich or lean in binder content.
  - Temperature controls and maximum target binder contents must be incorporated into the design specification to reduce the occurrence of defective surfaces.
  - If it is necessary to improve bonding characteristics and durability, polymer-modified binders should be used.

Noise Considerations

The two biggest keys to producing low noise asphalt pavements are surface texture and porosity (Newcomb and Scofield, 2004). A surface which is relatively flat with voids in it (i.e., negative texture) has better acoustical performance than one that has protrusions above the surface (i.e., positive texture).

For pavement–tire noise reduction, smaller maximum aggregate size and negative texture are better (Newcomb and Scofield, 2004). Larger sized surface texture tends to produce greater noise, which is why coarse chip and coarse-graded dense HMA surface mixes can be noisier than those having a smaller maximum aggregate size. Mixes containing a 0.18 or 0.25 in (5 or 6 mm) maximum aggregate size produce the quietest pavements, compared to reference dense-graded mixes containing a 0.55 or 0.62 in (14 or 16 mm) maximum aggregate size.

Porosity in the surface is a means to achieve even further pavement–tire noise reduction (Newcomb and Scofield, 2004). OGFC combined with a smaller aggregate size is very effective in reducing noise from traffic. Two-layer OGFCs (coarser underlying porous layer and finer porous surface layer) help maintain safety and reduce noise.

In closing, while macro-texture should be kept as low as practical—in the 0.4- to 2.0-in (10- to 50-mm) range—to reduce noise, it should not be done so at the price of good surface friction (Wayson, 1998).

Step 3—Identification of Concrete Pavement Texturing Technique

Concrete surface macro-texture is generally determined by the type of texturing applied to the surface of the concrete (whether freshly placed or hardened). As with asphalt surface mixes, designers must identify a texturing application that produces sufficient macro-texture (*MTD*) that, when combined with the aggregate PSV, satisfies the friction design requirements (Step 1). Extensive recommendations for applying the finishing methods listed in table 15 have been presented in several references, including FHWA *Technical Advisory T 5040.36* (FHWA, 2005). The recommendations provided can be used to enhance macro-texture for the texturing method selected.

Macro-Texture Durability

The strength/abrasion properties of the cement mortar/paste largely determine the wearing characteristics of new concrete surfaces. Increasing the cement content (in effect, decreasing the water-cement ratio) and implementing sound construction practices maximizes cement paste/mortar strength and, thus, abrasion resistance. Additionally, the use of air-entrained cement paste/mortar where freezing and thawing is encountered, can relieve pressure in the paste during freezing, thereby reducing the potential for the paste to crack.

Noise Considerations

Tine or groove depth, width, spacing, and orientation are all major factors affecting pavement-tire noise (Hoerner et al., 2003). Transverse tinings with uniformly spaced tines 0.5 in (13 mm) or greater have been found to produce an objectionable tonal quality (tire whine). Randomly varying the transverse tine spacing can reduce the tonal quality problems. Tire noise increases with tine width; research shows mixed data regarding impact of tine depth on noise.

Skewing of transverse tining has been found to reduce pavement-tire noise (Hoerner et al., 2003). Longitudinal tining, shallow turf drags, and abrading do not exhibit same prominent objectionable tonal spikes observed with uniform transverse tining (Hoerner et al., 2003).

Recommended transverse tining types, with respect to noise are as follows (Hoerner and Smith, 2002):

- Repeated random, with spacing of 0.4 to 3.0 in (10 to 76 mm), depth of 0.125 in to 0.25 in (3 to 6 mm), width of 0.125 in (3 mm), and skew of 1:6.
- Repeated random, with spacing of 0.4 to 2.0 in (10 to 51 mm), depth of 0.125 in to 0.25 in (3 to 6 mm), width of 0.125 in (3 mm), and skew of 1:6.

Recommended longitudinal tining type, with respect to noise are as follows (Hoerner and Smith, 2002):

- Uniform, with spacing of 0.75 in (19 mm), depth of 0.125 in to 0.25 in (3 to 6 mm), and width of 0.125 in (3 mm).

Finally, based on Wisconsin's results and Virginia's experience (FHWA, 1996), using transverse and longitudinal tining together (i.e., cross-hatching) produces consistently higher total noise.

Step 4—Development of Construction Specifications

All agencies have standard specifications for construction of pavement surfaces. The standards provide guidance on requirements for aggregates, mixes, handling, placement, compaction, curing, and protection of new surfaces. For some agencies, these specifications do not specifically address friction properties of the wearing surface. To ensure quality friction on new or rehabilitated pavement surfaces, requirements for aggregate properties and test methods presented in this section may be added to project specifications as needed.

<u>Special Provisions</u>

Each project has a unique set of requirements depending on the design and construction constraints and special demands. These include such items as aggregate blending, noise mitigation, and quality assurance (QA), which are clarified in the special provisions of the construction documents and specifications.

Blending

Normally, aggregates from two or more sources must be blended to meet the specification limits. Several studies have reported that the blended aggregate properties tend to be the same as the weighted average of the properties of the individual aggregates. Thus, the goal of blending aggregate is to set the percentages of each aggregate used such that the final blend has properties that lies within the specification limits of the tests to be performed.

Quality Assurance

A QA program often stipulates the frequency of testing aggregate sources. While no specific guidance on the extent and frequency of testing is provided in this Guide, it is strongly suggested that an aggregate source be tested extensively whenever substantially new aggregate deposits are to be used for pavement surfacing. The extent and frequency can be reduced as the agency becomes more familiar with the aggregate source and there is a history of performance for aggregates from the given source (Folliard and Smith, 2003).

Construction Issues

Construction deficiencies and poor construction practices can contribute to inadequate friction. Construction issues involve control of aggregate and mix quality during production, handling, stockpiling, mixing, placing, and finishing. Friction restoration treatments in particular, such as chip seals, slurry seals, micro-surfacing, and proprietary surfaces, are susceptible to providing less than expected friction, if poor construction practices are employed.

Step 5—Formulation of Design Strategies

Both monetary and non-monetary factors are considered in selecting preferred pavement design strategy the various feasible alternatives. The main inputs required are (1) estimates of costs, (2) estimates of benefits (if the benefit cost option is selected, not that benefit cost analysis is required only if there is a significant difference in benefits between alternatives, and (3) non-monetary factors.

Important cost elements related to the inclusion of surface friction in the design strategy are:

- Agency costs.
  - Additional design and engineering costs.
  - Aggregate materials with required frictional properties.
  - Additives, including polymers, to improve surface properties and performance.
  - Frequency/duration of restoration activities.
    - Design strategies involving frequent M&R are typically more costly overall because of the effects of highway user delay costs, traffic control, and so on.
    - Timing of M&R can significantly escalate costs if M&R to restore surface friction does not coincide with M&R to restore structural capacity.
  - Tort and legal exposure caused by inadequate pavement friction.

- User costs
  - Travel delays (time/delay) for friction restoration impact life cycle cost.
  - Friction can adversely influence pavement–tire factors such as tire wear, rolling resistance, and fuel consumption.
  - Safety associated factors that impact accident costs.
    - Frequency of accidents.
    - Value of accidents.

Benefits from ensuring adequate levels of friction throughout the pavement life are quantified through:

- Improved highway safety (i.e., reduction in accident costs).
  - Value of lives saved.
  - Value of injuries avoided (medical, loss income, psychological damage).
  - Savings in pain and suffering of crash victims and their families due to a reduction in accidents.
  - Reductions in property damage due to reduction in accidents.
- Reduction in legal exposure and cash settlements for legal claims.
  - Medical care.
  - Wage loss and other economic payments.
  - Pain and suffering, and other non-economic damages.
  - Legal fees.

Non-monetary factors can be included in the decision matrix and addressed through (1) agency policies and criteria on these factors and (2) appropriate weights to these factors to reflect the importance assigned to them by the agency. The non-monetary design considerations include (AASHTO, 1993):

- Service life.
- Duration of construction.
- Traffic control problems.
- Reliability, constructability, and maintainability of design.

Non-monetary factors attributed to pavement friction include:

- Pavement–tire noise.
- Splash and spray.
- Fuel consumption.
- Rolling resistance and tire wear.
- Reflectance and glare.

REFERENCES

Al-Qadi, I.L., G.W. Flintsch, D.S. Roosevelt, R. Decker, J.C. Wambold, and W.A. Nixon. 2002. "Feasibility of Using Friction Indicators to Improve Winter Maintenance Operations and Mobility," NCHRP Web Document 53, National Cooperative Highway Research Program (NCHRP), Washington, D.C.

American Association of State Highway and Transportation Officials (AASHTO). 1976. Guidelines for Skid-Resistant Pavement Design, Task Force for Pavement Design,
Andresen A. and J.C. Wambold. 1999. "Friction Fundamentals, Concepts and

American Concrete Pavement Association (ACPA). 2000. "Concrete Pavement Surface Textures," *Special Report No. SR902P*, ACPA, Skokie, Illinois.

Brown, R., B. Powell, R. West, and D. Timm. 2005. "Summary of NCAT Test Track Findings," Volume 4, Number 3 (Spring Issue) *Southeastern Superpave Center News*, National Center for Asphalt Technology (NCAT), Auburn, Alabama.

Dahir, S.H. and J.J. Henry. 1978. Alternatives for the Optimization of Aggregate and Pavement Properties Related to Friction and Wear Resistance, Report No. FHWA-RD-78-209, Federal Highway Administration (FHWA), Washington, D.C.

Davis, R.M. 2001. Comparison of Surface Characteristics of Hot-Mix Asphalt Pavement Surfaces at the Virginia Smart Road, Thesis submitted to the faculty of Virginia Polytechnic Institute and State University, Blacksburg, Virginia.

Emery, J.J., W. Schenk, J.J. Carrick, J.K. Davidson, W.K. MacInnis, and G.J.A. Kennepohl. 1993. "Stone Mastic Asphalt Trials in Ontario," *Transportation Research Record 1427*, Transportation Research Board, Washington, D.C.

Federal Highway Administration (FHWA). 1990. *Open-Graded Friction Courses*, Technical Advisory T 5040.13, FHWA Office of Pavement Technology, Washington, D.C.

Federal Highway Administration (FHWA). 1996. "PCC Surface Texture Technical Working Group Findings," FHWA, Washington, D.C.

Federal Highway Administration (FHWA). 2005. *Surface Texture for Asphalt and Concrete Pavements*, Technical Advisory T 5040.36, FHWA Office of Pavement Technology, Washington, D.C.

Flintsch, G.W., I.L. Al-Qadi, C.A. Via Jr., R. Davis, and K.K. McGhee. 2002. "Effect of HMA Properties on Pavement Surface Characteristics," Paper presented at *Pavement Evaluation 2002 Conference*, Roanoke, Virginia.

Flintsch G.W., E. De Leon, K.K. McGhee, and I.L. Al-Qadi. 2003. "Pavement Surface Macro-texture Measurement and Application," Transportation Research Board (TRB), Washington, D.C.

Folliard, K.J. and K.D. Smith. 2003. "Aggregate Tests for Portland Cement Concrete Pavements: Review and Recommendations," September edition (No. 281) of *NCHRP Research Results Digest*, National Cooperative Highway Research Program (NCHRP), Washington, D.C.

Gransberg, D. and D.M.B. James. 2005. "Chip Seal Best Practices," *NCHRP Synthesis 342*, National Cooperative Highway Research Program (NCHRP), Washington, D.C.

Gillespie, T.D. 1992. *Fundamentals of Vehicle Dynamics*, Society of Automotive Engineers (SAE), Warrendale, Pennsylvania.

Hanson, D.I. and B.D. Prowell. 2004. "Evaluation of Circular Texture Meter for Measuring Surface Texture of Pavements," NCAT Report No. 04-05, National Center for Asphalt Technology (NCAT), Auburn, Alabama.

Hanson, D.I. and B. Waller. 2005. "Evaluation of the Noise Characteristics of Minnesota Pavements," Final Report prepared for Minnesota Department of Transportation, St. Paul, Minnesota.

Harmelink, D. 2001. Stone Mastic Asphalt in Colorado, Report No. CDOT-DTD-R-2001-1, Colorado Department of Transportation, Denver, Colorado.

Hayes, G.G., D.L. Ivey, and B.M. Gallaway, "Hydroplaning, Hydrodynamic Drag, and Vehicle Stability," Special Technical Publication 793, American Society for Testing and Materials (ASTM), Philadelphia, Pennsylvania (1983).

Henry, J.J. 2000. "Evaluation of Pavement Friction Characteristics—A Synthesis of Highway Practice," *NCHRP Synthesis 291*, Transportation Research Board, Washington, D.C.

Hoerner, T.E., K.D. Smith, R.M. Larson, and M.E. Swanlund. 2003. "Current Practice of PCC Pavement Texturing," Paper presented at 82nd Annual Meeting of the Transportation Research Board, Washington, D.C.

Hoerner, T.E. and K.D. Smith. 2002. *High Performance Concrete Pavement: Pavement Texturing and Tire-Pavement Noise*, FHWA Report No. FHWA-IF-02-020, Federal Highway Administration, Washington, D.C.

Horne, W.B. and F. Buhlmann. 1983. "A Method for Rating the Skid Resistance and Micro/Macro-texture Characteristics of Wet Pavements," ASTM International STP No. 793, W. E Meyers and J. D. Walter, Editors American Society for testing and materials, Philadelphia, Pennsylvania.

Kandhal, P.S., F. Parker Jr., and R.B. Mallick. 1997. *Aggregate Tests for Hot Mix Asphalt: State of the Practice*, NCAT Report No. 97-6, National Center for Asphalt Technology (NCAT), Auburn, Alabama.

Kandhal, P.S. and F. Parker Jr. 1998. 1997. *Aggregate Tests Related to Asphalt Concrete Performance in Pavements*, NCHRP Report 405, National Cooperative Highway Research Program (NCHRP), Washington, D.C.

Kuemmel, D.A., J.R. Jaeckel, and A. Satanovsky. 2000. *Investigative Study of the Italgrip System: Noise Analysis*, Report No. WI/SPR-02-00Wisconsin Department of Transportation, Madison, Wisconsin.

Kulakowski, B.T., D.W. Harwood, D.R. Hiltunen, J.M. Mason, Jr., W.E. Meyer, S.L. Simoneau, and J.C. Wambold. 1990. "Skid Resistance Manual," Report No. PTI 9016, Pennsylvania State University, University Park, Pennsylvania.

Liang, R.Y. 2003. "Blending Proportions of High Skid and Low Skid Aggregate," Final Report prepared for Ohio Department of Transportation (ODOT), Columbus, Ohio.

Liang, R.Y. and L.L. Chyi. 2000. "Polishing And Friction Characteristics Of Aggregates Produced in Ohio," Report No. FHWA/OH-2000/001, Ohio Department of Transportation, Columbus, Ohio.

McDaniel, R.S. and B.J. Coree. 2003. "Identification of Laboratory Techniques to Optimize SuperPave HMA Surface Friction Characteristis," Phase I Final Report, SQDH 2003-6, HL 2003-19, Institute for Safe, Quiet, and Durable Highways (ISQDH), Purdue University.

McNerney, M.T., B.J. Landsberger, T. Turen, and A. Pandelides. 2000. "Comparative Field Measurements of Tire/Pavement Noise of Selected Texas Pavements," Report No. FHWA/TX-7-2957-2, Texas Department of Transportation, Austin, Texas.

Meegoda, J.N., C.H. Hettiarachchi, G.M. Rowe, N. Bandara, and M.J. Sharrock. 2002. Correlation of Surface Texture, Segregation, and Measurement of Air Voids, Final Report prepared for New Jersey Department of Transportation, Trenton, New Jersey.

Meininger, R.C. 1998. "Aggregate Tests Related to Performance of Portland Cement Concrete Pavement," Unpublished Final Report, NCHRP Project 4-20A, National Cooperative Highway Research Program (NCHRP), Washington, D.C.

Mergenmeier, A.J. 2004. Stone Matrix Asphalt—VDOT's Initiative for Longer Lasting Roads, Paper Presented at Annual Meeting of Southeastern Association of State Highway and Transportation Officials (SASHTO) held in Norfolk, Virginia.

Mockensturm, E.M., B.T. Kulakowski, and N.M. Hawk. 2002. "Measurement and Evaluation of Roadside Noise Generated by Transit Buses," Final Report, The Institute for Safe, Quiet, and Durable Highways (ISQDH), Purdue University.

National Highway Institute (NHI). 1998. *Techniques for Pavement Rehabilitation—A Training Course*, Participant's Manual, Federal Highway Administration, Washington, D.C.

Newcomb, D. and L. Scofield. 2004. "Quiet Pavements Raise the Roof in Europe: Scanning Tour Reveals European Practice for Noise Mitigation," September/October edition of *Hot Mix Asphalt Technology*.

Noyce, D.A., H.U. Bahia, J.M. Yambo, and G. Kim. 2005. Incorporating Road Safety into Pavement Management: Maximizing Asphalt Pavement Surface Friction for Road Safety Improvements," Draft Literature Review and State Surveys, Midwest Regional University Transportation Center (UMTRI), Madison, Wisconsin.

Ohio Department of Transportation (ODOT). 2001. "Pavement Preventive Maintenance Program Guidelines," ODOT Office of Pavement Engineering, Columbus, Ohio.

PennDOT, (2008) "Vanport Limestone Skid Resistance Analysis", Committee Report. Harrisburgh, PA

Permanent International Association of Road Congresses (PIARC). 1987. "Report of the Committee on Surface Characteristics," *Proceedings of the 18th World Road Congress*, Brussels, Belgium.

Prowell, B.D., J. Zhang, and E.R. Brown. 2005. "Aggregate Properties and the Performance of SuperPave-Designed Hot Mix Asphalt," *NCHRP Report 539*, National Cooperative Highway Research Program (NCHRP), Washington, D.C.

Rado, Z. 1994. "Analysis of Texture Models," PTI Report No. 9510, Pennsylvania Transportation Institute (PTI), Penn State University, State College, Pennsylvania.

Radt, H.S. and W.F. Milliken. 1960. *Motions of Skidding Automobiles*, Paper No. 600133 (205A), Society of Automotive Engineers (SAE), Warrendale, Pennsylvania.

Rao, S., H.T. Yu, L. Khazanovich, M.I. Darter, and J.W. Mack. 1999. "Longevity of Diamond Ground Concrete Pavements," Paper presented at 78th Annual Meeting of the Transportation Research Board, Washington, D.C.

Rasoulian, M. 2004. "Notes from February 19, 2004 teleconference with Mr. Masood Rasoulian, Louisiana Transportation Research Center," Champaign, Illinois.

Richardson, J.T.G. 1999. "Stone Mastic Asphalt in the U.K.," Society of Chemical Industry (SCI) Lecture Papers Series, London, United Kingdom.

Roads and Bridges. 2005. A Texture Message, September Issue *Roads and Bridges* Magazine.

Rowdan, L. 2004. "Notes from February 19, 2004 teleconference with Ms. LaDonna Rowdan, Illinois Department of Transportation," Champaign, Illinois.

Saito, K., T. Horiguchi, A. Kasahara, H. Abe, and J.J. Henry. 1996. "Development of Portable Tester for Measuring Skid Resistance and its Speed Dependency on Pavement Surfaces," Transportation Research Record No. 1536, Transportation Research Board, Washington, D.C.

Sandburg, U. 1998. "Influence of Road Surface Texture on Traffic Characteristics Related to Environment, Economy, and Safety: A State-of-the-Art Study Regarding Measures and Measuring Methods," VTI Report 53A-1997, Swedish National Road Administration, Borlange, Sweden.

Sandburg, U. and J.A. Ejsmont. 2002. *Tyre/Road Noise Reference Book*, ISBN 91-631-2610-9, Informex, Kisa, Sweden.

Schmiedlin, R.B. and D. Bischoff. 2002. "Stone Matrix Asphalt: The Wisconsin Experience," Report No. WI/SPR-02-02, Wisconsin Department of Transportation, Madison, Wisconsin.

Senior, S.A. and C.A. Rogers. 1991. "Laboratory Tests for Predicting Coarse Aggregate Performance in Ontario, Transportation Research Record 1301, Transportation Research Board, Washington, D.C.

Skerritt, W.H. 2004. "Notes from February 19, 2004 teleconference with Mr. Bill Skerritt of the New York Department of Transportation, Engineering Geology section of the Materials Bureau," Champaign, Illinois.

Stampley, B. 2004. "Notes from February 13, 2004 teleconference with Mr. Bryan Stampley, Pavement Management Engineer with Texas Department of Transportation," Champaign, Illinois.

Texas Department of Transportation (DOT). 2004. "Concrete Rated Source Quality Catalog and Bituminous Rated Source Quality Catalog," Material Producer List, Texas DOT, http://www.dot.state.tx.us/business/materialproducerlist.htm, Austin, Texas.

Uhlmeyer, J.S., L.M. Pierce, and J.T. Weston. 2003. Novachip®, Post Construction/Performance Report, Report No. WA-RD 568.1, Washington Department of Transportation (WSDOT), Olympia, Washington.

Wade, M., R. DeSombre, and D. Peshkin. 2001. High Voluem/High Speed Asphalt Roadway Preventive Maintenance Surface Treatments, Final Report, South Dakota Department of Transportation, Pierre, South Dakota.

Wallman, C.G. and H. Astrom. 2001. "Friction Measurement Methods and the Correlation Between Road Friction and Traffic Safety," Swedish National Road and Transport Research Institute, VTI Meddelande 911A, Linkoping, Sweden.

Wambold, J.C., C.E. Antle, J.J. Henry, and Z. Rado. 1995. "International PIARC Experiment to Compare and Harmonize Texture and Skid Resistance Measurements," AIPCR-01.04.T.

Washington Department of Transportation (WSDOT). 2005. "Factors Affecting HMA Permeability," Tech Notes, WSDOT Materials Laboratory, Olympia, Washington.

Washington Asphalt Pavement Association (WAPA). 2004. "Asphalt Pavement Guide," on-line website www.asphaltwa.com.

Wayson, R.L. 1998. "Relationship Between Pavement Surface Texture and Highway Traffic Noise," *NCHRP Synthesis 268*, National Cooperative Highway Research Program (NCHRP), Washington, D.C.

Wu, Y., F. Parker, and K. Kandhal. 1998. *Aggregate Toughness/Abrasion Resistance and Durability/Soundness Tests Related to Asphalt Concrete Performance in Pavements*, NCAT Report 98-04, National Center for Asphalt Technology (NCAT), Auburn, Alabama.

Yaron, R. and S. Nesichi. 2005. "Alleviating the Skid Resistance Problem: The Israeli Experience," Paper presented at *First International Conference on Surface Friction: Roads and Runways*, Christchurch, New Zealand.

Bibliography

- **<u>Concrete pavements surface texture (friction characteristics and measurement)</u>**

Texturing Concrete Pavement. ACI Committee 325, ACI-325.6R-88. American Concrete Institute, Detroit, Mich., 1988.

Dahir, S. H. M., and W. L. Gramling. NCHRP Synthesis of Highway Practice 158: Wet-Pavement Safety Programs. TRB, National Research Council, Washington, D.C., 1990.

Hibbs, B. O., and R. M. Larson. Tire Pavement Noise and Safety Performance— PCC Surface Texture Technical Working Group. FHWASA- 96-068. FHWA, U.S. Department of Transportation, 1996.

Concrete Pavement Surface Textures. Special Report SR902P. American Concrete Pavement Association, Skokie, Ill., 2000.

Report of the Committee on Surface Characteristics. In Proc., 18th World Road Congress, Brussels, Belgium, Permanent International Association of Road Congresses (PIARC), Paris, 1987.

Wu, C. L., and M. A. Nagi. Optimizing Surface Texture of Concrete Pavement. PCA Research and Development Bulletin RD111T. Portland Cement Association, Skokie, Ill., 1995.

Abe, H., A. Tamai, J. J. Henry, and J. Wambold. Measurement of Pavement Macrotexture Using the Circular Texture Meter. In Transportation Research Record: Journal of the Transportation Research Board, No. 1764, TRB, National Research Council, Washington, D.C., 2001, pp. 201–209.

Henry, J. J. NCHRP Synthesis of Highway Practice No. 291: Evaluation of Pavement Friction Characteristics. TRB, National Research Council, Washington, D.C., 2000.

Roe, P. G., A. R. Parry, and H. E. Viner. High and Low Speed Skidding Resistance: The Influence of Texture Depth. TRL Report 367. U.K. Transport Research Laboratory, Crowthorne, Berkshire, England, 1998.

International PIARC Experiment to Compare and Harmonize Texture and Skid Resistance Measurements. PIARC Report 01.04.T. PIARC, Paris, 1995.

Characterization of Pavement Texture Using Surface Profiles, Part 1: Determination of Mean Profile Depth. In Acoustics, ISO Standard 13473, International Standards Organization, Geneva, Switzerland, 1998.

Construction and Materials Manual. Chapter 8, Section 8.10. Wisconsin Department of Transportation, Madison, 2001.

Kuemmel, D. A., R. C. Sonntag, J. A. Crovetti, Y. Becker, J. R. Jaeckel, and A. Satanovsky. Noise and Texture on PCC Pavements—Results of a Multi-State Study. Report WI/SPR-08-99. Wisconsin Department of Transportation, Madison, 2000.

Smith, K. D. Status of High Performance Concrete Pavements. Report FHWA-IF-01-025. FHWA, U.S. Department of Transportation, 2001.

Descornet, G., F. Fuchs, and R. Buys. Noise-Reducing Concrete Pavements. In Proc., Fifth International Conference on Concrete Pavement Design and Rehabilitation, Purdue University, West Lafayette, Ind., 1993.

- **Aggregate Resistance to Polishing and Abrasion**

Abdul-Malak, M., Fowler, D., and Constantino, C. 1996. "Aggregate characteristics governing performance of seal coat highway overlays." Transportation Research Record. 1547, Transportation Research Board, Washington, D.C., 15–22.

Chandan, C., Sivakumar, K., Masad, E., and Fletcher, T. 2004. "Application of imaging techniques to geometry analysis of aggregate particles." J. Comput. Civ. Eng., Vol. 18 1 , pp 75–82.

Cooley, L. Jr., and James, R. 2003. "Micro-Deval testing of aggregates in the southeast." Transportation Research Record. 1837, Transportation Research Board, Washington, D.C., 73–79.

Crouch, L., and Dunn, T. 2005. "Identification of aggregates for Tennessee bituminous surface courses." Project No. TNSPR-RES1149, Final Rep., Tennessee Dept. of transportation TDOT, Cookeville, Tenn.

Dahir, S. 1979. "A review of aggregate selection criteria for improved wear resistance and skid resistance of bituminous surfaces." J. Test. Eval., 7, 245–253.

Gatchalian, D., Masad, E., Chowdhury, A., and Little, D. 2006. "Characterization of aggregate resistance to degradation in stone matrix asphalt mixtures." Transportation Research Record. 1962, Transportation Research Board, Washington, D.C., 55–63.

Kandhal, P., Parker, F. Jr., and Bishara, E. 1993. "Evaluation of Alabama limestone aggregates for asphalt wearing courses." Transportation Research Record. 1418, Transportation Research Board, Washington, D.C., 12–21.

Mahmoud, E. 2005. "Development of experimental methods for the evaluation of aggregate resistance to polishing, abrasion, and breakage." MS thesis, Texas A&M Univ., College Station, Tex.

Masad, E., Al-Rousan, T., Button, J., Little, D., and Tutumluer, E. _2007 "Test methods for characterizing aggregate shape, texture and angularity." NCHRP 4-30A Final Rep., Rep. No. 555, National Cooperative Highway Research Program, National Research Council, Washington, D.C.

Nitta, N., Saito, K., and Isozaki, S. 1990. "Surface characteristics of roadways: International research and technologies." ASTM Special Technical Publication No. 1031, ASTM, Philadelphia, 113–126.

Won, M., and Fu, C. 1996. "Evaluation of laboratory procedures for aggregate polish test." Transportation Research Record. 1547, Transportation Research Board, Washington, D.C., 23–28.

Wu, Y., Parker, F., and Kandhal, P. 1998. "Aggregate toughness/ abrasion resistance and durability/soundness tests related to asphalt concrete performance in pavements." Transportation Research Record. 1638, Transportation Research Board, Washington, D.C., 85–93.

- **Interaction between aggregate and cement mortar**

M.H. Zhang, O.E. Gjorv, Microstructure of the interfacial zone between lightweight aggregate and cement paste, Cem. Concr. Res. 20 (4) (1990) 610– 618.

R. Zimbelmann 1987, A method for strengthening the bond between cement paste and aggregates, Cem. Concr. Res. 17 (4) 651–660.

P.J.M. Monterio, J.C. Maso, J.P. Ollivier 1985, The aggregate– mortar interface, Cem. Concr. Res. 15 (6) 953–958.

J.A. Larbi, J.M.J.M. Bijen 1990, Orientation of calcium hydroxide at the Portland cement paste– aggregate interface in mortars in the presence of silica fume: A contribution, Cem. Concr. Res. 20 (3) 461– 470.

Y.L. Wong, L. Lam, C.S. Poon, F.P. Zhou 1999, Properties of fly ash-modified cement mortar – aggregate interfaces, Cem. Concr. Res. 29 1905– 1913.

M.G. Alexander 1993, Two experimental techniques for studying the effects of the interfacial zone between cement paste and rock, Cem. Concr. 23 567–575.

M. Saito, M. Kawamura 1986, Resistance of the cement–aggregate interfacial zone to propagation of cracks, Cem. Concr. Res. 16 (5) 653– 661.

U. Trende, O. Buyukozturk 1998, Size effect and influence of aggregate roughness in interface fracture of concrete composites, ACI Mater. J. 95 (4) 331– 338.

E.K. Tschegg, H.M. Rotter, P.E. Roelfstra, U. Bourgund, P. Jussel 1995, Fracture mechanical behavior of aggregate–cement matrix interfaces, J. Mater. Civ. Eng. 7 (4) 199– 203.

K.M. Lee, O. Buyukozturk 1995, Fracture toughness of mortar– aggregate interfaces in high-strength concrete, ACI Struct. J. 92 (6) 634– 642.